SOLAR HOT WATER SYSTEM USING LATENT HEAT THERMAL ENERGY STORAGE

By

Saeid Seddegh Kiyaroudi

B.Eng (Hons)(Mechanical Engineering)

M.Eng (Mechanical Engineering)

MIEAust

School of Engineering and ICT, University of Tasmania

A dissertation submitted for the degree of

Doctor of Philosophy

September 2016

SUMMARY

Latent heat thermal energy storage, based on the absorption or release of heat when a storage material undergoes phase change, has received significant research attention due to its high storage density and small temperature variation. A comprehensive literature review found that a common issue raised is the lack of understanding of the heat transfer mechanism as phase change material (PCM) melts and solidifies during the charging and discharging processes, respectively. Thus, this project largely focuses on investigation of the heat transfer mechanism across a complete charging and discharging cycle. A proper heat transfer model was developed to study the thermal behaviour and heat transfer characteristics of PCMs during the phase change process. Experimental studies were also performed to visualise the formation of heat transfer mechanism at different stages in PCMs. It was found that the heat transfer mechanism during charging is different from that during discharging.

The developed heat transfer model was first validated using experimental data available on literature. It was then used to investigate the heat transfer mechanism in a shell-and-tube latent heat energy storage system (LHTES). Results showed that the combined convection and conduction model can better describe the thermal behaviour of PCMs than a pure conduction model. This combined model was further used to study the effect of orientation of the LHTES on the system performance. The results showed that during the charging process for the horizontal orientation, convective heat transfer has a strong effect on melting of the upper part of the solid PCM and is less significant during melting of the lower half. However, in the vertical orientation, convective heat transfer maintains similar action during the entire charging process. In the discharging process, the thermal behaviour does not show any difference between horizontal and vertical systems.

As different mechanism of heat transfer was found in vertical and horizontal systems, further visualized experimental study focused on the vertical conical and cylindrical LHTES systems which were followed by the numerical analyses. It was revealed that during the charging process, there existed a vertical convective circulation channel around the heat transfer fluid (HTF) pipe. The width of this vertical channel did not show significant change once it was formed. Thermal energy was transferred from the HTF to the liquid PCM and then carried upward via vertical convective circulation in the channel. This thermal energy was further transferred in the liquid PCM accumulated at the upper part of the storage system through horizontal convective circulation. Hence heat transfer was more effective at the upper part of the system and PCM melting front moves downward from the top to the bottom of the system. Further comparison study showed that the vertical conical system had better energy storage performance than the cylindrical system. This indicated that a vertical storage unit with geometry having large volume in the upper part and small volume in the lower part could have better energy storage performance. During the discharging process, it was revealed that the PCM solidifies around the HTF pipe and the solidification front moves outward. Due to its low thermal conductivity, the PCM behaves as an insulation material and the rate of heat transfer from the HTF to the PCM is reduced. The comparative results show that both cylindrical and conical systems have similar trend and it takes almost the same time to complete the discharging process.

The study was then followed by an investigation of the effects of geometrical parameters on vertical cylindrical shell-and-tube LHTES systems. For this purpose, the temporal variations of four similar LHTES units with different HTF pipe diameters were measured and compared experimentally. The effect of different HTF inlet temperatures and flow rates were investigated. The results show that complete charging and discharging is highly dependent on the ratio of outside to the inside diameter as well as the HTF temperature. It is also concluded

that there is no significant difference in the charging and discharging time by increasing the HTF flow rate as far as the HTF flow is turbulent. It was suggested that the selection of operating conditions and geometrical parameter dimensions depends upon the required heat transfer rate and the time within which the energy has to be stored and delivered. This analysis provides useful information on design and optimization of the shell-and-tube LHTES system.

DECLARATION OF ORIGINALITY

"This thesis contains no material which has been accepted for a degree or diploma by the University or any other institution, except by way of background information and duly acknowledged in the thesis, and to the best of my knowledge and belief no material previously published or written by another person except where due acknowledgement is made in the text of the thesis, nor does the thesis contain any material that infringes copyright."

This thesis may be made available for loan and limited copying and communication in accordance with the Copyright Act 1968.

Saeid Seddegh Kiyaroudi

05/09/2016

ACKNOWLEDGEMENTS

I highly appreciate my primary supervisor Dr Xiaolin Wang for his much needed support, uncountable advices and precious inputs throughout the project over the whole period of my candidacy. I would also like to thank my co-supervisor, Dr Alan Henderson who made valuable contributions to the project. Thanks are extended to the workshop staff at the School of Engineering and ICT for their technical support and Mr Zane Smith who did the proof reading of the thesis.

This research would not have been possible without the support of my triangle of love; my father, my mother and specially my wife, to whom I dedicate this thesis.

STATE OF CO-AUTHORSHIP

The following people and institutions contributed to the publication of work undertaken as part of this thesis:

- **Candidate:** Saeid Seddegh, School of Engineering and ICT, University of Tasmania, Hobart, Tasmania, Australia.
- **Author 1:** Dr Xiaolin Wang, School of Engineering and ICT, University of Tasmania, Hobart, Tasmania, Australia, Primary Supervisor.
- **Author 2:** Dr Alan D. Henderson, School of Engineering and ICT, University of Tasmania, Hobart, Tasmania, Australia, Co-Supervisor.
- **Author 3:** Dr Ziwen Xing, School of Energy and Power Engineering, the Xi'an Jiaotong University, China.

Authors' details and their roles:

❖ **Paper 1:** Saeid Seddegh, Xiaolin Wang, Alan D. Henderson, Ziwen Xing. "Solar domestic hot water systems using latent heat energy storage medium: A review". Renewable and Sustainable Energy Reviews 49, PP. 517-533, ELSEVIER, 2015. (***Located in Chapter 2).***

For paper 1, the Candidate was the primary author who evaluated and classified the literature, wrote the first draft and finalized the manuscript. Author 1 enhanced the contents and was the corresponding author. Author 2 and 3 assisted with manuscript editing.

❖ **Paper 2:** Saeid Seddegh, Xiaolin Wang, Alan D. Henderson. "Numerical investigation of heat transfer in a vertical shell and tube latent energy storage

system". Applied Thermal Engineering 87, PP. 698-706, ELSEVIER, 2015. (***Located in Chapter 3).***

- **Paper 3:** Saeid Seddegh, Xiaolin Wang, Alan D. Henderson. "A comparative study of thermal behaviour of a horizontal and vertical shell-and-tube energy storage using phase change materials". Applied Thermal Engineering 93, PP. 348-358, ELSEVIER, 2016. (***Located in Chapter 4).***

  For papers 2, and 3, the Candidate was the primary author who evaluated the literature, develop the heat transfer method, performed the simulation, analysed the results, wrote the first draft and finalized the manuscript. Author 1 enhanced the contents and was the corresponding author. Author 2 assisted with manuscript editing.

- **Paper 4:** Saeid Seddegh, Xiaolin Wang. "Investigation of heat transfer in cylindrical and conical vertical shell-and-tube latent heat energy storage systems during charging processes". Submitted to the Journal of Renewable Energy, ELSEVIER. (***Located in Chapter 5).***

- **Paper 5:** Saeid Seddegh, Xiaolin Wang. "Heat transfer investigation of cylindrical and conical shell-and-tube latent heat thermal energy storage systems during discharging processes". Accepted for oral presentation in the 8th International conference on applied Energy, Beijing, China, October 8-11, 2016. (***Located in Chapter 6).***

  For papers 4, and 5, the Candidate was the primary author who evaluated the literature, developed the conceptual design, set up the experimental facilities, developed the simulation model, analyses the experimental and numerical data,

wrote the first draft and finalized the manuscript. Author 1 enhanced the contents, assisted with manuscript editing and was the corresponding author.

- **Paper 6:** Saeid Seddegh, Xiaolin Wang, "Experimental investigations of geometrical parameters affecting a cylindrical shell-and-tube latent heat thermal energy storage system". Submitted to the International Journal of Heat and Mass Transfer. ***(Located in Chapter 7).***

  For paper 6, the Candidate was the primary author who evaluated the literature, developed the conceptual design, set up the experimental facilities, analysed the data, wrote the first draft and finalized the manuscript. Author 1 enhanced the contents and was the corresponding author.

We the undersigned agree with the above stated "proportion of work undertaken" for each of the above published (or submitted) peer-reviewed manuscripts contributing to this thesis:

Signed:

Candidate:

Author 1:

Author 2:

Author 3:

Date: 23/08/2016

Dr Xiaolin Wang
Supervisor
School of Engineering and ICT
University of Tasmania

Professor Andrew Chan
Head of School
School of Engineering and ICT
University of Tasmania

NOMENCLATURE

A	Mushy zone constant	(kg/m^3·s)
c_p	Specific heat	(J/kg·K)
D	Pipe diameter	(m)
f	Liquid fraction or friction factor	
h	enthalpy	(J/kg)
H	Total enthalpy	(J/kg)
k	Thermal conductivity	(W/m·K)
L	Latent heat	(J/kg)
P	Pressure	(Pa)
S	Source term	
t	Time	(s)
T	Temperature	(K)
v	Velocity	(m/s)

Greek letter

ρ	Density	(kg/m^3)
μ	Dynamic viscosity	(kg/m·s)
ε	Numerical constant	
β	Volumetric expansion coefficient	(1/K)

Subscripts

i	Cell number
ini	Initial
mush	Mushy zone
o	Reference
stored	Stored energy
solid	Solid phase
liquid	Liquid phase

Table of Contents

List of Figures

List of Tables

Chapter 1: Introduction

1.1. Background

The current global reliance on fossil fuels for energy production presents environmental concerns. Increasing levels of greenhouse gas emissions and depletion of fossil fuels are the main driving force behind efforts to effectively utilise various sources of renewable energy. Renewable energy sources such as solar, wind, hydropower and biogas show strong potential to meet global energy requirements in a sustainable way. Solar thermal energy is the most abundant source, and is available in both direct as well as indirect forms. The Sun emits energy at a rate of 3.8×10^{23} kW, of which, approximately 1.8×10^{14} kW is intercepted by the earth. About 60% of this amount, or 1.08×10^{14} kW, is absorbed by the surface of the earth. The remainder is reflected into space and absorbed by the atmosphere. In just 1 hour, energy absorbed by the earth is more than the energy consumed in the whole world for 1 year. The annual solar energy that reaches the earth's surface is approximately 3,400,000 EJ. This is an order of magnitude greater than all the estimated (both discovered and undiscovered) non-renewable energy resources, including fossil fuels and nuclear [1].

Figure 1 shows the average annual growth rates of various renewable energy sectors over the period 2007 to 2012. During this five-year period, the installed capacity of many renewable energy technologies grew very rapidly, with the fastest growth occurring in the power sector. Demand has also increased rapidly in the heating/cooling sector, particularly for solar thermal systems, geothermal ground-source heat pumps, and bioenergy fuels and systems. The capacity of glazed solar water heaters has increased by an average exceeding 15% over the last five years. By 2012, the global solar thermal capacity reached an estimated 282 GW_{th} for all collector types, with the capacity of glazed water collectors reaching an estimated 255 GW_{th}.

The majority of installed solar heat capacity is in China and Europe, which accounts for more than 90% of the world market and 81% of total capacity in 2011 [2].

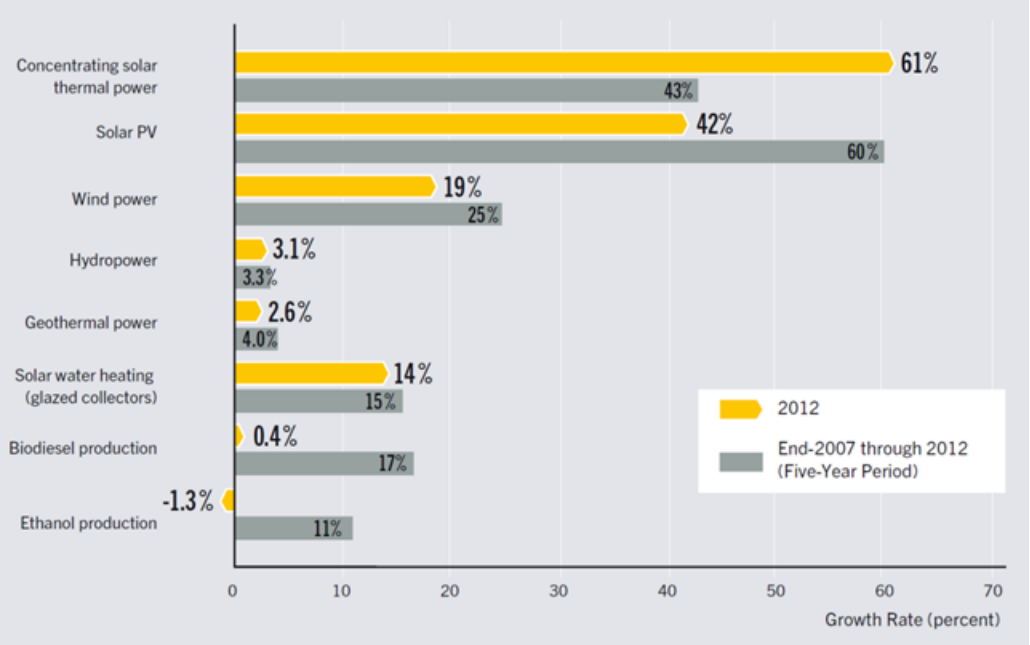

Fig. 1.1 Average annual growth rates of renewable energy capacity, for end 2007 to 2012 [2].

Australia has one of the highest levels of solar radiation per square meter of any continent in the world. The annual solar radiation falling on Australia is approximately 58 million petajoules (PJ), approximately 10,000 times Australia's annual energy consumption [3]. In Australia, solar energy is mainly used in small direct-use applications such as water heating, and in 2011-2012 it accounted for 0.2% of total energy consumption. Solar energy use in Australia is projected to increase by 5.9 per cent per year to 24 PJ in 2029-30 [3]. Although solar energy is a clean, abundant and easily accessible form of renewable energy, its intermittent and dynamic nature hinders its wide application. Therefore, an efficient thermal energy storage (TES) system is highly valuable for many solar applications to provide a reservoir of energy to adjust the mismatch between energy supply and demand, so that energy needs can be met at all times. There are three main methods used to store thermal energy: thermochemical, sensible heating, and latent heating storage [4]. These are shown in Fig. 2.

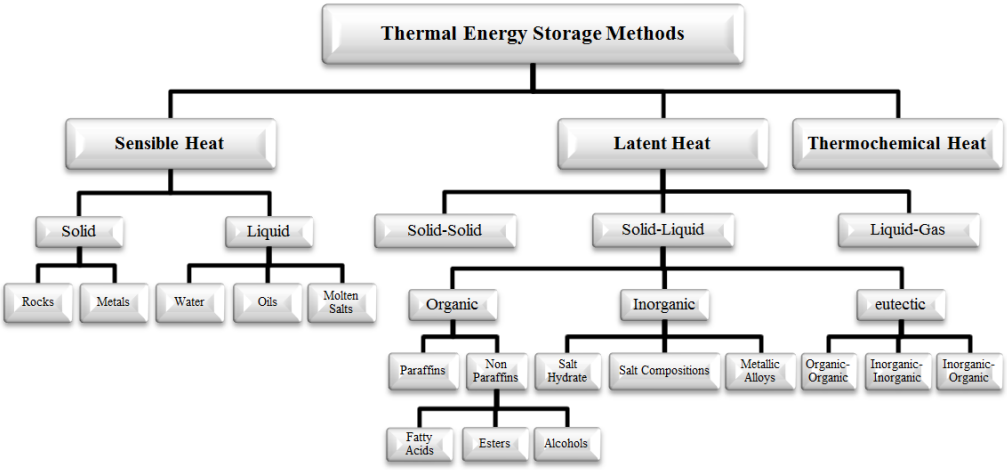

Fig. 1.2 Thermal energy storage methods (adapted from literature [4]).

Thermochemical storage relies on the energy absorbed and released in breaking and reforming molecular bonds in a reversible chemical reaction. In this case, the heat stored depends on the amount of storage material, the endothermic and exothermic heat of reaction, and the extent of the conversion [5].

In sensible heat thermal energy storage (SHTES), thermal energy is stored by raising the temperature of a solid or liquid. Sensible heat storage systems make use of a fluid's heat capacity, and the change in temperature of the working medium during the process of thermal charging and discharging. Water is often used as a storage medium in most low-temperature applications, and the temperature of the water increases as energy is stored. The amount of heat stored depends on the specific heat of the medium, the density, the temperature change, and the amount of storage material [6].

Latent heat thermal energy storage (LHTES) is based on the heat absorption or release when a storage material undergoes a phase change from solid to liquid, from liquid to gas, or vice versa. Latent heat storage is more attractive than sensible heat storage because of its high storage density and small temperature difference during charging or discharging. A comparison between latent and sensible heat storage shows that LHTES offers storage densities that are typically 5 to 10 times higher and require approximately half the volume of the SHTES. Latent

heat storage can be accomplished through solid-liquid, liquid-gas, solid-gas, and solid-solid phase transformations [4].

In solid–solid phase changes, heat is stored as the material is transformed from one crystalline state to another. These changes generally have smaller latent heat and volume changes than solid–liquid changes. Solid–gas and liquid–gas transitions have higher latent heat of phase change, but the associated volume change can lead to containment problems. Solid–liquid provide relatively less latent heat than liquid–gas transformations. However, these transformations involve only a small change (of the order of 10% or less) in volume. In addition, phase changes can take place at constant temperature and for many materials; the melting and freezing process can be repeated for an unlimited number of cycles with no change to the physical or chemical properties of the material. For these reasons, solid-liquid phase change processes have proved to be the most economically attractive for use in thermal energy storage systems [7].

1.2. Research objectives

The main research objective in this research aims to investigate heat transfer mechanism in a shell-and-tube latent heat thermal energy storage. It includes the following detailed research objectives:

- Review the different configuration of LHTES systems using phase change material (PCM) and the current cutting edge technologies.
- Develop a heat transfer model for the phase change problem for melting and solidification.
- Theoretically investigate the heat transfer mechanism in PCMs.
- Theoretically investigate the effect of LHTES orientation on the heat transfer mechanism and system performance.

- ❖ Experimentally investigate and visualize the mechanism of heat transfer in PCMs during the phase change.
- ❖ Develop the model to track the PCM solid-liquid interface during the charging and discharging processes.
- ❖ Experimentally investigate the effect of geometrical parameters in design of LHTES systems.
- ❖ Investigate the effect of operation parameters on the performance of storage systems.

1.2. Research outline

Latent heat thermal energy storage has gained significant research attention due to its high storage density with small temperature change during melting/solidification processes. Then, Chapter **2** started with a comprehensive review on LHTES in the solar domestic hot water (SDHW) application. Firstly, the SDHW systems were classified based on the working fluids and the thermal energy storage methods. Then, the review focused on the SDHW system containing a latent heat energy storage medium and the aspects that have not been well addressed in the literature. These aspects include the effect of PCM position on system performances, performance comparisons of SDHW systems with and without PCM units, the long term performance of SDHW systems and current research involving the latent heat storage units. *The findings of chapter 2 were published in the journal of Renewable and Sustainable Energy Reviews 49, PP. 517-533, ELSEVIER, 2015.*

It was concluded from Chapter 2 that the latent heat storage unit is the key component in the solar domestic hot water system using phase change materials. However, the low thermal conductivity of PCMs, has hindered the commercialization and widespread applications [8,9]. Two main research areas include the configuration of the latent heat storage unit to improve heat transfer inside the unit, and the heat transfer mechanism in the PCM, as this aims to improve understanding of the thermal behaviour inside a PCM unit. Then, the next two chapters

of this thesis were dedicated to the investigation of the heat transfer mechanism during melting (for the charging) and solidification (for the discharging) processes. **Chapter 3** focused on developing a proper heat transfer model to simulate the thermal behaviour and heat transfer characteristics of LHTES systems. A pure thermal conduction model and a combined conduction-convection heat transfer model were developed to study the thermal behaviour and heat transfer characteristics of a vertical cylindrical shell and tube LHTES unit. Results from a pure conduction model and combined conduction-convection model were compared and validated with available experimental data. The important parameters in the phase transition including transition times, temperature ranges, and propagation of the solid liquid interface were investigated. It is concluded that the combined convection and conduction model can better describe the energy transfer in PCMs. *The findings of chapter 3 were published in the journal of Applied Thermal Engineering 87, PP. 698-706, ELSEVIER, 2015.*

Chapter 4 was a continuation of chapter 3, where the combined conduction-convection heat transfer model was used to study the effect of the LHTES orientation on the heat transfer mechanism during charging and discharging processes. The thermal behavior and heat transfer characteristics in the horizontal and vertical shell-and-tube LHTES systems were investigated and compared using a combined conduction and convection model. The predicted results were validated using the published experimental data, and the effect of key parameters including the HTF inlet temperature and flow rate on the storage system performance in both horizontal and vertical heat storage units is examined during melting and solidification of the PCM. The results show that during the charging process, the convective heat transfer is the dominant heat transfer mechanism in both horizontal and vertical systems. In fact, for the horizontal orientation, natural convection has a strong effect on melting of the upper part of the solid PCM and is less significant during melting of the lower half of the solid PCM. However, in the vertical orientation, convective heat transfer is the same active during the entire charging

process. In the discharging process, the thermal behavior does not show any difference between horizontal and vertical systems. *The findings of chapter 4 were published in the journal of Applied Thermal Engineering 93, PP. 348-358, ELSEVIER, 2016.*

Despite significant research on the heat transfer mechanism, there is still a lack of experimental work to understand the physics of heat transfer in PCM in the vertical shell-and-tube LHTES system. As discussed in Chapter 4, most experimental work focused on heat transfer in the horizontal shell-and-tube LHTES system which was significantly different from that in the vertical shell-and-tube LHTES system. Thus, **Chapter 5** focuses on physics of heat transfer in PCM in the vertical cylindrical shell-and-tube LHTES system during charging processes. Visualized experiments are performed to observe the liquid-solid PCM interface evolutions during melting. A temporal variation of the experimental temperature is used to demonstrate the effect of convection on heat transfer during melting of the PCM. Then experimental images incorporating the theoretical velocity field inside PCM are further investigated to explain the heat transfer phenomena in the vertical LHTES system. Based on the research finding, a vertical conical shell-and-tube LHTES system is proposed and investigated. The performance of the vertical conical shell-and-tube LHTES system is further compared with the cylindrical vertical LHTES system. *The findings of chapter 5 were submitted to the journal of Renewable Energy.*

Chapter 6 was a continuation of chapter 5, where the physics of the heat transfer mechanism in vertical cylindrical and conical shell-and-tube LHTES systems during a discharging process were investigated by visualized experimental studies and simulation analyses. The comparative results show that both systems have similar trend and it takes almost the same time to complete the discharging process. *The findings of chapter 6 were accepted for publication in the 8th International conference on Applied Energy, Beijing, China, October 8-11, 2016.*

Chapter 7 studied the effect of the geometrical parameter on vertical cylindrical shell and tube LHTES systems. Four different shell to tube diameter ratios were considered with PCM is in the shell side and HTF passing through the tube side. The PCM temperature distributions are measured and compared experimentally. The results show that complete charging and discharging is highly dependent on the ratio of outer to the inside diameter. For the design purpose, this parameter is highly dependent on the hours of sunlight as well as the output temperature of the solar collector. *The findings of chapter 7 were submitted for review and publication to the International Journal of Heat and Mass Transfer.*

Chapter 8 summarizes the major outcomes of this research and the possibilities for future research on LHTES systems using PCM.

It is worthwhile to mention that Chapters 2 to 7 are self-contained in having their own introduction, methodology, results and discussions. In fact, the nature of the study makes the presentation of the outcomes more appropriate in a modular fashion without interruption of the flow of the thesis.

1.3. References

[1] Thirugnanasambandam M, Iniyan S, Goic R. A review of solar thermal technologies. Renewable and Sustainable Energy Reviews. 2010;14:312-22.

[2] Renewables 2013 Global Status Report, Renewable Energy Policy Network for the 21st Century, REN 21.

[3] L. carson, Australian Energy Resource Assessment, Second Edition Report, Geoscience Australia, Canbera, 2014 (http://www.industry.gov.au/Office-of-the-Chief-Economist/Publications/Documents/GA21797.pdf).

[4] Demirbas MF. Thermal energy storage and phase change materials: An overview. Energy Sources, Part B: Economics, Planning, and Policy. 2006;1:85-95.

[5] Sharma SD, Kitano H, Sagara K. Phase change materials for low temperature solar thermal applications. Res Rep Fac Eng Mie Univ. 2004;29:31-64.

[6] Sharma S, Sagara K. Latent heat storage materials and systems: a review. International Journal of Green Energy. 2005;2:1-56.

[7] Regin AF, Solanki S, Saini J. Heat transfer characteristics of thermal energy storage system using PCM capsules: a review. Renewable and Sustainable Energy Reviews. 2008;12:2438-58.

[8] S. Jegadheeswaran and S. D. Pohekar, Performance enhancement in latent heat thermal storage system: A review, Renewable and Sustainable Energy Reviews, 2009, 13 (9), 2225-2244.

[9] M. Kenisarin and K. mahkamov, Solar energy storage using phase change materials, Renewable and Sustainable Energy Reviews, 2007, 11 (9), 1913-1965.

[10] Liu S, Li Y, Zhang Y. Mathematical solutions and numerical models employed for the investigations of PCMs′ phase transformations. Renewable and Sustainable energy reviews. 2014;33:659-74.

Chapter 2: A review of thermal energy storage in solar domestic hot water systems

2.1. Chapter summary

This chapter reviews thermal energy storage (TES) technologies for solar water heating systems with a particular focus on techniques for integrating PCM into these systems. These techniques include integrated PCM storage vessels, integrated PCM solar collectors, and integrated a PCM unit inside the solar hot water circuit. It is found that the integrated PCM storage vessel is the most widely applied technique in SDHW systems using PCMs. Furthermore, this review presents recent findings on the performance comparison between conventional SDHW systems and SDHW systems containing PCMs and the long term performance of SDHW systems using PCMs are discussed. This review highlights the need for further research in several areas including performance evaluation of different integration techniques, numerical model for system optimization, and long-term performance of solar domestic hot water systems featuring PCMs.

This research contained within this chapter has been published as: Saeid Seddegh, Xiaolin Wang, Alan D. Henderson, Ziwen Xing. "Solar domestic hot water systems using latent heat energy storage medium: A review". Renewable and Sustainable Energy Reviews 49, PP. 517-533, ELSEVIER, 2015.

2.2. Background

The development of solar domestic hot water (SDHW) systems began in the 1760s in Geneva, Switzerland, when Horace-Bénédict de Saussure, a Swiss naturalist, observed that water fluid and surroundings become hotter when the sun's rays passed through a glass-covered structure. He put this hypothesis under scientific scrutiny in 1767 when he built an insulated box with its bottom painted black to absorb as much solar energy as possible.

In 1891, Clarence Kemp, an American plumbing and heating manufacturer, placed a black-painted storage vessel inside a glass-covered box of similar design to de Saussure's. This was the first commercial solar water heater called "The Climax" which produced hot water (38.8 °C) on sunny days. As California has a good supply of solar energy, by the late 19th century, about a third of the homes in Pasadena California had water heated from the sun. The Kemp's concept was further implemented as an integral collector storage solar water heater [1].

From the early 1900s, several researchers focused their attention on improving the design of SDHW systems to make them more durable and efficient. In 1909, William J. Bailey found a way of separating solar heating of water from its storage vessel. His solar collector consisted of water pipes housed inside a glass-covered box which was connected to an insulated remote storage tank located above the collector. As the solar energy heated the water, it became lighter, allowing cool water to enter from the bottom and hot water to rise into the storage tank. Bailey called his company the "Day and Night Solar Water Heater Company" and his products soon drove "The Climax" out of business and became the dominant solar water heater business in California, Arizona and Hawaii. Bailey's system was the first to use an insulated storage tank that relied upon the thermosyphon principle to circulate water between the solar collector and storage tank [1].

Since 1980, the use of SDHW systems has increased at a rate of about 30% annually [2]. The technology is now well-established. The achievement of this status is the outcome of a century of development. Solar water heaters are gaining popularity since they are relatively inexpensive, simple to fabricate and easy to maintain. Although SDHW technology is well established, there are opportunities to further improve system performance and reliability. One of the most important components in residential SDHW systems is thermal energy storage. Peak solar radiation occurs near noon, but peak heating demand is typically late evening or early morning when solar radiation is not available. The time mismatch between energy availability and energy demand with SDHW systems may be solved using energy storage.

Most energy storage systems typically employ water for thermal energy storage; however, water storage takes up considerable space and weight due to the large volume required under certain conditions. Systems that utilise the sensible energy of water require a high storage temperature and hence have large energy losses to the environment. Latent heat energy storage systems can offer valuable solutions to issues such as space, weight and a high storage temperature [3-10]. Storage systems using phase change materials (PCMs) use a material's latent heat of fusion [11-22], which represents a much larger energy exchange than from sensible heating of a single phase. Therefore, the space of the storage system is smaller in comparison to the sensible energy storage system. Since the energy release is due to the phase change of the material, the difference between the storage temperature and user required temperature can be small and reduce the energy loss to the environment.

Some researchers have reviewed SDHW systems [1-4]. Shukla et al. [1] summarized the investigation and analysis of a thermal energy storage with and without PCM for use in solar water heater. This study is classified according to the type of collector and storage. Sharma and Chen [2] reviewed energy storage using PCMs for solar hot water heating systems and attempted to summarize the investigation of these systems. Islam et al. [3] recently presented

an overview of various types of solar assisted water heating systems and their market potential. Nkwetta and Haghighat [4] discussed the existing simulation, design tools and experimental studies relating to PCM usage in hot water vessels and central thermal storage. This paper builds on previous reviews to update the latest available literature pertaining to SDHW systems. It focuses on the SDHW system containing a latent heat energy storage medium and the aspects that have not been well addressed in the literature. These aspects include the effect of PCM position on system performances, performance comparisons of SDHW systems with and without PCM units, the long term performance of SDHW systems and current research involving the latent heat storage units.

2.3. Classification of solar domestic hot water systems

The general classification of SDHW system is based on the types of working fluid or thermal energy storage system as shown in Fig. 2.1.

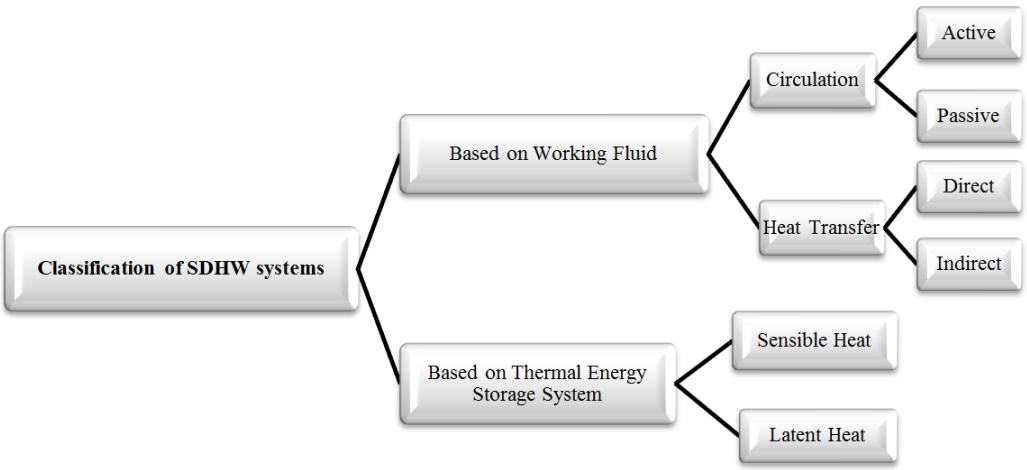

Fig. 2.1 Classification of SDHW systems.

Depending on the nature of heat transfer methods used for the working fluid, SDHW systems can be broadly classified into two types: direct systems and indirect systems. In direct systems, water is heated inside the collector in direct. In indirect systems, a heat transfer fluid is heated inside the collector which then passes through a condenser or heat exchanger to transfer its heat to the domestic or service water. Similarly, depending on the circulation of

working fluids, SDHW systems can be grouped into either passive or active circulation system. Passive circulation systems use thermosyphonic methods in which the density difference induces a circulation of the fluid. In contrast, active circulation methods use a pump to force a circulation of the working fluid. To provide protection against damage from freezing, recirculation and drain-down methods are used for direct solar water heating systems and the drain-back method is used for indirect water heating systems [23].

Furthermore, an efficient thermal energy storage (TES) system is highly valuable for many solar applications, especially SDHW systems provide a reservoir of energy to adjust the mismatch between energy supply and demand, so that energy needs can be met at all times. There are three methods to directly store thermal energy: thermochemical, sensible heat and latent heat storage. Latent heat thermal energy storage (LHTES) is based on the heat absorption or release when a storage material undergoes a phase change from solid to liquid or from liquid to gas or vice versa. It has gained research attention because of its high storage density with small temperature change during melting/solidification processes.

2.4. Solar domestic hot water system using PCM

2.4.1. Selection of PCMs

A suitable PCM with its melting point in the desired temperature range is one of the most important parameters in the design of a SDHW system using latent heat energy storage. An early study of PCMs was made by Telkes and Raymond [24] in the 1940s, but it did not receive much attention until the energy crisis in the late 1970s and early 1980s. Since then, it was extensively researched for use in different applications involving solar heating systems [25, 26]. A large range of PCMs is currently available that have melting temperatures ranging from -5 to 190 °C. These may be grouped into three categories: organic; inorganic; and eutectic, which is a mixture of organic and inorganic materials. Phase change materials intended for use

in the design of thermal storage systems should possess suitable thermodynamic, kinetic and chemical properties as listed in Table 2.1 [8]. Comprehensive details on various PCMs and their applications are available in the literature [5-22].

Table. 2.1. Desirable properties of PCMs.

Thermodynamic properties
• Melting temperature in the desired operating temperature range
• High latent heat of fusion per unit volume so that the required volume of the container to store a given amount of energy is less
• High specific heat to provide for additional significant sensible heat storage
• High thermal conductivity of both solid and liquid phases to assist the charging and discharging of energy to the storage system
• Small volume changes on phase transformation and small vapour pressure at operating temperatures to reduce the containment problem
• Congruent melting of the PCM for a constant storage capacity of the material with each freezing/melting cycle
• High density
• Favourable phase equilibrium
Kinetic properties
• High nucleation rate to avoid supercooling of the liquid phase
• High rate of crystal growth, so that the system can achieve rapid heat recovery from the storage system
Chemical properties
• Long term chemical stability
• Complete reversible freeze/melt cycle
• Compatibility with materials of construction
• No degradation after a large number of freeze/melt cycle
• Non-corrosiveness to the construction materials
• Non- toxic, non-flammable and non-explosive materials for safety
Economic properties
• Abundance
• Low cost
• Large scale availability

A common problem encountered with PCM usage is the lack of a comprehensive database of thermophysical properties, information about long term stability, corrosion, phase segregation, and sub-cooling. However, the most significant drawback limiting PCM widespread use in latent heat thermal storage systems is their low thermal conductivity, which typically ranges from 0.15 - 0.3 W/(m·K) for organic materials, and from 0.4 - 0.7 W/(m·K) for salt hydrates [15]. The effect of this low thermal conductivity is reflected during energy retrieval. Consequently, the rate of phase change process does not occur at levels suitable for large scale utilization [16].

Some fatty acids, including myristic, palmitic and stearic, with melting temperatures between 50-70 ºC have been recommended as suitable PCMs for SDHW systems [27-33]. Capric acid has been shown to have suitable properties. In addition, a eutectic mixture of palmitic (64.2 weight%) and stearic acid (35.8 weight%) with a melting point of 52.3 °C showed no sub-cooling during the solidification process. Furthermore, paraffins with a melting temperature of around 60 °C have been proven as a good storage material for SDHW systems due to their melting point, reliability, cost and non-corrosiveness [34-37].

The selection of the PCM is not an easy task and needs to carefully consider comprehensive thermal properties including melting point temperature, thermal conductivity, corrosiveness, reliability, cost and compatibility with the storage material. A case by case basis assessment is needed based on the design and installed location of the SDHW system.

2.4.2. Different methods of utilizing PCMs in SDHW systems

Utilization of the PCM in the SDHW system using latent heat energy storage medium can be split into three main methods: integrated PCM storage vessel, integrated PCM solar collector storage and separate PCM units in the solar hot water loop. The detailed research works in these three techniques are detailed in the following sessions.

2.4.2.1 Integrated PCM storage vessels

The integrated PCM storage vessel introduces latent heat storage into SDHW systems by placing PCMs inside the water storage vessel. This is the most common method and has been widely studied theoretically and experimentally [38-51]. Some researchers focused on the application of different PCMs [42-46] while others have focused on the structure of the storage unit [47-51].

Nallusamy et al. [42] experimentally investigated the thermal behaviour of a latent heat thermal energy storage unit that contained paraffin in the form of spherical capsules. These

capsules were packed into an insulated cylindrical storage tank and water was used as the heat transfer fluid. Tarhan et al. [43] investigated the effect of two different configured PCM storage units (myristic acid and lauric acid) on the temperature distributions in water tanks. A trapezoidal hot water system without the PCM storage unit was used as a control reference. It was concluded that the lauric acid storage could be used to stabilize the water temperature during the daytime, while the myristic acid storage unit could be used as a thermal barrier against heat loss during the night. This was because of its relatively high melting temperature and low heat conduction coefficient in its solid phase. The experimental results indicated that the thermal characteristics of the PCM and the configuration of the PCM storage unit could result in advantageous control of the water temperature rise and drop during both day and night. EL Qarnia [44] conducted a series of numerical simulations on a solar latent heat storage unit using three kinds of PCM (n-octadecane, paraffin wax and stearic acid) to find the optimum design for a given climatic conditions of Marrakech city, Morocco: solar radiation and ambient temperature. The optimization of the solar latent heat storage unit involves determination of the PCM mass, tube numbers and the water flow rate inside the solar collector. The study showed that the system containing stearic acid delivered an acceptable temperature range at the outlet. Reddy et al. [45] investigated different PCMs for SDHW applications by varying HTF flow rates (2, 4, and 6 litres/min) for spherical capsules of diameters of 38, 58, and 68 mm. The results showed that the flow rates of HTF did not have a very significant influence on the charging time and the quantity of thermal energy recovered. The charging time and the average temperature of hot water discharged was almost the same for all three capsule diameters. However, the quantity of hot water discharged was slightly greater for the 38 mm capsule diameter compared to the 68 mm diameter capsule. There was not much difference in performance between paraffin and stearic acid for the charging and discharging processes,

although the paraffin's performance was 5–7% higher due to differing latent heat and thermal conductivity.

Hassan and Beliveau [46] presented a new design that consisted of an integrated flat-plate collector and a PCM storage vessel. Automatic control of the solar thermal system was accomplished by modulating the flow direction in the fluid circuits. Fig. 2.2 shows a schematic drawing of the completed solar hot water system. Thermal energy is stored in the PCM (Rubithern RT 54) which is installed in a well-insulated cylindrical vessel as shown in Fig. 2.2 (b). The storage vessel contains a parallel array of copper pipes. These pipes were connected to the solar collector and used to transfer the hot fluid from the solar collector to the PCM. Section A is enlarged in Fig. 2.2 (c) to show the copper pipe serving the two PCM sections. The system consists of four fluid paths to suit different conditions. If the fluid outlet temperature of the solar collector ranges between 40°C and 60°C, Path A becomes operational and hot fluid is circulated between the solar collector and the building thermal zones, where hot water is used to satisfy the thermal load and hot water requirements. Once the fluid outlet temperature increases above 60°C, the fluid path is switched to Path B and hot fluid from the solar collector is directed to the storage tank, thereby storing the excess thermal energy while ensuring the fluid's temperature leaving the storage tank remains around 50°C. The fluid is then transferred to the thermal zones. If there is no change in fluid temperature when passing through the solar collector, the flow within the solar collector will be shut-off. During that time, the required energy will be drawn from either the PCM storage tank (Path C), or the electrical supply if the stored energy is not sufficient (Path D).

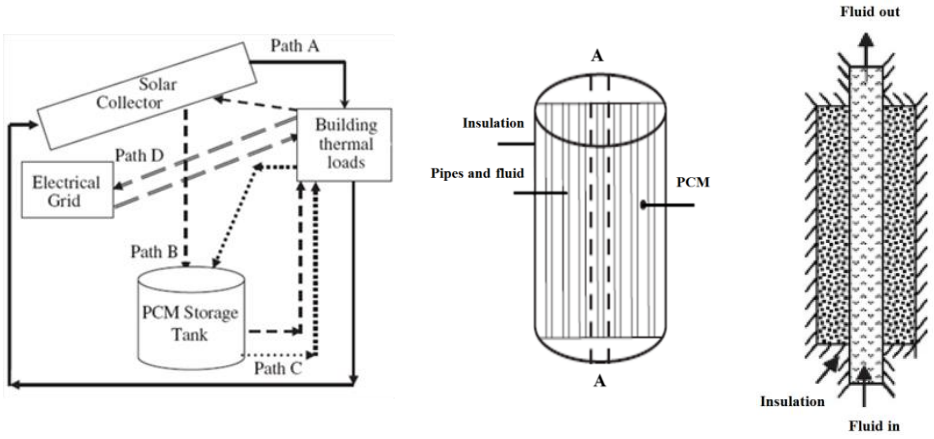

(a) **(b)** **(c)**

Figs. 2.2 (a) Energy supply paths, (b) PCM storage vessel and (c) Section "A" enlarged [48].

Some researchers [47-51] proposed adding a PCM module to the upper layer of a hot water storage vessel to enhance thermal stratification effects. This allows the top layer of the vessel to remain hot using stratification of the water. The addition of a PCM module increases the energy storage density, thus allowing reheating of the transition layer after partial unloading over a considerable time, as shown in Fig. 2.3 [47]. This approach combines the stratification effect and latent heat storage technology. It uses the low cost and high thermal capacity of water as the main storage medium and small amount of PCM as a secondary storage medium. This arrangement can significantly increase the storage capacity of the top layer and improve the overall system performance.

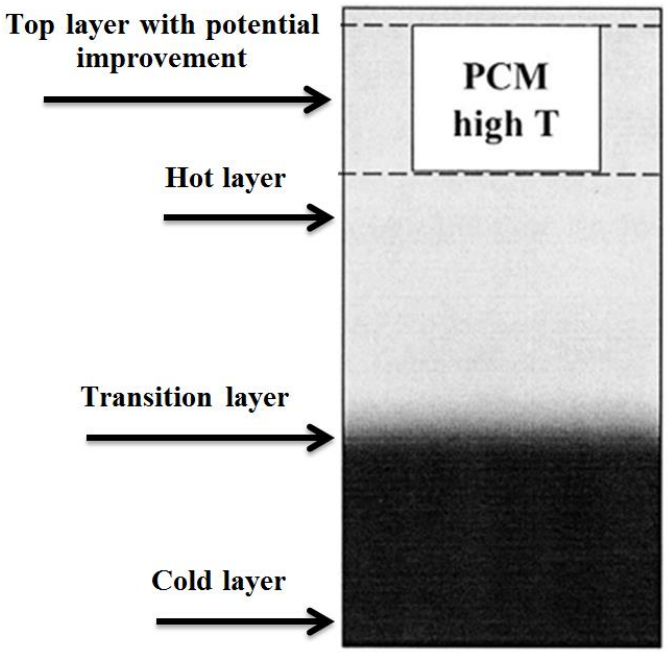

Fig. 2.3 Thermal energy storage with a PCM module at the top layer of the vessel [47].

Cabeza et al. [48, 49] further studied a similar type of system as shown in Fig. 2.4a. The PCM module geometry consisted of several cylinders located at the top of the storage vessel. Experiments with two, four and six PCM modules were performed using different PCMs (paraffins, sodium acetate trihydrate and fatty acids). The sodium acetate trihydrate showed superior performance and was chosen for a further set of studies [49]. The same authors [50] later studied ways to enhance heat transfer in the PCM storage vessel by mixing the graphite with sodium acetate (10:90 volume ratio). Mazman et al. [51] continued to investigate the effect of using PCM modules on the thermal performance of a SDHW system. The modules contained three kilograms of a paraffin and fatty acids mixture (80:20 mass mixtures). As shown in Fig. 2.4b, three cylindrical modules containing a mixture of paraffin and stearic acid (PS), paraffin and palmitic acid (PP), and stearic acid and myristic acid (SM) were introduced at the top of the storage vessel. During discharging, the average tank water temperature dropped below the PCM melting temperature range after approximately 6-12 h. The maximum drop in temperature occurred for the PS mixture, and the minimum for the SM mixture. During the charging

experiments, the PCM could increase the temperature of 14-36 L of water at the upper part of the SDHW vessel by 3-4 ^{o}C. The PS mixture gave the best results in the thermal performance enhancement of the SDHW vessel.

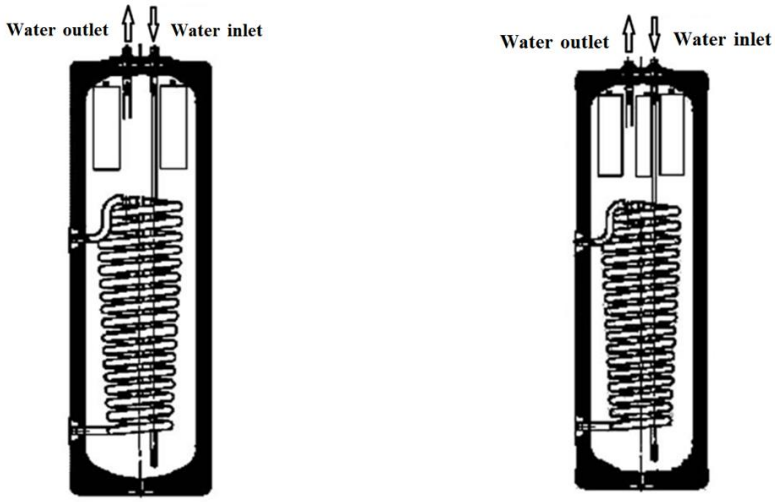

(a) **(b)**

Fig. 2.4 Solar domestic hot water vessel. a) Cabeza et al. [49] and b) Mazman et al. [51].

The above experimental work demonstrates that application of a PCM module into a SDHW storage vessel is a promising approach, as it helps to maintain the thermal stratification and increases the time the hot-water is made available. This improvement in reheating the upper portion of water in the storage vessel is critical since hot water is drawn from this location. Consequently, it is possible to reduce the size of the vessel while still providing the same delivery of hot water.

2.4.2.2 Integrated PCM solar collector storage

The integrated PCM solar collector storage concept is economically promising in low temperature solar water heating systems for domestic, agricultural and industrial applications. A system of this type combines the collection and storage of thermal energy into a single unit. This integrated solar collector storage water heater approach was developed from early systems

and comprised simply of a simple black vessel placed in the solar collector [52]. The thermal performance of the integrated PCM solar collector has been widely investigated [53-62].

Rabin et al. [55] developed an integrated PCM solar collector for a low-temperature SDHW system using salt hydrate eutectic mixture (48% $CaCl_2$, 4.5% KCl, 0.4% NaCl and 47.1% H_2O) where the PCM is held inside the collector and thermally discharged to cold water flowing through a heat exchanger, as shown in Fig. 2.5. Kumar [56] applied the same concept as shown in Fig. 2.6. A box type solar collector consisting of three finned heat exchangers and paraffin wax (melting temperature 54 ºC) was investigated and it was found that the studied system could provide hot water over a desirable temperature range.

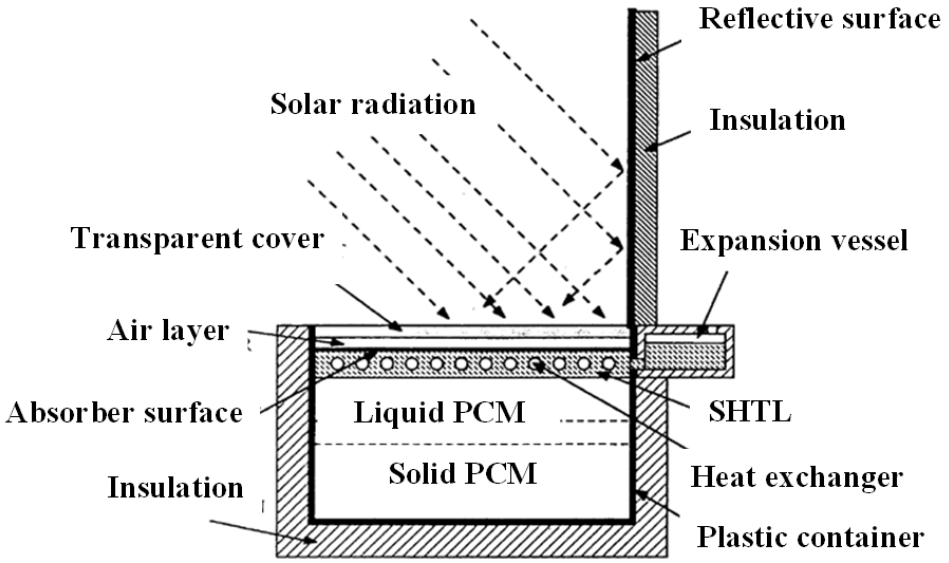

Fig. 2.5 Integrated PCM solar collector storage system designed by Rabin et al. [55].

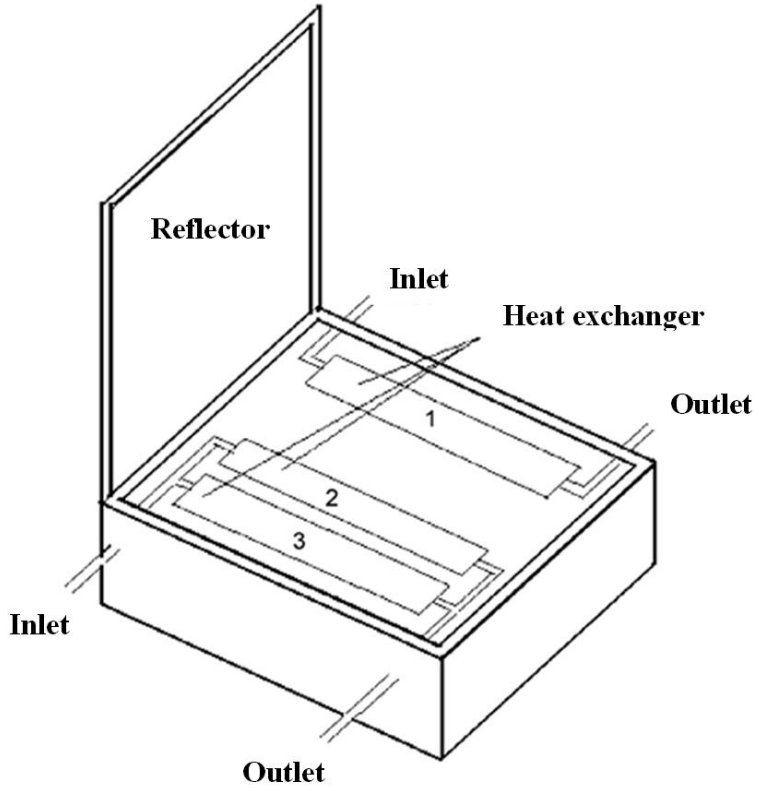

Fig. 2.6 Integrated PCM solar water heater designed by Kumar [56].

Kürklü et al. [57] developed a type of water-PCM solar collector consisting of two adjoining sections as shown in Fig. 2.7. One section is filled with water and the other with paraffin wax (melting temperature 45-50°C). The experimental results indicated that the water temperature could exceed 55 °C during a typical day of high solar radiation and remain over 30 °C during the whole night.

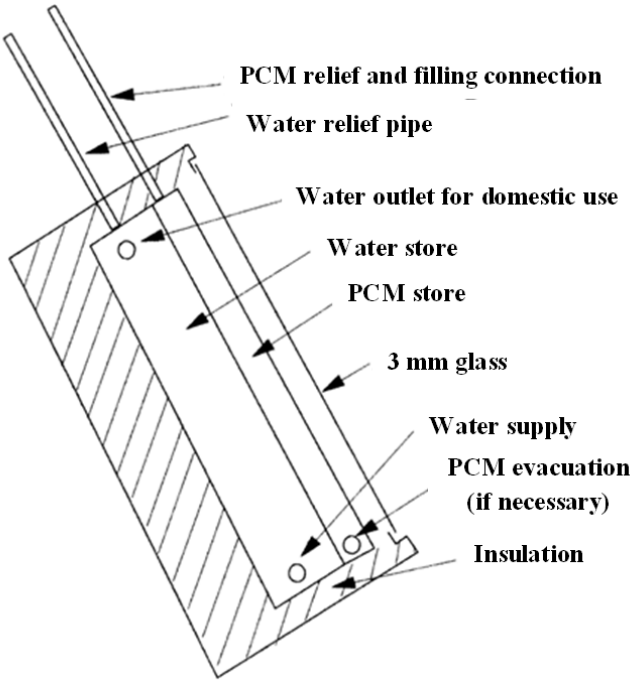

Fig. 2.7 Schematic view of the solar collector construction [57].

Mettawee and Assassa [58] proposed the integrated solar collector as shown in Fig. 2.8. In this system, the absorber plate unit performs the function of both absorbing solar energy and storing it in PCMs. In this case, solar energy was stored in paraffin wax and then discharged to cold water flowing in pipes located inside the PCM. The results showed that during the charging process, the average heat transfer coefficient increased sharply as the molten layer of paraffin increased in thickness with strengthening natural convection. The effect of mass flow rate on the heat recovery was also investigated in the study. It showed that both energy storage and release rate increased as the mass flow rate of the heat transfer fluid was increased. The same authors [59] also investigated a method of enhancing the thermal conductivity of paraffin wax by embedding aluminium powder inside it. The mass fraction of aluminium powder to PCM was examined and but no optimal mass fraction was found. With a mass fraction of 0.5, the experiment demonstrated that the useful heat gained increased substantially and reduced the charging time by 60%.

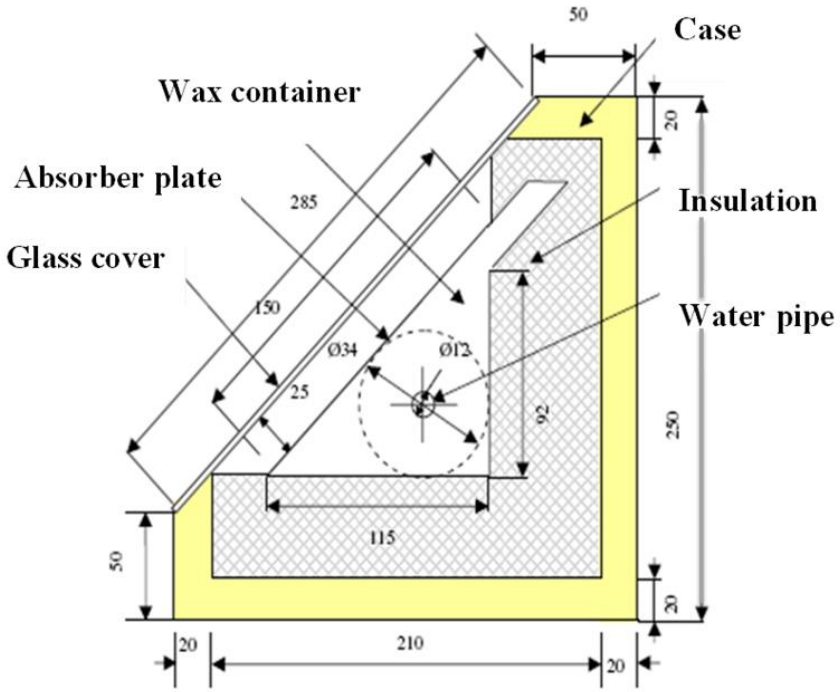

Fig. 2.8 Schematic of the experimental apparatus, cross section [58].

Khalifa et al. [60] investigated a PCM storage solar collector consisting of six 80 mm diameter copper pipes. The storage vessel featured a layer of paraffin wax as shown in Fig. 2.9. Outdoor experiments were carried out to demonstrate the potential of the solar energy storage system for water heating. The performance of the system was evaluated by calculating the various performance indexes such as heat loss coefficient (W/m^2 °C), plate temperature (°C), energy flux (W/m^2), and system efficiency of the collector. The plate temperature was found to increase up to a distance of 2.5 m from the inlet, after which an almost steady temperature was observed. The water continued to gain heat after sunset as the PCM continued to transfer energy to the water.

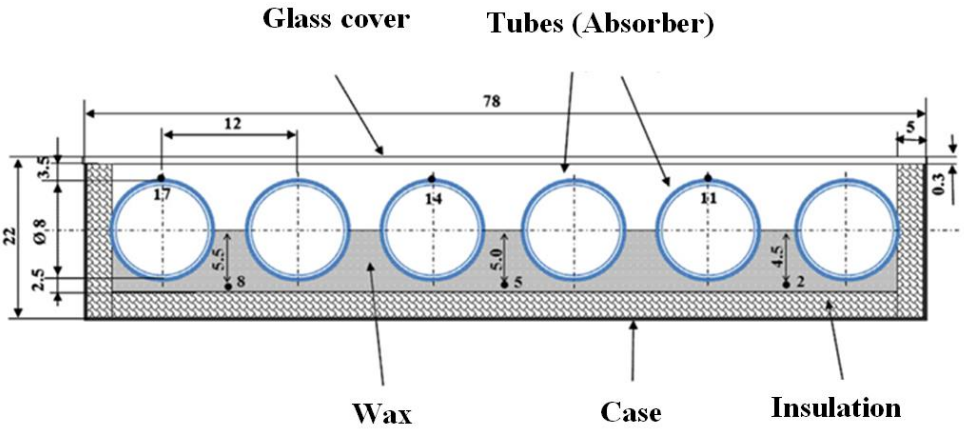

Fig. 2.9 Schematic diagram of the solar collector storage system [60].

Haillot et al. [61] proposed a new type of integrated solar collector storage system called ICS-CENG/PCM, which involved placing a composite made of compressed, expanded natural graphite (CENG) and phase change material (PCM) directly inside a flat plate solar collector. The composite ensured the sufficient capture of solar energy (absorption function) and storage of thermal energy (storage function). Several composites based on CENG and various storage materials (paraffin, stearic acid, sodium acetate trihydrate and pentaglycerin) were studied. A further performance study was performed numerically in another paper [62]. Figure 2.10 shows a schematic drawing of the proposed design. The solar collector including the composite plate was placed below the solar absorber and then surrounded by a polymer material to prevent any liquid PCM escaping (Fig. 2.10a). The system consisted of an absorber, glazing cover, insulation, heat transfer fluid and the composite plate with a surrounding polymer envelope as shown in Fig. 2.10b [62]. A numerical simulation of the whole SDHW system was performed and then validated with experimental data. The results showed that when a large amount of solar energy is available during summer months, adding a composite to the collector allowed excess heat to be stored. The release of this stored energy in the evening significantly increases the performance of the system, as the storage material was still at a significantly higher temperature after reheating of the storage vessel. During winter, when the available solar

energy is low, the system efficiency was reduced due to the presence of the storage composite. Despite this, the simulation results showed that the system efficiency was increased by adding a composite to the solar collector. The composite offered an alternative to replace the traditional copper-based solar absorber [62].

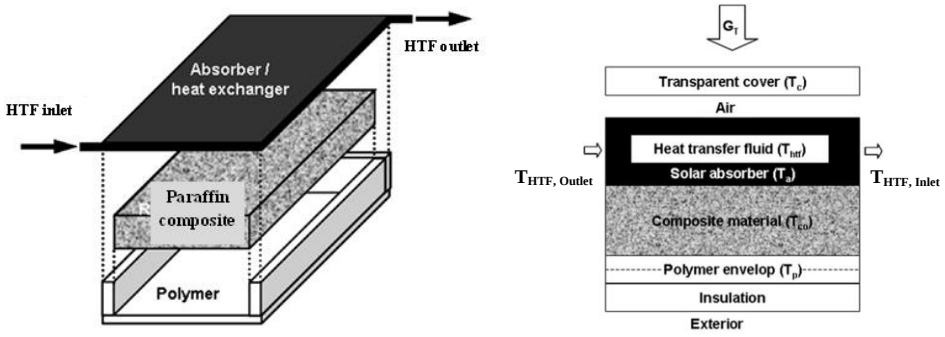

(a) **(b)**

Fig. 2.10 (a) ICS-CENG/PCM design, and (b) schematic view of the ICS-CENG/PCM [62].

In summary, using PCM in an integrated solar collector storage system presents several advantages when compared to conventional SDHW systems [62]:

- Reduction of collector maximum temperature. During stagnation, the absorber temperature reaches temperatures up to 170 °C. This can be responsible for severe reductions in solar collector life.
- Enhancement of useful efficiency. The solar collector operates predominantly in the melting temperature of the PCM, thus restricting significant heat losses when the solar collector is at its highest temperature. When excess solar energy is available, additional energy may be stored and released at a later time as required.
- The reduction in storage vessel volume. Part of the storage volume is inside the solar collector.

2.4.2.3 Integrated PCM solar heat transfer loop

Haillo et al. [62] highlighted two major problems inhibiting large improvements in system performance through the introduction of a PCM inside a solar collector: the heat losses from the collector, especially at night are too large to allow for efficient daily storage; and the storage medium imposes its temperature on the absorber thus lowering the efficiency under winter metrological conditions. Therefore, an alternative configuration that located a PCM storage unit inside the heat transfer loop was proposed. The results indicated an increase in the solar fraction from 58% to 66% (summer) and from 42% to 46% (winter) when compared to a system without PCM storage, as shown in Fig. 2.11.

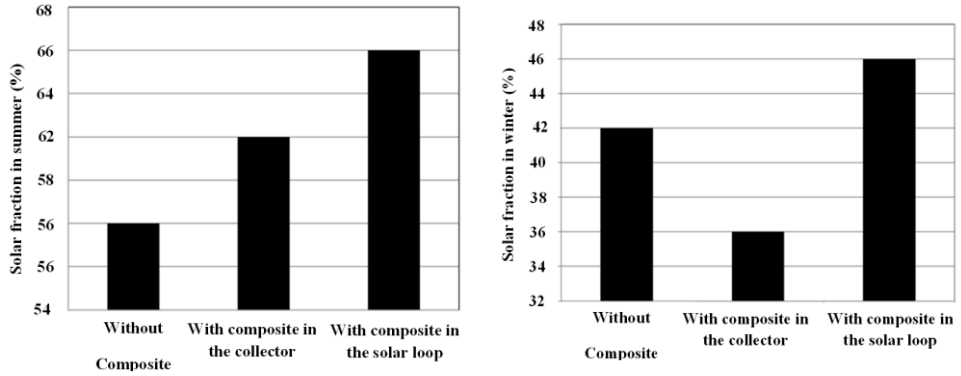

(a) **(b)**

Fig. 2.11 Solar fraction obtained in (a) summer and (b) winter [62].

Haillot et al. [63] further investigated the thermal behaviour of the system proposed in literature [62]. This system consisted of a SDHW vessel connected to flat plate collectors as shown in Fig. 2.12. A PCM storage unit was added between the SDHW vessel and the solar collector. The PCM was encapsulated in the cylinder and several tubes were embedded in the PCM. The heat transfer fluid was circulated inside the tubes where the heat transfer fluid could exchange heat with the PCM during the charging or discharging. A backup heating system was activated by the control system when the solar radiation was insufficient to meet hot water demands. Numerical simulations of the system were performed to investigate the effect of

several key parameters on the system performance, including PCM melting temperature and volume, volume of the water vessel, and meteorological conditions. For each set of parameters, solar fraction and the energy delivered by the electric auxiliary heater were numerically calculated. A genetic algorithm was then used to determine the system parameters needed to maximize the solar fraction and/or to minimize the energy delivered by the electric auxiliary heater. Optimal parameters of PCM volume and PCM melting point temperature were chosen as a function of meteorological conditions and storage vessel volume. The authors concluded that best system configurations are not unique, and are different for summer and winter. Therefore, further studies on this topic, including whole year simulations, various end user load profiles, and different system regulation are needed.

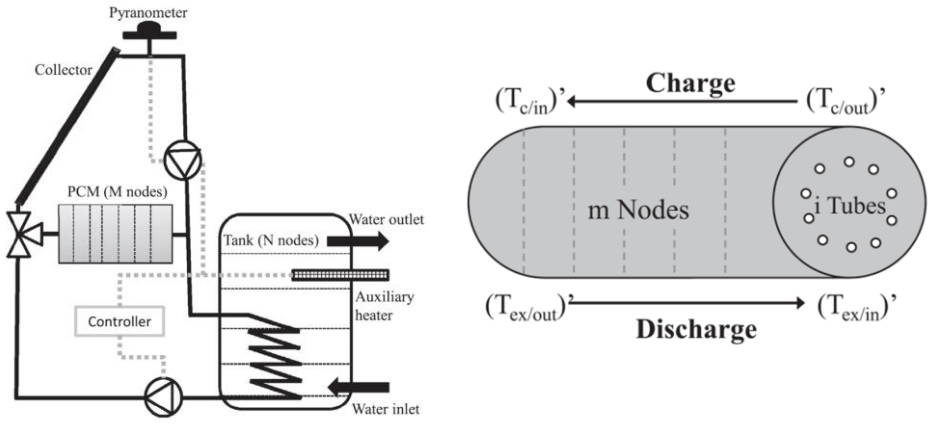

(a) **(b)**

Fig. 2.12 (a) Layout of the system and (b) the PCM unit [63].

2.5. Performance evaluation of solar domestic hot water systems

2.5.1. Performance comparison of SDHW systems with PCM

Chaurasia [64] presented a comparative study of solar energy storage systems using the latent heat storage and sensible heat storage techniques. Two identical storage units were studied: one containing 17.5 kg paraffin wax (with melting temperature of 54 ºC) packed into a heat exchanger made of the aluminium tubes, and the other simply containing water. Both

units were separately charged during the day by flat plate solar collectors of equal areas. The study revealed that the latent heat storage system comparable yields more hot water on the next day morning when compared with the sensible heat based storage system.

Kaygusuz [65] conducted an experimental and theoretical study to determine the performance of phase change, energy storage materials for solar water-heating systems. A storage vessel filled with 1500 kg of encapsulated PCM ($CaCl_2.6H_2O$ or $Na_2SO_4.10H_2O$) inside tubes was investigated over the entire heating season. Variants of the solar-supplied fraction of the load with storage mass and collector area for water-based systems with sensible and latent heat storage were examined. It was concluded that the PCM storage was preferable than the water and rock storage.

Canbazoglu et al. [66] calculated the total heat (sensible and latent) to compare the storage capacity of SDHW systems with PCMs to the conventional systems as shown in Fig. 2.13. Polyethylene bottles were filled with hydrated salts and set into the vessel in three rows. The bottles did not let the water flow in a horizontal direction due to their close arrangement, and it instead allowed flows through the vertical cavities between the bottles. The results indicated that the water temperature has a constant value of 46 ºC during the night until sunrise, as hot water was not drawn from the vessel. The temperature difference between the midpoint of the heat storage tank and the outlet of the collector was approximately 6 ºC greater than that in the system without PCM. Heat storage performances of the same solar water-heating system combined with the other salt hydrates-PCMs such as the zinc nitrate hexahydrate, disodium hydrogen phosphate dodecahydrate, calcium chloride hexahydrate and sodium sulphate decahydrate (Glauber's salt) were examined theoretically by using meteorological data and thermophysical properties of PCMs with some assumptions. It was concluded that the total energy stored in the SDHW system containing PCM was about 2.59-3.45 times of that in the conventional solar water-heating system.

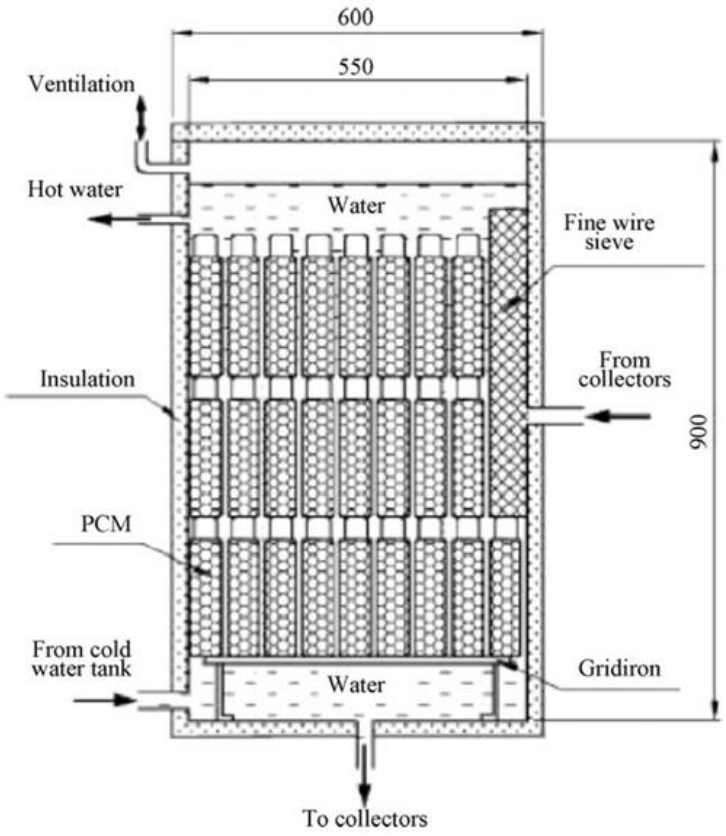

Fig. 2.13 Cross-section of the storage unit designed by Canbazoglu et al. [66].

Figure 2.14 shows a system using paraffin wax in small cylindrical aluminium containers which were placed in a commercially available cylindrical hot water storage vessel [67]. The advantage of the PCM energy storage was demonstrated under controlled energy input experiments with the aid of an electrical heater on an isolated storage tank. It was found that including the PCM could result in a 13-14 °C temperature advantage in stored hot water temperature over extended periods of time. The storage performance was also investigated when connected to flat plate collectors inside a closed-loop system with conventional natural circulation. Over a period of 24 hours, the stored water temperature remained at least 30 °C higher than the ambient temperature. The effect of limited periods of forced circulation on the performance of the system in general, and for reducing the time lag between the peak radiation and peak water temperature, were found to be minimal. It was also found that day-time consumption of moderate amounts of hot water withdrawn from the storage tank on sufficiently

spaced time intervals does not adversely affect the final water temperature or the overall performance of the system. Furthermore, in the case of extreme consumption during evening hours, the existence of PCM can partially recover the temperature of water, thus extending the effective operational time of the SDHW system.

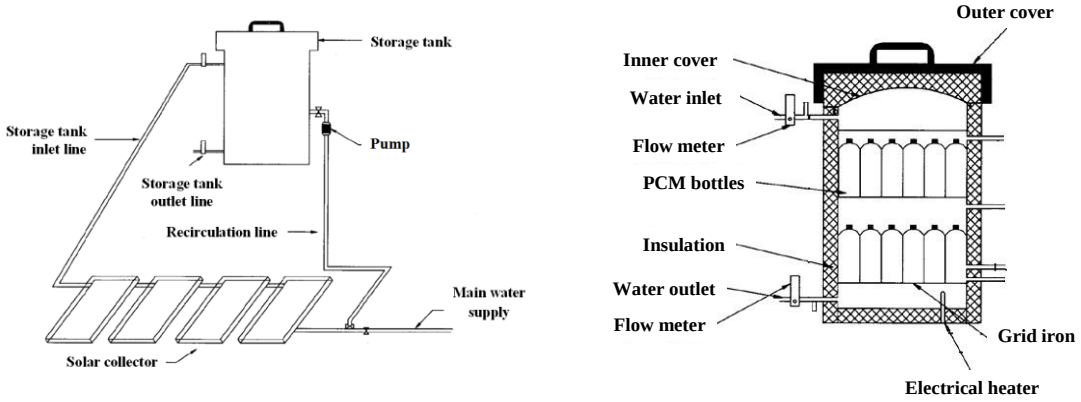

(a) **(b)**

Fig. 2.14 (a) Schematic of experimental set up, and (b) Cross section view of the storage tank with PCM [67].

More recently, Nkwetta et al. [68] numerically investigated and compared the SDHW system with and without PCMs. It was concluded that adding a PCM module (Sodium Acetate with 10% graphite) into a hot water tank substantially increases the amount of thermal storage. This stored energy was found to be directly proportional to the amount of PCM. Furthermore, the integration of PCM in the hot water tank improves the storage capacity with the potential to save energy and to shift and/or smooth peak power demand.

2.5.2. Long term performance of SDHW systems with PCM elements

A significant criterion for evaluating the performance of SDHW systems with PCM is to evaluate whether the presence of the PCM will lead to an overall annual increase in the solar fraction, i.e., a better use of solar energy collected and a reduction in the required amount of auxiliary energy supplied. This requires examining the long term performance of the SDHW

with PCM and the overall contribution, including PCM made to the energy delivered to the end-user under realistic operating conditions. Ibanez et al. [69] simulated a single family SDHW system in Lleida, Spain. The solar fraction was shown to increase by up to 8% due to the addition of PCM in the storage vessel. However, such results largely depend on many factors, including site conditions, load profile, type and amount of PCM.

Talmatsky and Kribus [70] numerically compared the annual performance of a storage vessel containing PCM to a standard vessel without PCM under identical conditions. A mathematical model was constructed to evaluate the performance of the storage systems. The model included a storage vessel with and without PCM, pump, collector, controller and auxiliary heater as shown in Fig. 2.15. Annual simulations were carried out for different sites (Tel Aviv, Israel represents warm climate and good insolation and Munich, Germany representing cold climate and low annual insolation), various user load profiles (step wise and statistical), different types of PCMs (composite sodium acetate trihydrate mixed with graphite particles (SAT-G) and RT42 paraffin in a graphite matrix (RT42-G)) and different PCM volume fraction (6%- 25%). Realistic environmental conditions and typical end-user requirements were imposed. The results showed that the application of PCMs in the storage vessel did not yield a significant benefit in energy provided to the end-user (less than 1% in yearly values).

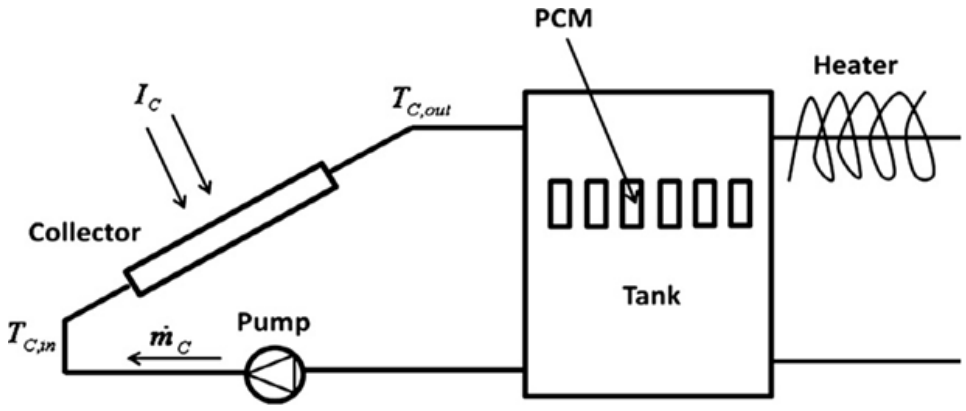

Fig. 2.15 Layout of the solar domestic hot water system with PCM [70].

Kousksou et al. [71] later analysed the conditions under which lower performance resulting from PCMs was found. The mathematical model reported in [70] was used and the simulation was performed over a complete year. The simulation results were consistent with the findings reported by Talmatsky and Kribus [70] and suggested that using PCM in SDHW systems might not offer substantial benefit.

2.6. Latent heat storage unit

Latent heat thermal energy storage (LHTES) unit is the key component in the solar domestic hot water system using phase change materials. The latent heat storage unit is found to be able to save up to 90% mass and space to store the same amount of thermal energy in comparison to the sensible thermal energy storage in materials such as concrete and water [72]. It has gained significant research attention due to its high storage density with small temperature change during melting/solidification processes. However, the low thermal conductivity of PCMs, typically between 0.15 and 0.3 W/mK for organic materials and between 0.4 and 0.7 W/m·K for salt hydrates, has hindered the commercialization and widespread applications.

In order to improve the energy storage and thermal performance of solar hot water systems, many researchers focused on improving the heat transfer inside the latent heat storage unit. Two main areas that researchers have focused on include the configuration of the latent heat storage unit to improve heat transfer inside the unit, and the heat transfer mechanism in the PCM, as this aims to improve understanding of the thermal behaviour inside a PCM unit.

2.6.1. Configuration of latent heat storage units

One solution to the problem of low thermal conductivity in PCMs is to improve the heat transfer rate between the heat exchang surface and the PCM. This can be achieved using different heat exchanger configurations with enhancement techniques to increase heat transfer

surface area. Many studies have been conducted across a range of heat exchanger configurations: plate type heat exchangers containing PCM, small diameter tubes, double pipe, tube in tube, compact, spiral, helical coil, shell and tube heat exchanger [73-75]. Recently, triplex tube heat exchanger (TTHX) with PCM in centre tube has been proposed to provide a larger heat transfer area and improve the heat transfer rate inside the LHTES [76-78]. Agyenim et al. [17] reviewed the materials, heat transfer and phase change problem formulation for latent heat thermal energy storage units and concluded that the most intensely studied LHS unit was the shell-and-tube storage, which accounted for around 70% of publications.

Also, heat transfer enhancement techniques such as using surface extension, encapsulated PCMs, multiple PCMs, and the use of thermal conductivity enhancement have been applied in the latent heat storage system as shown in Fig. 2.16 [17]. The majority of such techniques was based on concepts utilising fins embedded in the phase change material, as they are relatively simple, easy to fabricate and have low construction cost. Agyenim et al. [79-83] performed a series of experimental studies to investigate three practical heat transfer enhancement methods: circular fins, longitudinal fins, and a multi-tube with four heat transfer tubes on a horizontal shell and tube heat exchanger. The results showed that the longitudinal finned configuration is suitable for both charging and discharging processes as it achieved the best charge performance with insignificant sub-cooling during discharging. It was also concluded that the convection mode of heat transfer played an important role during the melting process, while conduction was significant during the solidification process.

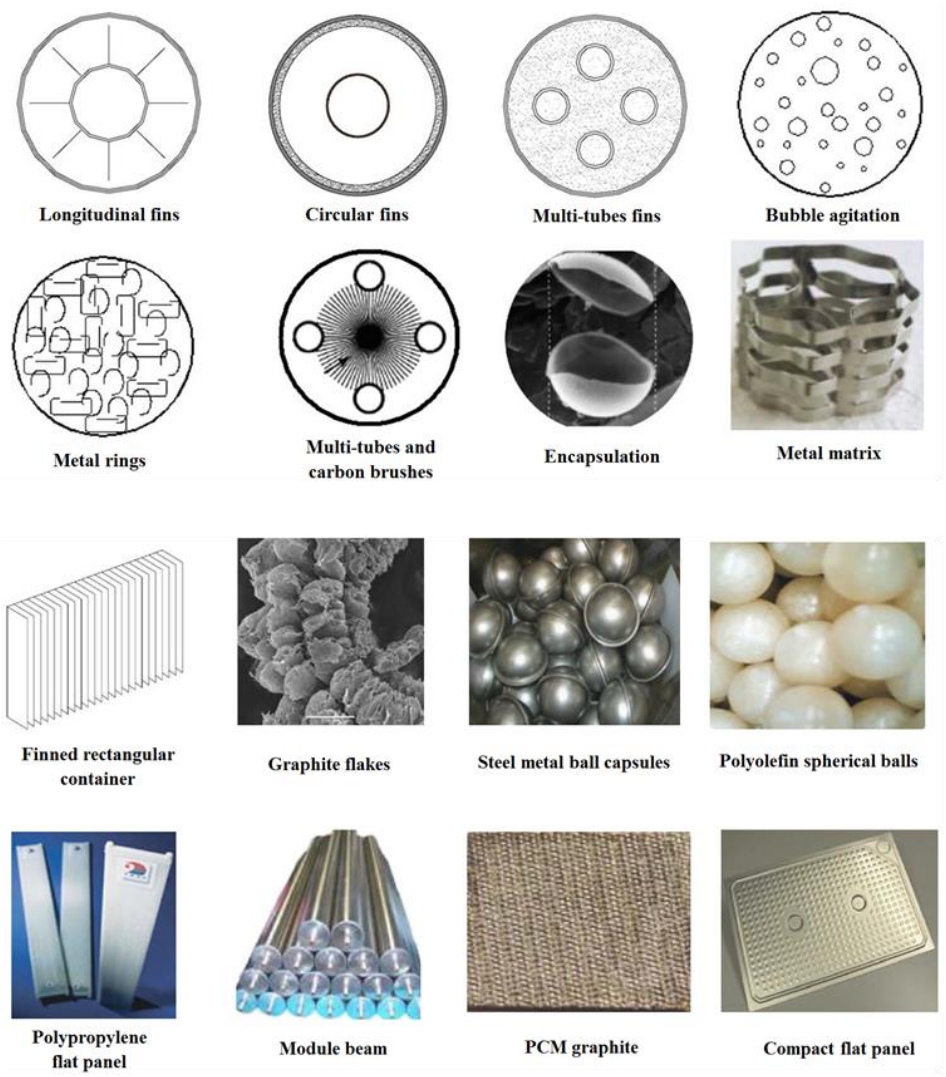

Fig. 2.16 Heat transfer enhancement methods employed in LHS systems [17].

Recently, Liu et al. [84] experimentally investigated the effectiveness of straight angles longitudinal fins in horizontal shell and tube LHS system. The experimental results showed that the charging and discharging performance of the angles longitudinal fins had insignificant difference from straight fins over a wide range of heat transfer fluid temperatures.

2.6.2. Heat transfer mechanism in latent heat storage units

During the melting and solidification processes, the possible heat transfer mechanisms are conduction, convection or a combination of both. However, the issue of which mechanism dominates the heat transfer at various stages in the energy charging and discharging has been

argued for decades. Despite of many research works in the heat transfer mechanism, the comprehensive reviews on the heat transfer analysis of PCMs [6, 17, 72, 85-87] revealed that still there is a challenge in the literature on how to weight the percentages of conduction and convection heat transfer and how the dominant heat transfer mechanism differs in various geometries during the charging and discharging processes.

2.6. Conclusion

The above literature review shows many vital areas for future research. The following important aspects need to be addressed in future work in this area.

Researchers have made a large effort to investigate integration techniques between solar collectors and PCM units. It is concluded that the PCM unit in a SDHW system substantially increases the energy storage capacity in comparison to the conventional SDHW system. However, the performance of the SDHW system is largely affected by selection of integration technique. Even when using the same integration technique, a different PCM configuration may yield a different system performance. No research finding in literature or model can predict which integration technique will perform the best for a specific case. In other words, there is still a lack of understanding on how to optimize SDHW systems with PCMs. A further experimental investigation needs to be performed to obtain adequate knowledge of SDHW systems containing PCMs to optimize the system design and performance. A general numerical model should be developed to simulate the SDHW system performance under different scenarios to optimize the system in terms of performance and economics.

This literature review shows that most of the current research efforts have focused on understanding the performance and heat transfer in the latent heat energy storage unit. Only limited type of PCMs and latent heat storage units have been applied in the SDHW system. Therefore, further research is required to incorporate the up-to-date technologies of PCM units

into SDHW systems and to better understand the SDHW system performance with these PCM units at different working conditions.

The long term performance of SDHW systems using PCM is also an important aspect needing further study. Although some researchers have successfully demonstrated an improvement in energy storage capacity by using a PCM unit, other researchers have found that the long term performance may not be as good as expected. The majority of simulation studies has been based on the part of European weather conditions. Further experimental work is needed to validate the findings reported by the aforementioned researchers and then the numerical study should be carried out to better understand the long term performance of different SDHW systems with PCM at different working conditions.

2.6. References

[1] Shukla A, Buddhi D, Sawhney R. Solar water heaters with phase change material thermal energy storage medium: A review. Renewable and Sustainable Energy Reviews. 2009;13:2119-25.

[2] Sharma A, Chen C. Solar Water Heating System with Phase Change Materials. International Review of Chemical Engineering. 2009;1:297-307.

[3] Raisul Islam M, Sumathy K, Ullah Khan S. Solar water heating systems and their market trends. Renewable and Sustainable Energy Reviews. 2013;17:1-25.

[4] Nkwetta DN, Haghighat F. Thermal energy storage with phase change material-A state-of-the art review. Sustainable Cities and Society. 2014;10:87-100.

[5] Hasnain S. Review on sustainable thermal energy storage technologies, part I: heat storage materials and techniques. Energy Conversion and Management. 1998;39:1127-38.

[6] Zalba B, Marín JM, Cabeza LF, Mehling H. Review on thermal energy storage with phase change: materials, heat transfer analysis and applications. Applied Thermal Engineering. 2003;23:251-83.

[7] Farid MM, Khudhair AM, Razack SAK, Al-Hallaj S. A review on phase change energy storage: materials and applications. Energy Conversion and Management. 2004;45:1597-615.

[8] Sharma A, Tyagi V, Chen C, Buddhi D. Review on thermal energy storage with phase change materials and applications. Renewable and Sustainable Energy Reviews. 2009;13:318-45.

[9] Zhou D, Zhao C-Y, Tian Y. Review on thermal energy storage with phase change materials (PCMs) in building applications. Applied Energy. 2012;92:593-605.

[10] Al-Abidi AA, Bin Mat S, Sopian K, Sulaiman M, Lim C, Th A. Review of thermal energy storage for air conditioning systems. Renewable and Sustainable Energy Reviews. 2012;16:5802-19.

[11] Demirbas MF. Thermal energy storage and phase change materials: An overview. Energy Sources, Part B: Economics, Planning, and Policy. 2006;1:85-95.

[12] Sharma SD, Kitano H, Sagara K. Phase change materials for low temperature solar thermal applications. Res Rep Fac Eng Mie Univ. 2004;29:31-64.

[13] Sharma S, Sagara K. Latent heat storage materials and systems: a review. International Journal of Green Energy. 2005;2:1-56.

[14] Regin AF, Solanki S, Saini J. Heat transfer characteristics of thermal energy storage system using PCM capsules: a review. Renewable and Sustainable Energy Reviews. 2008;12:2438-58.

[15] Kenisarin M, Mahkamov K. Solar energy storage using phase change materials. Renewable and Sustainable Energy Reviews. 2007;11:1913-65.

[16] Jegadheeswaran S, Pohekar SD. Performance enhancement in latent heat thermal storage system: a review. Renewable and Sustainable Energy Reviews. 2009;13:2225-44.

[17] Agyenim F, Hewitt N, Eames P, Smyth M. A review of materials, heat transfer and phase change problem formulation for latent heat thermal energy storage systems (LHTESS). Renewable and Sustainable Energy Reviews. 2010;14:615-28.

[18] Baetens R, Jelle BP, Gustavsen A. Phase change materials for building applications: A state-of-the-art review. Energy and Buildings. 2010;42:1361-8.

[19] Cabeza L, Castell A, Barreneche C, De Gracia A, Fernández A. Materials used as PCM in thermal energy storage in buildings: a review. Renewable and Sustainable Energy Reviews. 2011;15:1675-95.

[20] Zhao C-Y, Zhang GH. Review on microencapsulated phase change materials (MEPCMs): fabrication, characterization and applications. Renewable and Sustainable Energy Reviews. 2011;15:3813-32.

[21] Huang M, Eames P, McCormack S, Griffiths P, Hewitt N. Microencapsulated phase change slurries for thermal energy storage in a residential solar energy system. Renewable Energy. 2011;36:2932-9.

[22] Kuznik F, David D, Johannes K, Roux J-J. A review on phase change materials integrated in building walls. Renewable and Sustainable Energy Reviews. 2011;15:379-91.

[23] Kalogirou SA. Solar thermal collectors and applications. Progress in Energy and Combustion Science. 2004;30:231-95.

[24] Telkes M, Raymond E. Storing solar heat in chemicals. Ind Heat Engr. 1950;12:119.

[25] Telkes M. Thermal storage for solar heating and cooling. Proceedings of the Workshop on Solar Energy Storage Subsystems for the Heating and Cooling of Buildings, Charlottesville (Virginia, USA)1975.

[26] Telkes M. Trombe wall with phase change storage material. Proceeding of II National Passive Solar Conference.1978:283-87.

[27] Sari A, Kaygusuz K. Thermal energy storage system using stearic acid as a phase change material. Solar Energy. 2001;71:365-76.

[28] Sarı A, Kaygusuz K. Thermal performance of myristic acid as a phase change material for energy storage application. Renewable Energy. 2001;24:303-17.

[29] Sari A, Kaygusuz K. Thermal performance of palmitic acid as a phase change energy storage material. Energy Conversion and Management. 2002;43:863-76.

[30] Sarı A, Kaygusuz K. Some fatty acids used for latent heat storage: thermal stability and corrosion of metals with respect to thermal cycling. Renewable Energy. 2003;28:939-48.

[31] Sarı A. Thermal reliability test of some fatty acids as PCMs used for solar thermal latent heat storage applications. Energy Conversion and Management. 2003;44:2277-87.

[32] Baran G, Sari A. Phase change and heat transfer characteristics of a eutectic mixture of palmitic and stearic acids as PCM in a latent heat storage system. Energy Conversion and Management. 2003;44:3227-46.

[33] Sharma A, Won LD, Buddhi D, Park JU. Numerical heat transfer studies of the fatty acids for different heat exchanger materials on the performance of a latent heat storage system. Renewable Energy. 2005;30:2179-87.

[34] Gu Z, Liu H, Li Y. Thermal energy recovery of air conditioning system-heat recovery system calculation and phase change materials development. Applied thermal engineering. 2004;24:2511-26.

[35] Sharma A, Sharma S, Buddhi D. Accelerated thermal cycle test of acetamide, stearic acid and paraffin wax for solar thermal latent heat storage applications. Energy Conversion and Management. 2002;43:1923-30.

[36] Hosseini M, Ranjbar A, Sedighi K, Rahimi M. A combined experimental and computational study on the melting behavior of a medium temperature phase change storage material inside shell and tube heat exchanger. International Communications in Heat and Mass Transfer. 2012;39:1416-24.

[37] Hosseini M, Rahimi M, Bahrampoury R. Experimental and computational evolution of a shell and tube heat exchanger as a PCM thermal storage system. International Communications in Heat and Mass Transfer. 2014;50:128-36.

[38] Bhargava AK. A solar water heater based on phase-changing material. Applied Energy. 1983;14:197-209.

[39] Prakash J, Garg H, Datta G. A solar water heater with a built-in latent heat storage. Energy Conversion and Management. 1985;25:51-6.

[40] Tiwari G, Rai S, Ram S, Singh M. Performance prediction of PCCM collection-cum-storage water heater: quasi-steady state solution. Energy Conversion and Management. 1988;28:219-23.

[41] Bansal N, Buddhi D. An analytical study of a latent heat storage system in a cylinder. Energy Conversion and Management. 1992;33:235-42.

[42] Nallusamy N, Sampath S, Velraj R. Experimental investigation on a combined sensible and latent heat storage system integrated with constant/varying (solar) heat sources. Renewable Energy. 2007;32:1206-27.

[43] Tarhan S, Sari A, Yardim MH. Temperature distributions in trapezoidal built in storage solar water heaters with/without phase change materials. Energy Conversion and Management. 2006;47:2143-54.

[44] El Qarnia H. Numerical analysis of a coupled solar collector latent heat storage unit using various phase change materials for heating the water. Energy Conversion and Management. 2009;50:247-54.

[45] Reddy RM, Nallusamy N, Reddy KH. Experimental studies on phase change material-based thermal energy storage system for solar water heating applications. Renewable Energy and Application. 2012;2:1-6.

[46] Hassan MM, Beliveau Y. Modelling of an integrated solar system. Building and Environment. 2008;43:804-10.

[47] Mehling H, Cabeza L, Hippeli S, Hiebler S. PCM-module to improve hot water heat stores with stratification. Renewable Energy. 2003;28:699-711.

[48] Cabeza L, Nogues M, Roca J, Illa J, Hiebler S, Mehling H. PCM-module to improve hot water heat stores with stratification: first tests in a complete solar system. 9th international conference on thermal energy storage. 2003:273-8.

[49] Cabeza LF, Ibanez M, Sole C, Roca J, Nogués M. Experimentation with a water tank including a PCM module. Solar Energy Materials and Solar Cells. 2006;90:1273-82.

[50] Cabeza L, Mehling H, Hiebler S, Ziegler F. Heat transfer enhancement in water when used as PCM in thermal energy storage. Applied Thermal Engineering. 2002;22:1141-51.

[51] Mazman M, Cabeza LF, Mehling H, Nogues M, Evliya H, Paksoy HÖ. Utilization of phase change materials in solar domestic hot water systems. Renewable Energy. 2009;34:1639-43.

[52] Smyth M, Eames P, Norton B. Integrated collector storage solar water heaters. Renewable and Sustainable Energy Reviews. 2006;10:503-38.

[53] Boy E, Boss R, Lutz M. A collector storage module with integrated phase change material. Proceeding ISES. Pergamon Press, Hamburg, 1987.

[54] Al-Jandal S, Sayigh A. Thermal performance characteristics of STC system with phase change storage. Renewable Energy. 1994;5:390-9.

[55] Rabin Y, Bar-Niv I, Korin E, Mikic B. Integrated solar collector storage system based on a salt-hydrate phase-change material. Solar Energy. 1995;55:435-44.

[56] Kumar B. Design, development and performance evaluation of a latent heat storage unit for evening and morning hot water using a box type solar collector. Project Report, M Tech(Energy Management), Indore, India: School of Energy and Environmental Studies, Devi Ahilya University. 2001.

[57] Kürklü A, Özmerzi A, Bilgin S. Thermal performance of a water-phase change material solar collector. Renewable Energy. 2002;26:391-9.

[58] Mettawee E-BS, Assassa GM. Experimental study of a compact PCM solar collector. Energy. 2006;31:2958-68.

[59] Mettawee E-BS, Assassa GM. Thermal conductivity enhancement in a latent heat storage system. Solar Energy. 2007;81:839-45.

[60] Khalifa AJN, Suffer KH, Mahmoud MS. A storage domestic solar hot water system with a back layer of phase change material. Experimental Thermal and Fluid Science. 2013;44:174-81.

[61] Haillot D, Goetz V, Py X, Benabdelkarim M. High performance storage composite for the enhancement of solar domestic hot water systems: Part 1: Storage material investigation. Solar Energy. 2011;85:1021-7.

[62] Haillot D, Nepveu F, Goetz V, Py X, Benabdelkarim M. High performance storage composite for the enhancement of solar domestic hot water systems: Part 2: Numerical system analysis. Solar Energy. 2012;86:64-77.

[63] Haillot D, Franquet E, Gibout S, Bédécarrats J-P. Optimization of solar DHW system including PCM media. Applied Energy. 2012; 109:470-75.

[64] Chaurasia P. Phase change material in solar water heater storage system. Proceedings of the 8th International Conference on Thermal Energy Storage. 28 August – 1 September, 2000, Stuttgart, Germany.

[65] Kaygusuz K. Experimental and theoretical investigation of latent heat storage for water based solar heating systems. Energy Conversion and Management. 1995;36:315-23.

[66] Canbazoğlu S, Şahinaslan A, Ekmekyapar A, Aksoy ÝG, Akarsu F. Enhancement of solar thermal energy storage performance using sodium thiosulfate pentahydrate of a conventional solar water-heating system. Energy and Buildings. 2005;37:235-42.

[67] Al-Hinti I, Al-Ghandoor A, Maaly A, Abu Naqeera I, Al-Khateeb Z, Al-Sheikh O. Experimental investigation on the use of water-phase change material storage in conventional solar water heating systems. Energy Conversion and Management. 2010;51:1735-40.

[68] Nkwetta DN, Vouillamoz P-E, Haghighat F, El Mankibi M, Moreau A, Desai K. Phase change materials in hot water tank for shifting peak power demand. Solar Energy. 2014;107:628-35.

[69] Ibanez M, Cabeza LF, Solé C, Roca J, Nogués M. Modelization of a water tank including a PCM module. Applied Thermal Engineering. 2006;26:1328-33.

[70] Talmatsky E, Kribus A. PCM storage for solar DHW: An unfulfilled promise? Solar Energy. 2008;82:861-9.

[71] Kousksou T, Bruel P, Cherreau G, Leoussoff V, El Rhafiki T. PCM storage for solar DHW: From an unfulfilled promise to a real benefit. Solar Energy. 2011;85:2033-40.

[72] Liu S, Li Y, Zhang Y. Mathematical solutions and numerical models employed for the investigations of PCMs′ phase transformations. Renewable and Sustainable Energy Reviews. 2014;33:659-74.

[73] H. A. Adine and H. E. Qarnia, Numerical analysis of the thermal behaviour of a shell and tube heat storage unit using phase change matherials, Applied Mathematical Modelling, 33 (4), 2009, 2132-2144.

[74] M. Akgun, O. Aydin, K. Kaygusuz, Thermal energy storage performance of paraffin in a novel tube in shell system, Applied thermal Engineering, 2008, 28 (5), 405-413.

[75] A. Erek, Z. Llken, M. A. Acar, Experimental and numerical investigation of thermal energy storage with a finned tube, International Journal of Energy Research, 2005, 29 (4), 283-301.

[76] B. Basal, A. Unal, Numerical evaluation of a triple concentric tube latent heat thermal energy storage, Solar Energy, 92, 2013, 196-205.

[77] A. A. Al-Abidi, S. B. Mat, K. Sopian, M. Y. Sulaiman, A. T. Mohammad, Internal and external fin heat transfer enhancement technique for latent heat thermal energy storage in triplex tube heat exchangers, Applied Thermal Engineering, 2013, 53 (1), 147-156.

[78] A. A. Al-Abidi, S. B. Mat, K. Sopian, M. Y. Sulaiman, A. T. Mohammad, Experimental study of melting and solidification of PCM on a triplex tube heat exchanger with fins, Energy and Building, 68 (A), 2014, 33-41.

[79] Agyenim F, Eames P, Smyth M. Heat transfer enhancement in medium temperature thermal energy storage system using a multitube heat transfer array. Renewable Energy. 2010;35:198-207.

[80] Agyenim F, Eames P, Smyth M. A comparison of heat transfer enhancement in a medium temperature thermal energy storage heat exchanger using fins. Solar Energy. 2009;83:1509-20.

[81] Agyenim F, Eames P, Smyth M. Experimental study on the melting and solidification behaviour of a medium temperature phase change storage material (Erythritol) system augmented with fins to power a LiBr/H2O absorption cooling system. Renewable Energy. 2011;36:108-17.

[82] Agyenim F, Hewitt N. Experimental investigation and improvement in heat transfer of paraffin PCM RT58 storage system to take advantage of low peak tariff rates for heat pump applications. International Journal of Low-Carbon Technologies. 2012;8:260-70.

[83] Agyenim F, Hewitt N, Eames P, Smyth M. Numerical and experimental development of medium temperature thermal energy storage (Erythritol) system for the hot side of LiBr/H2O air conditioning applications. World Renewable Energy Congress. 19-25 July, 2008, Glasgow, Scotland.

[84] Liu C, Groulx D. Experimental study of the phase change heat transfer inside a horizontal cylindrical latent heat energy storage system. International Journal of Thermal Sciences. 2014;82:100-10.

[85] Hu H, Argyropoulos SA. Mathematical modelling of solidification and melting: a review. Modelling and Simulation in Materials Science and Engineering. 1996;4:371.

[86] Sharma A, Tyagi V, Chen C, Buddhi D. Review on thermal energy storage with phase change materials and applications. Renewable and Sustainable Energy Reviews. 2009;13:318-45.

[87] Al-abidi AA, Bin Mat S, Sopian K, Sulaiman M, Mohammed AT. CFD applications for latent heat thermal energy storage: a review. Renewable and Sustainable Energy Reviews. 2013;20:353-63

Chapter3: Mathematical modelling of heat transfer in a latent heat thermal energy unit

3.1. Chapter summary

In this chapter, pure thermal conduction model and a combined conduction-convection heat transfer models have been used to study the thermal behaviour and heat transfer characteristics of a vertical cylindrical shell and tube latent heat thermal energy storage (LHTES) unit. The results from numerical simulation are validated with published experimental data which indicate that the combined convection and conduction model can better describe the energy transfer in the phase change materials (PCMs) during the melting process. In contrast, heat transfer by conduction is most significant during the solidification process. In terms of total solidification time, the two models show little difference.

This research contained within this chapter has been published as: Saeid Seddegh, Xiaolin Wang, Alan D. Henderson. "Numerical investigation of heat transfer in a vertical shell and tube latent energy storage system", Applied Thermal Engineering 87, PP. 698-706, ELSEVIER, 2015.

3.2. Introduction

A common problem raised in the literature is the lack of understanding of the heat transfer mechanisms during melting (for the charging) and solidification (for the discharging) processes. The possible heat transfer mechanisms are conduction, convection or a combination of both. However, the issue of which mechanism dominates at various stages during energy charging and discharging has been argued for decades [1-4]. Conduction was initially believed to play the most important role during phase transformation processes [5-7]. However, many researchers argued that natural convection is the most important mechanism in the phase change process, and in particular in the melting process [8, 9]. Sparrow et al. [8] performed a pioneering study and concluded that natural convection could not be ignored in the analysis of a phase change problem. Yao and Chen [9] performed a numerical study using an approximate solution and found that the heat transfer mechanism strongly depended on the Rayleigh number. In 1994, Hasan [10] concluded that the convection heat transfer active an important role in the melting process, and a simplified model that only considering conduction will not describe the melting process properly. Later, Lacroix & Duong [11] and Velraj et al. [12] reported the similar findings in their research and reported that natural convection is the main heat transfer mechanism during the melting process. Natural convection occurs in the melt layer which results in the heat transfer rate increasing compared to the solidification process. Buddhi et al. [13] presented an explanation for this phenomenon: the density difference between the solid and liquid PCM phase induces the buoyancy, which causes convective motion in the liquid phase. However, Zhang and Yi [14] believed that the convection motions were due to the volume increase as the solid PCM melted into liquid during the melting process.

The effect of natural convection on the constrained melting of PCM within spherical containers has been conducted numerically [15] and experimentally [16]. Results showed that in the early stages of a melting process, the conduction mode of heat transfer is dominant. As

the melting progresses natural convection caused by buoyancy in the liquid PCM is strengthened. Khillarkar et al. [17] numerically investigated the free convection dominated melting of a PCM contained inside concentric horizontal annuli with different configurations: a square external tube with a circular tube inside and a circular external tube with a square tube inside. It was concluded that the thermal stratification occurs in the upper section of the cavity. Darzi et al. [18] carried out a 2D numerical study for symmetric melting of N-eicosane between two horizontal cylinders in concentric and eccentric arrays. The predicted results show that when the inner cylindrical tube moves downwards, the melting rate increases sharply due to the larger zone of dominant natural convection heat transfer in the PCM. Hosseini et al. [19-20] experimentally and computationally studied the characteristics of a medium temperature PCM in a horizontal shell-and-tube heat exchanger. It was concluded that during the melting process, convection drives recirculation inside the liquid region. Then the upper section reaches a higher temperature than the lower section due to natural convection. Contrary to the melting process, solidification is dominated by conduction, although initially convective heat transfer accompanies the prevailing conduction.

Although there are some experimental results for vertical shell-and-tube heat exchangers [21-23], there are limited computational studies of vertical cylindrical tube systems [24-25] and vertical cylindrical shell-and-tube systems which are commonly used in the thermal energy storage. In this study, a numerical simulation was conducted to investigate the heat transfer mechanism inside a vertical cylindrical shell-and-tube latent heat energy storage system during different charging and discharging stages. The effect of natural convection in the storage system in charging/discharging mode was studied, respectively. Results from a pure conduction model and combined conduction-convection model were compared and analyzed. The important parameters in the phase transition, including transition times, temperature ranges, and propagation of the solid liquid interface were investigated. The analyses would

provide useful information on the heat transfer mechanism in the LHTES and design of more efficient systems.

3.3. System description

Fig. 3.1 shows the schematic drawing of the studied system which consists of two vertical concentric tubes with the PCM in the annulus and heat transfer fluid in the tube. The outer surface of the system is well-insulated. For model validation purposes, the temperature monitor locations are selected based on the experimental measurement points in the annulus as was done by Rathod and Banerjee [26-27]. Water is used as the heat transfer fluid (HTF), which is circulated through the inner tube, and the annulus is filled with paraffin wax with the thermal properties shown in Table 3.1. During the charging process, hot water is circulated through the inner tube. Cold water is circulated through the inner tube during the discharging process.

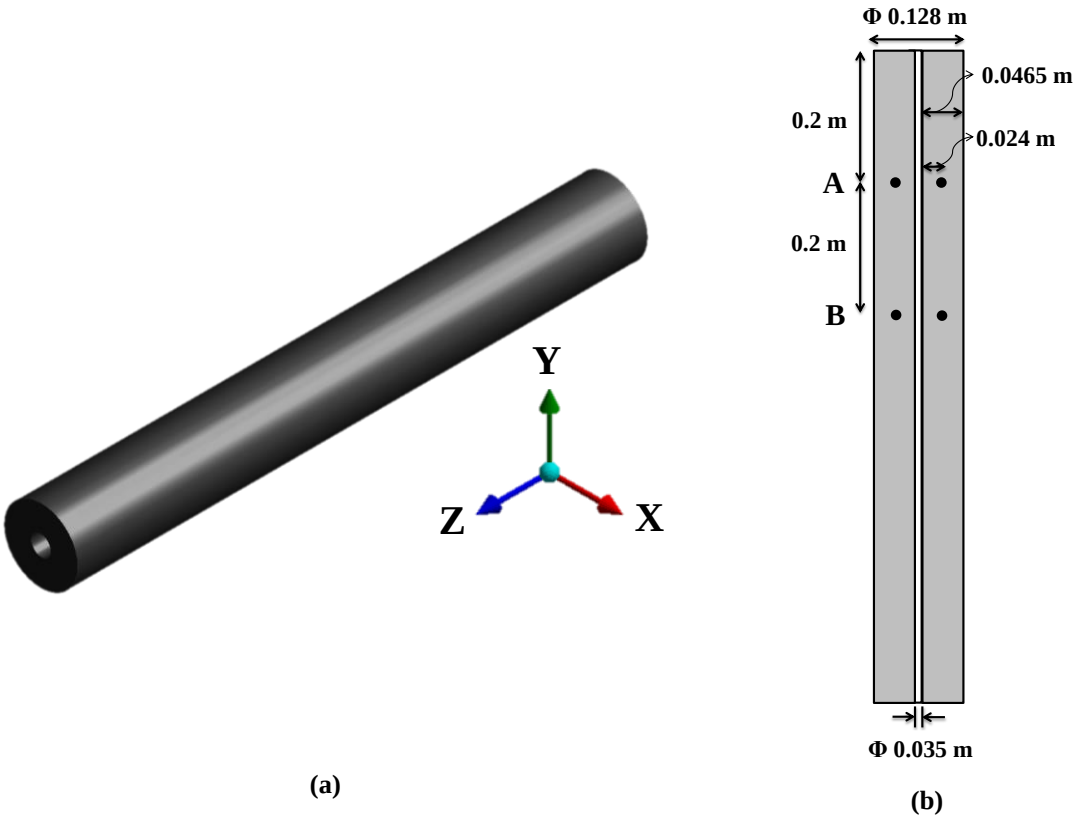

Fig.3.1 a) Schematic drawing of the LHTES unit, Fig.3.1 b) the location of thermocouple (marks represent the temperature point).

Table 3.1: PCM and HTF thermo-physical properties.

PCM	Melting Temperature (K)	Latent heat of fusion (kJ/kg)	Density (kg/m^3)		Specific heat (J/kgK)		Thermal conductivity (W/mK)	
			Solid	Liquid	Solid	Liquid	Solid	Liquid
Paraffin wax	331-333	213.0	861	778	1850	2384	0.40	0.15
Heat transfer fluid (HTF)	**Charging Temperature**	**Discharging temperature**	**Density (kg/m^3)**		**Specific heat (J/kgK)**		**Thermal conductivity (W/mK)**	
Water	358	301	998		4183		0.58	

3.4. Numerical approach

In this study, the enthalpy method is applied due to its advantages: (i) the governing equations are similar to the single-phase equation; (ii) no explicit conditions are needed to be satisfied at the solid-liquid interface; (iii) the enthalpy formulation involves the solution within a mushy zone, involving both solid and liquid materials, between the two standard phases; and (iv) the phase change problem can be solved more easily [28].

3.4.1. Numerical model

In the enthalpy method, the governing equation is the same for both the solid and liquid phases and the solid-liquid interface position is not explicitly tracked. The interface is indicated by a mushy zone, which separates the two phases [29]. The energy conservation is expressed in terms of total volumetric enthalpy and temperature for constant thermo-physical properties by

$$\frac{\partial \rho H}{\partial t} + \nabla \cdot \left(\rho v H \right) = \nabla \cdot \left(k \nabla T \right) + S \qquad (1)$$

where H is the total volumetric enthalpy which is the sum of sensible and latent heats as Eq. (2 and 3), and h_{ref} is the sensible heat at T_{ref} :

$$H = h + fL \tag{2}$$

$$h = h_{ref} + \int_{T_{ref}}^{T} C_P dT \tag{3}$$

where *f* refers to liquid fraction and indicates the fraction of a cell volume in liquid form and is associated with each cell in the domain given by Eq. (4). The mushy zone is a region wherein the liquid fraction lies between 0 and 1.

$$f = \begin{cases} 0 & T < T_{Solidus} \\ \dfrac{T - T_{Solidus}}{T_{Liquidus} - T_{Solidus}} & T_{Solidus} \le T \le T_{Liquidus} \\ 1 & T > T_{Liquidus} \end{cases} \tag{4}$$

applying Eq. (2-4), the energy equation is written as

$$\frac{\partial \rho h}{\partial t} + \nabla \cdot (\rho v h) = \nabla \cdot (k \nabla T) - \frac{\partial \rho f L}{\partial t} - \nabla \cdot (\rho v f L) + S \tag{5}$$

In order to account for the effect of natural convection melting from the density change, the momentum equation is written as

$$\frac{\partial \rho v}{\partial t} + \nabla \cdot (\rho v v) = -\nabla P + \nabla \cdot (\mu \nabla v) + \rho g + \frac{(1-f)^2}{f^3 + \varepsilon} v A_{mush} \tag{6}$$

where ν is velocity, the term A_{mush} is a constant reflecting the mushy zone morphology which describes how steeply the velocity is reduced to zero when the material solidifies. The constant ε is a small number to prevent division by zero.

The Boussinesq approximation was used [29] and is valid if the density variation is small, as it provides faster convergence than other temperature dependent models. The model assumes the fluid density is constant in all terms of the momentum equation except the body force term, and it is modeled based on reference density (ρ_0) and temperature (T_0), and the volumetric expansion coefficient (β). Then the momentum equation is written as

$$\frac{\partial \rho_0 v}{\partial t} + \nabla \cdot (\rho_0 v v) = -\nabla P + \nabla \cdot (\mu \nabla v) + (\rho - \rho_0) g + \frac{(1-f)^2}{f^3 + \varepsilon} v A_{mush} \quad (7)$$

$$(\rho - \rho_0) g = -\rho_0 \beta (T - T_0) \quad (8)$$

The continuity is given as:

$$\frac{\partial \rho}{\partial t} + \nabla \cdot (\rho v) = 0 \quad (9)$$

In the pure conduction model, Eqs. (5) and (9) are solved while Eqs. (5), (7-9) are solved to consider the combined conduction/convection heat transfer mechanism. The liquid fraction is computed during each iteration at each cell in the domain based on enthalpy balance. The mushy zone is modeled as a ‘‘pseudo’’ porous medium in which the porosity decreases from 1 to 0 as the material solidifies. When the material has fully solidified in a cell, the porosity becomes zero, and the velocity drops to zero [28]. The following parameters were used in the simulation: A_{mush} =10^5, ε =0.001, β=0.002 1/K and T_{ref} = 298.15 K.

The computational study is performed using the Fluent application of the ANSYS 15 software. The solidification and melting models are solved for laminar flow with Navier-Stokes equations using the enthalpy-porosity technique. A 2D vertical slice of the cylinder is modeled to reduce computational time. Following previous numerical studies using Fluent [18, 25], the transient simulation with the pressure staggering option (PRESTO) scheme is used for the pressure correction equation, and a Coupled algorithm was used for pressure-velocity coupling. A second order upwind scheme was used to solve the momentum and energy equations.

3.4.1.1 Boundary/Initial conditions

In both models, the boundary conditions on the outer wall surface and the top and bottom caps are well insulated. The boundary condition used for the inner surface of the pipe (HTF wall) is convective heat transfer which corresponds to the case in the experimental study. The heat transfer coefficient is calculated by [30].

$$h = Nu\frac{k}{D} \quad (10)$$

$$Nu = \frac{\left(\frac{f}{8}\right)\left(\mathrm{Re}_d - 1000\right)\mathrm{Pr}}{1 + 12.7\left(\frac{f}{8}\right)^{\frac{1}{2}}\left(\mathrm{Pr}^{\frac{2}{3}} - 1\right)} \quad (11)$$

where Pr is the Prandtl number, and the correlation is valid for $0.5 \le \mathrm{Pr} \le 2000$ and $3000 \le \mathrm{Re}_d \le 5\times10^6$, $\mathrm{Re_d}$ is the Reynolds number expressed by

$$\mathrm{Re}_d = \frac{4\dot{m}}{\pi D\mu} \quad (12)$$

f is the friction factor calculated as

$$f = \left(1.58\ln \mathrm{Re}_d - 3.28\right)^{-2} \quad (13)$$

The PCM is initially set to solid with a temperature of 303 K during the melting process and set to liquid with a temperature of 353 K in the solidification process. The HTF flow in the inner pipe is 5 L/min with Re_d of 32152. The HTF temperature is 358 K for charging and 301 K for discharging. From the experimental data [26, 27] and initial energy analysis, the change of the HTF temperature down the tube during charging and discharging is less than 0.5 °C. In order to simplify the problem, this change of the HTF temperature is not considered in the simulation.

3.4.1.2 Assumption

In both the conduction only and conduction-convection model, the following assumptions are made:

- Thermophysical properties of the materials are constant with temperature.
- The motion of the liquid PCM is laminar, unsteady, and incompressible.

- Viscous dissipation is negligible.

3.5. Results and discussion

The model was verified to check the dependency of time steps size and element size prior to simulation. Three mesh sizes: 645, 2010, and 5678 elements; and three time-step sizes: 0.05 s, 0.1 s, and 0.2 s were examined. It can be seen that the model with 2010 cells and time steps of the 0.05 s and 0.1 s produces a similar temperature variation. Increasing the number of elements to 5678 produces no significant change. Furthermore, the limit 2010 cells grid and 0.1 s time step are sufficient to achieve a predetermined convergence threshold for the energy equation ($1E^{-6}$).

3.5.1. Charging process

Figs. 3.2a and 3.2b show contours of temperature and liquid fraction in the PCM for a charging process using the pure conduction model. As shown in Fig. 3.2a, there is no temperature difference in the vertical direction. This can be explained by the conduction heat transfer in the PCM. The temperature of the PCM is controlled by energy being absorbed by the PCM from the HTF, heat is transferred from the hot PCM to the adjacent layer of cold PCM. Depending on the rates of these two energy transfer processes, the temperature at a position in the vessel may remain constant or increase. In the pure conduction model, the total heat transfer rate is almost the same along the vertical direction from the inner tube surface to PCM interface due to conduction. Therefore, the melting front along the axial direction moves at the same rate from the inner tube surface to the inner surface of the cylinder. This result indicates that there is no difference between liquid regions in axial direction of the cylinder and the liquefied PCM in the radial direction as shown in Fig. 3.2b.

However, the results obtained from the combined conduction and convection model are quite different. Fig. 3.3a shows contours of temperature in the PCM using the combined

conduction and convection model during a charging process. The PCM temperature changes substantially in the axial direction at different charging times. In the combined model, the heat transfer from the wall of the inner tube to the PCM is initially through conduction before the PCM starts melting. As the PCM melts, a thin layer of liquid is formed between the inner tube outer wall and the solid phase material, and natural convection starts to take place. As the melted zone becomes larger, the convection becomes stronger and the interface front moves faster. The heat transfer in the cylinder relies on two mechanisms: (1) in the liquid PCM, the interface between the liquid PCM and inner tube surface and the interface between the liquid PCM and the solid PCM, heat transfer is mainly controlled by convection and (2) in the solid PCM, heat transfer is by conduction. Due to buoyancy, the liquid PCM rises up and gradually fills the upper region of the system. The melting front moves in the axial direction from the top to the bottom of the cylinder as shown in Fig. 3.3b. Hence, the melting front is not cylindrical in shape, and is visualized as a conical shape. The upper part of the PCM in the cylinder melts much faster than the lower part. This finding is consistent with that observed during experiments [26-27].

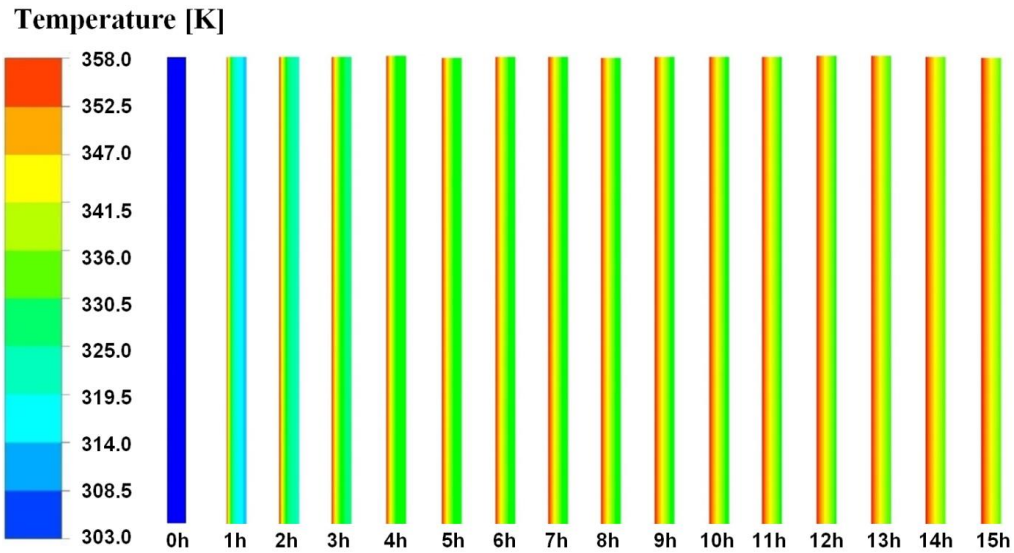

Fig. 3.2a Contours of temperature using the pure conduction model during a charging process (from the inner tube surface to shell surface, same for the Figs. 2b, 3a and 3b).

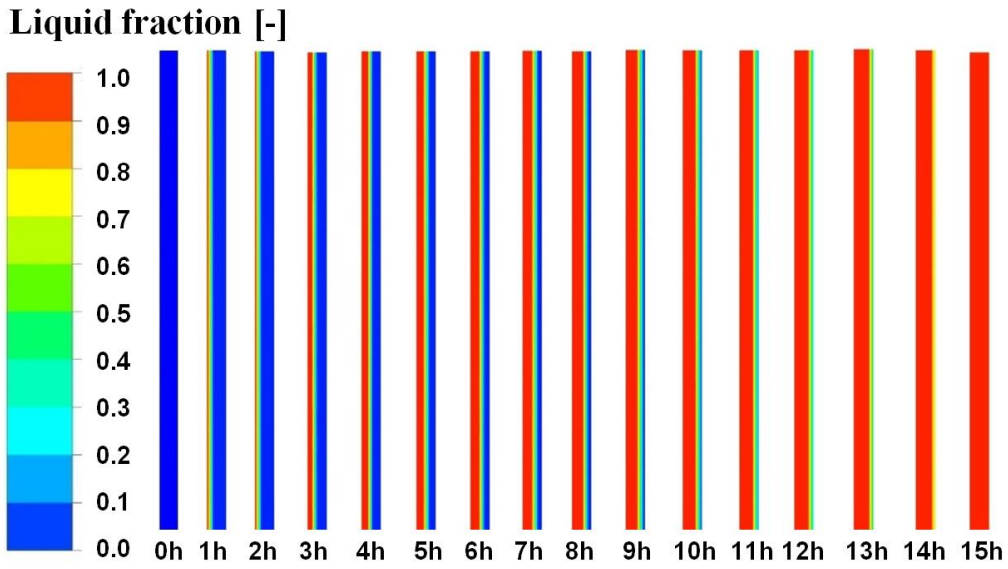

Fig. 3.2b Contours of liquid fraction using the pure conduction model during a charging process.

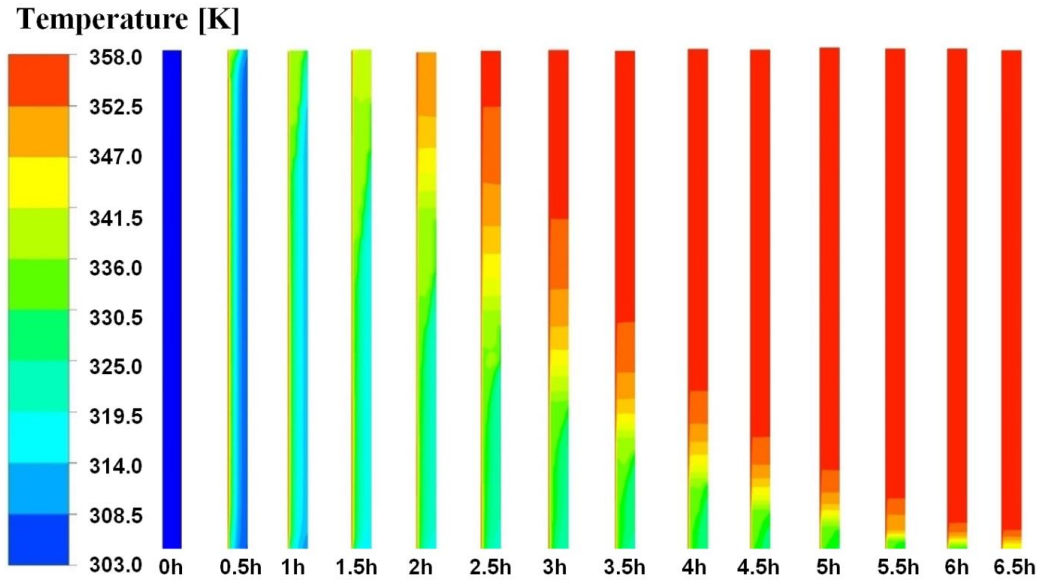

Fig. 3.3a Contours of temperature using the combined conduction and convection model during a charging process.

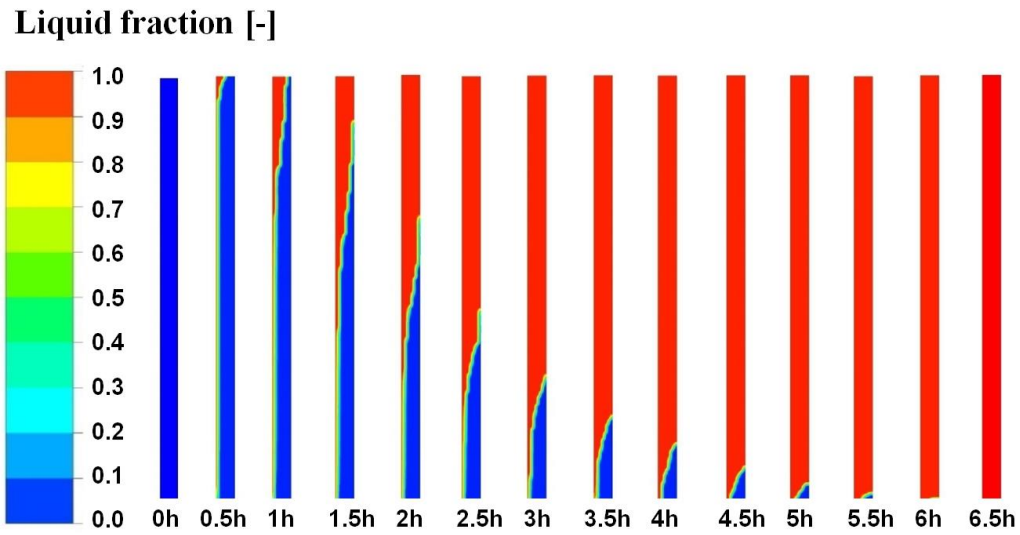

Fig. 3.3b Contours of liquid fraction using the combined conduction and convection model during a charging process.

In order to investigate the model most accurately describes the heat transfer in the PCM, the temperatures inside the domain is monitored and compared with experimental data [26, 27]. Fig. 3.4 shows a comparison between the experimental and simulated PCM temperature during a charging process. Using the Root Mean Square (RMS) method of statistical analysis, the RMS value of the difference between the simulated temperature of the conduction model and experimental data is 22 K at point A and 19 K at point B, respectively. The RMS value of the difference between the predicted temperature from the combined conduction-convection model and experimental data is 2.2 K at point A and 3.9 K at point B, respectively. It is obvious that the PCM temperatures obtained from the combined conduction-convection model agree far better with the experimental data than those obtained from the pure conduction model. It can be seen that the temperature difference is very small at the beginning of charging process before the PCM temperature reaches the melting point. This confirms that conduction dominates the heat transfer during this initial charging period and there is no significant difference between the two models. Once the PCM temperature reaches the melting point, the combined conduction-convection model can still predict the PCM temperature accurately while the pure

conduction model cannot. This change is mainly caused by natural convection. As soon as the PCM melts, a thin layer of liquid PCM is formed near the HTF wall. The heat transfer is dominated by natural convection, which speeds up the melting of the PCM. Liquid PCM rises up and the natural convection is stronger in the upper part than the lower part. Therefore, the PCM temperature in the upper part is higher than that in the lower part as evidenced by the PCM temperatures at point A and B in Fig. 3.4. The experimental results show that the time taken for all the PCM to reach 358 K is 6.5 hrs. This time is almost the same as the simulated total charging time using the combined conduction-convection model; in contrast, it takes about 28 hours using the pure conduction model. The above comparison results indicate that the charging process is mainly controlled by the natural convection and that conduction almost becomes negligible. Therefore, the combined conduction-convection model can better describe the heat transfer in the PCMs in comparison to the pure conduction model. Heat is transferred to the solid PCM initially by conduction and then by natural convection as the solid PCM melts. Since the sensible heat is much smaller than the latent heat, conduction is less significant and the natural convection is the major heat transfer mechanism during the charging process.

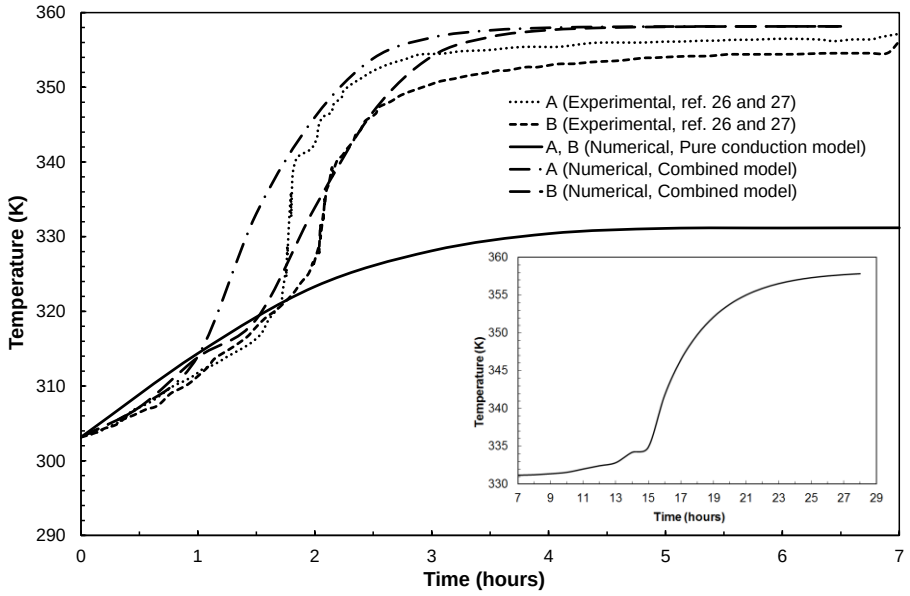

Fig. 3.4 Comparison of the PCM temperature variation during charging process (inserted picture shows the PCM temperature after 7 hour obtained from the pure conduction model).

3.5.2. Discharging process

Fig. 3.5a and 3.5b show contours of temperature and liquid fraction in the PCM for the pure conduction model during a discharging process. Once again, the temperature in the axial direction does not show significant difference in Fig. 3.6a since the total heat transfer rate from the outer surface of the inner tube to the inner surface of the cylinder is almost the same along the vertical. Therefore, there is little difference between the solid region in axial direction of the cylinder and the PCM solidified in the radial direction as shown in Fig. 5b. All the PCM is solidified within 9 hours and it takes another 4 hours for all PCM temperatures to drop to 303 K due to low temperature difference between the cold HTF and the solid PCM. Figs 3.6a and 3.6b show contours of temperature and liquid fraction during a discharging process using the combined conduction-convection model. As shown in Fig. 3.6a, in comparison to the pure conduction model, the PCM temperature drops much faster from the initial temperature to freezing point due to convection in the liquid PCM. Due to the buoyancy, the liquid PCM rises and the PCM temperature slightly varies along the axial direction. However, this temperature variation in the axial direction during the solidification process is not as large as that observed in the charging process, which implies that solidification front moves mostly in the radial direction as shown in Fig. 3.6b. As the solidification front moves outward, the rate of heat transfer is slowed down by increasing the thickness of solid PCM and hence the conduction thermal resistance. That is why, according to the experimental data and numerical simulations, the observed discharging is much slower than charging.

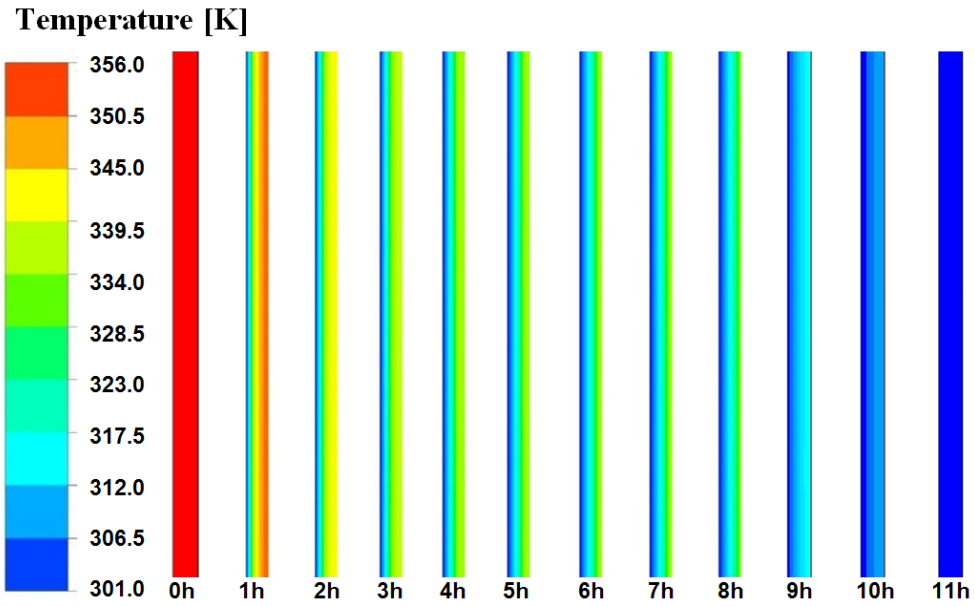

Fig. 3.5a Contours of temperature using the pure conduction model during the discharging process.

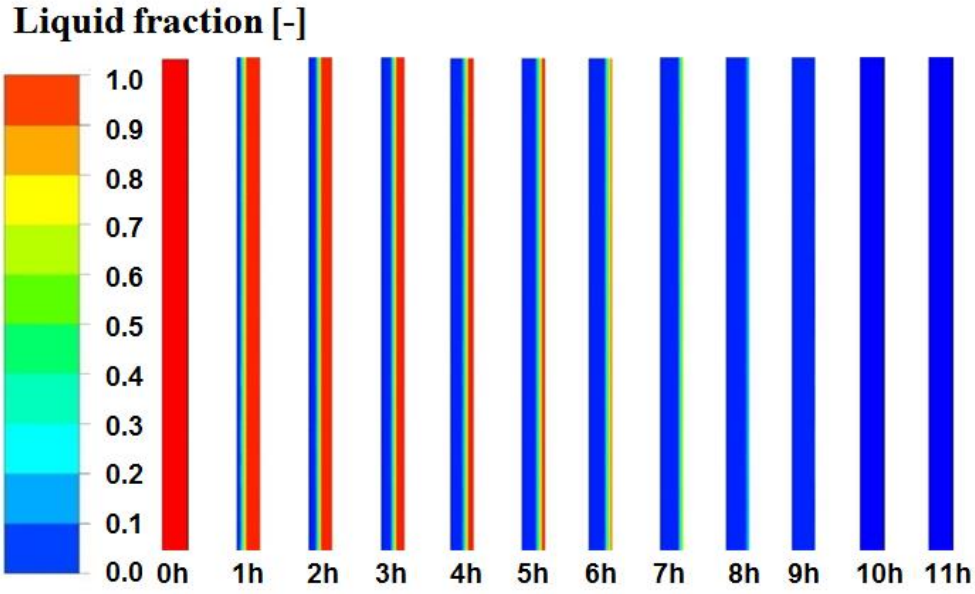

Fig. 3.5b Contours of liquid fraction using the pure conduction model during the discharging process.

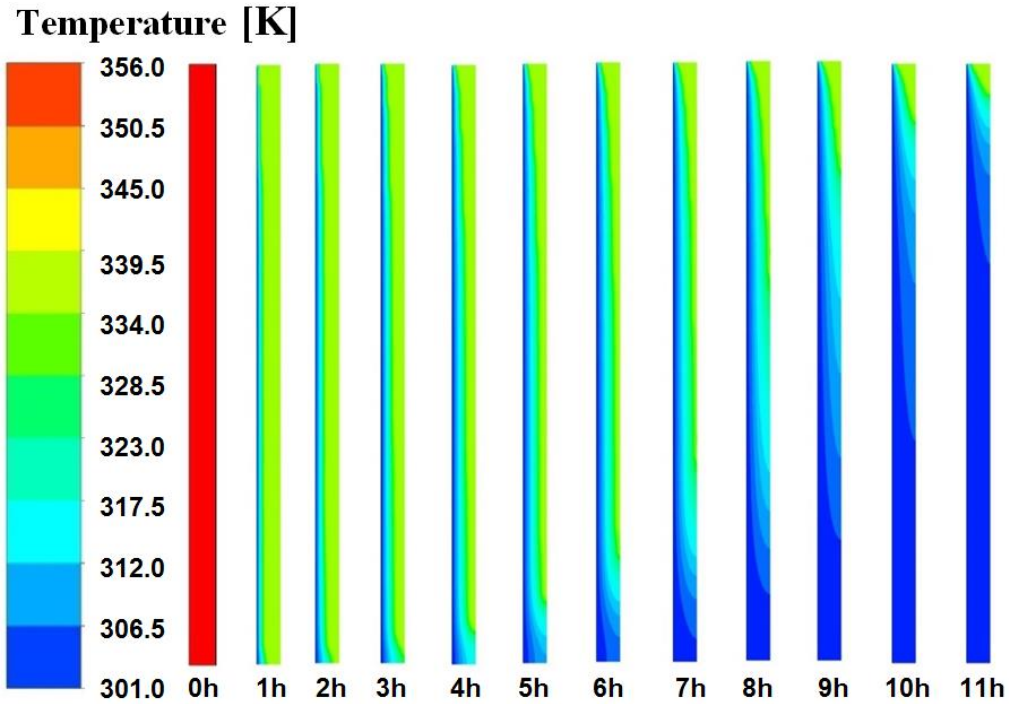

Fig. 3.6a Contours of temperature using the combined conduction-convection model during the discharging process.

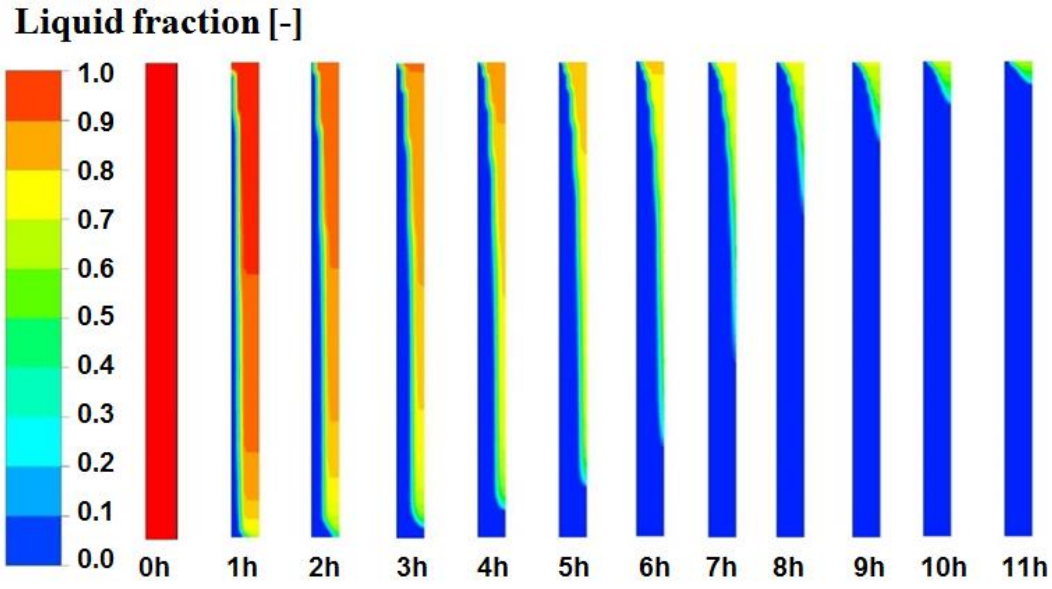

Fig. 6b Contour of liquid fraction using the combined conduction-convection model during the discharging process.

Fig. 3.7 shows a comparison between the experimental and simulated PCM temperatures during a discharging process. At the beginning, the experimental data shows that the liquid PCM temperature drops very fast at the beginning of the discharging process until it reaches

the freezing point of PCM (about 330 K). However, the simulated PCM temperature using the pure conduction model is higher than the experimental results during this period. In contrast, the predicted temperatures using combined conduction-convection model agree well with the experimental data. This demonstrates that natural convection plays a major role in the liquid phase PCMs during this period. Due to natural convection, the sensible form of thermal energy in the liquid PCM is depleted very quickly and the PCM temperature of the whole cylinder drops very fast. No PCM is solidified before the temperature lowers to the freezing point.

After the PCM temperature lowers to the freezing point, the PCM closer to the inner tube surface starts to solidify. The heat transfer in the solidified PCM around the inner tube, then changes in conduction which becomes the dominant heat transfer in the PCM storage system during the solidification process due to the low thermal conductivity. The total solidification time of the PCM is the same for the two simulation models and experiment. It takes approximately 13 hours for the PCM temperature to drop from 353 K to 303 K during a discharging process. This implies that the conduction heat transfer dominates the energy transfer during the whole discharging process, although the convective heat transfer is involved at the beginning.

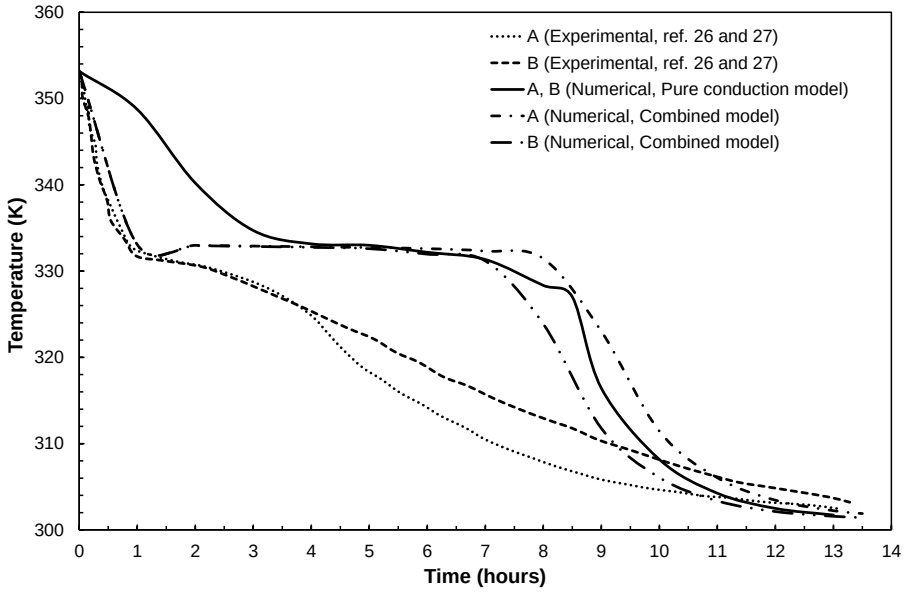

Fig. 3.7 Comparison of the PCM temperature variation during the discharging process.

Another interesting observation is that the PCM temperature during the experiment does not show a constant temperature solidification process. The simulated results clearly show the constant temperature for quite some time at the freezing point when the PCM temperature drops to the solidification temperature. Energy is transferred from the solid PCM to the solid/liquid PCM interface and the temperature of mushy zones remains constant which attributes to the large latent heat of the PCM. This finding is not discussed in the literature [26, 27].

Fig. 3.8 shows the variation of the energy stored fraction with time during both charging and discharging processes. The energy stored fraction is defined as the ratio of energy stored in the system at a given point in time to the maximum possible stored energy during charging and discharging processes. It is seen that during charging process, the energy stored fraction calculated from the combined model is much higher than that obtained from the pure conduction model. This further indicates that the convection heat transfer plays a significant role in the charging process. However, the energy stored fraction during the discharging process does not show significant differences between the two models. This is mainly because the heat transfer in the PCM during the discharging process is dominated by the thermal conduction. The effect of convection on the discharging process is negligible.

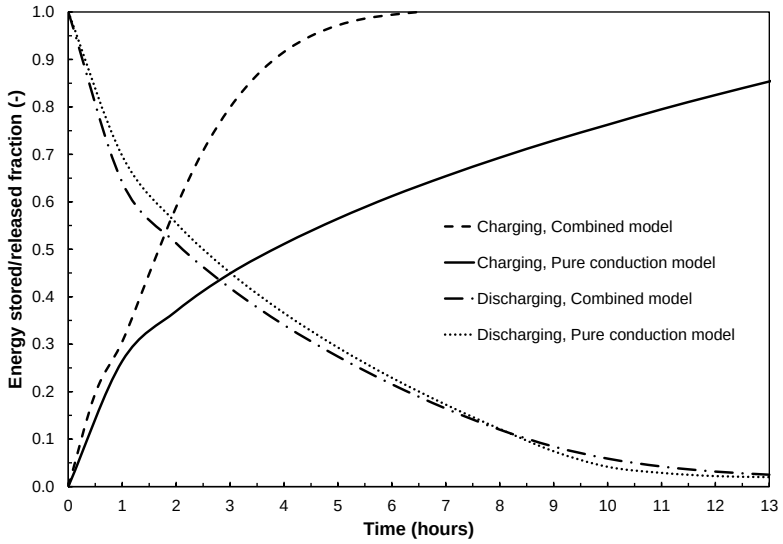

Fig. 3.8 Variation of the energy stored/released fraction with time during the charging and the discharging processes.

3.6. Conclusion

In this chapter, the heat transfer mechanism inside a vertical shell and tube LHTES unit was studied using a pure conduction and a combined conduction-convection model. The comparison results showed that the predicted results obtained from the combined model agreed well with the experimental data. This indicated that the combined model can better describe the thermal behavior of the PCM than the pure conduction model. The analyses show that natural convection is the dominant mode of heat transfer in the PCM in the charging process, while the heat transfer in the discharging process is dominated by conduction.

3.6. References

[1] Hu H, Argyropoulos SA. Mathematical modelling of solidification and melting: a review. Modelling and Simulation in Materials Science and Engineering. 1996;4:371.

[2] Zalba B, Marín JM, Cabeza LF, Mehling H. Review on thermal energy storage with phase change: materials, heat transfer analysis and applications. Applied Thermal Engineering. 2003;23:251-83.

[3] Sharma A, Tyagi V, Chen C, Buddhi D. Review on thermal energy storage with phase change materials and applications. Renewable and Sustainable Energy Reviews. 2009;13:318-45.

[4] Liu S, Li Y, Zhang Y. Mathematical solutions and numerical models employed for the investigations of PCMs′ phase transformations. Renewable and Sustainable Energy Reviews. 2014;33:659-74.

[5] Silva PD, Gonçalves LC, Pires L. Transient behaviour of a latent-heat thermal-energy store: numerical and experimental studies. Applied Energy. 2002;73:83-98.

[6] Tan Z, Lim K, Khoo BC. An adaptive mesh redistribution method for the incompressible mixture flows using phase-field model. Journal of Computational Physics. 2007;225:1137-58.

[7] Mackenzie J, Robertson M. A moving mesh method for the solution of the one-dimensional phase-field equations. Journal of Computational Physics. 2002;181:526-44.

[8] Sparrow EM, Patankar SV, Ramadhyani S. Analysis of Melting in the Presence of Natural Convection in the Melt Region. Journal of Heat Transfer. 1977;99:520-6.

[9] Yao LS, Chen FF. Effects of Natural Convection in the Melted Region Around a Heated Horizontal Cylinder. Journal of Heat Transfer. 1980;102:667-72.

[10] Hasan A. Phase change material energy storage system employing palmitic acid. Solar Energy. 1994;52:143-54.

[11] Lacroix M, Duong T. Experimental improvements of heat transfer in a latent heat thermal energy storage unit with embedded heat sources. Energy Conversion and Management. 1998;39:703-16.

[12] Velraj R, Seeniraj R, Hafner B, Faber C, Schwarzer K. Heat transfer enhancement in a latent heat storage system. Solar Energy. 1999;65:171-80.

[13] Buddhi D, Bansal N, Sawhney R, Sodha M. Solar thermal storage systems using phase change materials. International Journal of Energy Research. 1988;12:547-55.

[14] Yinping Z, Yi J. A simple method, the-history method, of determining the heat of fusion, specific heat and thermal conductivity of phase-change materials. Measurement Science and Technology. 1999;10:201-6.

[15] J. M. Khodadadi and Y. Zhang, Effect of buoyancy-driven convection on melting within spherical containers, International Journal of Heat and Mass Transfer, 2001, 44 (8), 1605-1618.

[16] F. L. Tan, S. F. Hosseinizadeh, J. M. Khodadadi, L. Fan, Experimental and computational study of constrained melting of phase change materials (PCM) inside a spherical capsule, International Journal of Heat and Mass Transfer, 2009, 52 (15-16), 3464-3472.

[17] D. B. Khillarkar, Z. X. Gong, A. S. Mujumdar, Melting of a phase change material in concentric horizontal annuli of a arbitrary cross-section, Applied Thermal Engineering, 2000, 20 (10), 893-912.

[18] A. R. Darzi, M. Farhadi, K. Sedighi, Numerical study of melting inside concentric and eccentric horizontal annulus, Applied Mathematical Modelling, 2012, 36 (9), 4080-4086.

[19] M. J. Hosseini, A. A. Ranjbar, K. Sedighi, M. Rahimi, A combined experimental and computational study on the melting behaviour of a medium temperature phase change storage material inside shell and tube heat exchanger, International Communications in Heat and Mass Transfer, 2012, 39 (9), 1416-1424.

[20] M. J. Hosseini, M. Rahimi, R. Bahrampoury, Experimental and computational evalution of a shell and tube heat exchanger as a PCM thermal storage system, International Communications in Heat and Mass Transfer, 2014, 50, 128-136.

[21] A. Sari and K. Kaygusuz, Thermal and heat transfer characteristics in a latent heat storage system using lauric acid, Energy Conversion and Management, 2002, 43 (18), 2493-2507.

[22] R. E. Murray and D. Groulx, Experimental study of the phase change and energy characteristics inside a cylindrical latent heat energy storage system: Part 1 consecutive charging and discharging, Renewable Energy, 2014, 62, 571-581.

[23] R. E. Murray and D. Groulx, Experimental study of the phase change and energy characteristics inside a cylindrical latent heat energy storage system: Part 2 simultaneous charging and discharging, Renewable Energy, 2014, 63, 724-734.

[24] B. J. Jones, D. Sun, S. Krishnan, S. V. Garimella, Experimental and numerical study of melting in a cylinder, International Journal of Heat and Mass Transfer, 2006, 49 (15-16), 2724-2738.

[25] H. Shmueli, G. Ziskind, R. Letan, Melting in a vertical cylindrical tube: Numerical investigation and comparison with experiments, International Journal of Heat and Mass Transfer, 2010, 53 (19-20), 4082-4091.

[26] M. K. Rathod and J. Banerjee, Experimental investigations on latent heat storage unit using paraffin wax as phase change material, Experimental Heat Transfer: A Journal of Thermal Energy Generation, Transport, Storage, and Conversion, 2014, 27 (1).

[27] M. K. Rathod and J. Banerjee, Thermal performance enhancement of shell and tube latent heat storage unit using longitudinal fins, Applied Thermal Engineering, 2015, 75, 1084-1092.

[28] A. A. Al-Abidi, S. B. Mat, K. Sopian, M. Y. Sulaiman, A. T. Mohammad, CFD applications for latent heat thermal energy storage: a review, Renewable and Sustainable Energy Reviews, 2013, 20, 353-363.

[29] Y. Dutil, D. R. Rousse, N. B. Salah, S. Lassue, L. Zalewski, A review on phase change materials: Mathematical modelling and simulations, Renewable and Sustainable Energy Reviews, 2011, 15 (1), 112-130.

[30] T. L. Bergman, A. S. Lavine, F. P. Incropera, D. P. Dewitt, Fundamentals of heat and mass transfer, 7th Edition, John Wiley & Sons, 2011.

Chapter4: The effect system orientation on heat transfer mechanism in a latent heat thermal energy unit

4.1. Chapter summary

In this chapter, thermal behaviour in a vertical and horizontal shell-and-tube energy storage system using phase change materials (PCMs) is investigated and compared using a combined conduction and convection heat transfer model. The model is first evaluated using published experimental data available in literature and then used to study the temperature variation, solid-liquid interface, phase distribution, total melting and solidification time during charging and discharging processes of PCMs. The simulated results show that during the charging process for the horizontal orientation, convective heat transfer has a strong effect on melting of the upper part of the solid PCM and is less significant during melting of the lower half of the solid PCM. However, in the vertical orientation, convective heat transfer is the same active during the entire charging process. In the discharging process, the thermal behavior does not show any difference between horizontal and vertical systems. The results indicate that the horizontal orientation has superior thermal performance during charging and in particular during part-load energy charging. The results also show that increasing the hot heat transfer fluid (HTF) inlet temperature substantially reduces the total charging time for both orientations. However, increasing the flow rate does not greatly affect the charging and discharging processes.

This research contained within this chapter has been published as: Saeid Seddegh, Xiaolin Wang, Alan D. Henderson. "A comparative study of thermal behaviour of a horizontal and vertical shell-and-tube energy storage using phase change materials", Applied Thermal Engineering 93, PP. 348-358, ELSEVIER, 2016.

4.2. Introduction

One solution to the problem of low thermal conductivity in PCMs is to improve heat transfer in the PCM unit which can be achieved using different heat exchanger configurations [1]. Much research on latent heat energy storage has been conducted theoretically. Zivkovic and Fuji [2] numerically compared the melting time of the isothermal phase change of PCMs encapsulated in rectangular and cylindrical containers. The rectangular container was found to require half of the melting time of the cylindrical container for an equal volume and heat transfer area between the heat transfer fluid and the container wall. Vyshak and Jilani [3] theoretically conducted a comparative study of the total melting time of PCMs packed with three containers of different geometric configurations: rectangular, cylindrical and shell-and-tube. It was concluded that the shell-and-tube vessel took the least time for storing an equal amount of energy, and this geometric effect was more pronounced with an increase in the mass of the PCMs. Furthermore, Mosaffa et al. [4] performed an approximate analytical study to compare the solidification time of the PCMs inside a shell-and-tube and rectangular. The results indicated that the PCMs solidified more quickly in the shell and tube storage. Agyenim et al. [5] reviewed the development of latent heat thermal energy storage systems. The review examined the geometry and configurations of PCM containers and concluded that the most intensely studied LHTES unit was the shell-and-tube energy storage system.

Esen et al. [6] developed a theoretical model to predict the heat transfer between the heat transfer fluid (HTF) and PCM in two different shell-and-tube configurations: the PCMs were packed inside the tube and the HTF flowed parallel to it on the shell side and vice versa. It was

found that the later configuration could store much more energy than the other. He and Zhang [7] presented a theoretical and experimental analysis on the thermal performance of a shell-and-tube heat exchanger applied at a high temperature application. The effect of tube length, HTF inlet temperature, mass flow rate and the thickness of phase change material on the heat transfer performance of the unit was investigated. Ismail and his collaborators developed a convection based model for a PCM vertical storage unit [8, 9]. The effect of the geometrical and operational parameters on the solid-liquid interface, stream function, energy stored and melt mass fraction was investigated. The numerical solution was further extended to analyse the phase change problem around a horizontal cylinder in the presence of natural convection in the melt region [10, 11]. The numerical predictions demonstrated the effects of Rayleigh and Stefan numbers as well as the wall temperature at the time for complete fusion and total melt volume. Ismail and Jesus [12, 13] incorporated the interface immobilization technique and the finite volume method for the solution of the solidification of PCM around a cold cylinder considering pure conduction as the heat transfer mechanism. Nagano et al. [14] studied a mixture of magnesium nitrate hexahydrate as a base material and magnesium chloride hexahydrate as an additive to store the energy at temperatures of 60 - 90 ºC using a heat storage tank with a simple vertical heat exchange unit. The results showed that the effective use of the phase change temperature region resulted in an available enthalpy of 2 - 2.5 times of the equivalent sensible heat storage in water. Akgün et al. [15] experimentally analysed the latent heat thermal energy storage system using the shell-and-tube heat exchanger with different paraffin-based PCMs. Aldine and Qarnia [16] numerically investigate the thermal behaviour of a shell-and-tube heat storage unit using PCMs with a low melting temperature (27.7 ºC and 50 ºC) and examined the impact of HTF inlet temperature and mass flow rate on the thermal performance of the storage unit. Agyenim et al. [17] further experimentally compared a shell-and-tube configuration with one heat transfer tube, and a unit with multi-tubes. The results

showed that the multi-tube configuration could result in strong convective heat transfer in the PCMs. Shmueli et al. [18] numerically investigated melting of a PCM in a vertical cylindrical tube and compared the results with experimental data. It revealed that the dominant heat transfer mechanism in the PCM is natural convection. More recently, Hosseini et al. [19, 20] experimentally and computationally studied the thermal behaviour and heat transfer characteristics of a medium temperature PCM in a shell-and-tube heat exchanger.

As reviewed by Liu et al. [21], many mathematical solutions have been employed to investigate the PCM phase transformation in the latent heat thermal energy storage systems. However, very few studies have reported the effect of the vertical or horizontal orientation of the shell-and-tube heat exchanger on the thermal behaviour of PCMs in the storage unit. Hasan [22, 23] conducted an experimental study on a shell-in-tube heat exchanger storage system where the PCM was in the tube and the water was on the shell side. It was concluded that a faster phase transition was realized by placing the heat exchanger in a horizontal position rather than a vertical one. Sari and Kaygusuz [24] claimed the similar findings in a shell-and- copper tube heat storage unit with PCM in the shell side and water in the tube. However, there was no detailed discussion and evidence presented in theses literature.

In this chapter, the thermal behaviour in the horizontal and vertical shell-and-tube heat energy storage units is investigated and compared using a combined convection and conduction model [25]. The simulation results are validated using published data in the literature [19, 20]. Then the thermal behaviour and heat transfer characteristics of the two systems during charging and discharging processes are studied and compared. The effect of key parameters including the HTF inlet temperature and flow rate on the storage system performance in both horizontal and vertical heat storage units is examined during melting and solidification of the PCM.

4.3. System description

Fig. 4.1 shows the schematic drawing of the studied shell-and-tube LHTES unit which consists of two concentric tubes with the PCM in the annulus and HTF in the tube. For model validation purpose, the dimensions of the system are chosen to be the same as the horizontal shell-and-tube heat exchanger experimentally studied by Hosseini et al. [19, 20]. The inner diameter of the HTF tube is 0.022 m, the diameter of the shell is 0.085 m and the height of the system is 1 m. Water is used as the HTF, which is circulated through the inner tube. The shell side is filled with paraffin wax (RT 50) as the PCM and its thermal properties are shown in Table 1. During the charging process, constant temperature hot water is circulated through the inner tube while the constant temperature cold water is circulated through the inner tube during the discharging process. Although the specific dimension of the LHTES unit is chosen in this study, the findings are valid for shell-and-tube LHTES units with different dimensions and configurations since the thermo-fluid process involving convection, conduction and phase change is similar in shell-and-tube LHTES units.

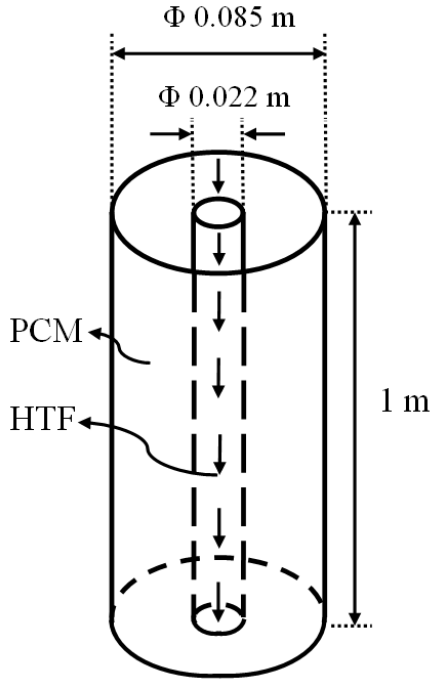

Fig. 4.1 Schematic drawing of the shell-and-tube storage system.

Table 4.1: Thermophysical properties

PCM	Melting Temperature (K)	Latent heat of fusion (kJ/kg)	Density (kg/m^3)		Specific heat (J/kg-K)	Thermal conductivity (W/mK)	Thermal expansion coefficient (1/K)
			Solid	Liquid	2000	0.2	0.0006
Paraffin wax (RT50)	318-324	168	880	760			
Heat transfer fluid (HTF)	**Charging temperature (K)**	**Discharging temperature (K)**	**Density (kg/m^3)**		**Specific heat (J/kg-K)**	**Thermal conductivity (W/m-K)**	
Water	358	301	998		4183	0.58	

4.3. Numerical approach

The thermo-fluid processes in the phase change energy storage system involve natural convection, conduction and phase change, which are similar in the horizontal and vertical shell-and-tube storage systems during the charging and discharging processes. In this study, the enthalpy method is applied due to its advantages: (i) the governing equations are similar to the single-phase equation; (ii) no explicit conditions are needed to be satisfied at the solid-liquid interface; (iii) the enthalpy formulation involves the solution within a mushy zone, involving both solid and liquid materials, between the two standard phases; and (iv) the phase change problem can be solved more easily [27]. These advantages ensure that the enthalpy method can easily capture the thermal behaviour of the horizontal and vertical shell-and-tube energy storage systems during the charging and discharging processes.

4.3.1. Numerical model

In the enthalpy method, the governing equation for energy conservation is the same for both the solid and liquid phases. The solid-liquid interface is indicated by a mushy zone, which separates the two phases [27-29]. Energy conservation is expressed in terms of total volumetric enthalpy and temperature for constant thermo-physical properties as

$$\frac{\partial \rho H}{\partial t} + \nabla \cdot \left(\rho v H \right) = \nabla \cdot \left(k \nabla T \right) + S \qquad (1)$$

where ρ is PCM density, v is velocity, S is a source term, and H is the total volumetric enthalpy which is the sum of sensible and latent heats as Eq. (2 and 3), and h_{ref} is the sensible heat at the reference temperature, T_{ref} :

$$H = h + fL \tag{2}$$

$$h = h_{ref} + \int_{T_{ref}}^{T} c_p dT \tag{3}$$

where c_p is the specific heat and f refers to liquid fraction that indicates the fraction of a cell volume in liquid form and is associated with each cell in the domain given by Eq. (4). The mushy zone is a region wherein the liquid fraction lies between 0 and 1.

$$f = \begin{cases} 0 & T < T_{Solidus} \\ \dfrac{T - T_{Solidus}}{T_{Liquidus} - T_{Solidus}} & T_{Solidus} \le T \le T_{Liquidus} \\ 1 & T > T_{Liquidus} \end{cases} \tag{4}$$

Applying Eqs. (2-4) into Eq. (1), the energy equation is written as

$$\frac{\partial \rho h}{\partial t} + \nabla \cdot (\rho v h) = \nabla \cdot (k \nabla T) - \frac{\partial \rho f L}{\partial t} - \nabla \cdot (\rho v f L) + S \tag{5}$$

Where k is thermal conductivity and L is latent heat of fusion. In order to account for the effect of natural convection melting from the density change, the momentum equation is written as [27].

$$\frac{\partial \rho v}{\partial t} + \nabla \cdot (\rho v v) = -\nabla P + \nabla \cdot (\mu \nabla v) + \rho g + \frac{(1 - f)^2}{f^3 + \varepsilon} v A_{mush} \tag{6}$$

where v is velocity, the term A_{mush} is a constant reflecting the mushy zone morphology which describes how steeply the velocity is reduced to zero when the material solidifies. The constant ε is a small number to prevent division by zero.

The Boussinesq approximation is used [27-29] due to small density variation. The model assumes the fluid density is constant in all terms of the momentum equation except the body

force term, and it is modelled based on a reference density (ρ_0) and temperature (T_0), and the volumetric expansion coefficient (β). Then the momentum equation is written as

$$\frac{\partial \rho_0 v}{\partial t} + \nabla \cdot (\rho_0 v v) = -\nabla P + \nabla \cdot (\mu \nabla v) + (\rho - \rho_0) g + \frac{(1-f)^2}{f^3 + \varepsilon} v A_{mush} \quad (7)$$

$$(\rho - \rho_0) g = -\rho_0 \beta (T - T_0) \quad (8)$$

The continuity is given as:

$$\frac{\partial \rho}{\partial t} + \nabla \cdot (\rho v) = 0 \quad (9)$$

The liquid fraction is computed each iteration at each cell in the domain based on enthalpy balance. The mushy zone is modelled as a ‘‘pseudo’’ porous medium in which the porosity decreases from 1 to 0 as the material solidifies. When the material has fully solidified in a cell, the porosity becomes zero, resulting in the drop of velocities to zero [26]. The following parameters were used in this simulation [27-29]: A_{mush} =10^5, ε =0.001, and T_{ref} = 298.15 K.

The computational study is performed using the Fluent application of the ANSYS 15 software. The solidification and melting models are studied by solving the Navier-Stokes equations for laminar flow using an enthalpy-porosity technique. The transient simulation with the pressure staggering option (PRESTO) scheme is used for the pressure correction equation, and a Coupled algorithm is used for pressure-velocity coupling [27-29]. A second order upwind scheme was used to solve the momentum and energy equations.

4.3.1.1 Boundary/Initial conditions

In this model, the boundary conditions on the outer wall surface, top and bottom ends are made adiabatic to simulate insulation. The boundary condition used for the inner surface of the pipe (HTF wall) is convective heat transfer which corresponds to the forced convection heat transfer from the HTF fluid, as was the case in the experimental study. The heat transfer coefficient can be calculated by [30, 31]:

$$h = Nu\frac{k}{D} \tag{10}$$

$$Nu = \frac{\left(\frac{f}{2}\right)\left(\mathrm{Re}_d - 1000\right)\mathrm{Pr}}{1+12.7\left(\frac{f}{2}\right)^{\frac{1}{2}}\left(\mathrm{Pr}^{\frac{2}{3}}-1\right)} \tag{11}$$

where Pr is Prandtl number, Re_d is the Reynolds number expressed by

$$\mathrm{Re}_d = \frac{4\dot{m}}{\pi D\mu} \tag{12}$$

f is the friction factor calculated as

$$f = \left(1.58\ln \mathrm{Re}_d - 3.28\right)^{-2} \tag{13}$$

The PCM is initially set to solid with a temperature of 293 K during the charging process and set to liquid with a temperature of 343 K in the discharging process. The HTF flow in the inner pipe is 1 L/min. The HTF temperature is 343 K for charging and 293 K for discharging.

4.3.1.2 Assumption

A combined conduction and natural convection heat transfer model is applied, and the following assumptions are made:

- Thermophysical properties of the materials are constant with temperature.
- The PCM motion in the liquid state is laminar, unsteady, and incompressible.
- Viscous dissipation is negligible.
- No viscous stress and convective flux at the pipe outlet.

4.4. Results and discussion

4.4.1. Model verification and validation

The model was verified to check the dependency on time steps and cell size prior to simulation. For the horizontal system, three mesh sizes: 3000, 6000, and 12000 cells; and three time-step sizes: 0.05 s, 0.1 s, and 0.2 s were examined. The model with 6000 cells and time step sizes of 0.05 s and 0.1 s produced a very similar variation in PCM average temperature. The results did not show significant change as the number of cells increases to 12000. As for the vertical system, three mesh sizes: 1200, 3600, and 8000 cells; and three time-step sizes: 0.05 s, 0.1 s, and 0.2 s were examined and the model with 3600 cells and time steps of the 0.05 s and 0.1 s produced a similar variation of PCM average temperature. Increasing the number of elements to 8000 did not show significant change in the results. Therefore, in order to save the computational time, a mesh of 6000 cells for the horizontal system and 3600 cells in the vertical system and a time step size of 0.1 s were found to be sufficient to achieve the predetermined convergence level of the energy equation ($1E^{-6}$).

The simulation was first performed on a horizontal shell-and-tube heat exchanger energy storage unit which is the same as that studied in literature [19, 20]. Fig. 4.2 compares the simulated PCM average temperature and liquid fraction with the experimental data reported in literature [19, 20] during a charging process under the same conditions. The HTF flow rate is 1 L/min and the HTF inlet temperature is 343 K. Both simulated average PCM temperature and liquid fraction during charging process shows good agreement with the experimental data. Using statistical analysis, the root mean square (RMS) of the relative average PCM temperature and liquid fraction deviation between the simulated and experimental data are 6.5% and 6%, respectively. This RMS value may be due to the measurement error. Due to the phase change, it was really difficult to accurately measure the average PCM temperature. The measurement

accuracy was not discussed in literature [19, 20]. However, the good agreement in the trend demonstrates that the model can be used to analyse the thermal behaviour and heat transfer characteristics of the shell-and-tube energy storage unit.

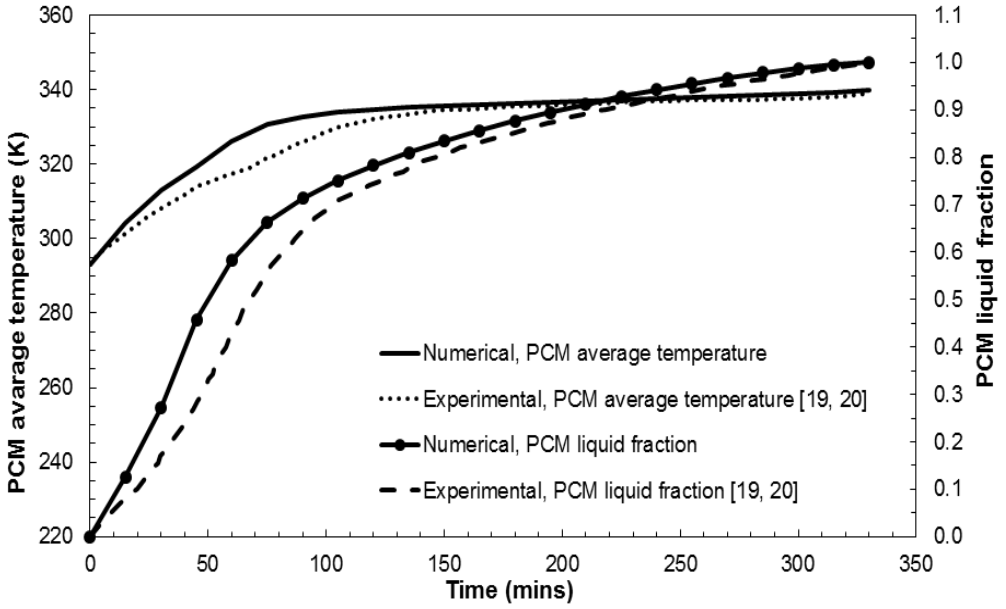

Fig. 4.2 Average PCM temperature and liquid fraction in the horizontal system during the charging process.

4.4.2. Comparison of Horizontal and Vertical Orientations

The thermal behaviour and heat transfer characteristics of the horizontal and vertical LHTES systems during charging and discharging processes are investigated and compared in the following sections. The HTF flow rate and inlet temperature are 1 L/min and 343 K, respectively.

4.4.2.1 Charging process

Fig. 4.3a and 4.3b show the contours of PCM liquid fraction and temperature during a charging process in the horizontal LHTES units, respectively. In the horizontal system, the solid PCM around the HTF tube absorbs thermal energy from the hot HTF via the tube surface and starts melting when the temperature reaches the melting point. The melted liquid PCM forms a recirculation region normal to the tube direction and around the tube. The recirculation

induces a strong convective heat transfer between the liquid PCM and HTF tube, and between the solid and liquid PCM interface, which dominates the heat transfer in the PCM and expedites melting of the PCM. Initially, the rate of PCM melting is very high. The liquid PCM rises directly upwards to the solid PCM above the tube due to buoyancy and results in a high melting rate as shown by the sharp temperature gradient near the solid interface in Fig. 4.3b. The liquid PCM rapidly fills the upper part of the energy storage unit as shown in the figure. Once the upper half of the energy storage unit is full of liquid PCM, the temperature in the liquid PCM becomes more uniform [32], reducing the strength of the convection. The temperature contours in Fig. 4.3b show that the liquid PCM begins to stratify in the region below the tube and solid PCM. The liquid temperature near the liquid-solid interface is relatively lower than that above the tube, further reducing the melting rate. The stratification is present long after all solid PCM has melted. This is shown in Fig. 4, where the slope of the PCM liquid faction curve shows that the rate of PCM melting is initially very high and then reduces at the time when the liquid PCM is full of the upper half of the horizontal energy storage unit.

In the vertical system, the contours of PCM liquid fraction and temperature during a charging process are shown in Fig. 4.3c and 4.3d, respectively. The solid PCM around the HTF tube absorbs thermal energy from the HTF via the tube surface and starts melting. Due to buoyancy, the liquid PCM rises up adjacent to the tube. This movement induces convective heat transfer between the liquid PCM and HTF tube surface, and between the solid and liquid PCM interface. The liquid PCM gradually fills the upper region of the vertical energy storage unit. However, the PCM always surrounds the vertical tube and the aforementioned movement exists throughout the entire charging process. The convective heat transfer is active throughout the whole melting process. The melting rate remains almost constant for the entire process as shown by the slope of the PCM liquid fraction curve in Fig. 4.4. The temperature contours in

Fig. 4.3d show that the stratification of the liquid phase does not occur as in melting for the horizontal case.

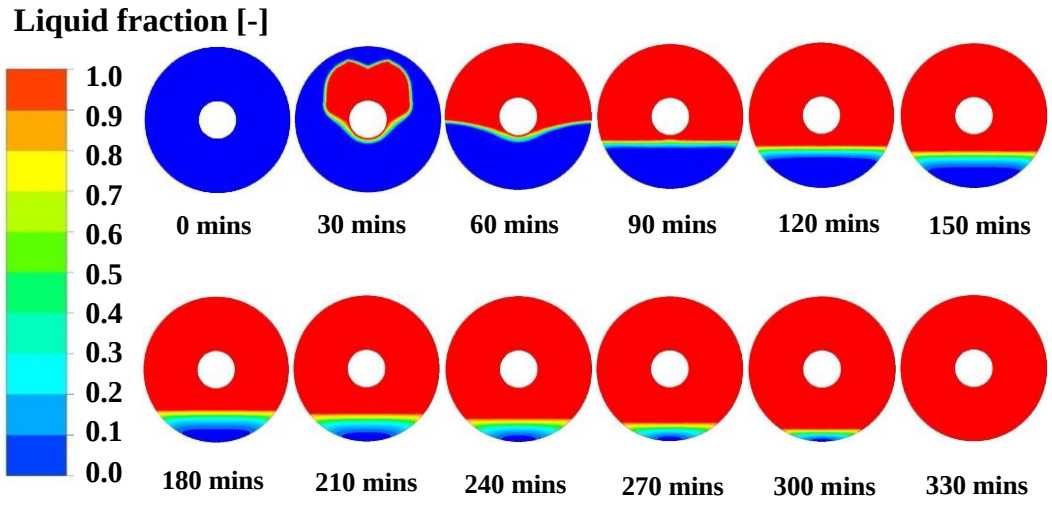

Fig. 4.3a Contours of PCM liquid fraction during charging process in a horizontal LHTES unit.

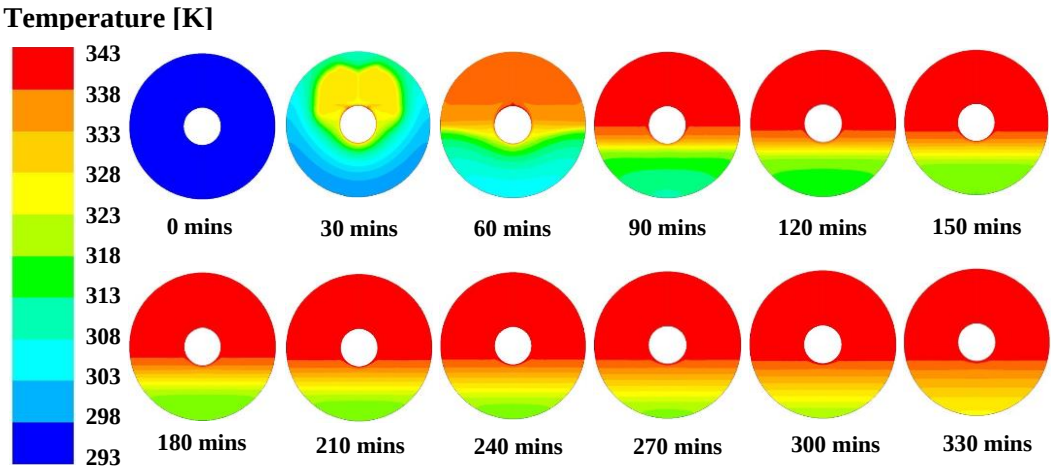

Fig. 4.3b Contours of PCM temperature during charging process in a horizontal LHTES unit.

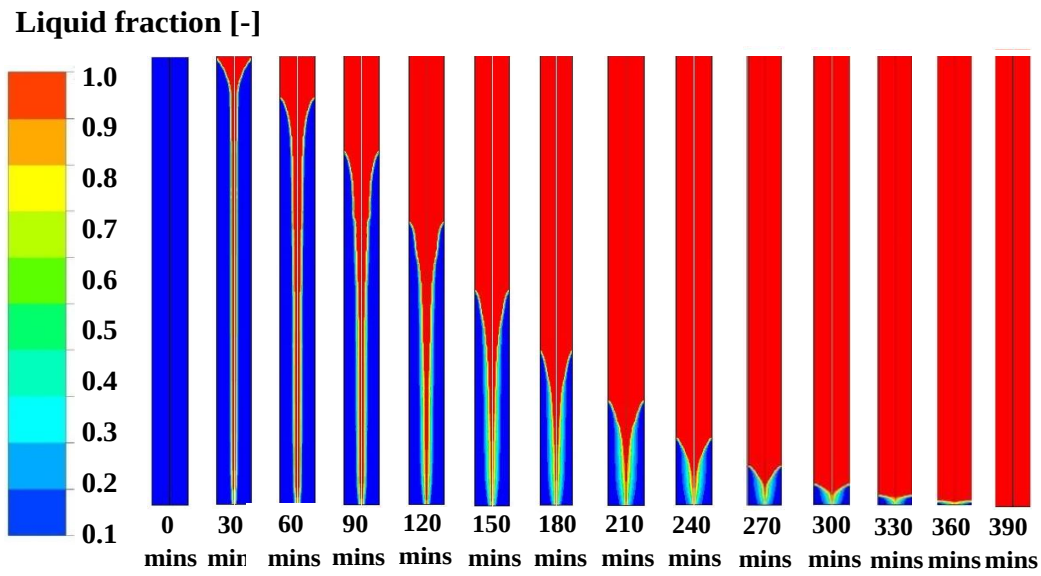

Fig. 4.3c Contours of PCM liquid fraction during charging process in a vertical LHTES unit.

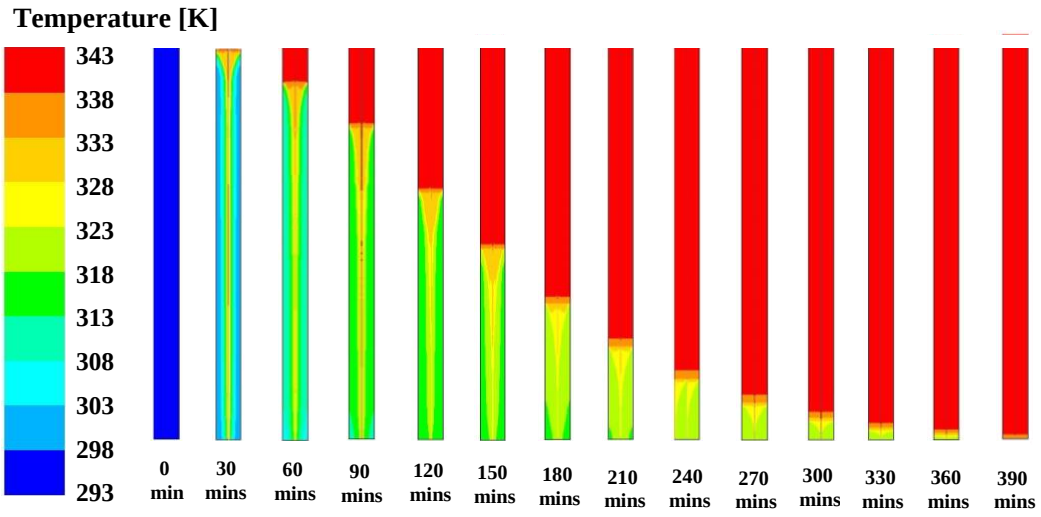

Fig. 4.3d Contours of PCM temperature during charging process in a vertical LHTES unit.

Fig. 4.4 shows a comparison of the average PCM temperature and liquid fraction during a charging process for the horizontal and vertical LHTES units. The average PCM temperature and liquid fraction in the horizontal unit remain higher than in the vertical unit for most of the charging cycle. The slope of the liquid fraction curve clearly shows that the melting rate of the PCM in the horizontal unit is higher than that in the vertical system while the upper part of the solid PCM is melting, and then it is reduced to less than the vertical system afterwards. This melting rate difference has been explained in the above session. In the horizontal system, once

PCM starts melting, the liquid PCM forms a recirculation region, which induces a strong convective heat transfer due to buoyancy. This recirculation region is along the axial direction. It is much larger than the recirculation region along the radial direction in the vertical unit. Hence the melting rate of the horizontal system is much higher than that in the vertical system initially. However, as the upper part PCM is fully melted, the recirculation in the horizontal system weakens due to small temperature difference in the liquid PCM and the liquid PCM begins to stratify in the region below the HTF tube and solid PCM. Hence the strength of convective heat transfer in the horizontal system reduces. In contrast, in the vertical system, the recirculation region remains the same during the whole charging process. As a result, the melting rate in the horizontal unit is reduced to lower than that in the vertical system in the second half of the charging process. This change in the melting rate indicates that the heat transfer in the horizontal storage system is more effective during the first half of PCM melting and less effective during the second half of PCM melting when compared with the vertical storage system. These results indicate that the horizontal system is more effective in the energy charging, in particular during the part-load operation in comparison to the vertical system.

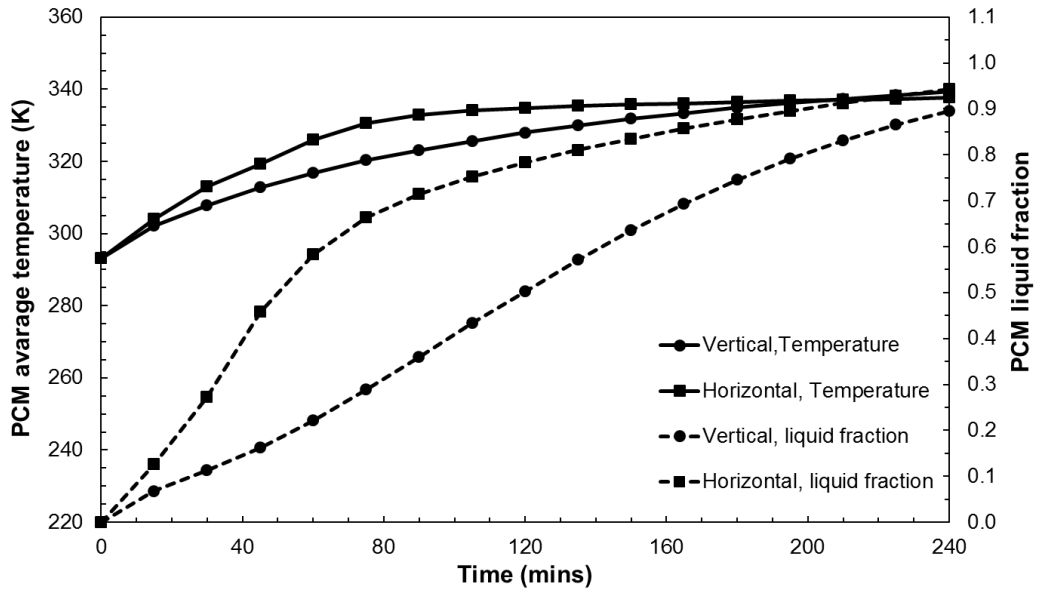

Fig. 4.4 PCM average temperature and liquid fraction in vertical and horizontal units during charging process.

4.4.2.1 Discharging process

Fig. 4.5 shows the contours of PCM liquid fraction during a discharging process for the horizontal and vertical orientation, respectively. At the beginning of the discharging process, natural convection in the liquid PCMs dominates heat transfer in the storage unit, which quickly removes the sensible heat of the PCM, dropping the temperature down to the freezing point in a very short time. Once the PCM surrounding the HTF tube is solidified, the solid PCM behaves as an insulation material due to its low thermal conductivity. The rate of heat transfer from the HTF to the PCM is slowed down. This rate decreases as the solidification front moves outward and the thickness of the solid PCM increases along the radial direction. Fig. 5 also shows that the liquid PCM moves up and solidification process is faster in the lower half of the shell-and-tube heat exchange. This movement is also due to buoyancy and the convective heat transfer between the solid and liquid phases. However, the thermal conductivity of the PCM is so low that the overall heat transfer is dominated by the thermal conduction in the solid phase between the HTF tube and solid/liquid interface. Over the discharging process, the heat transfer is dominated by the thermal conduction, which gives ample time for slow solidification. Further analysis shows that no significant difference is found in discharging process between the horizontal and vertical systems as shown in Fig. 4.6.

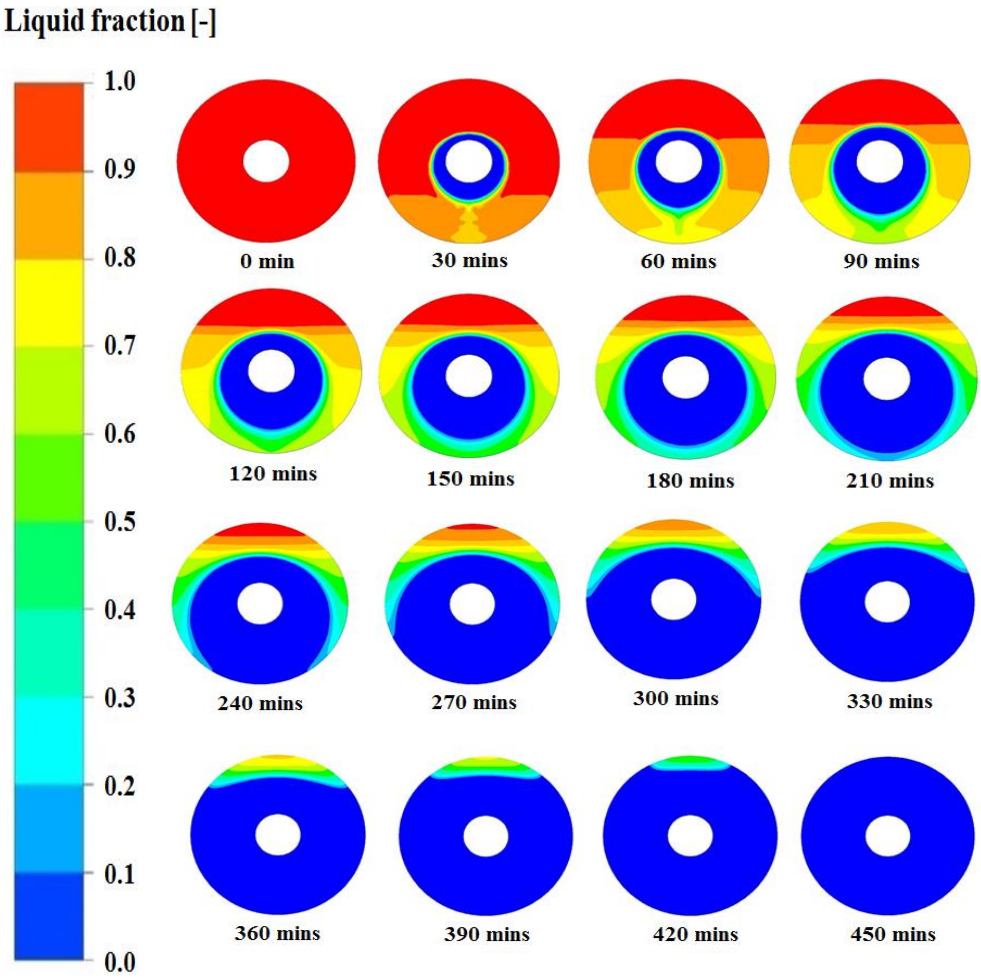

Fig. 4.5 Contours of liquid fraction during discharging process. a) horizontal system and b) vertical system.

A comparison of the average temperature and the liquid fraction of the PCM during a complete discharging process is shown in Fig. 4.6. It is observed that the average PCM temperature in both horizontal and vertical storage orientations is nearly the same during the entire process. The liquid fraction curve shows the same slope in the two systems, which indicates the same discharging rate found in the two systems. These findings are mainly due to the low thermal conductivity of the PCM, which slows down the solidification process. Once the PCM starts to solidify, the HTF tube is surrounded by the solid PCM. The heat transfer between the HTF and PCM is dominated by thermal conduction. As the solidification front moves outward, the thickness of the solid PCM around the HTF tube increases, which increases

the conduction thermal resistance and hence slows down the heat transfer rate in the discharging process. This phenomenon is almost the same in both horizontal and vertical systems. Therefore, the heat transfer in the horizontal and vertical units has similar effectiveness in the discharging process.

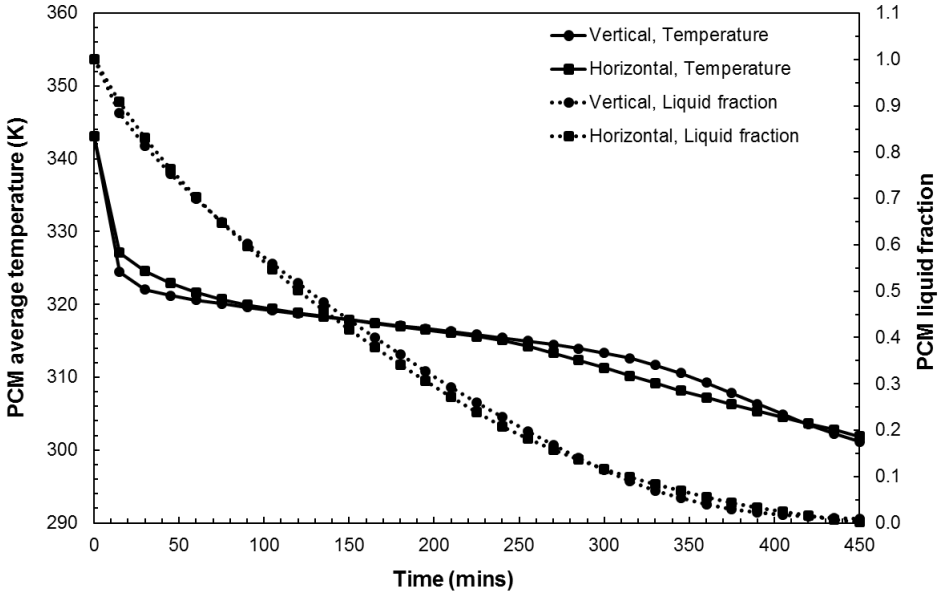

Fig. 4.6 PCM average temperature and liquid fraction in vertical and horizontal units during discharging process.

4.4.2.1 Energy storage fraction

Fig. 4.7 shows a comparison of the energy stored fraction in the horizontal and vertical systems during both charging and discharging processes. The energy stored fraction is defined as the ratio of energy stored in the system at a given point in a time to the maximum possible stored energy during charging and discharging processes. During the charging process, energy stored in the horizontal systems is faster than that in the vertical system, in particular during the first 100 minutes. As explained before, this is because the natural convective heat transfer in the horizontal system is more effective than that in the vertical system, particularly during the partial charging process. As a result, the energy charging in the horizontal system is faster than in the vertical system. The figure also indicates that the energy stored fraction during the

discharging process does not show significant differences between the two systems. This finding is mainly because the heat transfer in the PCM during the discharging process is dominated by the thermal conduction which has similar effectiveness in both horizontal and vertical systems.

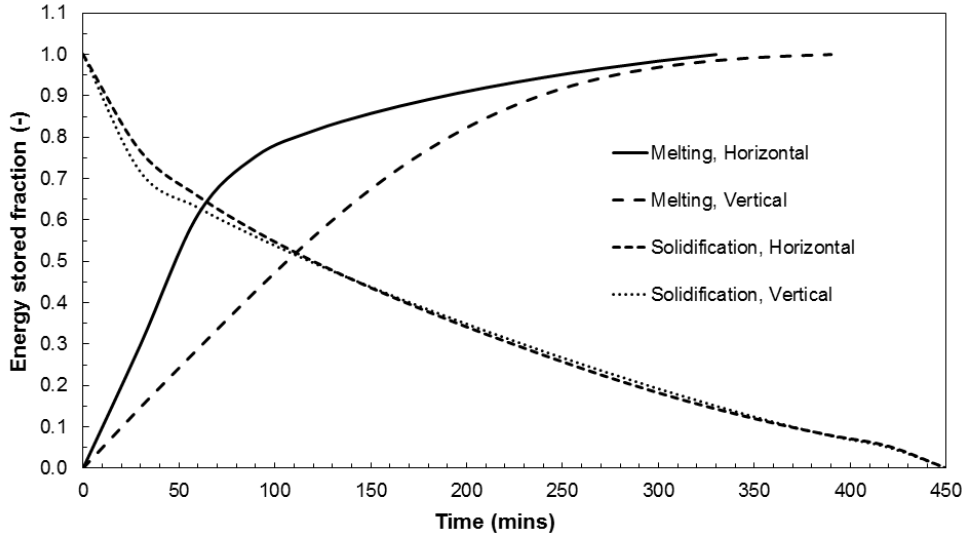

Fig. 4.7 Comparison of the energy stored fraction in the horizontal and vertical systems during charging and discharging processes.

4.4.3. Effect of important parameters

4.4.3.1 Effect of hot HTF inlet temperature

The effect of the hot HTF inlet temperature on the thermal behaviour of the horizontal and vertical units is investigated at three different temperatures: T=343K, 348K and 353K. In all cases, the constant hot HTF flow rate is 1 L/min. Fig. 4.8 shows the comparison of the liquid fraction of the PCM during complete melting. The total melting time is found to decrease in both horizontal and vertical LHTES units as the hot HTF inlet temperature increases. This decrease is due to high temperature gradient near the HTF tube which strengthens buoyancy and the convective heat transfer, and consequently the rate of energy transfer in the PCM increases. The figure also shows that the total melting time is decreased by 14% and 27% in

the horizontal system and by 12% and 27% in the vertical system, respectively, as the HTF temperature is increased from 343 K to 348 and then 353 K.

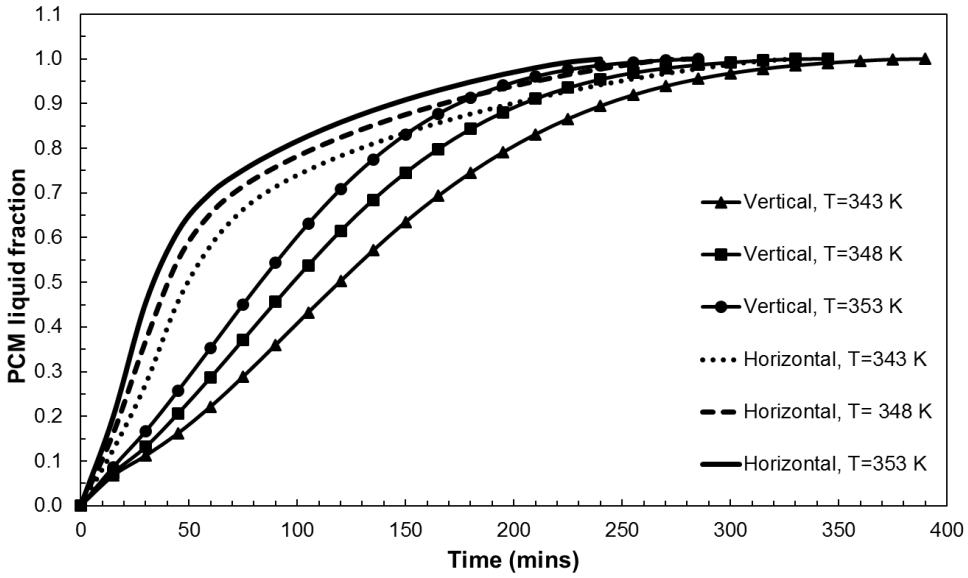

Fig. 4.8 PCM liquid fraction in vertical and horizontal units during the charging process at different HTF inlet temperatures.

4.4.3.2 Effect of hot HTF flow rate

Fig. 4.9 shows a comparison of the PCM liquid fraction during a complete charging process in the horizontal and vertical storage units under different hot HTF flow rates. The hot HTF inlet and the initial PCM temperatures are 343 K and 293 K, respectively. At all flow rates, the heat transfer in the horizontal system is slightly better for complete energy charging process and much more effective in the part-load energy storage process in comparison to the vertical system. However, for individual horizontal and vertical system, the increase of flow rate does not show significant changes in the total melting time during the charging process. This finding is consistent with the experimental findings reported in literature [19, 20]. It can be explained by the heat transfer mechanism. Heat transfer between the HTF and tube surface is forced convection which has much higher heat transfer coefficient in comparison to natural convection in the liquid PCM. During the charging process, heat transfer in both storage units is dominated by natural convection caused by buoyance. A change in the forced convective

heat transfer by increasing the flow rate does not enhance the heat transfer in the PCM which is dominated by natural convection. Therefore, increasing the HTF flow rate has little effect on the thermal behavior for either horizontal or vertical orientations.

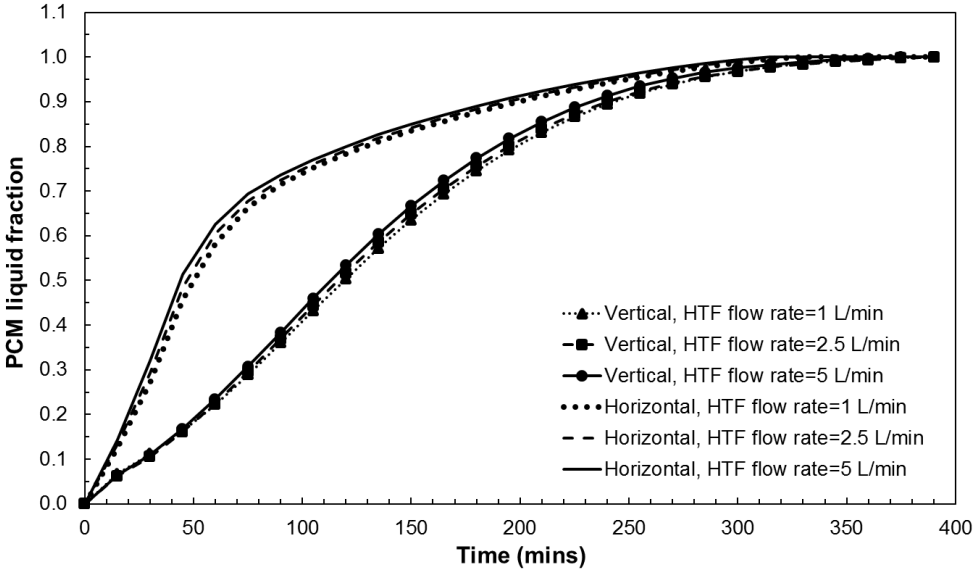

Fig. 4.9 PCM liquid fraction during charging with different HTF flow rates.

Fig. 4.10 shows a comparison of the PCM liquid fraction during a complete discharging process in the horizontal and vertical orientations at a cooling inlet temperature of 293 K and an initial PCM temperature of 343 K. The change in the cooling HTF flow rate does not show any significant effect on the heat transfer in the discharging process as evidenced by the liquid fraction at each solidification time. In the discharging process, heat transfer in both storage systems is dominated by thermal conduction which is much less effective than the forced convective heat transfer between the HTF and tube surfaces. A change in the forced convective heat transfer by varying the HTF flow rate does not alter the heat transfer rate in the PCM in the two systems.

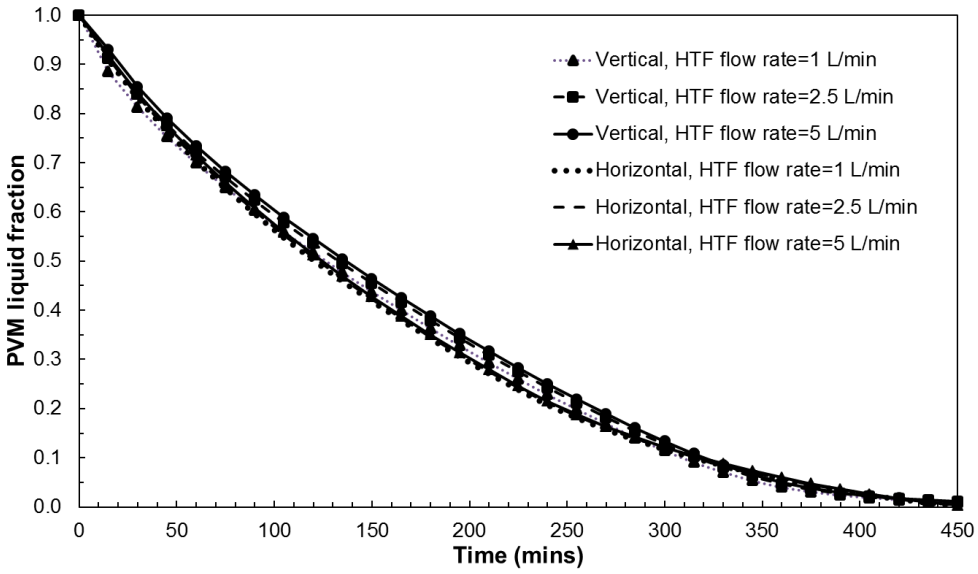

Fig. 4.10 PCM liquid fraction during discharging with different HTF flow rates.

4.5. Conclusion

In this chapter, thermal behavior and heat transfer characteristics in the horizontal and vertical shell-and-tube thermal energy storage systems were investigated and compared using a combined conduction and convection model. The predicted results were validated using the published experimental data. The conclusions are summarized below:

- During a charging process, the heat transfer in the horizontal unit is more effective while the upper half of PCM melts and less effective as the lower half of PCM melts. However, the effectiveness of heat transfer in the vertical unit is almost constant during the entire charging process. A comparison indicates that the horizontal energy storage system has better heat transfer performance, in particular during part-load energy charging.
- In the discharging process, thermal conduction dominates heat transfer in both horizontal and vertical energy storage units. Thermal behavior does not show any significant difference in the horizontal and vertical energy storage units.

- The hot HTF inlet temperature shows a large effect on heat transfer in both horizontal and vertical systems during the charging process. However, the HTF flow rate has little effect on both charging and discharging processes in the energy storage units.
- The geometry can alter the heat transfer performance and the effect of natural convection in the horizontal shell-and-tube LHTES system is significantly different from that in the vertical shell-and-tube LHTES

4.6. References

[1] Seddegh S, Wang X, Henderson AD, Xing Z. Solar domestic hot water systems using latent heat energy storage medium: A review. Renewable and Sustainable energy reviews. 2015;49:517-33.

[2] B. Zivkovic, I. Fujii, An analysis of isothermal phase change of phase change material within rectangular and cylindrical containers, Solar Energy 70 (1) (2001) 51-61.

[3] N.R. Vyshak, G. Jilani, Numerical analysis of latent heat thermal energy storage system, Energy conversion and management 48 (7) (2007) 2161-2168.

[4] A.H. Mosaffa, F. Talati, H.B. Tabrizi, M.A.Rosen, Analytical modeling of PCM solidification in a shell and tube finned thermal storage for air conditioning systems, Energy and Buildings 49 (2012) 356-361.

[5] F. Agyenim, N. Hewitt, P. Eames, M. Smyth, A review of materials, heat transfer and phase change problem formulation for latent heat thermal energy storage systems (LHTESS), Renewable and Sustainable Energy Reviews 14 (2) (2010) 615-628.

[6] M. Esen, A. Durmus, A. Durmus, Geometric design of solar-aided latent heat store depending on various parameters and phase change materials, Solar Energy 62 (1) (1998) 19-28.

[7] Q. He, W. Zhang, A study on latent heat storage exchangers with the high temperature phase change material, International Journal of Energy Research 25 (4) (2001) 331-341.

[8] K.A.R. Ismail, C.A. Melo, Convection based model for a PCM vertical storage unit, International Journal of Energy Research, 22 (1998) 1249-1265.

[9] K.A.R. Ismail, M.M. Abugderah, Performance of a thermal storage ystem of the vertical tube type, Energy Conversion and Management, 41(11) (2000) 1165-1190.

[10] K.A.R. Ismail, M.D.G.E. Da Silva, Numerical solution of the phase change problem around a horizontal cylinder in the presence of natural convection in the melt region, International Journal of Heat and Mass Transfer 46(10) (2003) 1791-1799.

[11] K.A.R. Ismail, M.D.G.E. Da Silva, Melting of PCM around a horizontal cylinder with constant surface temperature, International Journal of Thermal Science 42(12) (2003) 1145-1152.

[12] K.A.R. Ismail, A. B. De Jesus, Modeling and solution of the solidification problem of PCM around a cold cylinder, Numerical Heat Transfer, Part A (36) (1999) 95-114.

[13] K.A.R. Ismail, A. B. De Jesus, Parametric study of solidification of PCM around a cylinder for ice-bank applications, International Journal of Refrigeration 24(8) (2001) 809-822.

[14] K. Nagano, K. Ogawa, T. Mochida, K. Hayashi, H. Ogoshi, Performance of heat charge/discharge of magnesium nitrate hexahydrate and magnesium chloride hexahydrate mixture to a single vertical tube for a latent heat storage system, Applied Thermal Engineering 24 (2-3) (2004) 209-220.

[15] M. Akgun, O. Aydin, K. Kaygusuz, Thermal energy storage performance of paraffin in a novel tube in shell system, Applied Thermal Engineering 28 (5-6) (2008) 504-413.

[16] H.A. Adine, H.E. Qarnia, Numerical analysis of the thermal behaviour of a shell-and-tube heat storage unit using phase change materials, Applied Mathematical Modelling 33 (4) (2009) 2132-2144.

[17] F. Agyenim, P. Eames, M. Smyth, Heat transfer enhancement in medium temperature thermal energy storage system using a multitube heat transfer array, Renewable Energy 35 (1) (2010) 198-207.

[18] H. Shmueli, G. Ziskind, R. Letan, Melting in a vertical cylindrical tube: numerical investigation and comparison with experiments, International Journal of Heat and Mass Transfer 53 (19-20) (2010) 4082-4091.

[19] M.J. Hosseini, A.A. Ranjbar, K. Sedighi, M. Rahimi, A combined experimental and computational study on the melting behavior of a medium temperature phase change storage material inside shell and tube heat exchanger, International Communications in Heat and Mass Transfer 39 (9) (2012) 1416-1424.

[20] M.J. Hosseini, M. Rahimi, R. Bahrampoury, Experimental and computational evolution of a shell and tube heat exchanger as a PCM thermal storage system, International Communications in Heat and Mass Transfer 50 (2014) 128-136.

[21] S. Liu, Y. Li, Y. Zhang, Mathematical solutions and numerical models employed for the investigations of PCMs′ phase transformations, Renewable and Sustainable Energy Reviews 33 (2014) 659-674.

[22] A. Hasan, Thermal energy storage system with stearic acid as phase change material, Energy Conversion and Management 35 (10) (1994) 843-856.

[23] A. Hasan, Phase change material energy storage system employing palmitic acid, Solar Energy 52 (2) (1994) 143-154.

[24] A. Sari, K. Kaygusuz, Thermal energy storage system using stearic acid as a phase change material, Solar Energy 71 (6) (2001) 365-376.

[25] S. Seddegh, X. Wang, A.D. Henderson, Numerical investigation of heat transfer mechanism in a vertical shell and tube latent heat energy storage system, Applied Thermal Engineering 87 (2015) 698-706.

[26] A.A. Al Abidi, S.b. Mat, K. Sopian, M.Y. Sulaiman, A.T, Mohammed, CFD applications for latent heat thermal energy storage: a review, Renewable and Sustainable Energy Reviews 20 (2013) 353-363.

[27] A.A. Al Abidi, S. Mat, K. Sopian, M.Y. Sulaiman, A. Th, Internal and external fin heat transfer enhancement technique for latent heat thermal energy storage in triplex tube heat exchangers, Applied Thermal Engineering 53 (1) (2013) 147-156.

[28] A.A. Al Abidi, S. Mat, K. Sopian, M.Y. Sulaiman, A. Th, Numerical study of PCM solidification in a triplex tube heat exchanger with internal and external fins, International Journal of Heat and Mass Transfer 61 (2013) 684-695.

[29] S. Mat, A.A. Al Abidi, K. sopian, M.Y. Sulaiman, A. Th, Enhance heat transfer for PCM melting in triplex tube with internal–external fins, Energy Conversion and Management 74 (2013) 223-236.

[30] T.L. bergman, A.S.Lavine, F.P. Incropera, D.P. Dewitt, Fundamentals of Heat and Mass transfer, Seventh ed, John Wiley & Sons, 2011, pp. 518-593.

[31] A. J. Ghajar, L. Tam, Heat transfer measurements and correlations in the transition region for a circular tube with three different inlet configurations, Experimental Thermal and Fluid Science, 8 (1994) 79-90.

[32] F.L. Tan, S.F. Hosseinizadeh, J.M. Khodaddi, L. Fan, Experimental and computational study of constrained melting of phase change materials (PCM) inside a spherical capsule, International Journal of Heat and Mass Transfer, 52 (2009) 3464-3472.

Chapter5: Investigation of heat transfer in cylindrical and conical vertical shell-and-tube latent heat energy storage systems during charging processes

5.1. Chapter summary

In this chapter, physics of the heat transfer mechanism in cylindrical and conical shell-and-tube latent heat thermal energy storage (LHTES) systems is studied during a charging process. Visualized experiments are performed to investigate the evolution of the liquid/solid phase change material (PCM) interface. The temporal variation of the experimental temperature is then used to investigate effects of natural convection on heat transfer in PCM. A combined conduction and convection model is further applied to investigate the formation of convection circulation in the storage system. The results show that liquid PCM ascends to the upper part of the system and the melting region extends downwards. Thermal energy is first transferred from the heat transfer fluid (HTF) to the liquid PCM and then carried to the upper part of the storage system through vertical convection in the liquid PCM channel around the HTF pipe. It induces horizontal convective circulation inside the liquid PCM at the upper part of the system and is transferred outward towards the shell. A comparison study is further performed between the cylindrical and conical LHTES systems. Results show that the conical system has better energy storage performance for the same storage volume during charging processes.

This research contained within this chapter has been submitted for review and publication as: Saeid Seddegh, Xiaolin Wang, "Investigation of heat transfer in cylindrical and conical vertical shell-and-tube latent heat energy storage systems during charging process", Renewable Energy Journal.

5.2. Introduction

Latent heat thermal energy storage (LHTES) has received significant research attention in past decades [1, 2]. It offers high storage density and minimizes energy loss through energy storage at a nearly constant temperature. However, low thermal conductivity of phase change material (PCM) used in the LHTES system has hindered commercialization and widespread applications of these systems [3]. One solution to the problem of the low thermal conductivity of PCM is to enhance heat transfer by designing a proper heat exchanger system in the PCM unit. This requires a deep understanding of heat transfer mechanism in the LHTES system.

Some researchers believed that conduction played the most important role during phase transformation processes [4 - 7]. Zivkovic and Fuji [6] and later Vyshak and Jilani [7] applied this model and compared melting process of PCM packed in three containers of different geometric configurations: rectangular, cylindrical and shell-and-tube. The shell-and-tube storage was found to take the least time for storing an equal amount of energy.

However, many researchers demonstrated that natural convection was the most important heat transfer mechanism in the phase change process, especially during the melting process. Sparrow et al. [8] performed a pioneering study and concluded that natural convection could not be ignored in the analysis of a phase change process. Buddhi et al. [9] presented an explanation for the natural convection phenomenon: the density difference between the solid and liquid PCM phase induced buoyancy, which caused convection motion in the liquid phase. Later, Lacroix and Duong [10] experimentally demonstrated that natural convection was the main heat transfer mechanism during the melting process. This finding was further experimentally proven by Velraj et al. [11]. Hamdan and Al-Hinti [12] analytically investigated the melting process of a PCM contained in a rectangular enclosure heated from a vertical side

at a constant heat flux. The model well predicted the liquid/solid interface propagation at the initial stages of the melting process and under-predicted it at the later stage of melting. Fan et al. [13] studied constrained melting heat transfer of a PCM in a circumferentially finned spherical capsule. Local natural convection was found to emerge from above and underneath the fin surface. Caron-Soupart et al. [14] experimentally investigated the importance of natural convection in liquid PCM in a single stainless steel tube with longitudinal fins and a copper tube with helical fins energy storage systems, respectively. Ezan et al. [15] investigated the natural convection and flow parametric effects on charging and discharging periods of water in a shell-and-tube LHTES unit. Experimental results indicated that natural convection was the dominant heat transfer mechanism after a short heat conduction dominated period for both solidification and melting processes. The HTF inlet temperature had considerable effect on the energy storage capacity during charging process and energy rejection for discharging period.

Recent experimental and computational studies have revealed that the heat transfer mechanism in PCM is a combination of convection and conduction in the LHTES system [16-24]. Agyenim et al. [16] performed a series of experimental studies on a horizontal shell-and-tube heat exchanger LHTES system. Convection heat transfer was found to play an important role during the melting process, while conduction heat transfer was significant during the solidification process. Hosseini et al. [17-18] investigated heat transfer characteristics of a horizontal shell-and-tube heat exchanger LHTES system using RT50 (melting temperature of 50 ºC) as the PCM. It was found that recirculation was driven by convection inside the liquid region during the melting process. Avic and Yazici [19] experimentally recorded the time histories of a paraffin (P56-58) as the PCM in a horizontal shell-and-tube heat exchanger LHTES. It was concluded that the molten PCM ascended to the upper part of the storage unit and the melt region extended radially upward as a result of natural convection. Contrary to the melting process, in the solidification process natural convection has been observed to be

initially effective and then suppressed by conduction. Rosler and Bruggemann [20] performed numerical and experimental study of convection dominated phase change around a single cylinder in a horizontal shell-and-tube LHTES system. Industrial grade paraffin wax (RT42) was used as the PCM and water as the HTF. The calculated temperature, liquid fraction, and velocity field indicated that the phase boundary moved upward due to natural convection induced in the melting of the paraffin wax. Wang et al. [21] numerical studied the charging and discharging characteristics of a shell-and-tube phase change heat storage unit. The results showed that charging processes had three stages due to effect of convection and conduction: rapidly changing period, slowly changing period and more slowly changing period.

Murray et al. [22] experimentally studied heat transfer mechanisms in a vertical cylindrical shell-and-tube LHTES system. The effect of natural convection in the melting process was found to be significant since more melted PCM was observed at the top of the container. Seddegh et al. [23] numerically compared thermal behavior and heat transfer characteristics of a vertical cylindrical shell-and-tube unit using a pure thermal conduction model and a combined conduction-convection heat transfer model. The results indicated that convection heat transfer dominated the melting process while conduction dominated the solidification process. The same authors [24] further compared the heat transfer in the horizontal and vertical shell-and-tube LHTES systems using the combined model.

Furthermore, some researchers studied the effect of eccentricity on horizontal shell-and-tube LHTES system during the charging [25] and discharging [26] processes. Darzi et al. [25] numerically investigated the melting of N-eicosane as the PCM in concentric and eccentric cylindrical tubes. Results showed that the melting rate in upper half was faster than the lower half of the cylinder. As the HTF tube moves downward of the center, the melting rate increases sharply due to convective heat transfer in the most area of PCM. Yazici et al. [26] conducted an experimental study to investigate the solidification characteristics of paraffin when the HTF

tubes moves upward/downward around the center of the outer shell. It was found that increasing the eccentricity of the HTF tube, either upward or downward, make the total solidification time longer. Therefore, the concentric geometry is preferred for the solidification process in order to have better performance. Akgün et al. [27] experimentally investigated a vertical shell-and-tube LHTES unit with a novel design in which the shell was inclined with an angle of 5 degrees. The effects of the Reynolds number and the Stefan number on the melting and solidification behaviors were analyzed. The studied design showed promising results.

Despite significant research on the heat transfer mechanism, there is still a lack of experimental work to understand the physics of heat transfer in PCM in the vertical shell-and-tube LHTES system. As discussed above, most experimental work focused on heat transfer in the horizontal shell-and-tube LHTES system which was significantly different from that in the vertical shell-and-tube LHTES system [24]. Thus, this paper focuses on physics of heat transfer in PCM in the vertical cylindrical shell-and-tube LHTES system during charging processes. Visualized experiments are performed to observe the liquid-solid PCM interface evolutions during melting. A temporal variation of the experimental temperature is used to demonstrate the effect of convection on heat transfer during melting of the PCM. Then experimental images incorporating the theoretical velocity field inside PCM are further investigated to explain the heat transfer phenomena in the vertical LHTES system. Based on the research finding, a vertical conical shell-and-tube LHTES system is proposed and investigated. The performance of the vertical conical shell-and-tube LHTES system is further compared with the cylindrical vertical LHTES system. The research provides useful information and guidance to researchers and engineers for design and optimization of a vertical shell-and-tube LHTES system.

5.3. Experimental set up

5.3.1. Apparatus

Fig. 5.1 shows an experimental setup which consists of a hot water tank, a cold water tank, PCM storage systems, hot and cold water pumps, flow meter, data acquisition module, thermocouples, valves and a lot of piping systems. Water is used as both the hot and cold heat transfer fluid (HTF).

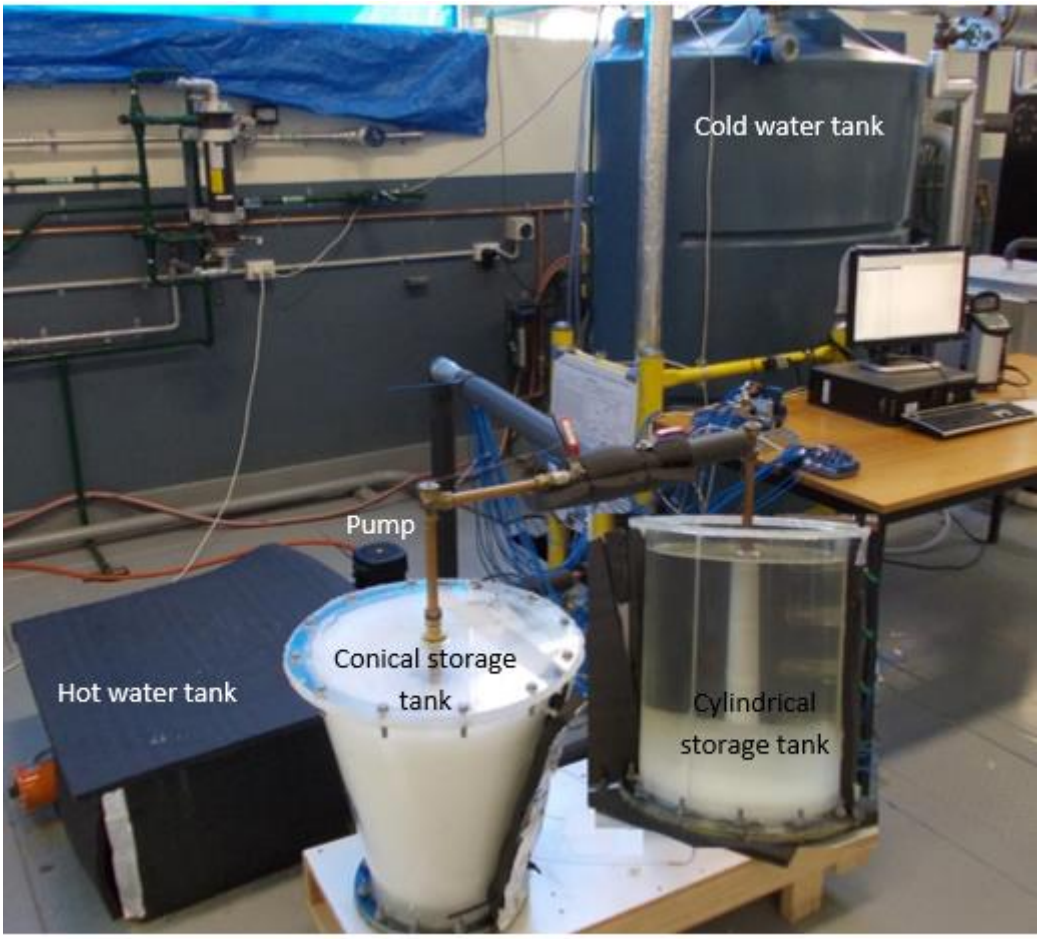

Fig. 5.1 A photograph of whole experimental rig.

During the charging process, the hot HTF is heated up to the pre-set temperature using two 2.4 kW thermal electric immersion heaters (model number TWI50240) with externally adjustable thermostats in the hot water tank with a capacity of 108 L. The hot water is circulated by a Grundfos vertical, multistage centrifugal pump (model number: CR 1-4 A-A-A-E-HQQE)

through the inner pipe in the PCM container where PCM is filled between the inner pipe and cylindrical/conical shell. Then the hot water is channelled back to the hot water tank from the exit of the storage system. During the discharging process, the cold water is maintained at a required temperature using a 20 kW chiller (model number HWP020-3BB) in the cold tank with a capacity of 1575 L. The cold water is circulated by an Onga horizontal, centrifugal pump (model number: 413) through the inner pipe in the PCM container to cool the PCM. A Flomec oval gear positive displacement flow meter with pulse output is placed at the position between the container outlets and hot/cold water tanks to monitor the hot and cold water flow rates. The temperatures and water flow rates are recorded by the data acquisition system (National Instruments NI9411).

5.3.2. PCM storage containers

Two different geometric containers with a height of 0.5 m and a capacity of 48.11 L are used in the experiment: the first one is a vertical cylinder with a diameter of 0.35 m, and the second one is a vertical conical cylinder with a diameter of 0.25 m at the bottom and 0.44 m at the top. Each tank contains 25 kg PCM, and a DN20 copper pipe is installed at the centre of the container. Both containers are made of transparent polypropylene (thermal conductivity k is 0.1 w/m·K) with a thickness of 6 mm for observing the melting process. The containers are insulated with Armaflex sheets with a thermal conductivity of 0.036 W/m·K.

The PCM temperatures inside the two containers are measured by Type-T thermocouples with an accuracy of ±0.2 °C. The position of the thermocouples is shown in Fig. 5.2. In order to compare the thermal behavior between PCM in the vertical cylindrical container and PCM in the vertical conical container, four series A thermocouples are located on four levels in the same radial position being 115.5 mm away from the center of the HTF pipe, and four series B thermocouples are located at four levels in the same radial position being 5 mm away from the outer surface of both containers. The water temperatures at the inlet and outlet of the containers

are measured by the same type of thermocouples. The PCM used in the test is RT60 paraffin wax from the Rubitherm Gmbh. PCM thermal properties and testing conditions are listed in Table 1.

Table 5.1: Thermophysical properties and test conditions

PCM	Melting Temperature (°C)	Latent Heat of Fusion (J/kg)	Density (kg/m3)		Specific Heat (J/kgK)	Thermal conductivity (W/mK)	Volume expansion (%)	Dynamic viscosity (mPa)
Paraffin wax (RT60)	55-61	123506	Solid (15°C)	Liquid (80°C)	2000	0.2	12.5	At 100°C
			880	770				3
Heat transfer fluid (HTF)	**Charging temperature (°C)**		**Density (kg/m^3)**		**Specific heat (J/kg-K)**	**Thermal conductivity (W/m-K)**		
Water	80		998		4183	0.58		

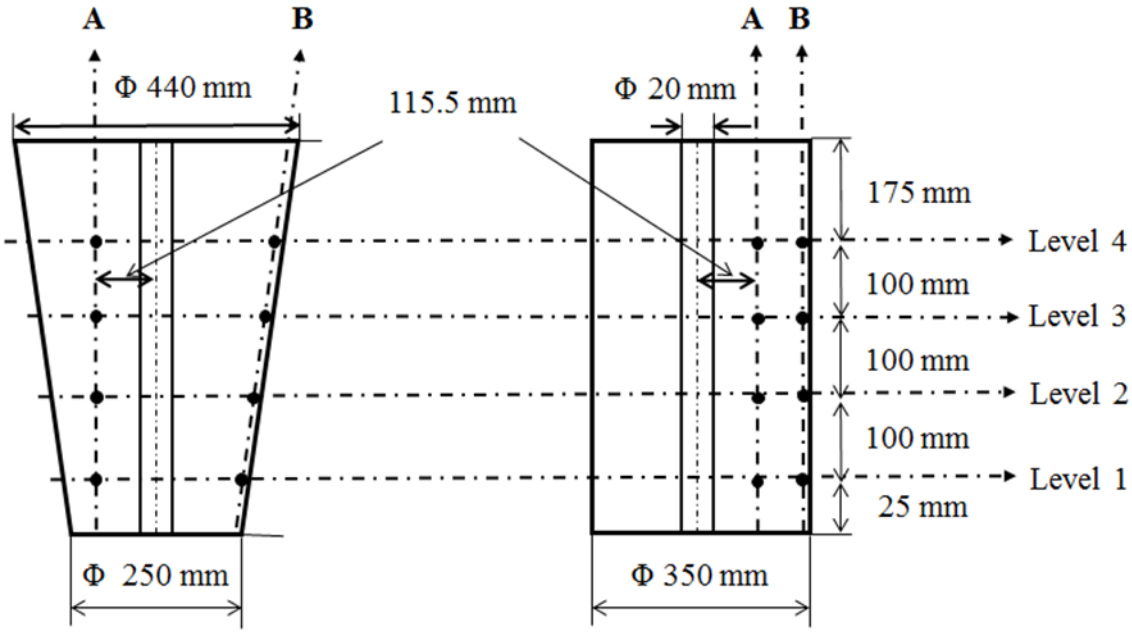

Fig. 5.2 locations of thermocouples a) Conical container, b) Cylindrical container (bold points represent the positions of thermocouples).

5.4. Numerical approach

In order to investigate the finding from the experiment, the combined conduction and convection model is used to investigate natural convection in PCM. The model is detailed in literature [23, 24] and is summarized below:

The energy conservation is expressed in terms of total volumetric enthalpy and temperature for thermo-physical properties as:

$$\frac{\partial \rho H}{\partial t} + \nabla \cdot (\rho v H) = \nabla \cdot (k \nabla T) + S \qquad (1)$$

The total volumetric enthalpy is calculated by:

$$H = h + fL \qquad (2)$$

$$h = h_o + \int_{T_o}^{T} C_P dT \qquad (3)$$

where h_o is the PCM sensible enthalpy at the reference temperature T_o, f refers to liquid fraction that indicates the fraction of a cell volume in liquid form and is associated with each cell in the domain given by Eq. (4).

$$f = \begin{cases} 0 & T < T_{Solidus} \\ \dfrac{T - T_{Solidus}}{T_{Liquidus} - T_{Solidus}} & T_{Solidus} \le T \le T_{Liquidus} \\ 1 & T > T_{Liquidus} \end{cases} \qquad (4)$$

By combining the Eqs. (2) to (4), the energy conservation equation can be simplified as:

$$\frac{\partial \rho h}{\partial t} + \nabla \cdot (\rho v h) = \nabla \cdot (k \nabla T) - \frac{\partial \rho f L}{\partial t} - \nabla \cdot (\rho v f L) + S \qquad (5)$$

The momentum equation is based on the Boussinesq approximation which assumes the fluid density is constant in all terms of the momentum equation except the body force term, and it is modelled based on a reference density (ρ_0) and temperature (T_0), and the volumetric expansion coefficient (β).

Momentum equation:

$$\frac{\partial \rho_0 v}{\partial t} + \nabla \cdot (\rho_0 vv) = -\nabla P + \nabla \cdot (\mu \nabla v) + (\rho - \rho_0) g + \frac{(1-f)^2}{f^3 + \varepsilon} v A_{mush} \quad (6)$$

Boussinesq approximation:

$$(\rho - \rho_0) g = -\rho_0 \beta (T - T_0) \quad (7)$$

Continuity equation:

$$\frac{\partial \rho}{\partial t} + \nabla \cdot (\rho v) = 0 \quad (8)$$

The energy (Q_{stored}) stored in the system at a given time is calculated by

$$Q_{stored} = \sum_{i=1}^{i=n} m_i (H_i(T_t) - H_{ini}) \quad (9)$$

The computational study is performed using the Fluent application of the ANSYS 17 software. The following parameters are used in this simulation [23-24]: $A_{mush} = 10^5$, $\varepsilon = 0.001$, and T_o = 298.15 K. The boundary conditions on the outer wall surface, top and bottom ends are made adiabatic to simulate insulation. The boundary condition for the outer surface of the HTF pipe is assumed as constant surface temperature. The PCM is initially set to solid state with a temperature of 15 °C and the HTF inlet temperature is 80 °C during the charging process.

Although this model has been validated in the previous study [23, 24], it was further verified to check the dependency on time step and cell size prior to simulation. Three mesh sizes: 58000, 83000, and 128000 cells; and three time-step sizes: 0.05 s, 0.1 s, and 0.2 s were examined in the cylindrical system. The model with 83000 cells and time step sizes of 0.05 s and 0.1 s produced a very similar variation in PCM average temperature. The results did not show significant change as the number of cells increase to 128000. As for the conical system, three mesh sizes: 53000, 78000, and 118000 cells; and three time-step sizes: 0.05 s, 0.1 s, and 0.2 s were examined and the model with 78000 cells and time steps of the 0.05 s and 0.1 s

produced a similar variation of PCM average temperature. Increasing the number of elements to 118000 did not show significant change in the results. Therefore, in order to save the computational time, a mesh of 83000 cells for the cylindrical system and 78000 cells for the conical system and a time step size of 0.1 s were found to be sufficient to achieve the predetermined convergence level of the energy equation (1E-6). Fig. 5.3 showed the comparison of the PCM temperature between the experimental data and simulation results for the first 10 hours of charging process. The simulation results were found to agree well with the experimental data, which was consistent with the finding in literature [23, 24].

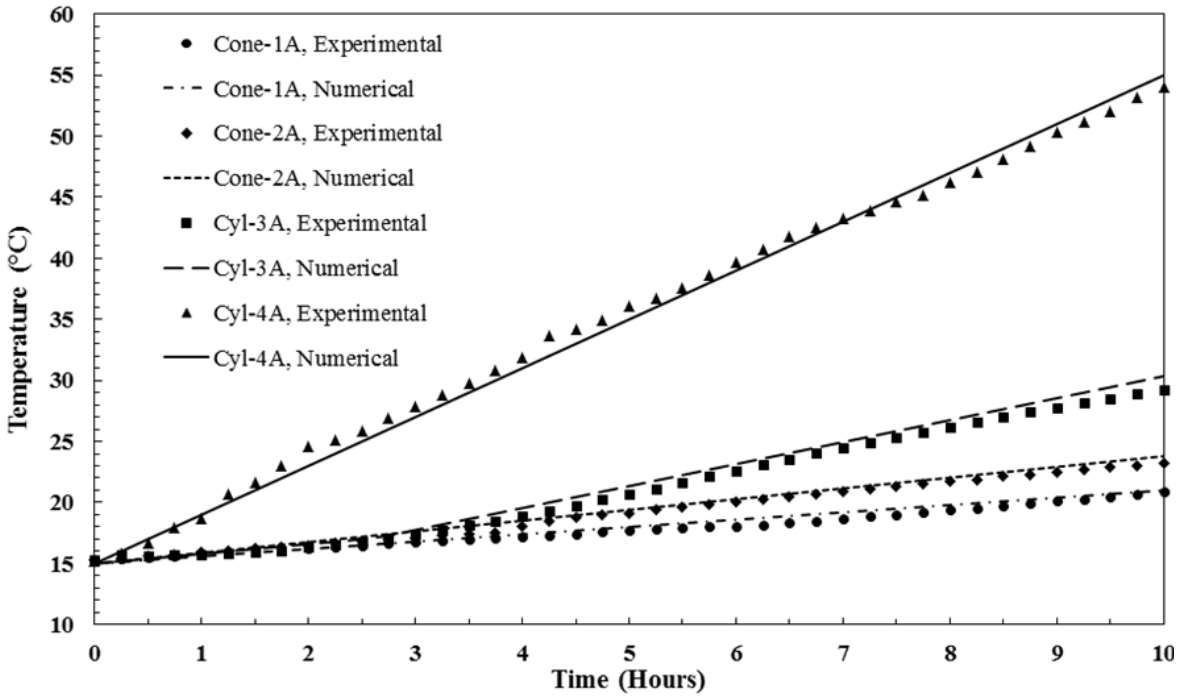

Fig. 5.3 Comparison between the simulated results and experimental data at the selected temperature points.

5.5. Results and discussion

The experiment is first performed to investigate heat transfer in the vertical cylindrical LHTES system at a charging HTF temperature of 80 °C and a flow rate of 10 L/min. The temporal variation of the experimental temperature inside the PCM and experimental images are used to investigate natural convection. Then the simulated velocity and temperature fields are used to explain the finding in the experiment. Finally, the heat transfer performance between the vertical cylindrical and conical storage systems is compared.

5.5.1. Heat Transfer in the cylindrical unit

Fig. 5.4 shows the PCM temperature variations with time at positions A and B in the cylindrical storage unit. The temperatures at the four levels are found to decrease from the top to the bottom of the storage unit at both positions A and B. This indicates that the heat transfer in the PCM cannot be only thermal conduction since conduction only leads to an almost identical temperature along the vertical direction. The temperatures of the upper levels PCM always increase much faster than those of the lower levels PCM. This can only be explained by natural convection which brings high temperature melted PCM upward, and leads to stronger heat transfer in the upper levels PCMs. This can be evidenced by the visualized images shown in Fig. 5.5.

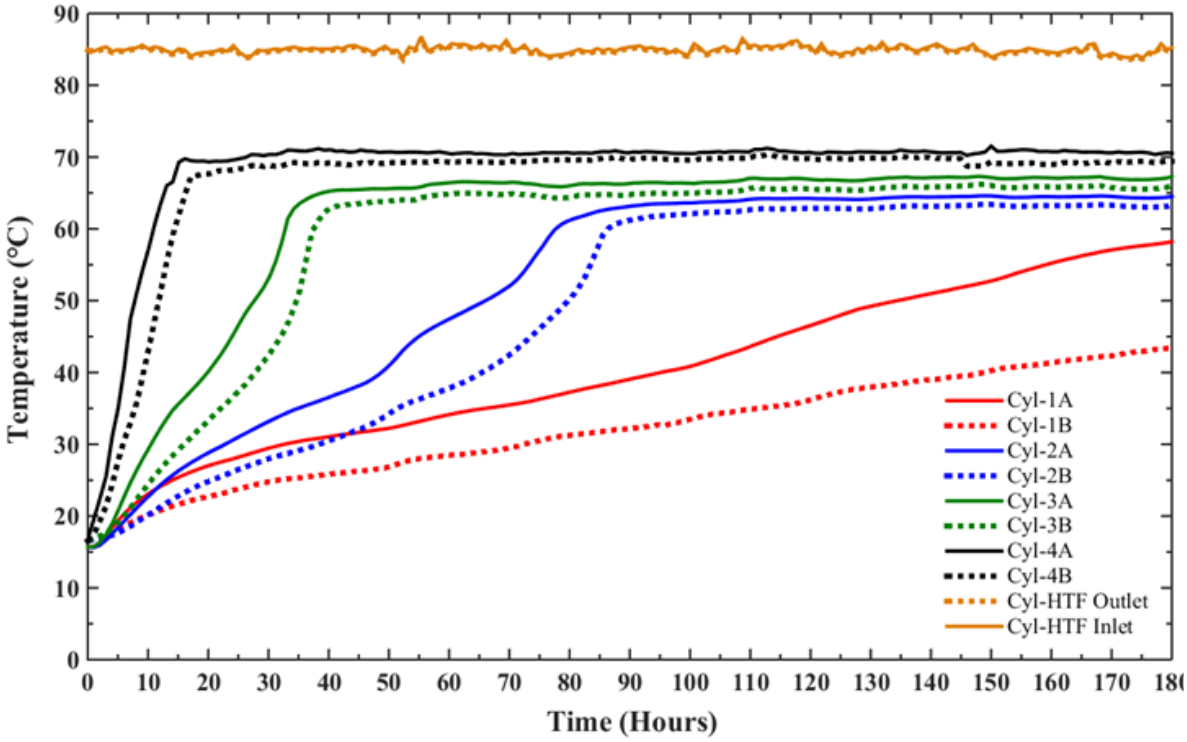

Fig. 5.4 PCM temperature variations in the cylindrical system during the charging process.

Fig. 5.5 shows the liquid and solid PCM interface evolutions. The liquid PCM accumulates at the top of the storage unit and forms a conical shape of the interface. The conic liquid/solid interface surface gradually moves down. This indicates that the PCM melts from the top to the bottom along the conic liquid/solid interface in the storage unit. This is different to previous understanding from thermal conduction that the PCM absorbs energy from the HTF pipe and melts from the centre of the cylinder to the edge in a radial direction. This finding clearly demonstrates that natural convection plays an important role in the heat transfer. Furthermore, it is observed that a thin vertical liquid PCM channel exists around the HTF pipe. The change in the width of this liquid PCM channel is found insignificant in the whole charging process as shown in Fig. 5.6. This is an interesting finding which has never been reported in any literature previously. In order to better understand these phenomena, the theoretical analysis is performed.

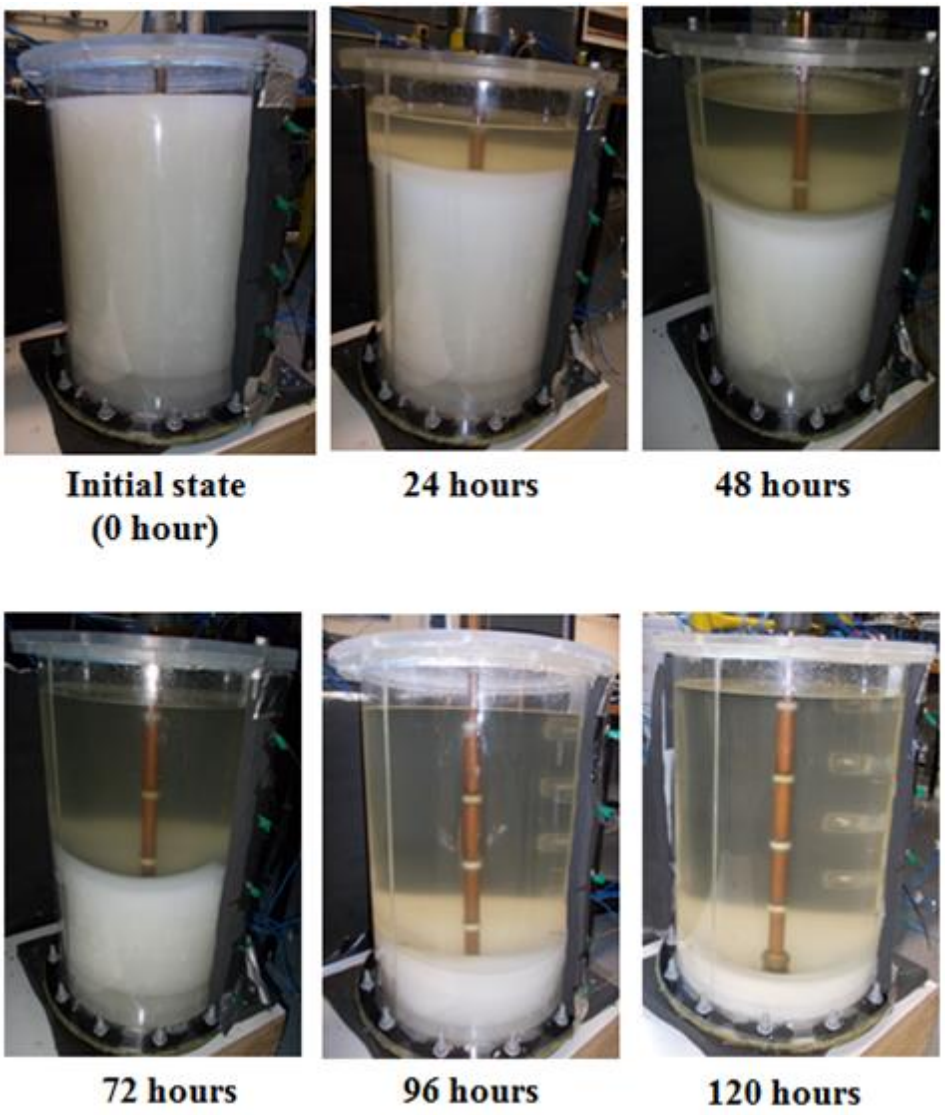

Fig. 5.5 Experimental photos of the cylindrical unit during charging process.

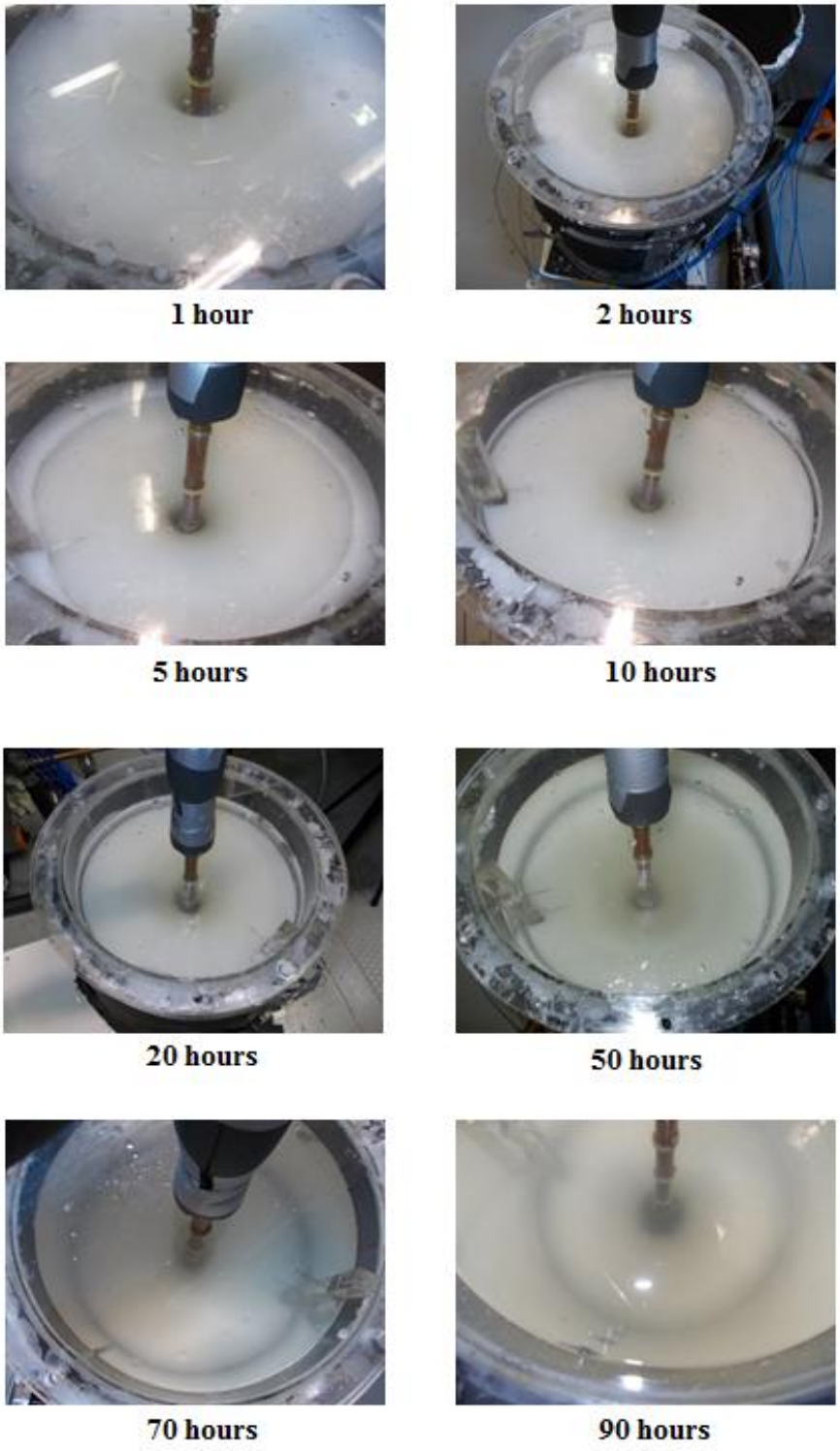

Fig. 5.6 Photos of the vertical liquid channel around the HTF pipe during the experimental charging process.

Fig. 5.7 shows simulated contours of the PCM liquid fraction (left side) and temperature field (right side) for the cylindrical storage unit using the mathematical model. The liquid

fraction contours show that most molten PCM ascends to the upper levels of the storage unit and extends vertically downward. A small portion of liquid PCM is found to exist in a vertical channel around the HTF pipe and the channel width does not show significant change over the charging process once it is formed. The temperature profile shows that the temperature along the vertical lateral surface decreases from the top to the bottom. It also shows that the temperature inside the vertical liquid channel decreases along radial direction. These findings are consistent with those presented in the experiments thus theoretically proving the significant role of convection heat transfer in the charging process.

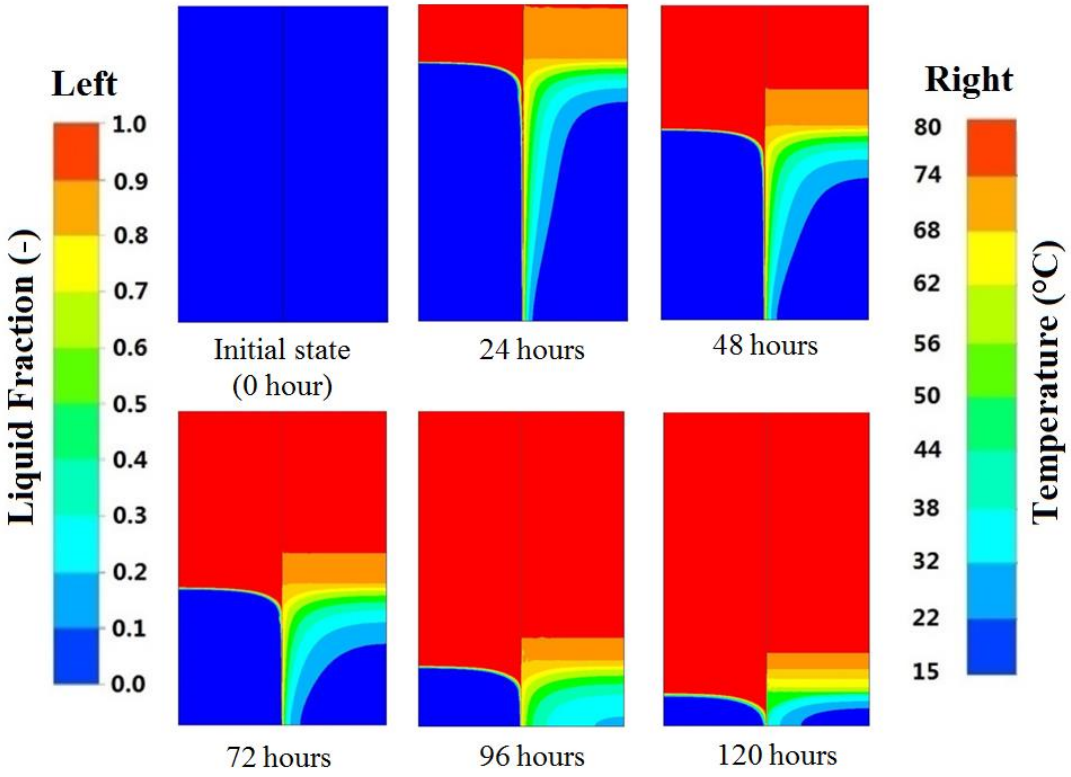

Fig. 5.7 The contour of the liquid fraction (left) and temperature (right) for the cylindrical unit.

Fig. 5.8 presents the simulated velocity field which helps in understanding the convection circulation in the liquid PCM. In region 1, the liquid PCM is found to circulate vertically in the confined channel. The high temperature liquid PCM around the HTF pipe flows up and low temperature liquid PCM flows downward along the solid/liquid PCM interface from the region 2 to make up the PCM in the confined channel. This vertical circulation induces the convective

heat transfer, which dominates heat transfer between the HTF pipe surface and liquid PCM, and brings thermal energy to the upper part of the storage unit. According to the calculation, the velocity of the liquid PCM flow is less than 0.02 m/s and the Reynolds number of the flow is very small, which indicates that the flow in the channel is laminar. When the melt layer is sufficiently thick, laminar thermal boundary layers are established adjacent to the wall of the inner pipe as well as near the liquid/solid PCM interface. In this situation, thermal energy from the HTF is difficult to transfer across the boundary layer. It is only transported by convective currents and moved towards the top of the storage unit. As a consequence, the thermal energy from the HTF is carried upward and less energy is transported to melt the PCM along the solid/liquid interface around the vertical PCM channel. This explains why the width of this confined liquid channel does not change during the charging process.

In the region 2, the liquid PCM is separated into two streams. One stream flows down due to pressure difference to make up the PCM in the confined channel and another stream is induced by the high temperature liquid PCM flowing up. Along the solid/liquid PCM interface, the convection enhances the heat transfer and the solid PCM melts. In region 3, the liquid PCM along the solid/liquid PCM interface forms a laminar flow circulation along the cross-section surface. This flow circulation induces natural convection which enhances heat transfer between the solid and liquid PCM and hence the solid PCM along this surface melts quickly. In region 4, the liquid PCM forms a larger flow circulation circuit which enhances heat transfer in the liquid PCM and unifies the liquid PCM temperature.

Natural convection was found to play an important role during the charging process, a vertical convective circulation channel around the HTF pipe was found and its width did not show significant change once it was formed. Thermal energy was found to be transferred from the HTF to the liquid PCM and then carried upward via the vertical convective circulation in the channel. This thermal energy was further transferred in the liquid PCM accumulated at the

upper part of the storage system through horizontal convective circulation. Hence heat transfer was more effective at the upper part of the system and PCM melting front moves downward from the top to the bottom of the system.

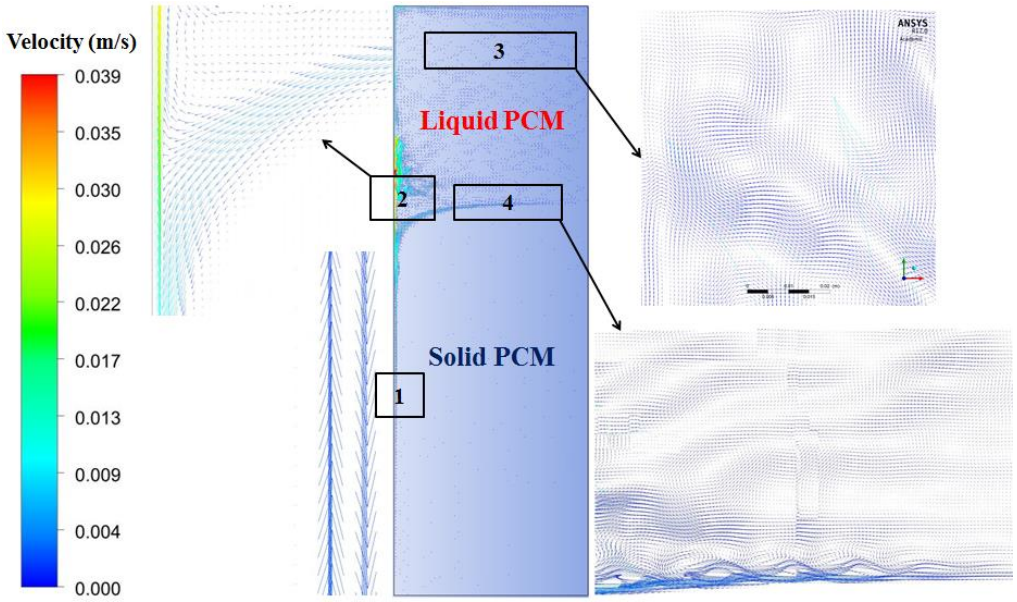

Fig. 5.8 The vector of velocity for the cylindrical unit.

5.5.2. Comparison between the conical and cylindrical storage unit

Fig. 5.9 shows the experimental PCM temperature variations with time in positions A and B in the conical storage unit. The experimental conditions are the same as those in the cylindrical storage unit. With the same HTF inlet temperature of 80 °C and flow rate of 10 L/min, it is found that the temperature profile is similar to that in the cylindrical unit. Temperatures at the upper level (Cone3A and Cone4A) reach steady state much more quickly than those in the lower level (Cone1A and Cone2A) of the conical unit. The PCM also melts from the top to the bottom. Once again, it demonstrates that natural convection plays an important role in the charging process and it is stronger in the upper part than the lower part. Contrary to the cylindrical unit, the distance between levels A and B is reducing downward to

the conical unit. At level 1, both Cone1A and 1B thermocouples are at almost the same location which resulted in a very similar temperature trend.

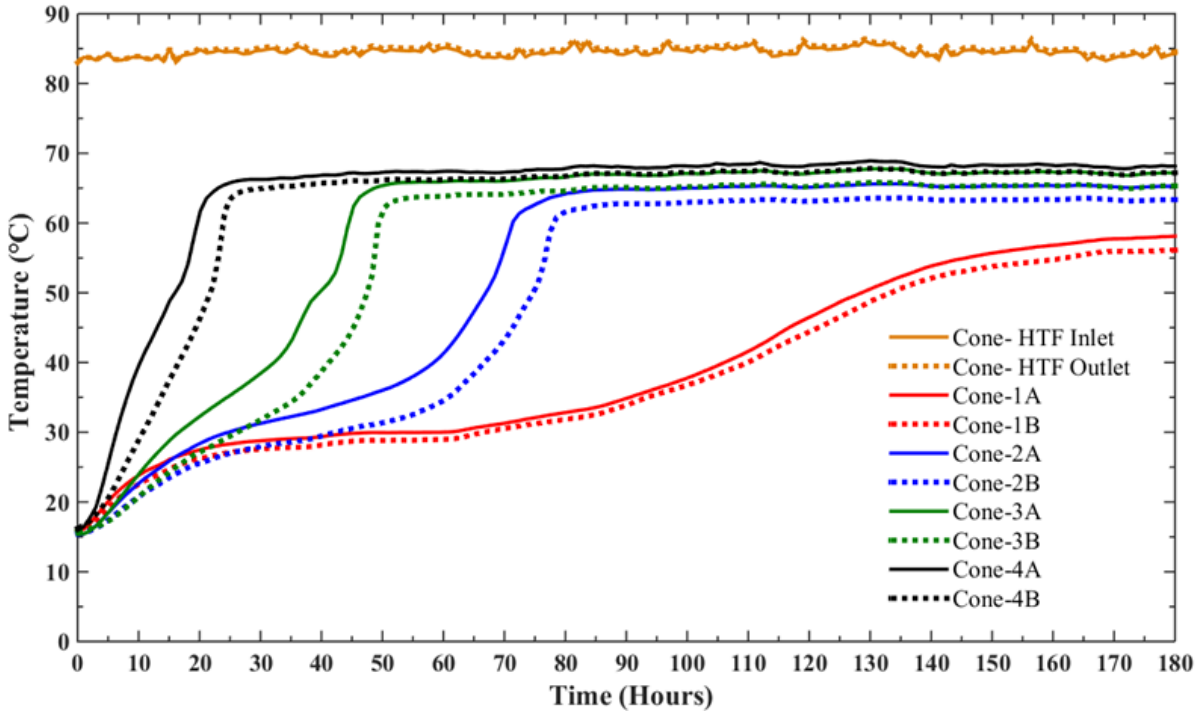

Fig. 5.9: PCM temperature variations of the conical system during the charging process.

In order to compare the thermal behavior between cylindrical and conical storage units during the charging process, Fig. 5.10 compares the PCM temperature at position A which has four thermocouples, with the same distance from the center of the HTF pipe in both cylindrical and conical systems. Temperatures in the upper level of the conical unit (Cone3A and 4A thermocouples) take a much longer time to reach steady state in comparison to those at the same positions in the cylindrical unit (Cyl3A and 4A). This is due to the packing of PCM. In the conical storage unit, more PCM is packed in the upper part of the conical system which requires more energy to melt the PCM in comparison to the cylindrical unit in which PCM is packed uniformly from the top to the bottom. Although heat transfer in the conical unit is stronger, it takes more time to melt all PCM in the upper part due to excessive PCM. This large amount of PCM also explains the low stable temperature at position A4 in the conical unit. For the thermocouples in levels Cone1A and Cone2A, initially the temperature in the conical unit

is lower because a large amount of energy is used to melt the upper part PCM. After a certain period, the temperatures at 1A and 2A in the conical unit increase to be higher than those in the cylindrical unit because less PCM is placed in the lower part of the conical unit. Therefore, the temperatures at levels Cone1A and 2A in the conical unit take a shorter time to eventually reach stability.

In both cylindrical and conical units, it is found that the temperature of positions A and B at all four levels reaches a different stable temperature although all these temperatures are located in the melting temperature range. The temperature difference between positions A and B for each level is due to thermal loss. Although the storage units are insulated by Armaflex with a thermal conductivity of 0.036 w/m·K, there is no ideal insulation in practice and heat is always lost to the environment through the shell surface. Position B is very close to the shell surface and hence the temperature is largely affected by the thermal loss. This thermal loss causes temperatures at position B to be lower than those in position A. For positions A or B at different levels, the difference between the stabilized temperatures is due to two reasons: One is thermal stratification. Since the storage system is heated up from the top to the bottom due to natural convection, thermal stratification appears in the whole heating process; the other reason is low heat transfer rate, which is not high enough to melt the PCM and quickly increase the PCM temperature at different levels.

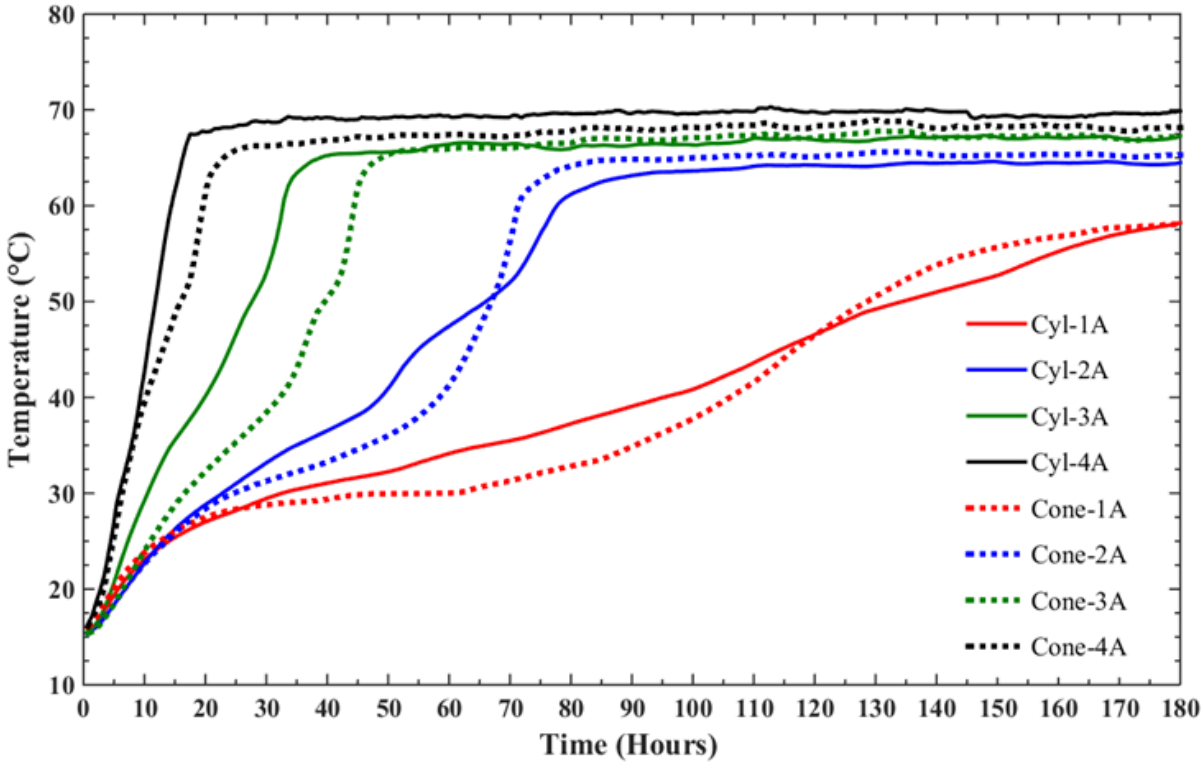

Fig. 5.10: Temperature profile comparison for cylindrical and conical systems during charging.

Fig. 5.11 shows a comparison of the simulated energy storage fraction and liquid fraction in the cylindrical and conical storage units. The energy storage fraction is defined as the ratio of stored energy at a given time to the total maximum energy which can be stored in the system. At the initial stage, energy fraction and liquid fraction do not show any differences between these two systems. This is due to thermal conduction which dominates heat transfer in the two storage units during this period. Since the height and the HTF size are the same in both storage units, energy transferred from the HTF to the surrounding PCM, and energy absorbed by the PCM, remain the same during this period. Therefore, the energy fraction and liquid fraction are the same in both systems. As the PCM melts, the liquid PCM forms natural circulation due to buoyancy and convective heat transfer gradually dominates energy transfer in the PCM until all the PCM melts. During this convective heat transfer period, the conical system gradually shows better storage performance. This can be understood from the previous analysis. Since liquid PCM accumulates at the top of the storage unit, convective heat transfer only happens

in the liquid PCM and at the interface between the liquid and solid PCM. In the conical storage unit, the volume of the upper part is larger in comparison to the cylindrical unit. More PCM is packed in the upper part of the conical unit where convective heat transfer is stronger and energy transfer is faster. Therefore, PCM in the conical unit receives thermal energy faster than that in the cylindrical unit and hence PCM in the conical unit melts faster as well. This finding could be further evidenced by experimental temperatures at position B.

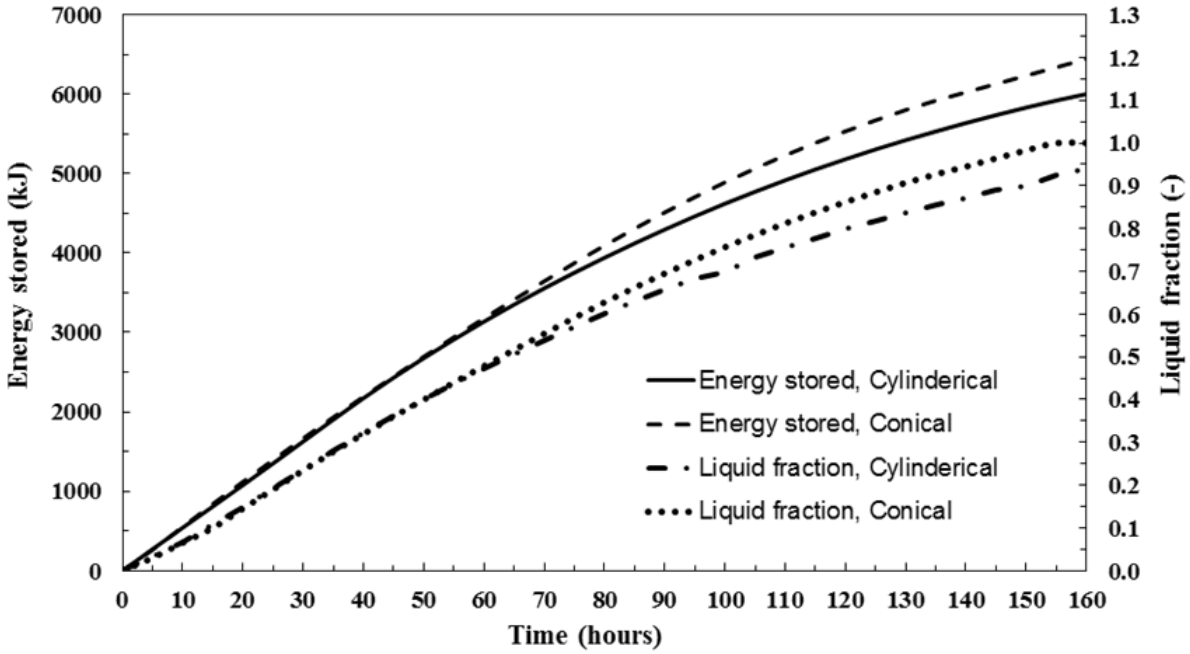

Fig. 5.11 Comparison of simulated energy stored and liquid fraction between the conical and cylindrical storage units.

Fig. 5.12 shows a comparison of experimental temperatures at different levels in position B. For the thermocouples at levels 3B and 4B, the temperatures inside the conical storage unit take longer to reach stability in comparison to the cylindrical unit. This is due to the amount of PCM at the upper part of the system as discussed before. However, for the thermocouples at levels 1B and 2B, it is found that these temperatures in the conical unit reach a steady temperature much faster than those in the cylindrical unit. It should be noted that position B thermocouples are located at about 5 mm away from the inner surface of the shell side. The temperatures at these locations indirectly represent energy transferred to the PCM close to the

edge of the storage unit. In other words, if the temperatures at these locations reach stability, it means that the PCM above this position has been all melted. As shown in Fig. 12, the temperatures at locations 1B and 2B in the conical unit reach the melting temperature or steady temperature much faster than those in the cylindrical unit. Since the volume of the conical system is larger than that of the cylindrical system at the same horizontal level according to the geometry, this temperature profile indicates that the PCM melts faster and energy stores quicker in the conical system. This demonstrates that the simulated results are reasonable and the conical system has better performance in comparison to the cylindrical system.

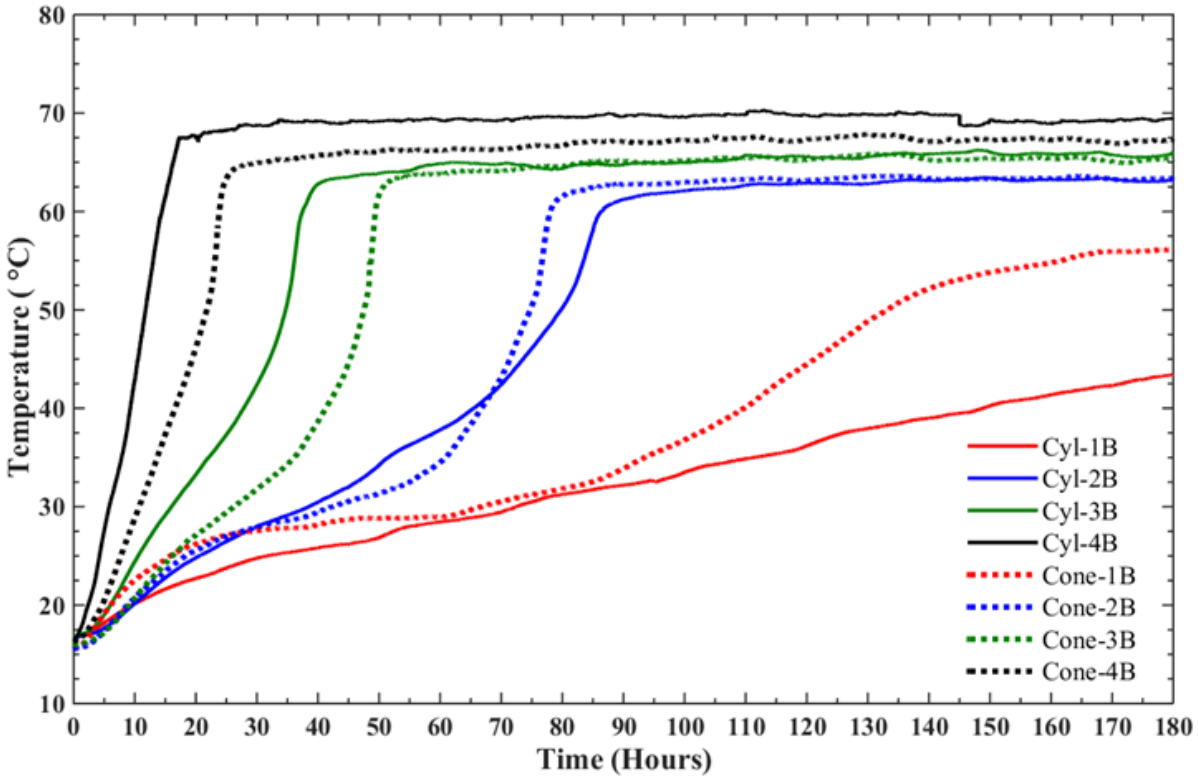

Fig. 5.12: Temperature profile comparison for cylindrical and conical systems during charging.

5.5.3. Effect of the HTF flow rate on the conical and cylindrical storage units

Figs. 5.13 and 5.14 show the PCM temperature comparison at the HTF flow rates of 10 and 20 L/min for the cylindrical and conical systems during the charging process, respectively. It shows that the HTF flow rate has no significant effect on the heat transfer in both systems

under the studied flow rates. This can be explained by the large heat transfer coefficient between the HTF and HTF pipe inner surface. Due to the large Reynolds number of the HTF flow in the HTF pipe, the convective heat transfer coefficient in the HTF pipe is much higher than that between the liquid PCM and the HTF outer surface. Hence the thermal resistance between the HTF outer surface and liquid PCM restricts the energy transfer from the HTF to the liquid PCM. Further increasing the convective heat transfer coefficient of the HTF by increasing the HTF flow rate in the HTF pipe will not substantially reduce the total thermal resistance between the HTF and PCM, and hence will not enhance heat transfer in the PCM.

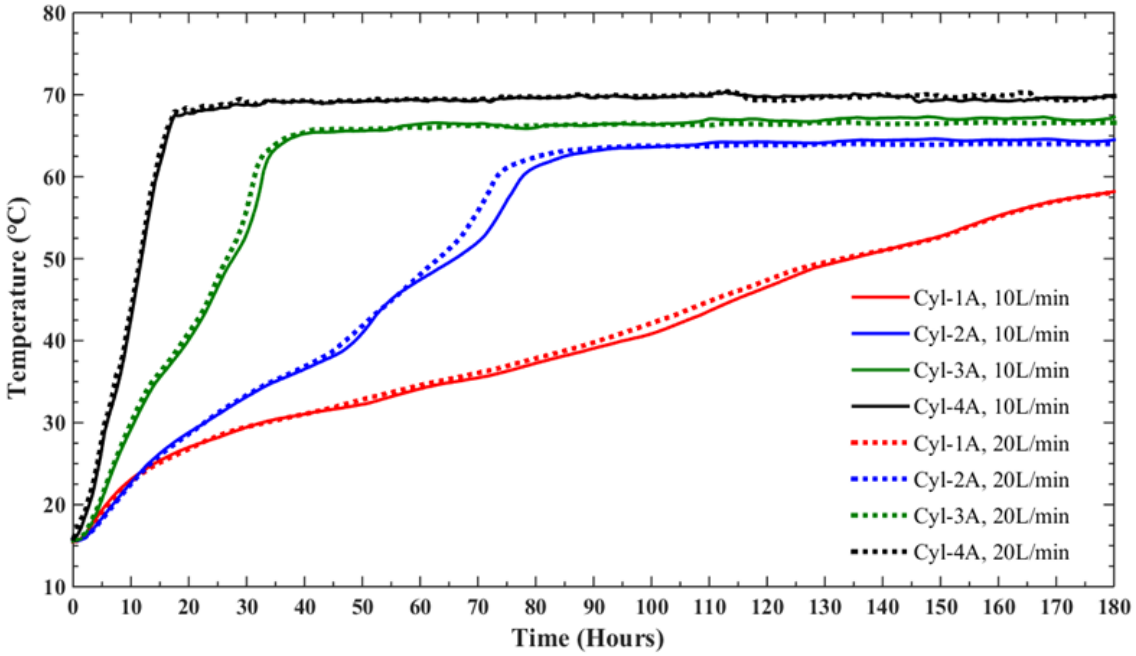

Fig. 5.13: Temperature profile comparison at position A with different HTF flow rate in the cylindrical unit during the charging process.

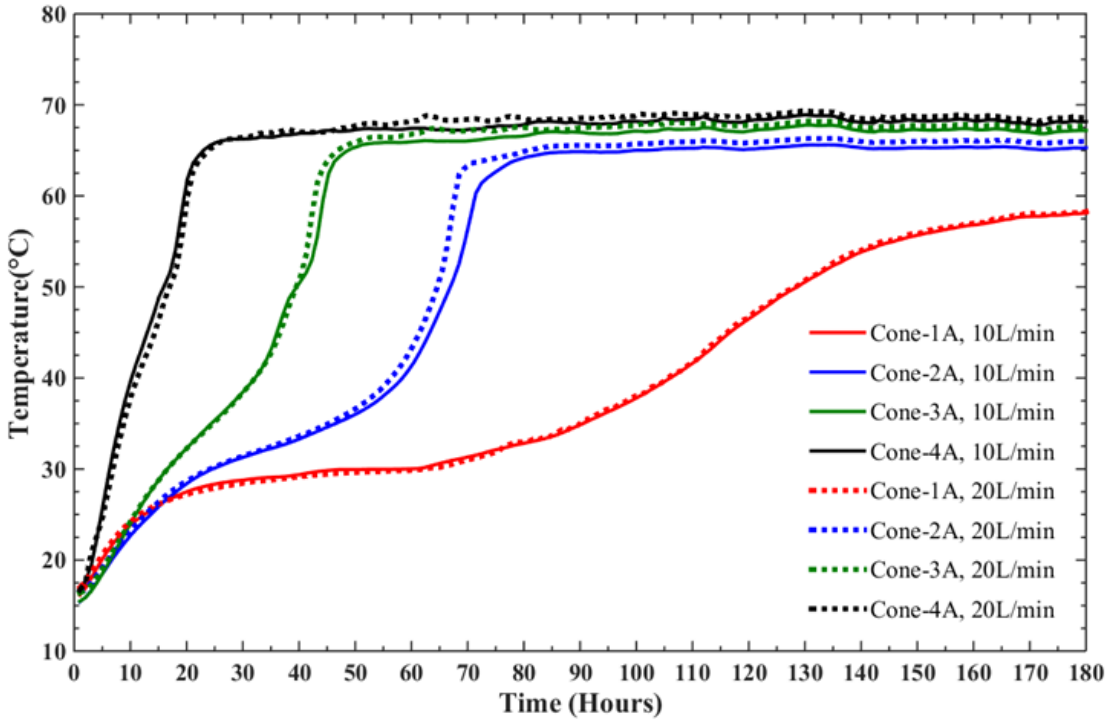

Fig. 5.14: Temperature profile comparison at position A with different HTF flow rate in the conical unit during the charging process.

5.6. Conclusion

In this chapter, thermal behavior in vertical conical and cylindrical shell-and-tube energy storage units were investigated experimentally and theoretically. It was found that natural convection dominated heat transfer during the charging process and thermal behavior in both systems were very similar. The results showed that there existed a vertical convective circulation channel around the HTF pipe. The width of this vertical channel did not show significant change once it was formed. Thermal energy was transferred from the HTF to the liquid PCM via convection and was then carried upward via vertical convective circulation in the channel. This thermal energy was further transferred in the liquid PCM accumulated in the upper part of the storage system through convection. Hence the heat transfer was more effective at the upper part of the system and PCM melted downwards from the top to the bottom of the system. The further comparison study showed that the vertical conical system had better energy

storage performance than the cylindrical system. This indicated that a vertical storage unit with geometry having large volume in the upper part and small volume in the lower part could have better energy storage performance. It is also found that increasing the HTF flow rate does not improve the overall performance of these systems.

5.6. References

[1] B. Zalba, J.M. Marín, L.F. Cabeza, H. Mehling, Review on thermal energy storage with phase change: materials, heat transfer analysis and applications. Applied Thermal Engineering, 2003, 23, 251-283.

[2] V. Kapsalis, D. Karamanis, Solar thermal energy storage and heat pumps with phase change materials. Applied Thermal Engineering, 2016, 99, 1212-1224.

[3] S. Seddegh, X. Wang, A.D. Henderson, Z. Xing, Solar domestic hot water systems using latent heat energy storage medium: A review. Renewable and Sustainable Energy Reviews, 2015, 49, 517-533.

[4] P.D. Silva, L.C. Gonçalves, L. Pires, Transient behaviour of a latent-heat thermal-energy store: numerical and experimental studies. Applied Energy, 2002, 73, 83-98.

[5] A. Sharma, L.D. Won, D. Buddhi, J.U. Park, Numerical heat transfer studies of the fatty acids for different heat exchanger materials on the performance of a latent heat storage system. Renewable Energy, 2005, 30, 2179-2187.

[6] B. Zivkovic, I. Fujii, An analysis of isothermal phase change of phase change material within rectangular and cylindrical containers. Solar Energy, 2001, 70, 51-61.

[7] N. Vyshak, G. Jilani, Numerical analysis of latent heat thermal energy storage system. Energy Conversion and Management, 2007,48,2161-2168.

[8] E.M. Sparrow, S.V. Patankar, S. Ramadhyani, Analysis of Melting in the Presence of Natural Convection in the Melt Region. Journal of Heat Transfer, 1977, 99, 520-526.

[9] D. Buddhi, N. Bansal, R. Sawhney, M. Sodha, Solar thermal storage systems using phase change materials. International Journal of Energy Research, 1988, 12, 547-555.

[10] M. Lacroix, T. Duong, Experimental improvements of heat transfer in a latent heat thermal energy storage unit with embedded heat sources. Energy Conversion and Management, 1998, 39, 703-716.

[11] R. Velraj, R. Seeniraj, B. Hafner, C. Faber, K. Schwarzer, Heat transfer enhancement in a latent heat storage system. Solar Energy, 1999, 65, 171-180.

[12] M. Hamdan, A. Al-Hinti, Analysis of heat transfer during the melting of a phase change material. Applied Thermal Engineering, 2004, 24(12), 1935-1944.

[13] L. Fan, Z. Zhu, S. Xiao, M. Liu, H. Lu, Y. Zeng, Z. Yu, K. Cen, An experimental and numerical investigation of constrained melting heat transfer of a phase change material in a circumferentially finned spherical capsule for thermal energy storage. Applied Thermal Engineering, 2016, 100, 1063-1075.

[14] A. Caron-Soupart, J. Fourmigue, P. Marty, R. Couturier, Performance analysis of thermal energy storage systems using phase change material. Applied Thermal Engineering, 2016, 98, 1286-1296.

[15] M. A. Ezan, M. Ozdogan, A. Erek. Experimental study on charging and discharging periods of water in a latent heat storage unit, International Journal of Thermal Sciences, 2011, 50, 2205-2219.

[16] F. Agyenim, P. Eames, M. Smyth, Experimental study on the melting and solidification behaviour of a medium temperature phase change storage material (Erythritol) system augmented with fins to power a LiBr/H2O absorption cooling system. Renewable Energy, 2011, 36, 108-117.

[17] M. Hosseini, A. Ranjbar, K. Sedighi, M. Rahimi, A combined experimental and computational study on the melting behavior of a medium temperature phase change storage material inside shell and tube heat exchanger. International Communications in Heat and Mass Transfer, 2012, 39 (9), 1416-1424.

[18] M. Hosseini, M. Rahimi, R. Bahrampoury, Experimental and computational evolution of a shell and tube heat exchanger as a PCM thermal storage system. International Communications in Heat and Mass Transfer, 2014, 50, 128-136.

[19] M. Avci, M.Y.Yazici, Experimental study of thermal energy storage characteristics of a paraffin in a horizontal tube-in-shell storage unit. Energy Conversion and Management. 2013, 73, 271-277.

[20] F. Rosler, D. Bruggemann. Shell-and-tube type latent heat thermal energy storage: numerical analysis and comparison with experiments, Heat Mass Transfer, 2011, 47, 1027-1033.

[21] W. Wang, K. Zhang, L. Wang, Y. He, Numerical study of the heat charging and discharging characteristics of a shell-and-tube phase change heat storage unit. Applied Thermal Engineering, 2015, 58 (1-2), 542-553.

[22] R.E. Murray, D. Groulx, Experimental study of the phase change and energy characteristics inside a cylindrical latent heat energy storage system: Part 1 consecutive charging and discharging. Renewable Energy, 2014, 62, 571-581.

[23] S. Seddegh, X. Wang, A.D. Henderson, Numerical investigation of heat transfer mechanism in a vertical shell and tube latent heat energy storage system. Applied Thermal Engineering, 2015, 87, 698-706.

[24] S. Seddegh, X. Wang, A.D. Henderson, A comparative study of thermal behaviour of a horizontal and vertical shell-and-tube energy storage using phase change materials. Applied Thermal Engineering, 2016, 93, 348-358.

[25] A. R. Darzi, M. Farhadi, K. Sedighi. Numerical study of melting inside concentric and eccentric horizontal annulus, Applied Mathematical Modelling, 2012, 36, 4080-4086.

[26] M. Y. Yazici, M. Avic, O. Aydin, M. Akgun. On the effect of eccentricity of a horizontal tube-in-shell storage unit on solidification of a PCM, Applied Thermal Engineering, 2014, 64, 1-9.

[27] M. Akgün, O. Aydin, K. Kaygusuz. Thermal energy storage performance of paraffin in a novel tube-in-shell system, Applied Thermal Engineering, 2008, 28, 405-413.

Chapter6: Heat transfer investigation of cylindrical and conical vertical shell-and-tube latent heat energy storage systems during discharging processes

6.1. Chapter summary

In this chapter, physics of the heat transfer mechanism in conical and cylindrical vertical shell-and-tube latent heat thermal energy storage (LHTES) systems is studied experimentally and theoretically during a discharging process. Visualized experiments are performed to observe the liquid–solid interface evolutions and the time history of phase change material (PCM) temperature is recorded. A combined conduction and convection heat transfer model is then developed to investigate the formation of the solid PCM. The results demonstrate that the PCM solidifies around the heat transfer fluid (HTF) pipe and the solidification front moves outward. Due to its low thermal conductivity, the PCM behaves as an insulation material and the rate of heat transfer from the HTF to the PCM is reduced. The comparative results show that both systems have similar trend and it takes almost the same time to complete the discharging process. It is also found that increasing the HTF flow does not improve the overall performance of these systems.

This research contained within this chapter has been accepted for oral presentation as: Saeid Seddegh, Xiaolin Wang, "Heat transfer investigation of cylindrical and conical shell-and-tube latent heat thermal energy storage systems during discharging processes", The 8th International Conference on Applied Energy, Beijing, Chain, October 8-11, 2016.

6.2. Introduction

Latent heat thermal energy storage (LHTES) has gained research attention because of its high storage density and small temperature change during charging/discharging processes [1]. The low thermal conductivity of PCMs, however, has hindered the commercialization and widespread applications. One solution to the problem of the low thermal conductivity of PCMs is to improve the heat transfer rate by designing a proper heat exchange system. This requires a deep understanding of heat transfer mechanisms in the LHTES system.

Some researchers such as Zivkovic and Fuji [2] and later Vyshak and Jilani [3] believed that conduction played the most important role during phase transformation processes. Given this assumption, the charging and discharging processes should be the same in all essential features. Recent experimental and computational studies of LHTES systems, however, have revealed that the heat transfer mechanism in the PCM is a combination of convection and conduction [4-13]. Agyenim et al. [4-6] performed a series of experimental studies on a horizontal shell-and-tube heat exchanger LHTES system. Convection heat transfer was found to play an important role during the melting process, while conduction heat transfer was significant during the solidification process. Hosseini et al. [7-8] experimentally and computationally investigated heat transfer characteristics of a horizontal shell-and-tube heat exchanger LHTES system using RT50 as the PCM. It was found that thermal conduction is the main heat transfer during the discharging process. Avic and Yazici [9] experimentally recorded time histories of a paraffin (P56-58) PCM in a horizontal shell-and-tube heat exchanger LHTES. It was concluded that natural convection has been observed to be initially effective on the heat transfer, but is then suppressed by conduction. Murray et al. [10, 11] experimentally studied heat transfer mechanisms in a vertical cylindrical shell-and-tube LHTES system. It was found that charging and discharging occurred independently when the PCM between the two heat transfer fluid pipes was solid during the simultaneous operation mode. Seddegh et al. [12]

numerically compared thermal behaviour and heat transfer characteristics of a vertical cylindrical shell-and-tube unit using a pure thermal conduction model and a combined conduction-convection heat transfer model. The results indicated that the discharging process was dominated by conductive heat transfer in the PCM. The same authors [13] further compared heat transfer in the horizontal and vertical shell-and-tube LHTES systems. It was found that heat transfer in these two systems was significant in the melting process due to convection, but there was no significant difference in the solidification process because conduction dominated.

Recent review papers [14, 15] have revealed that despite significant research on the heat transfer mechanism, there is still a lack of experimental work to explain the physics of PCM heat transfer in vertical shell-and-tube LHTES systems Most experimental work has focused on heat transfer in the horizontal shell-and-tube LHTES system. This paper thus focuses on the physics of PCM heat transfer in the vertically cylindrical and conical shell-and-tube LHTES system during discharging processes. A temporal variation of experimental temperature fields is first used to investigate conductive heat transfer in PCMs. Experimental images incorporating theoretical temperature and liquid fraction contours are then further investigated and used to explain the heat transfer phenomena inside the vertical LHTES system PCM. Furthermore, the heat transfer mechanism in the conical system is compared with the standard vertical cylindrical system.

6.2. Experimental set up

Two different geometry containers are used in the experiment, each with a height of 0.5 m, and a capacity of 48.11 L. The first is a vertical cylinder with a diameter of 0.35 m, and the second is a vertical conical cylinder with a diameter of 0.25 m at the bottom and 0.44 m at the top. Each tank contains 25 kg PCM, and a DN20 copper pipe is installed at the centre of the container [16]. Water is used as the cold heat transfer fluid (HTF) in this experiment. As shown

in Fig. 6.1, during the discharging process, cold water is maintained at a required temperature using a 20 kW chiller in a cold tank with a capacity of 1575 L. The PCM temperatures inside the two containers are measured by Type-T thermocouples with an accuracy of ±0.2 °C. The position of the thermocouples is shown in Fig. 1b. In order to compare PCM thermal behavior between the vertical cylindrical and vertical conical containers, five series A thermocouples are located at four levels in the same position being 115.5 mm away from the center of the HTF pipe, and five series B thermocouples are located at four levels in the same position being 5 mm away from the outer surface of both containers. Water temperatures at the inlet and outlet of the containers are measured by the same type of thermocouples. All these temperature readings are recorded by National Instrument NI9214.

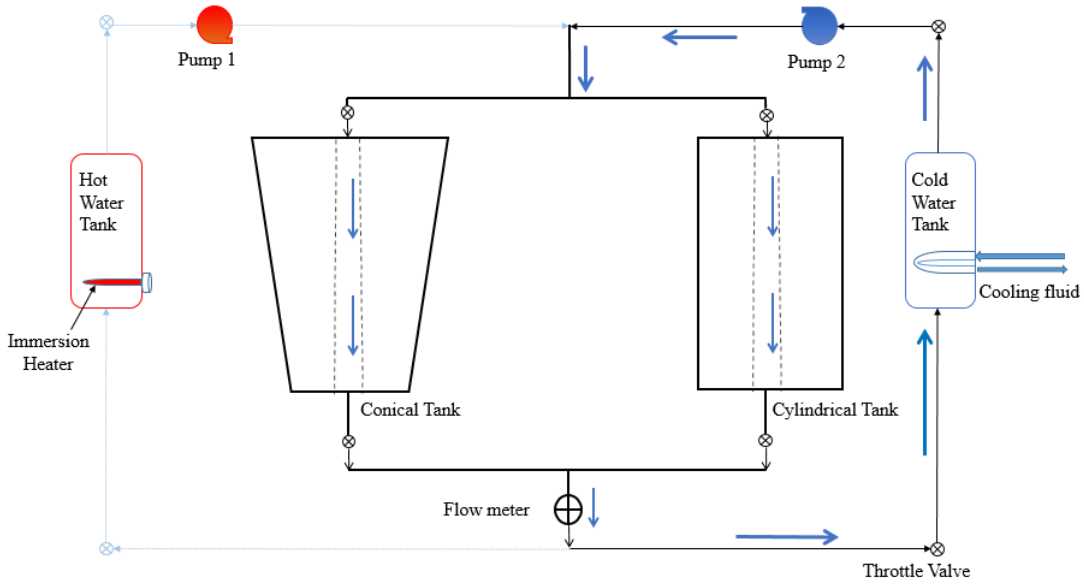

Fig .6.1: The schematic of the discharging process.

The PCM used in the test is RT60 paraffin wax from Rubitherm Gmbh. It is a safe, relatively inexpensive material with a melting temperature around 60 °C, which is a desirable temperature for solar domestic hot water appliances. Thermal properties and testing conditions are listed in Table 1.

Table 6.1. Thermophysical properties and test conditions

PCM	Melting Temperature (°C)	Latent Heat of Fusion (kJ/kg)	Density (kg/m^3)		Specific Heat (J/kgK)	Thermal conductivity (W/mK)	Volume expansion (%)	Dynamic viscosity (Kg/ m S)
RT60	55-61	123506	Solid	Liquid	2000	0.2	12.5	3.705E^{-5}
			880	770				
HTF	**Discharging Temperature (°C)**		**Density (kg/m^3)**		**Specific Heat (J/kgK)**		**Thermal conductivity (W/mK)**	
Water	10		998		4183		0.58	

6.4. Results and discussion

Once the PCM has completely melted, the experiment is performed to investigate the heat transfer mechanism of LHTES systems at a discharging HTF temperature of 10 °C and a flow rate of 10 L/min. First the temporal variation of the experimental temperature field inside the PCM is studied, along with the experimental images, to identify the heat transfer mechanism during the discharging process. In order to explain phenomena found in the experiment, a mathematical simulation developed in the previous research in chapter 3 and 4 is used to further investigate the temperature field and liquid fraction in the PCM. Variations of PCM temperature in both cylindrical and conical units are then compared.

6.4.1. Cylindrical storage unit

Fig. 6.2 shows the PCM temperature variations over time at positions A and B in the cylindrical storage unit during the discharging process. It is seen that the temperatures decreased rapidly at the beginning of the solidification period due to the convective heat transfer in the liquid which quickly transfers the stored sensible energy to the cold HTF. No PCM is solidified before the temperature lowers to the freezing point, and then a longer time is needed to transfer the latent heat during the phase change.

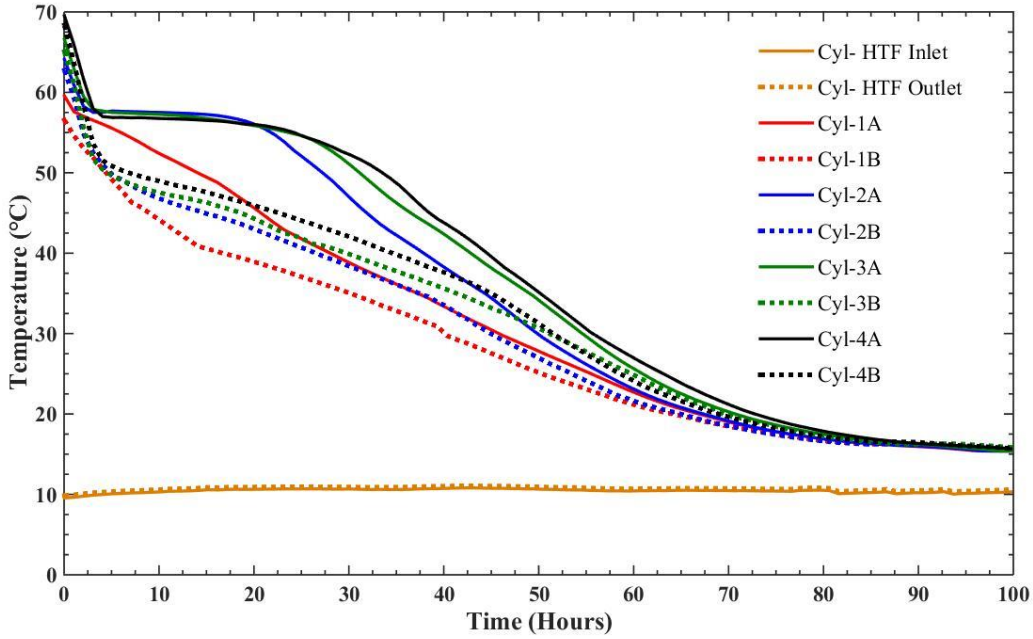

Fig. 6.2: PCM temperature variations for the cylindrical system during discharging process.

As it is shown in Fig. 6.2, the PCM temperature variation in the axial direction is not significant. This is mainly due to the following reasons. The PCM adjacent to the HTF tube begins to freeze and forms a solid layer of PCM around the HTF pipe which increases the thermal resistance between the cold HTF and liquid PCM. The heat transfer rate decreases as the thickness of the solid PCM increases. At the same time, natural convection dominates the heat transfer in the liquid PCM. This natural convective heat transfer rate is much higher than the conduction heat transfer rate. That is why the PCM temperature does not show much difference before the PCM solidifies. In particular, in the positions B, due to the low heat transfer rate, the PCM exists in liquid form for quite long time as shown by the flat line. The temperature profile also shows that both conduction and convection heat transfer exist in the solidification process which can be explained in Fig. 6.3.

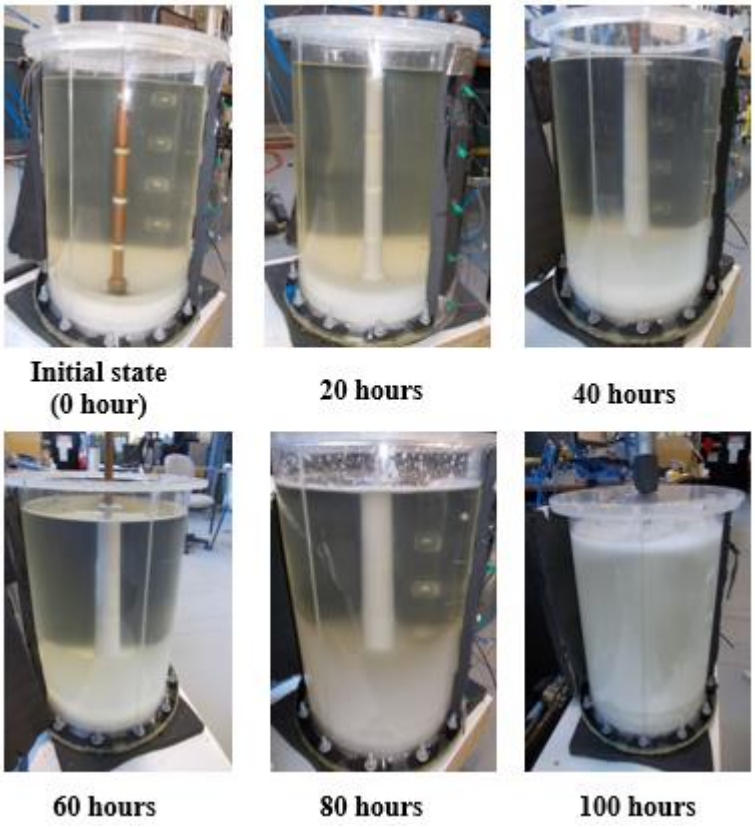

Fig. 6.3: Experimental photos of the cylindrical unit during discharging process.

As shown in Fig. 6.3, the solidification front moves along both radial and axial directions at the same time. When the cold HTF removes the heat from the PCM, the PCM solidifies and its temperature decreases which further solidifies the PCM next the solidification front. At the same time, the liquid PCM moves upward to buoyance, and the solid PCM sits at the bottom of the container due to higher density. Liquid PCM forms natural convection which enhances heat transfer between the solid and liquid PCM.

Fig. 6.4 shows simulated contours of the PCM liquid fraction (left side) and temperature field (right side) for the cylindrical storage unit using the mathematical model. The liquid fraction contours clearly show that the solidification front moves along the both axial and radial directions. The temperature profiles show that the temperature along the axial direction is different once the PCM solidifies. However, before it is solidified, the PCM temperature almost maintains at the frozen point. This phenomenon clearly show that the convection always exists

in the liquid PCM during the solidification process. In the discharging process, there exists both conduction and convection heat transfer. This finding is different from the finding presented in literature before.

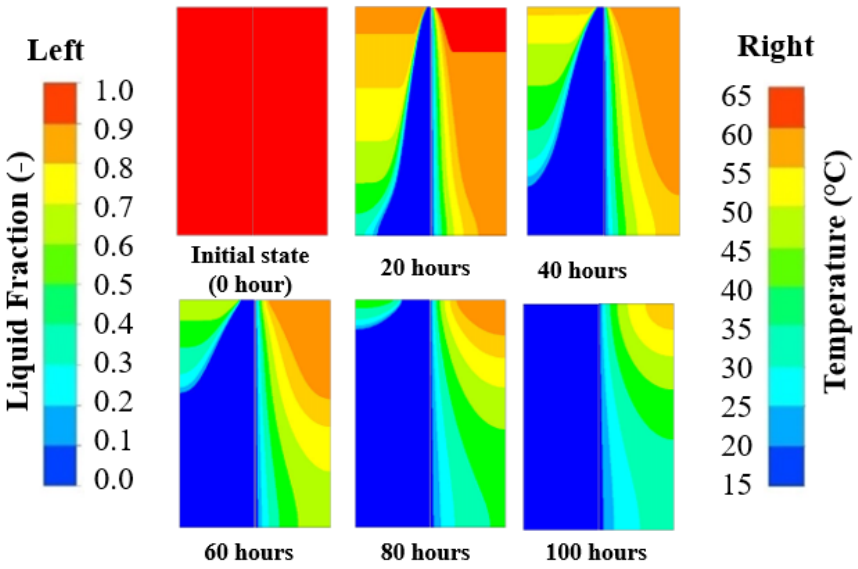

Fig. 6.4: The contour of the PCM liquid fraction (left) and temperature (right) in the cylindrical system during the discharging process.

6.3.2. Conical storage unit

Fig. 6.5 shows the experimental PCM temperature variations over time in positions A and B in the conical storage unit. The experimental condition is the same as that in the cylindrical storage unit with the same HTF inlet temperature of 10 °C and flow rate of 10 L/min. The temperature profile is almost the same as that presented in the cylindrical storage unit. This indicates that the heat transfer mechanism in the conical storage unit is the same as that in the cylindrical unit.

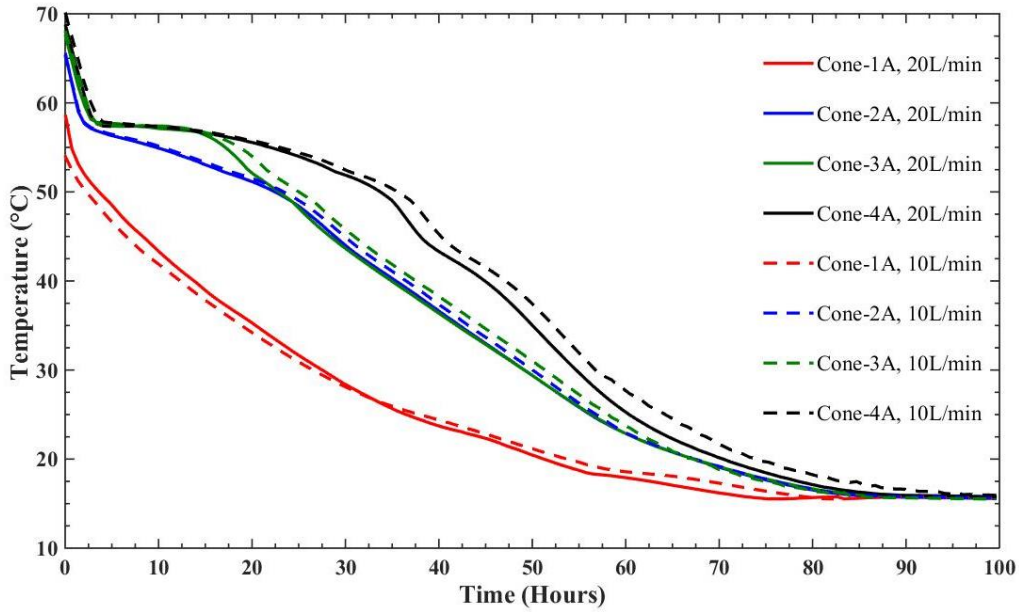

Fig. 6.5: PCM temperature profile for the conical system during the discharging process.

Fig. 6.6 shows simulated contours of the PCM liquid fraction (left side) and temperature field (right side) for the conical storage unit using the mathematical model. The liquid fraction contours show similar behaviour as the cylindrical one, the solidification front moves along both the axial and radial directions.

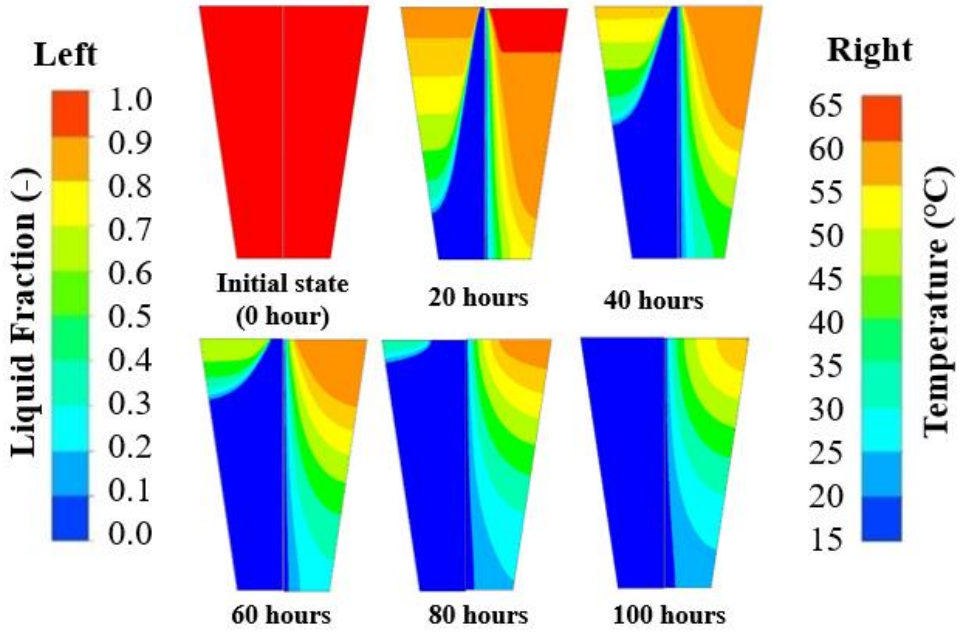

Fig. 6.6: The contour of the PCM liquid fraction (left) and temperature (right) in the conical system during the discharging process.

6.4.3. Comparison between the conical and cylindrical storage unit

In order to compare the thermal behavior between cylindrical and conical storage units during the charging process, Fig. 6.7 compares the PCM temperature at position A which has four thermocouples along axial direction, with the same distance from the center of the HTF pipe in both cylindrical and conical systems. It is found that the thermocouples at the positions 1A and 2A of the conical system drops much faster than those at same positions in the cylindrical system. This indicates that the energy recovered from the conical system is much faster than that in the cylindrical system initially. The temperatures at position 3A and 4A does not show much difference between the two systems. This is mainly due to the convective effect. In the upper part of the system, the convection heat transfer dominates the energy transfer in the system and hence the temperatures in both systems are similar. This indicates that the energy recovered from the both systems are almost the same during this stage. It can be further evidenced by all temperatures reaches the thermal equilibrium at almost the same time.

Fig. 6.8 shows a comparison of experimental temperatures at different levels in position B where thermocouples are located at about 5 mm away from the inner surface of the shell side. These temperatures indirectly represent energy recovered from the PCM close to the edge of the storage unit. In other words, if the temperatures at these locations reach stability, it means that the PCM below this position has all been solidified. It confirms that there is no significant difference between the total discharging times for the conical and cylindrical units. The temperatures at 1A and 2A position of the conical system are lower than those at the same position in the cylindrical position. This is because there is less PCM at the bottom of the conical system due to the geometry and hence the temperature of the PCM lowers faster. The temperatures at 3A and 4A positions indicated that the energy recovered from the two systems are almost at the same rate since conduction dominates the heat transfer in the solidification process.

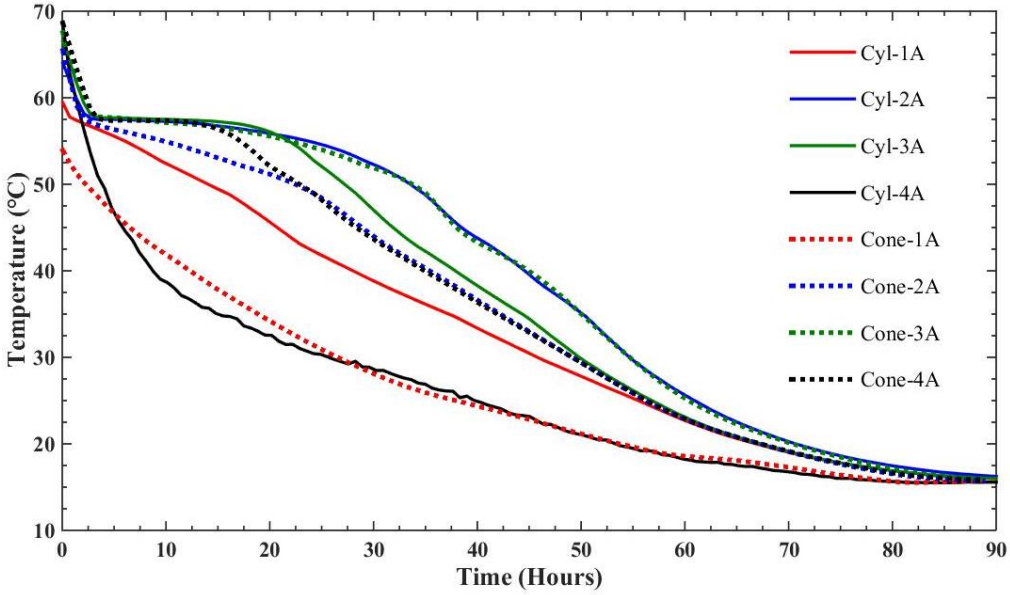

Fig. 6.7: Temperature profile comparison for cylindrical and conical systems at level A during the discharging process.

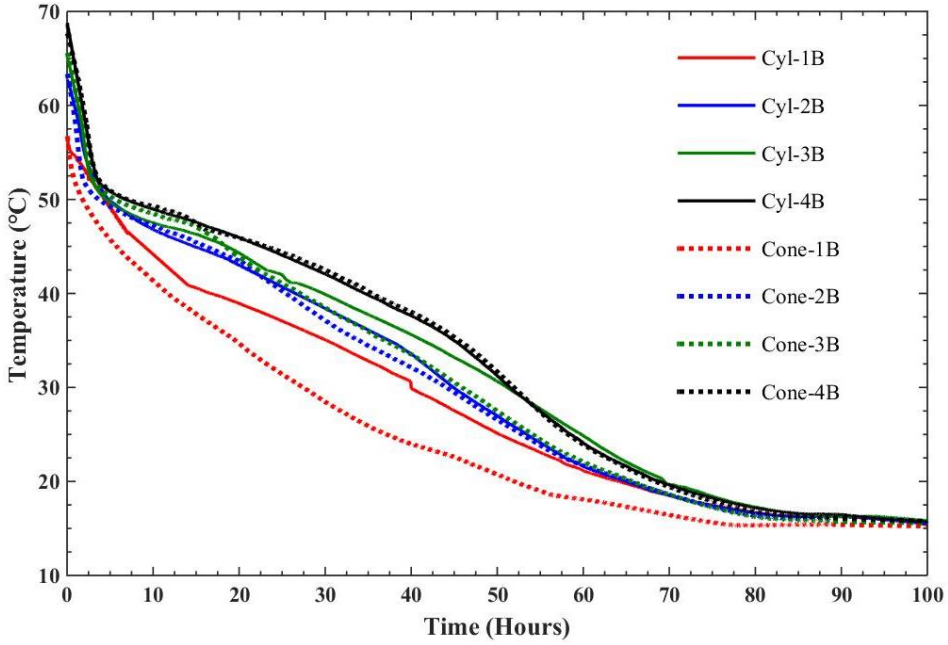

Fig. 6.8: Temperature profile comparison for cylindrical and conical systems at level B during the discharging process.

6.3.3. Effect of HTF flow rate during the discharging process

Figs. 6.9 shows the PCM temperature comparison with the flow rates of 10 and 20 L/min for cylindrical and conical systems during the discharging process. It is found that the mass

flow rate of the HTF does not show significant effect on the heat transfer rate in the PCM in the two systems. This is because the flow in the HTF is turbulent flow leading to high heat transfer rate. This heat transfer rate is much higher than the heat transfer flow rate between the HTF pipe and PCM caused by natural convection. Therefore, the heat transfer bottle-neck is the thermal resistance between the HTF pipe and PCM in the thermal resistance circuit. Further enhancing the heat transfer in the HTF side will not have big effect on the total thermal resistance and hence the flow rate does not show significant effect on the charging and discharging process under the studied flow region.

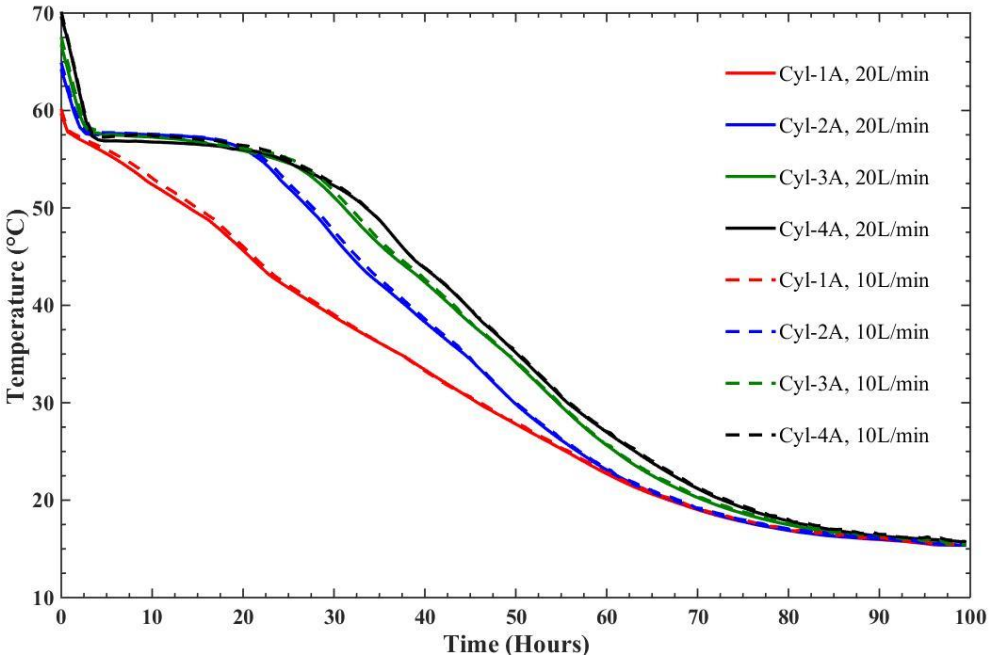

(a)

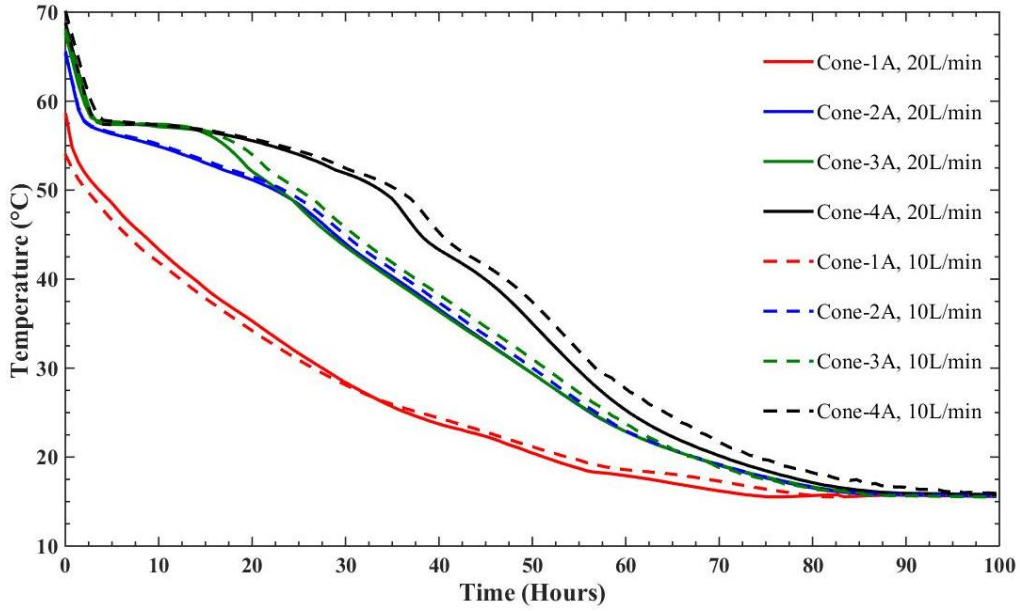

(b)

Fig. 6.9: PCM temperature variations during the discharging process with different HTF flow rates a) cylindrical and b) conical systems.

6.4. Conclusion

In this chapter, thermal behavior and heat transfer characteristics in conical and cylindrical shell-and-tube energy storage units were investigated during a discharging process. The experimental and theoretical results showed that the PCM solidifies around the HTF pipe and the solidification front moves both outward and upward. Due to its low thermal conductivity, the PCM behaves as an insulating material and the rate of heat transfer from the HTF to the PCM is reduced. The comparative results show that both systems have similar trend and it takes almost the same time to complete the discharging process. It is also found that increasing the HTF flow rate does not improve the overall performance of these systems.

6.5. References

[1] Seddegh S, Wang X, Henderson AD, Xing Z. Solar domestic hot water systems using latent heat energy storage medium: A review. Renewable and Sustainable energy reviews. 2015;49:517-33.

[2] Zivkovic B, Fujii I. An analysis of isothermal phase change of phase change material within rectangular and cylindrical containers. Solar Energy. 2001;70:51-61.

[3] Vyshak N, Jilani G. Numerical analysis of latent heat thermal energy storage system. Energy conversion and management. 2007;48:2161-8.

[4] F. Agyenim, P. Eames, M. Smyth, A comparison of heat transfer enhancement in a medium temperature thermal energy storage heat exchanger using fins, Solar Energy, 83 (9), 2009, 1509-1520.

[5] F. Agyenim, P. Eames, M. Smyth, Heat transfer enhancement in medium temperature thermal energy storage system using a multitube heat transfer array, Renewable Energy, 35 (1), 2010, 198-207.

[6] Agyenim F, Eames P, Smyth M. Experimental study on the melting and solidification behaviour of a medium temperature phase change storage material (Erythritol) system augmented with fins to power a LiBr/H2O absorption cooling system. Renewable energy. 2011;36:108-17.

[7] Hosseini M, Ranjbar A, Sedighi K, Rahimi M. A combined experimental and computational study on the melting behavior of a medium temperature phase change storage material inside shell and tube heat exchanger. International Communications in Heat and Mass Transfer. 2012.

[8] Hosseini M, Rahimi M, Bahrampoury R. Experimental and computational evolution of a shell and tube heat exchanger as a PCM thermal storage system. International Communications in Heat and Mass Transfer. 2014;50:128-36.

[9] Avci M, Yazici MY. Experimental study of thermal energy storage characteristics of a paraffin in a horizontal tube-in-shell storage unit. Energy conversion and management. 2013;73:271-7.

[10] Murray RE, Groulx D. Experimental study of the phase change and energy characteristics inside a cylindrical latent heat energy storage system: Part 1 consecutive charging and discharging. Renewable energy. 2014;62:571-81.

[11] Murray RE, Groulx D. Experimental study of the phase change and energy characteristics inside a cylindrical latent heat energy storage system: Part 2 simultaneous charging and discharging. Renewable energy. 2014;63:724-34.

[12] Seddegh S, Wang X, Henderson AD. Numerical investigation of heat transfer mechanism in a vertical shell and tube latent heat energy storage system. Applied thermal engineering. 2015;87:698-706.

[13] Seddegh S, Wang X, Henderson AD. A comparative study of thermal behaviour of a horizontal and vertical shell-and-tube energy storage using phase change materials. Applied Thermal Engineering. 2016; 93:348-358.

[14] Al-abidi AA, Bin Mat S, Sopian K, Sulaiman M, Mohammed AT. CFD applications for latent heat thermal energy storage: a review. Renewable and Sustainable energy reviews. 2013;20:353-63.

[15] Liu S, Li Y, Zhang Y. Mathematical solutions and numerical models employed for the investigations of PCMs′ phase transformations. Renewable and Sustainable energy reviews. 2014;33:659-74.

[16] Seddegh S, Wang. Heat transfer investigation of cylindrical and conical shell-and-tube latent heat thermal energy storage systems during charging processes. Accepted for publication with minor revision in the journal of Applied Thermal Engineering.

Chapter7: Experimental investigation of the effect of geometrical parameter on a cylindrical shell-and-tube latent heat thermal energy storage system

7.1. Chapter summary

The main objective of this chapter is to study the effect of the geometrical parameter on vertical cylindrical shell-and-tube latent heat thermal energy storage (LHTES) systems. Four different shell to tube diameter ratios are considered with the phase change material (PCM) in the shell side and the heat transfer fluid (HTF) flowing inside the tube. The PCM temperature distributions are measured and compared experimentally. The results show that complete charging and discharging is highly dependent on the ratio of outside to the inside diameter as well as the HTF temperature. The effects of HTF flow rate were also examined experimentally. It is concluded that there is no significant difference in the charging and discharging time by increasing the HTF flow rate as far as the HTF flow is turbulent. For the design purpose, this parameter is highly dependent on the hours of sunlight as well as the output temperature of the solar collector.

This research contained within this chapter has been submission for review and publication as: Saeid Seddegh, Xiaolin Wang, Zane Smith. "Experimental investigations of the geometrical parameter on cylindrical shell and tube latent heat thermal energy storage system", International Journal of Heat and Mass Transfer.

7.2. Introduction

The most intensely analysed type of latent heat thermal energy storage (LHTES) unit is the shell-and-tube system, accounting for more than 70% of the systems studied. This is because such system is simple and heat loss from a shell-and-tube system is minimal [1, 2]. Lacroix [3] performed a pioneering numerical study to assess the effect of various thermal and geometric parameters on the heat transfer process of a shell-and-tube LHTES system during the charging process. N-octadecane with a melting temperature of 26 °C was used as the phase change material (PCM) filling the shell space, and water as the heat transfer fluid (HTF) flowing inside the tubes (R_i=0.00635 m, R_o=0.0129 m, L=1 m). results showed that the whole PCM melting time depended not only upon thermal and geometric parameters, but also on the thermophysical properties of the PCM. Esen et al. [4] undertook a series of numerical tests to investigate the effects of various PCMs, cylinder and pipe radii, total PCM volume, HTF mass flow rate and temperature on the charging time. The results showed that the stored energy growed as the HTF inlet temperature increased. Further, Ismail and his collaborators [5, 6] developed a two-dimensional model to study the effect of the ratio of outer to inner tube radii (R_0/R_i) for the PCM around a vertical cylinder. The results indicated that the solidification mass fraction decreased with R_0/R_i and the time necessary for the complete fusion increased.

Trap et al. [7] performed a numerical study to evaluate the influence of tube length, shell radius, HTF inlet velocity and temperature on the amount of stored and recovered energy during the melting and solidification processes. It was concluded that the selection of operating conditions and geometrical parameter dimensions depended on the required heat transfer rate and the time in which the energy was to be stored and delivered. Tao and He [8] developed a two-dimensional mathematical model to study the effect of non-steady state HTF inlet conditions in a water/n-octadecane shell-and-tube LHTES unit (R_i=0.00635 m, R_o=0.01135 m,

L=1 m). It was revealed that the PCM melting time decreased with the increase in initial HTF inlet mass flow rate and temperature, when the hourly average of these parameters were fixed.

Avic and Yazici [9] experimentally recorded the time histories of a paraffin (P56-58) PCM in a horizontal shell-and-tube heat exchanger LHTES (R_i=0.028 m, R_o=0.103 m, L=0.5 m). It was found that increasing (for the charging process) or decreasing (for discharging process) the HTF inlet temperature enhanced PCM melting and solidification, respectively. Hosseini et al. [10] experimentally and computationally investigated heat transfer characteristics of a horizontal shell-and-tube heat exchanger LHTES system (R_i=0.022 m, R_o=0.085 m, L=1 m) using RT50 with a melting temperature of 50 ºC as the PCM. It was revealed that as the inlet HTF temperature increased from 70 to 80 °C, the total melting time decreased by 37%, and the theoretical efficiency in charging and discharging processes rised from 81.1% to 88.4% and from 79.7% to 81.4%, respectively. Seddegh et al. [11] compared heat transfer in the horizontal and vertical shell-and-tube LHTES systems. It was shown that the hot HTF inlet temperature has a large effect on heat transfer in both horizontal and vertical systems. However, the HTF flow rate has little effect on both charging and discharging processes in the energy storage units.

Wang et al. [12] numerically investigated the effects of HTF inlet temperature and mass flow rate on a horizontal shell-and-tube heat exchanger LHTES (R_i=0.0127 m, R_o=0.0258 m, L=1 m). The results showed that the HTF inlet temperature greatly affected the time taken to complete the charging or discharging process. However, the HTF mass flow rate has little influence on the amount of energy stored, and the time needed to complete the charging or discharging process decreased nonlinearly as the HTF mass flow rate increased. The same authors [13] later showed that as the length of the tube increased, the energy efficiency ratio reduced, but the heat storage rate increased. In addition, increasing the outer radius decreased

both the energy efficiency ratio and the heat storage rate. Thus, more attention should be paid to the outer tube's radius in the design process.

More recently, Tehrani et al. [14] reviewed low to medium temperature shell-and-tube LHTES systems and showed that the majority of the studies were numerical. In addition, researchers used different PCMs and HTFs based on the application as well as various geometrical parameters such as shell-to-tube ratio and unit length. Such extensive analyses complicated the comparison and optimization of the shell-and-tube system. This chapter therefore focused on determining the effect of the shell-to-tube ratio on the performance of vertical cylindrical shell-and-tube LHTES systems. For this purpose, the temporal variations of four similar LHTES units with different HTF pipe diameters were measured and compared. The effects of HTF temperature and flow rate were also examined experimentally.

7.3. Experimental Set up

7.3.1. Apparatus

Fig. 7.1 shows an experimental setup which consists of a hot water tank, a cold water tank, PCM storage systems, hot and cold water pumps, flow meter, data acquisition module, thermocouples, valves and extensive piping systems. Water is used as both the hot and cold heat transfer fluid (HTF).

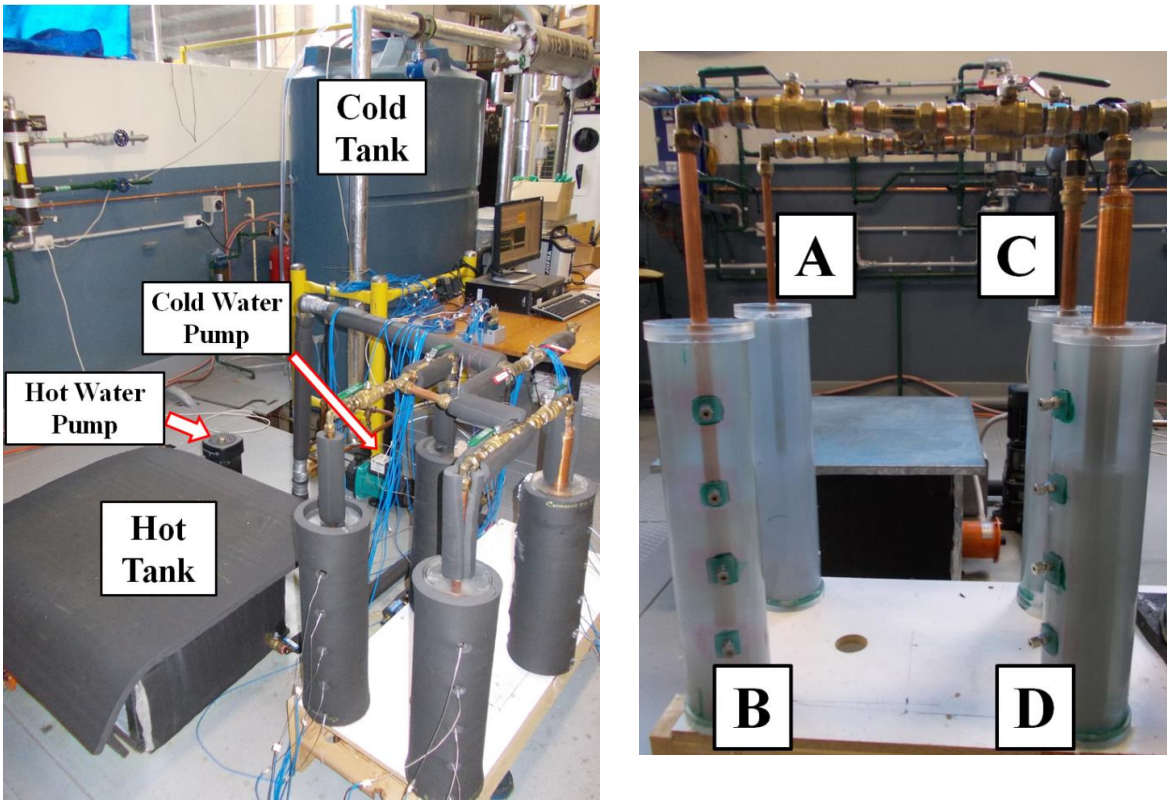

Fig. 7.1: A photograph of whole experimental rig.

During the charging process, the hot HTF is heated up to the pre-set temperature in the 108 L capacity hot water tank using two 2.4 kW thermal electric immersion heaters (model number TWI50240) with externally adjustable thermostats. The hot water is circulated by a Grundfos vertical, multistage centrifugal pump (model number: CR 1-4 A-A-A-E-HQQE) through the inner pipe in the PCM container where PCM is packed between the inner pipe and cylindrical shell. The hot water is then channelled back to the hot water tank from the exit of the storage system. During the discharging process, the cold water is maintained at the required temperature using a 20 kW chiller (model number HWP020-3BB) in the 1575 L capacity cold tank. The cold water is circulated by an Onga horizontal, centrifugal pump (model number: 413) through the inner pipe in the PCM container to cool the PCM. A Flomec oval gear positive-displacement flow meter with pulse output is placed in position between the container outlets and hot/cold water tanks to monitor the hot and cold water flow rates. Temperatures

and water flow rates are recorded by the data acquisition system (National Instruments NI9411).

7.3.2. PCM storage containers

Four containers of 0.5 m height and 0.1 m outer diameter with different inner diameters of 12.7 mm (0.5 inch), 19.05 mm (0.75 inch), 25.04 mm (1 inch), 38.1 mm (1.5 inch) at the centre to allow the HTF to pass through were constructed as seen in Fig. 7.1. All containers are made of transparent polypropylene (with thermal conductivity k of 0.1 W/m·K) with a thickness of 6 mm for observing the melting process. The containers are insulated with Armaflex sheets with a thermal conductivity of 0.036 W/m·K. Table 7.1 shows the specification of each shell-and-tube unit.

Table 7.1: Specification of shell and tube systems

LHTES Unit	Length (m)	Outer diameter (m)	Inner diameter (m)	Diameter ratio	Amount of PCM (kg)
	L (m)	D_o	D_i	D_o/D_i	M
Cylinder A	0.5	0.1	0.01270	8.1	3.0
Cylinder B	0.5	0.1	0.01905	5.4	2.9
Cylinder C	0.5	0.1	0.02504	4.0	2.7
Cylinder D	0.5	0.1	0.03810	2.7	2.4

The PCM temperatures inside the four containers are measured by Type-T thermocouples with an accuracy of ±0.2 °C. The position of the thermocouples is shown in Fig. 7.2. In order to compare the PCM thermal behavior between these vertical cylindrical containers, four thermocouples are located on four levels in the same radial position being 20 mm away from the outer surface of the HTF pipe. Another four thermocouples are located at four levels in the same radial position being 5 mm away from the inner surface of containers to identify if the PCM completely melted or solidified above this position. The PCM used in the test is RT60 paraffin wax from Rubitherm Gmbh. PCM thermal properties and testing conditions are listed in Table 7.2.

Table 7.2: Thermophysical properties and test conditions

PCM	Melting Temperature (°C)	Latent Heat of Fusion (kJ/kg)	Density (kg/m^3)		Specific Heat (J/kgK)	Thermal conductivity (W/mK)	Volume expansion (%)	Dynamic viscosity (Kg/ m S)
Paraffin wax (RT60)	55-61	123506	Solid (15 °C)	Liquid (80 °C)	2000	0.2	12.5	3.705E^{-5}
			880	770				
Heat transfer fluid (HTF)	**Charging Temperature (°C)**	**Discharging Temperature (°C)**	**Density (kg/m^3)**		**Specific Heat (J/kgK)**		**Thermal conductivity (W/mK)**	
Water	70 and 80	10	998		4183		0.58	

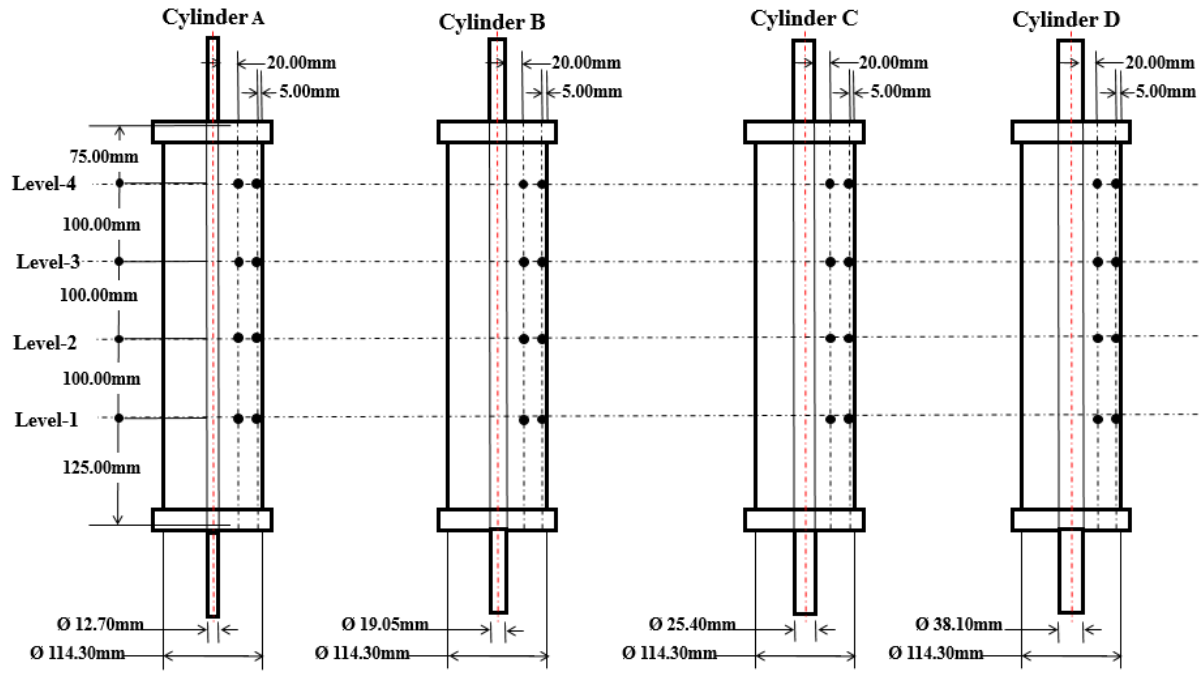

Fig. 7.2 locations of thermocouples (bold points represent the positions of thermocouples).

7.4. Results and discussion

The experiments were performed at different HTF inlet temperatures and flow rates. The thermal behaviour of the four different latent heat thermal energy storage systems were investigated and compared as detailed in the following sections.

7.4.1. Charging process

Before running the charging process, cold water with the temperature of 10 °C is passed through the HTF pipe to set the PCM temperature in all thermocouple to 15 °C. Then, water

with the temperature of 70 °C and the flow rate of 10 L/min is passed to melt the PCM during the charging process.

7.4.1.1 Charging process- 5 mm thermocouple

Fig. 7.3 (a-d) shows temperature variations in thermocouple probes located 5 mm away from the inner surface of the acrylic cylinder within each container during the charging process. It can be seen that PCM temperatures at different levels reach steady state at different times. The time needed for PCM to reach steady state for higher levels is shorter than for lower levels. This is due to natural convection heat transfer coming from the boussinesq effect. The entire mass of PCM in each cylinder must be completely melted when the thermocouple located 5 mm away from the inner surface of the acrylic cylinder in level 1 shows a steady temperature. Comparing the total melting time for different cylinders shows that increasing the inner radii reduces the required charging time. It is due to the fact that the bigger inner diameter provides more heat transfer surfaces. Reducing the outer to inner diameter ratio from 8.1 to 2.7 in cylinders A to D respectively, decreases the charging time up to 28%.

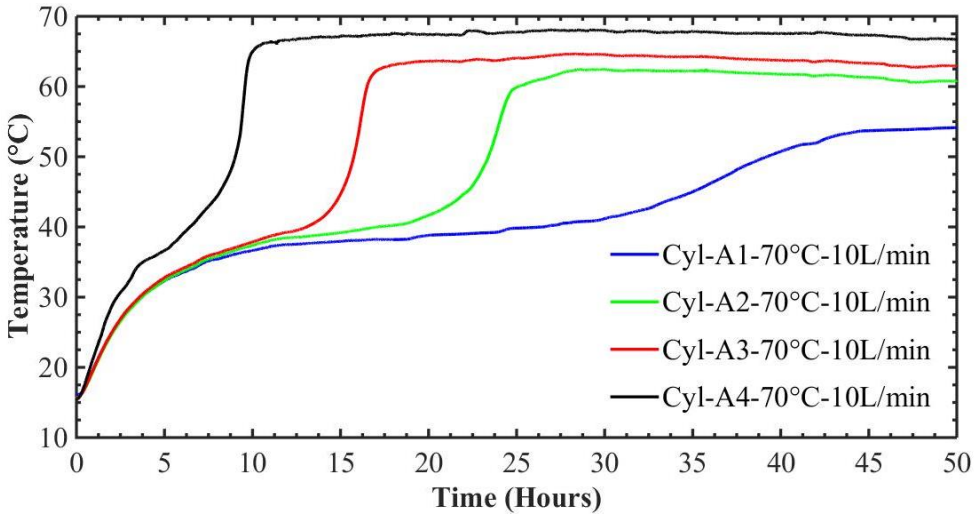

(a) Cylinder A

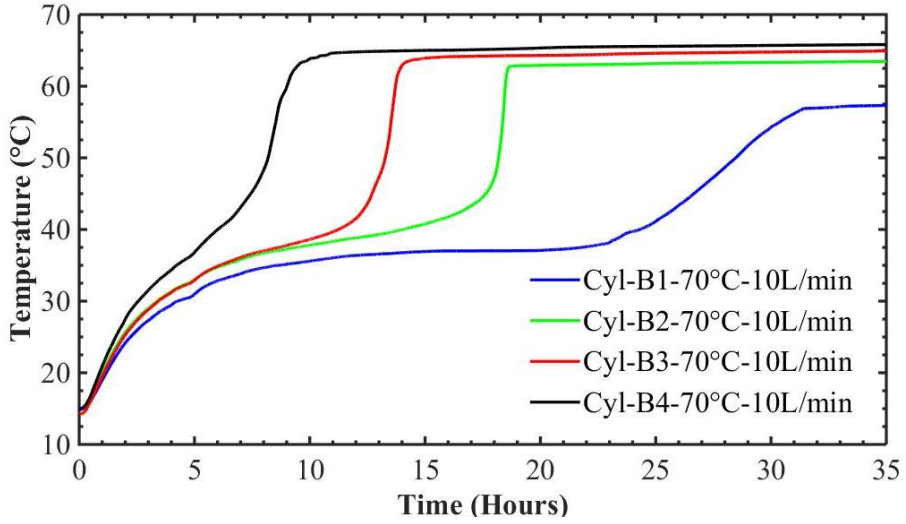

(b) Cylinder B

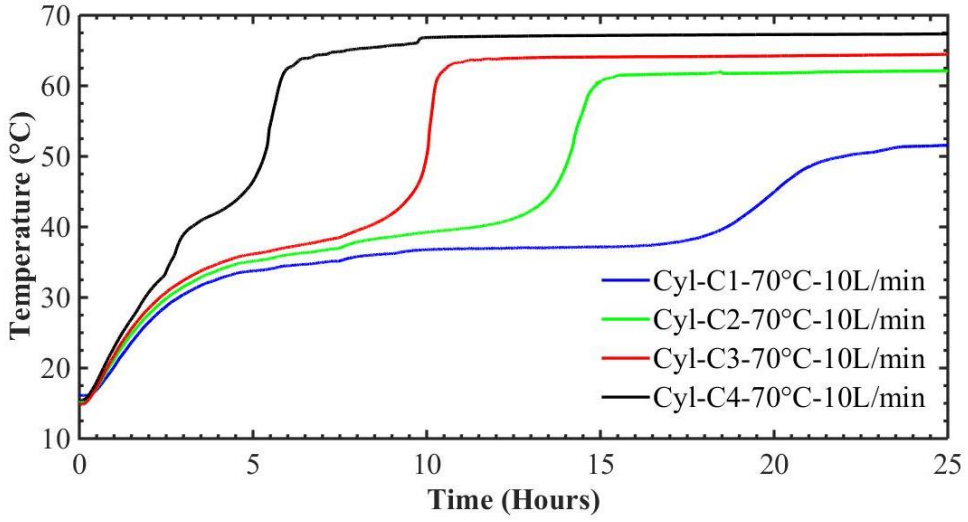

(c) Cylinder C

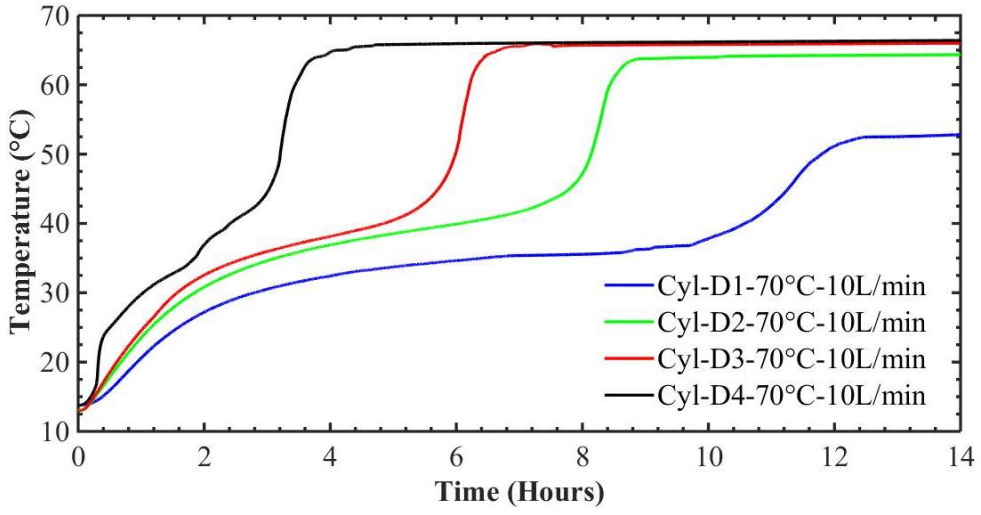

(d) Cylinder D

Fig. 7.3: Comparison of thermocouple probes located 5 mm away from HTF pipe during the charging process.

7.4.1.2 Charging process- 20 mm thermocouple

Fig.7.4 (a-d) compares temperature variations of thermocouple probes located 20 mm away from the HTF pipe at each level for the HTF charging temperature of 70 °C and the flow rate of 10 L/min. Since the distance of each thermocouple was kept constant from the outer of HTF tube, it obviously shows the significant effect of HTF surface on the variation of PCM temperature. The time is needed for PCM on level 1 to reach steady state decreases from 26 to 6 hour from cylinders A to D respectively. This time difference is 9, 6, and 4 hours in levels 2, 3, and 4 respectively. This reveals that at higher levels, the influence of the diameter ratio decreases as the time delay reduces. This is mainly due to natural convective heat transfer, which is more dominant at higher levels since the liquid PCM raises up due to the Boussinesq effect.

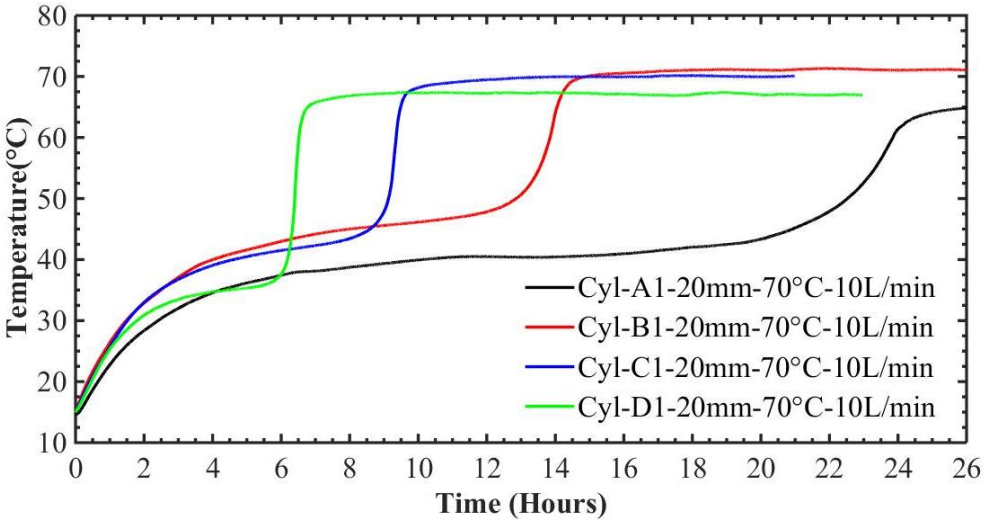

(a) Level 1

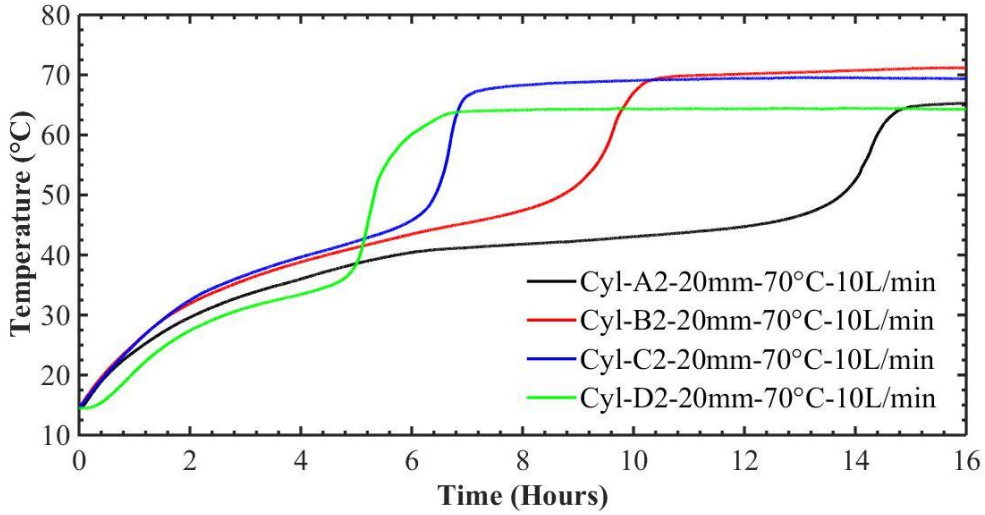

(b) Level 2

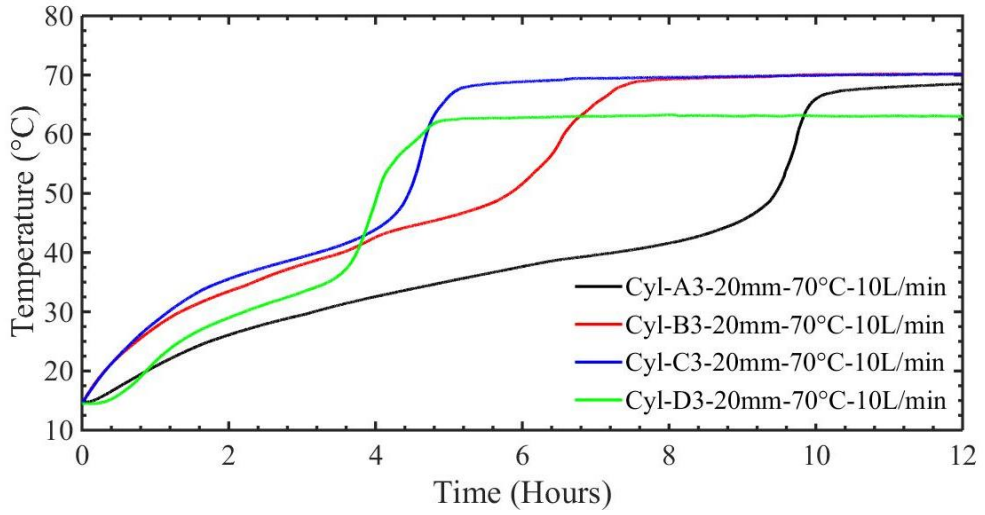

(c) Level 3

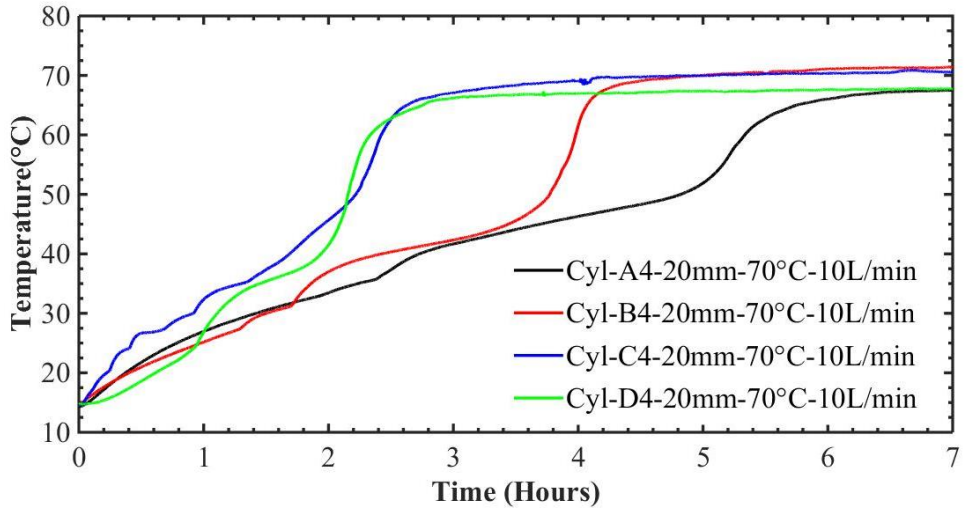

(d) Level 4

Fig. 7.4: Comparison of thermocouple probes located 20 mm away from HTF pipe during charging process.

7.4.2. Discharging process

After finishing the charging process, the cylinders were immediately discharged by passing cold HTF at a temperature of 10°C and flow rate of 10 L/min.

7.4.2.1 Discharging process- 5 mm thermocouple

Fig. 7.5 (a-d) shows the temperature variation in thermocouple probes located 5mm away from the inner surface of the acrylic cylinder within each container during the discharging process. It can be seen that for each cylinder, the PCM at different thermocouple locations solidify at almost the same time because conduction is the main heat transfer mechanism in the discharging process. Comparing the total solidification time for each of the different cylinders, it is concluded that increasing the inner radii reduces the required discharging time which is due to providing more heat transfer surfaces. Reducing the outer to inner diameter ratios from 8.1 to 2.7 between cylinders A and D, decreases the discharging time to 44%.

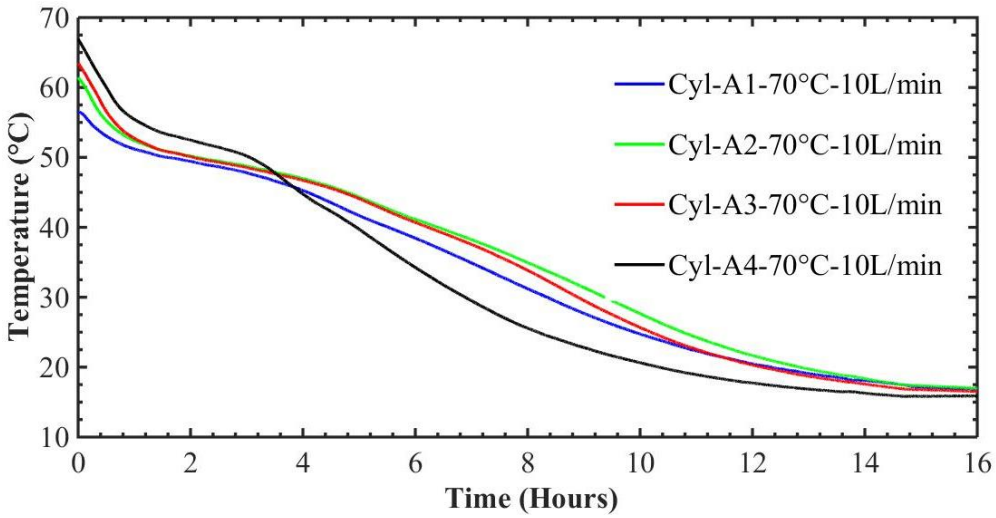

(a) Cylinder A

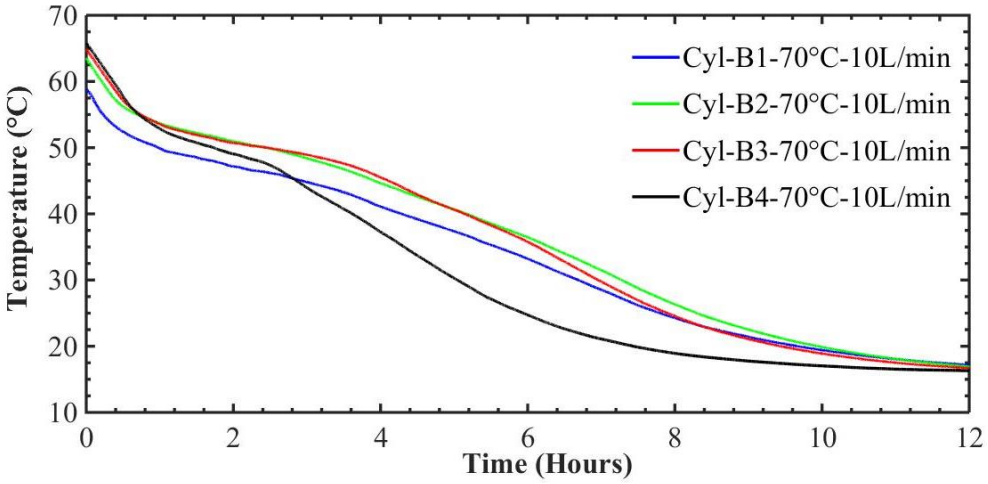

(b) Cylinder B

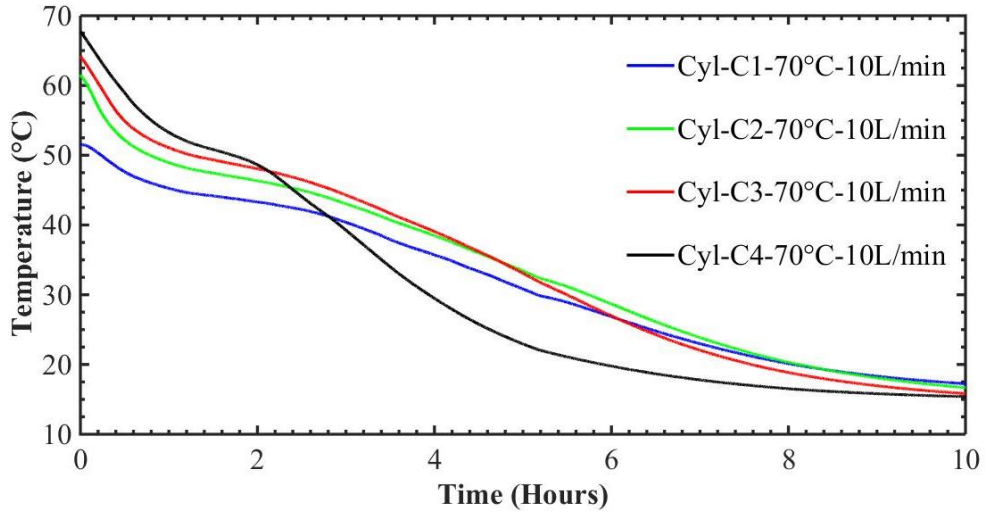

(c) Cylinder C

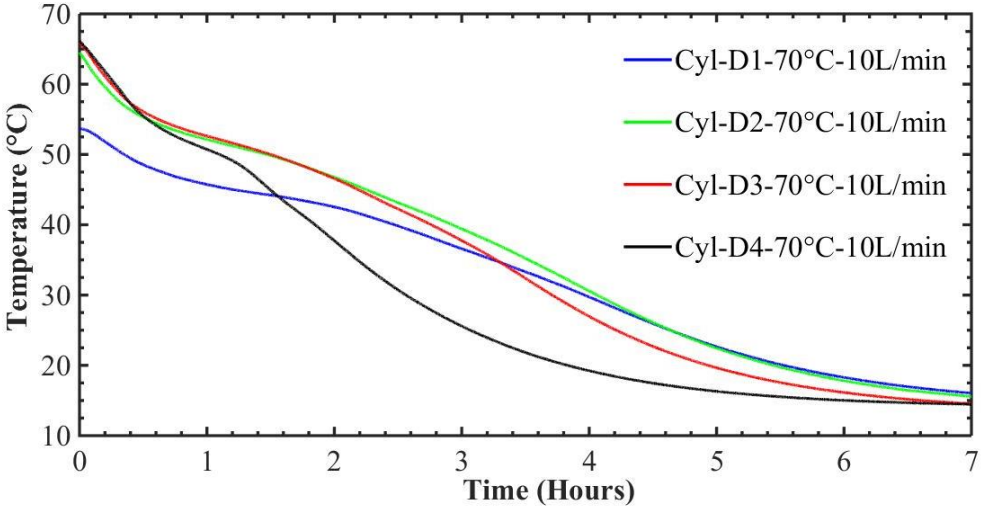

(d) Cylinder D

Fig. 7.5: Comparison of thermocouple probes located 5 mm away from HTF pipe during discharging process.

7.4.2.2 Discharging process- 20 mm thermocouple

Fig. 7.6 (a-d) compares the temperature variation at each level for the thermocouple probes located 20mm away from the HTF pipe and initially charged with HTF at temperatures of 70 °C and the flow rate of 10 L/min. It can be seen that contrary to the charging process, the time needed for PCMs in different locations to solidify does not change significantly in different levels. This is due to the fact that the main heat transfer mechanism during the discharging process is conduction. It takes almost 10 hours for the PCM temperature to decrease from 70 °C to 20 °C in all thermocouple located at 20 mm away from the HTF pipe. It can be concluded that different diameter ratios do not significantly reduce the time is needed for the PCMs at the same distance from the outer of HTF pipe to solidify.

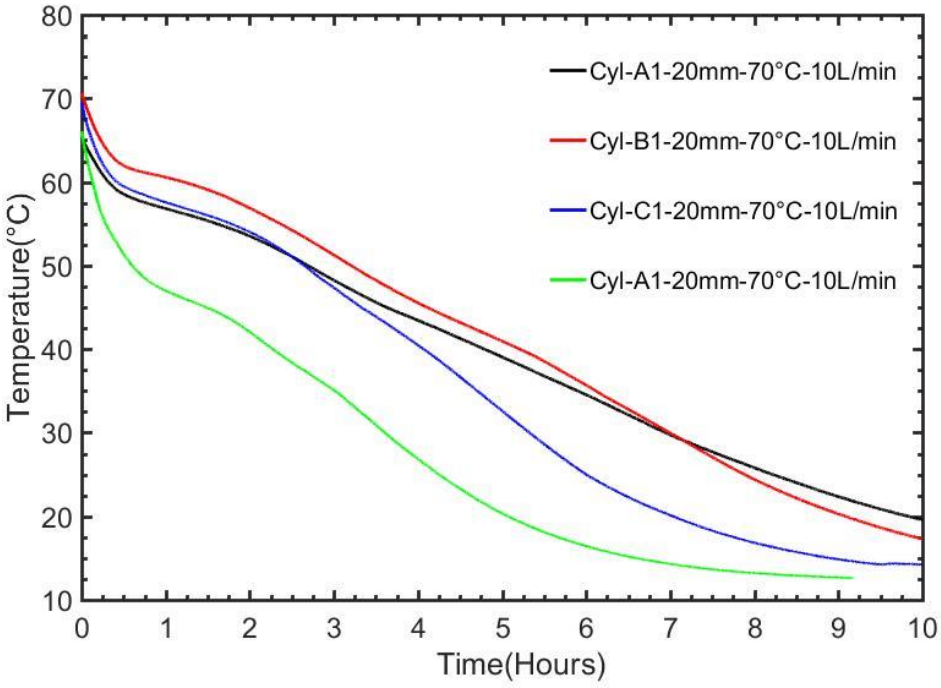

(a) Level 1

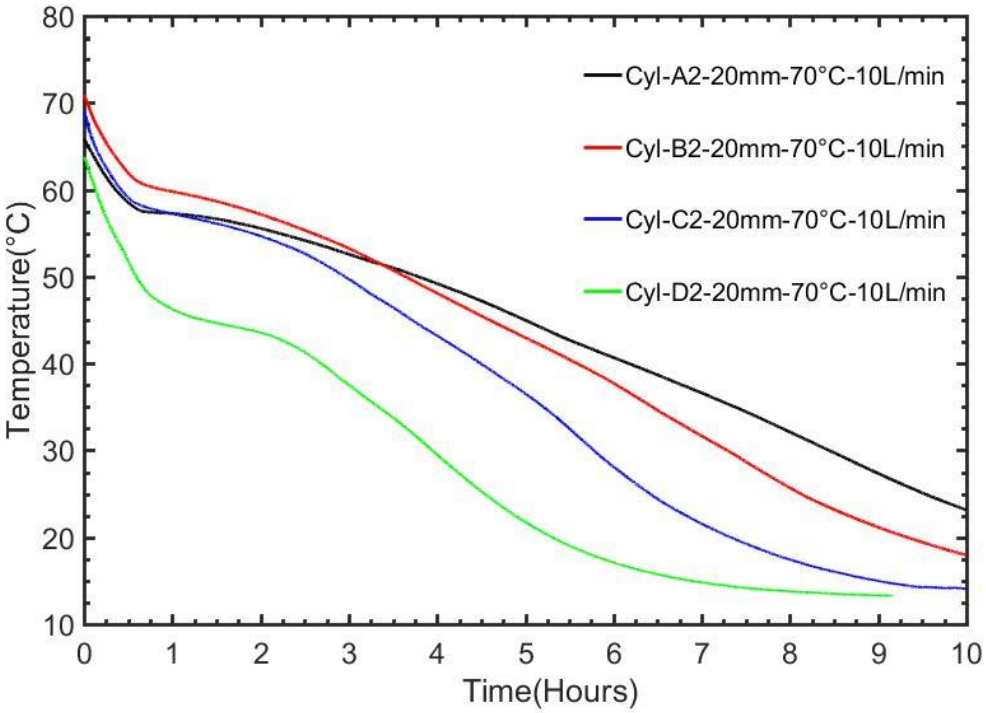

(b) Level 2

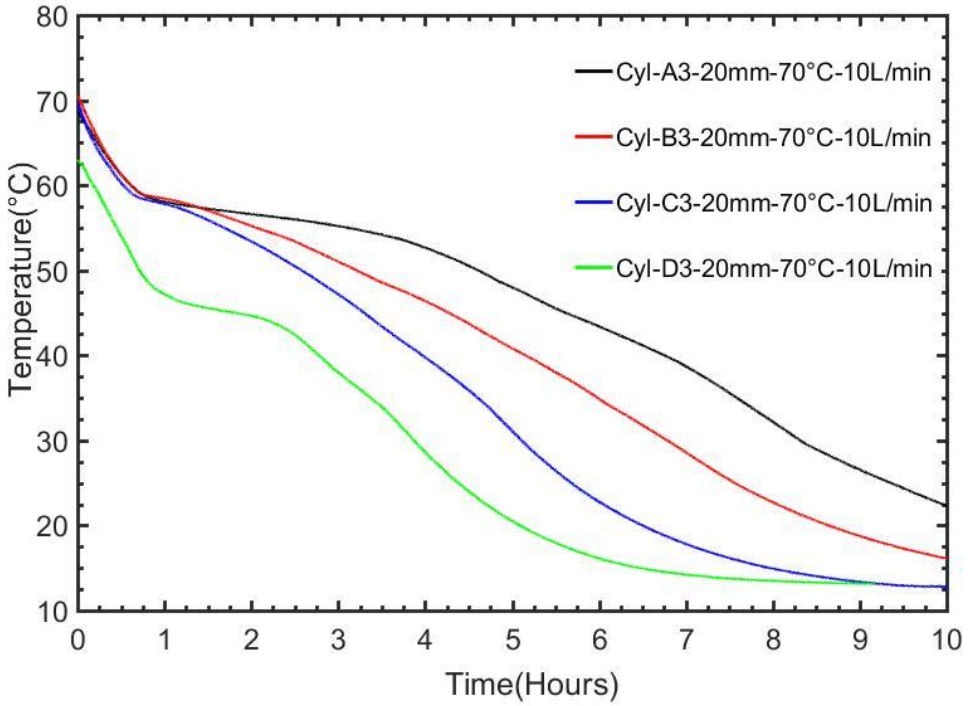

(c) Level 3

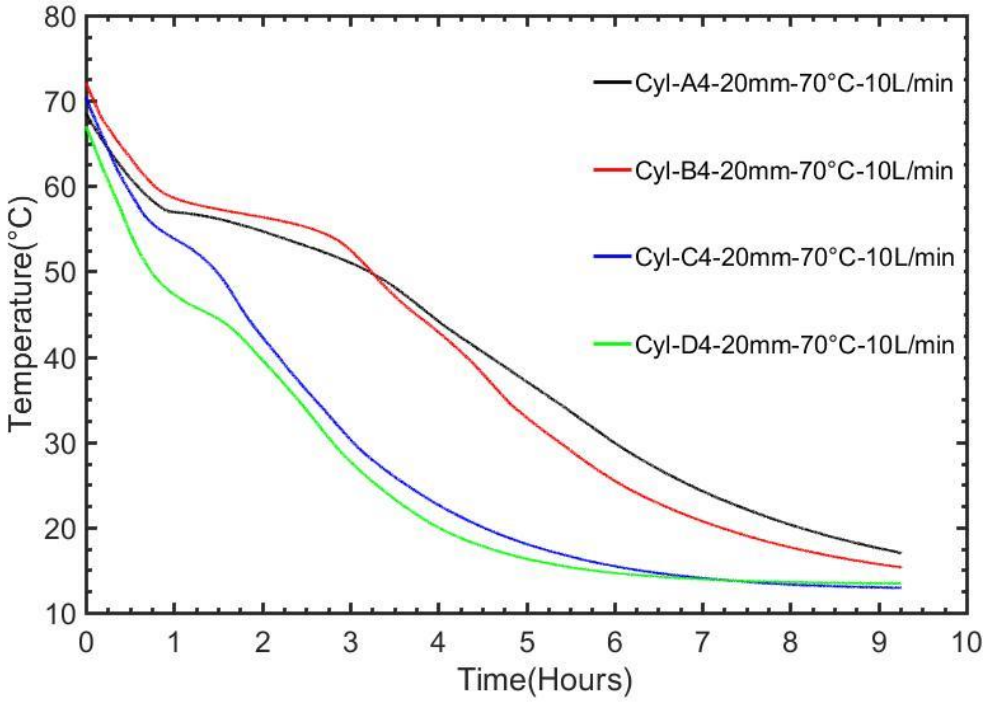

(d) Level 4

Fig. 7.6: Comparison of thermocouple probes located 20 mm away from HTF pipe during discharging process.

7.4.3. Comparing LHTES units based on the HTF temperature

7.4.3.1 Charging Process

The LHTES systems were charged by the HTF temperature of 70°C and 80°C while the HTF flow was kept constant at 10 L/min. Fig. 7.7 (a-d) shows the comparison of the PCM temperature variations for thermocouple probes located 5 mm away from the inner diameter of the acrylic cylinder after being charged with HTF at 70°C and 80°C. It is concluded that increasing the HTF temperature from 70 to 80 °C reduces the total charging time by 68%, 63%, 60%, and 54% in cylinders A, B, C, and D respectively. It is concluded that the effect of increasing the HTF inlet temperature decreases as the outer to inner radii reduce from cylinder A to D.

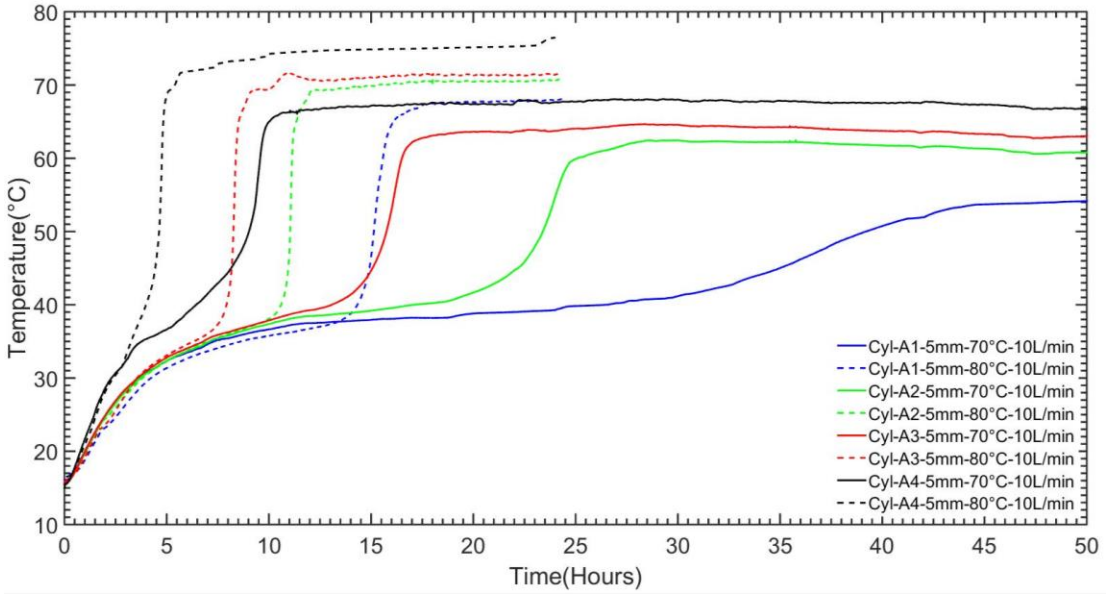

(a) Cylinder A

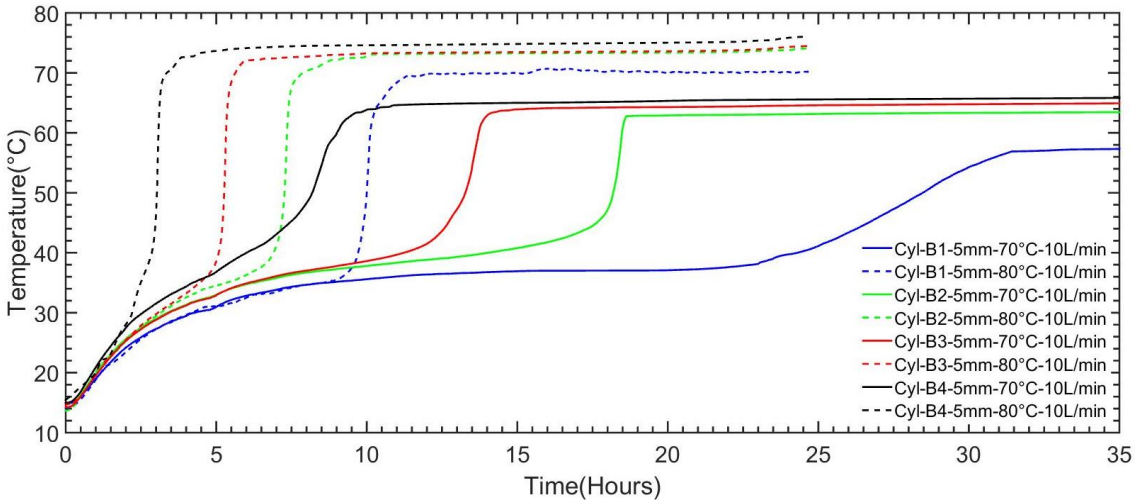

(b) Cylinder B

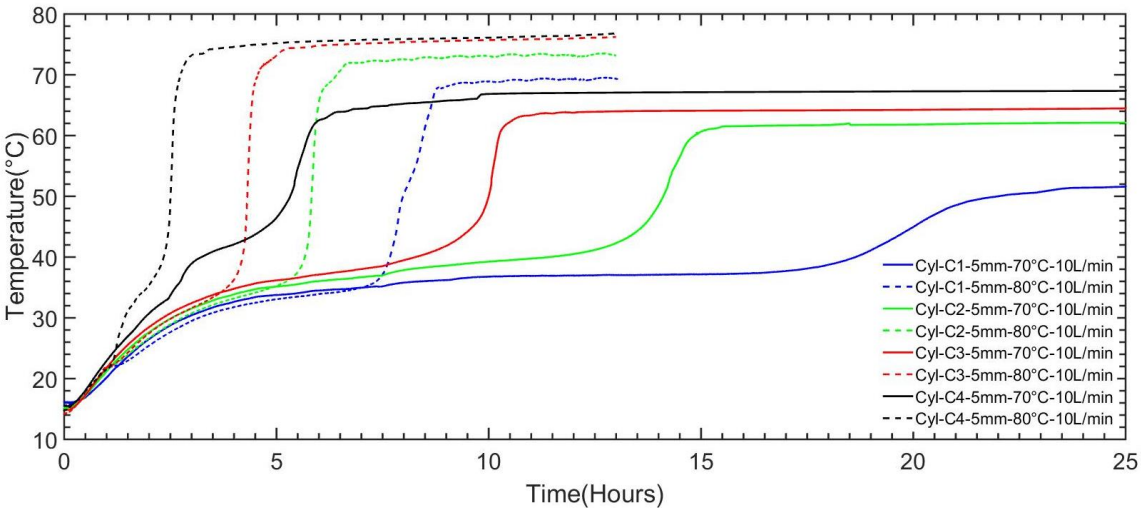

(c) Cylinder C

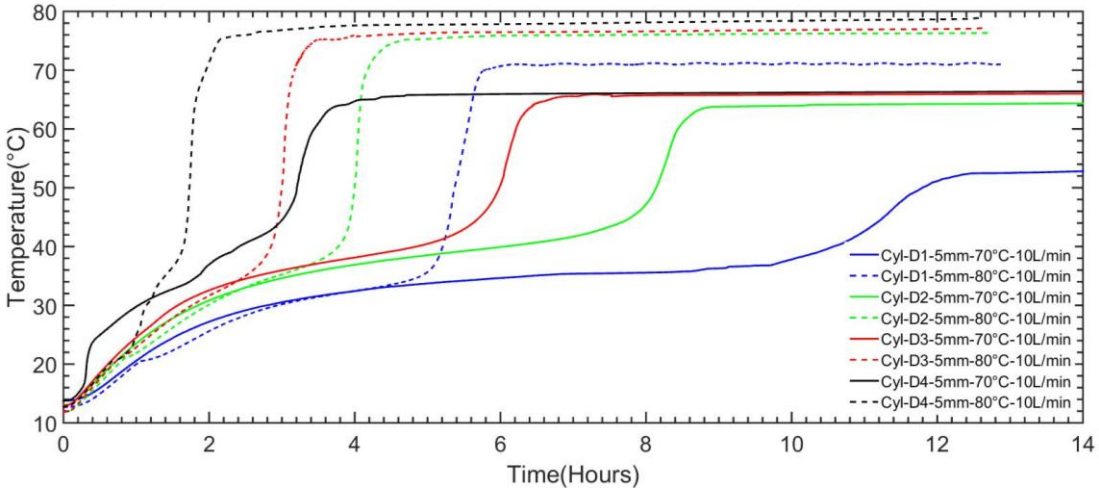

(d) Cylinder D

Fig. 7.7: Comparison of thermocouple probes located 5 mm away from HTF pipe during charging at 70°C and 80°C with the flow rate kept constant at 10 L/min.

Fig. 7.8 (a-d) shows the temperature variations for thermocouple probes located 20 mm away from the inner diameter of the acrylic cylinder after being charged with HTF at 70°C and 80°C. It can be seen that the influence of increasing the HTF temperature decreases from cylinder D to A in each level. It means that at higher outer to inner radii, increasing the HTF temperature is more pronounced.

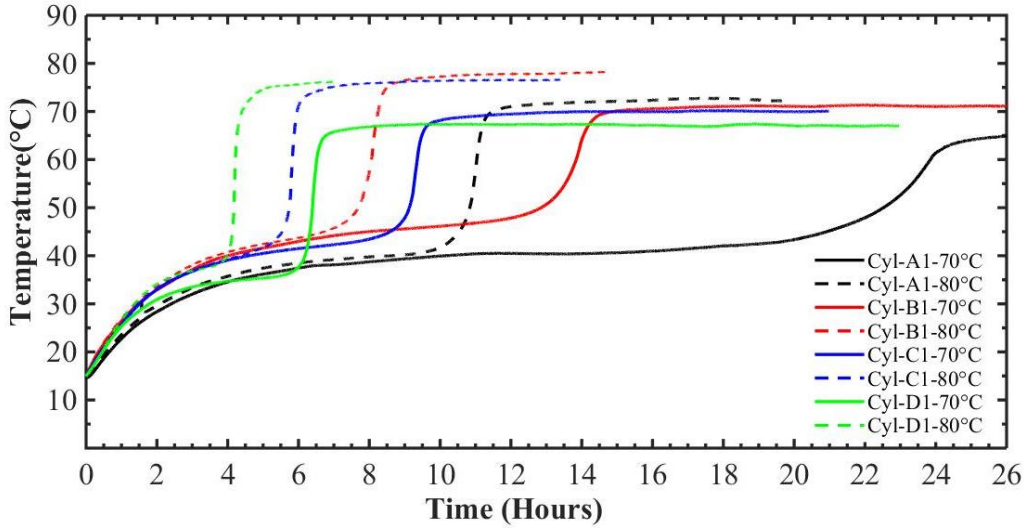

(a) Level 1

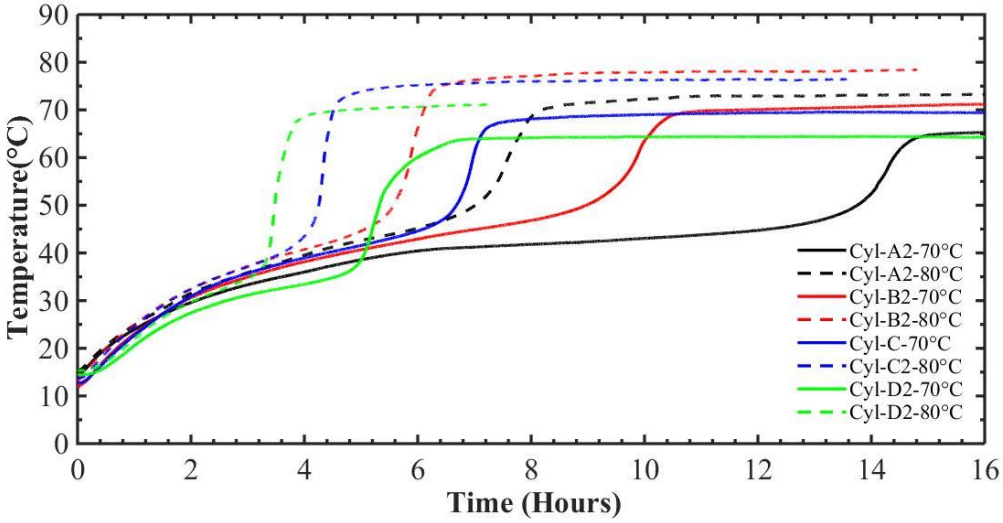

(b) Level 2

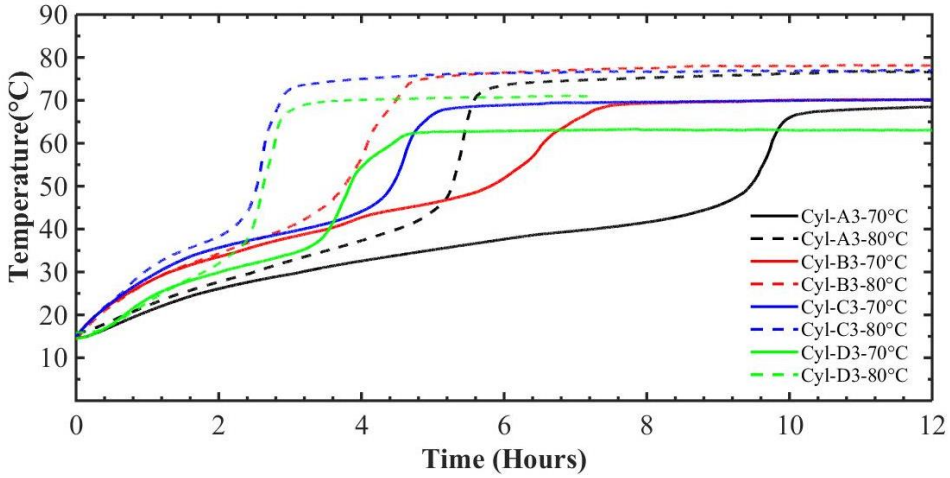

(c) Level 3

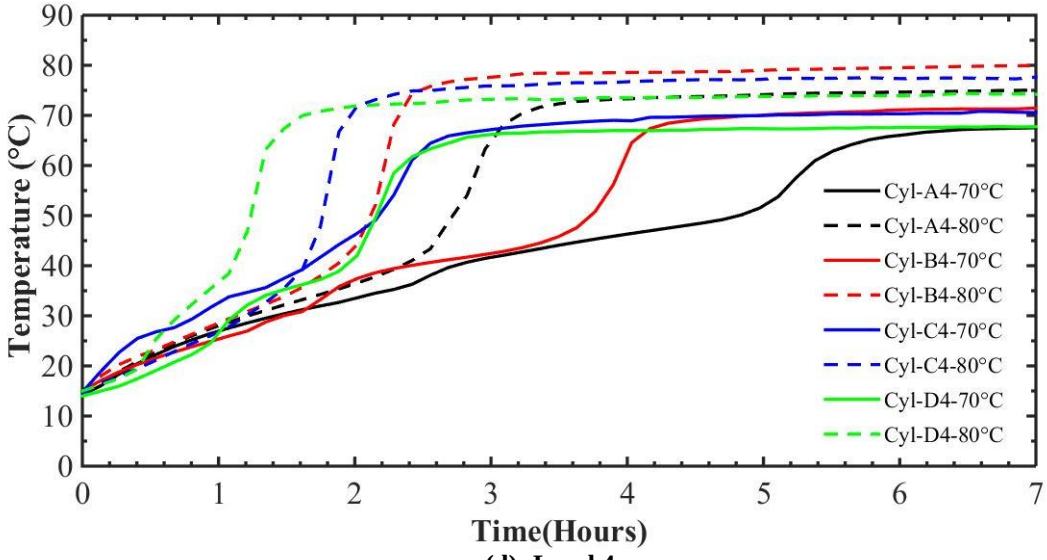

(d) Level 4

Fig. 7.8: Comparison of thermocouple probes located 20 mm away from the inner diameter of the acrylic cylinder during charging at 70 °C and 80 °C and 10 L/min flow rate.

7.4.3.2 Discharging Process

Fig. 7.9 (a-d) shows the temperature variations for thermocouple probes located 5 mm away from the inner diameter of the acrylic cylinder during the discharging process with the HTF temperature of 10°C after being charged with HTF at 70°C and 80°C while the flow rate is kept constant at 10 L/min. It can be seen that initial HTF charging temperature does not have any significant effect on the total discharging time in each LHTES unit.

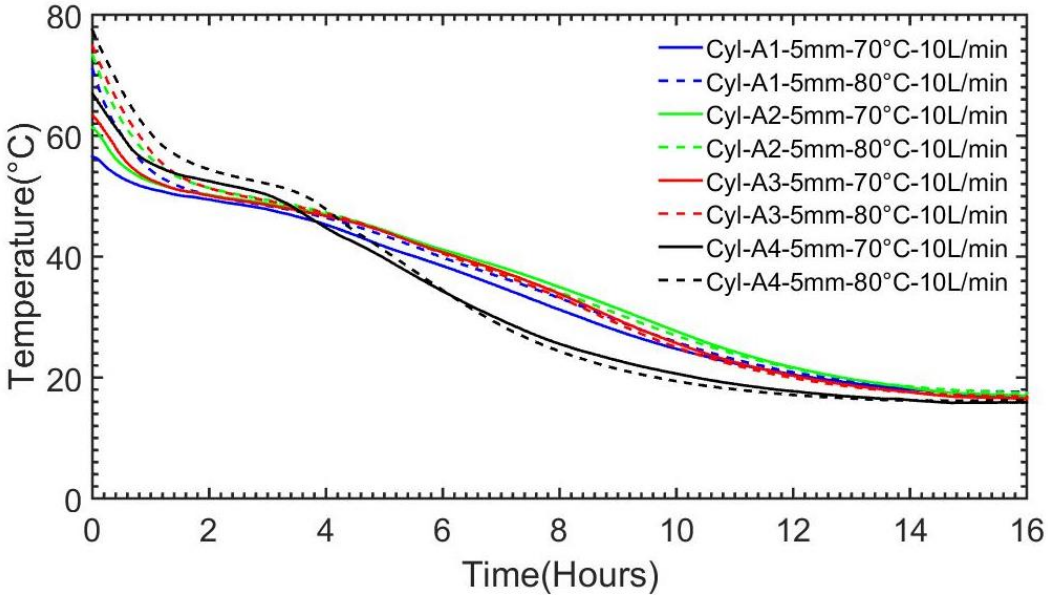

(a) Cylinder A

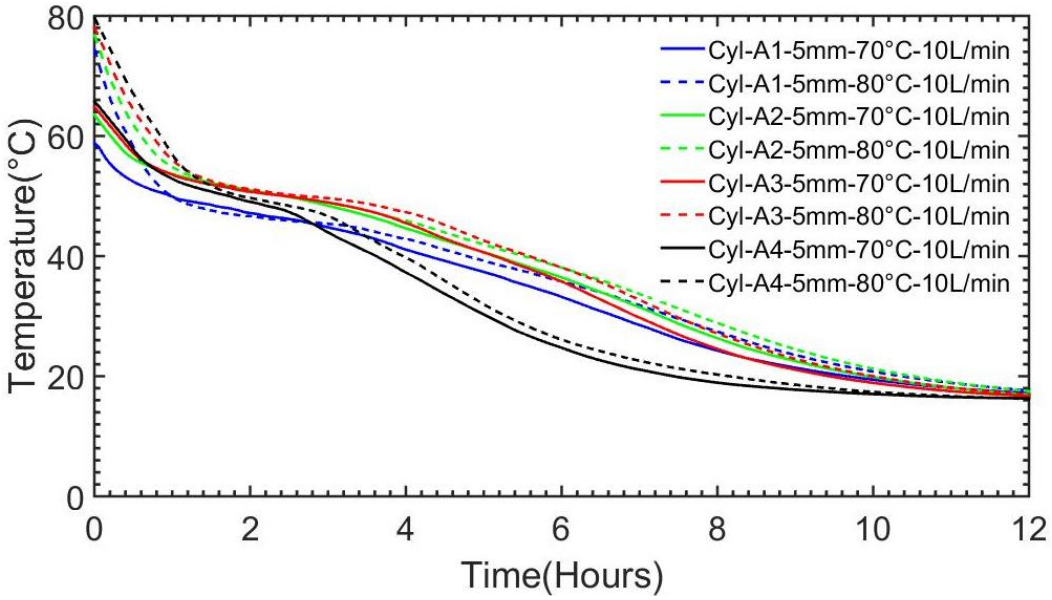

(b) Cylinder B

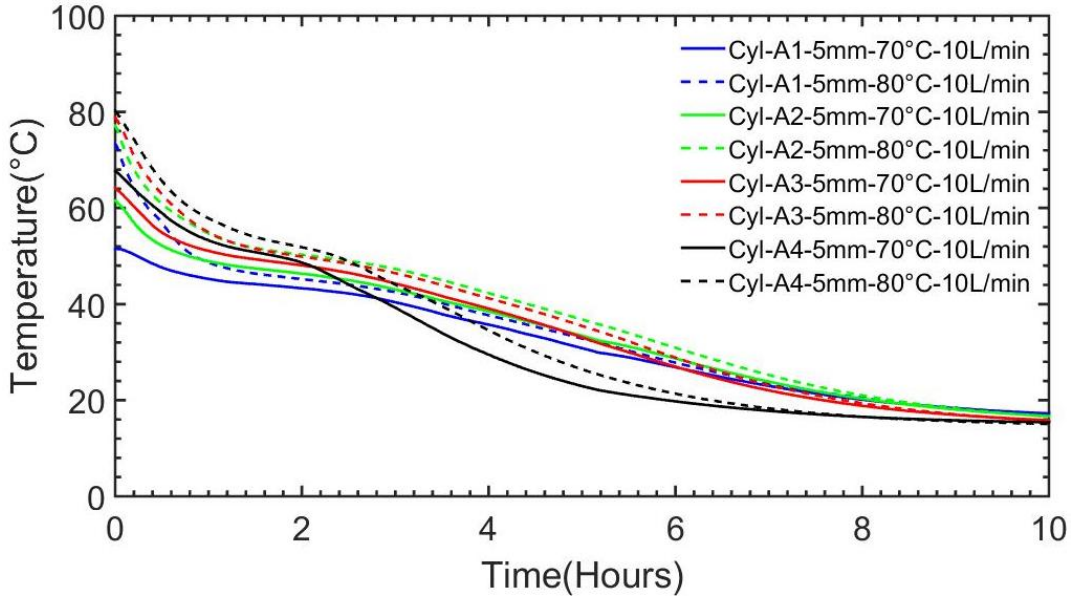

(c) Cylinder C

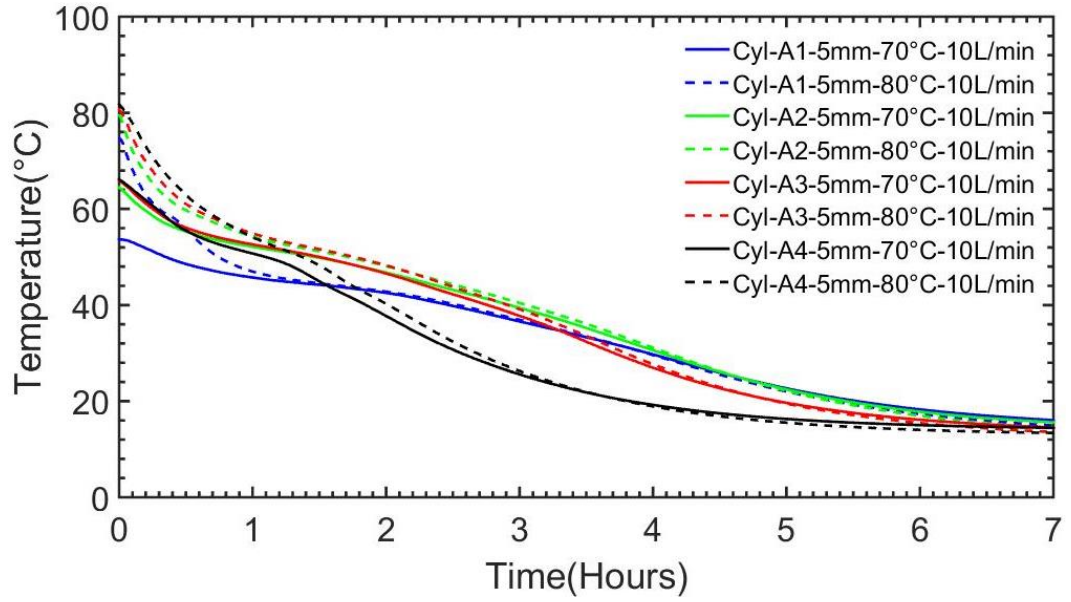

(d) Cylinder D

Fig. 7.9: Comparison of thermocouple probes located 5 mm away from HTF pipe during discharging with HTF at 10 °C after charging at 70 °C and 80 °C and 10 L/min flow rate.

Fig. 7.10 (a-d) compares the temperature variation at each level for the thermocouple probes located 20mm away from the HTF pipe discharging process which were initially charged with HTF at temperatures of 70 °C and 80 °C. It can be seen that the PCM temperature drops rapidly at the beginning of the discharging process due to the dominant convection heat

transfer, and initial HTF charging temperature does not have any significant effect on the time taken to reach 20 °C in all thermocouple locations.

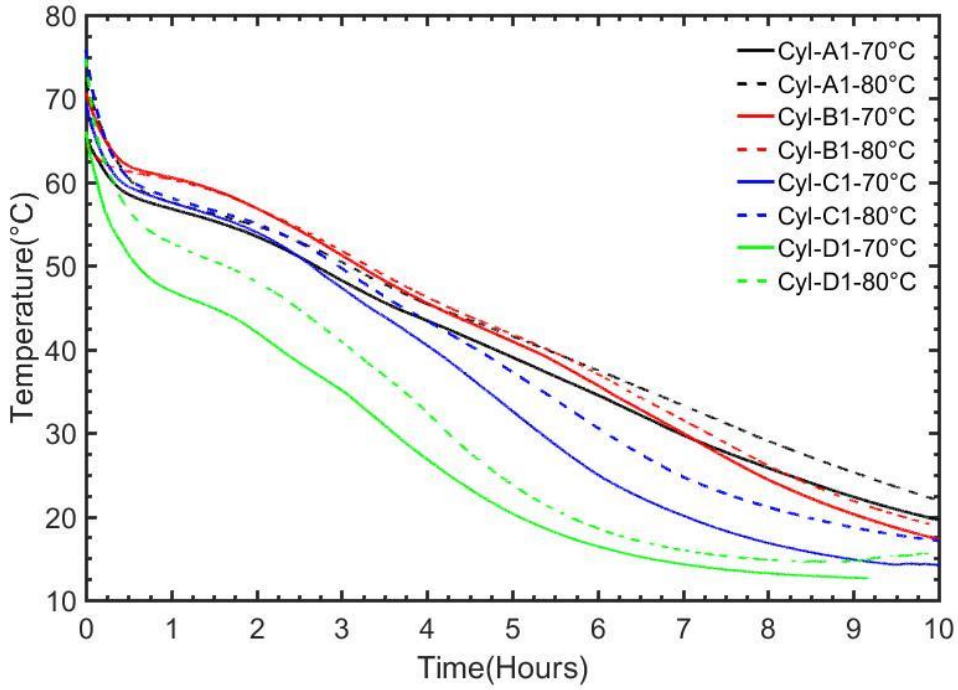

(e) Level 1

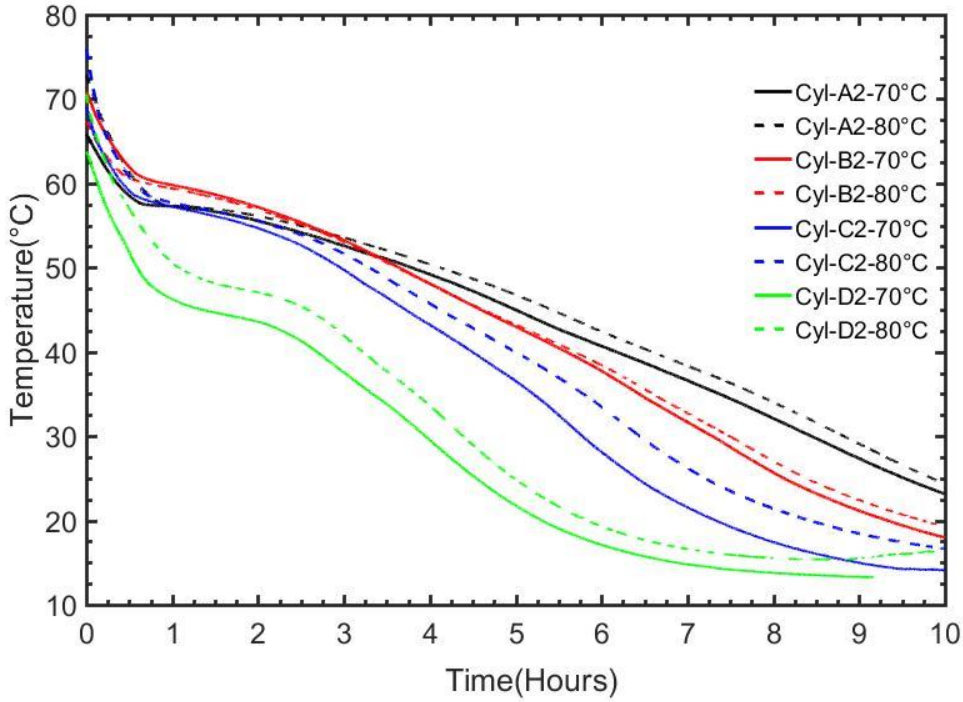

(f) Level 2

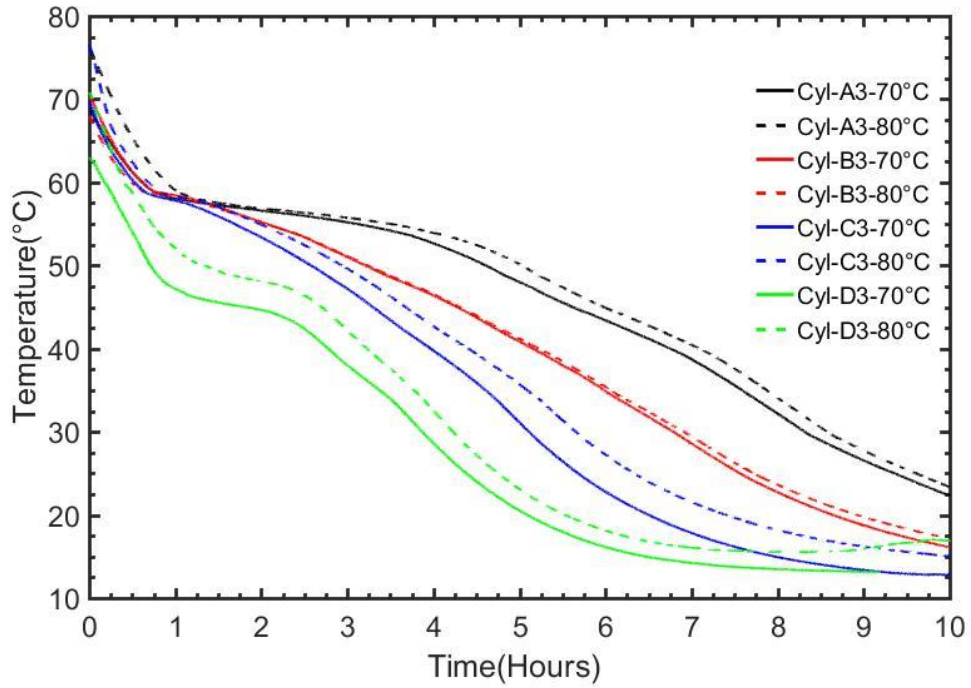

(g) Level 3

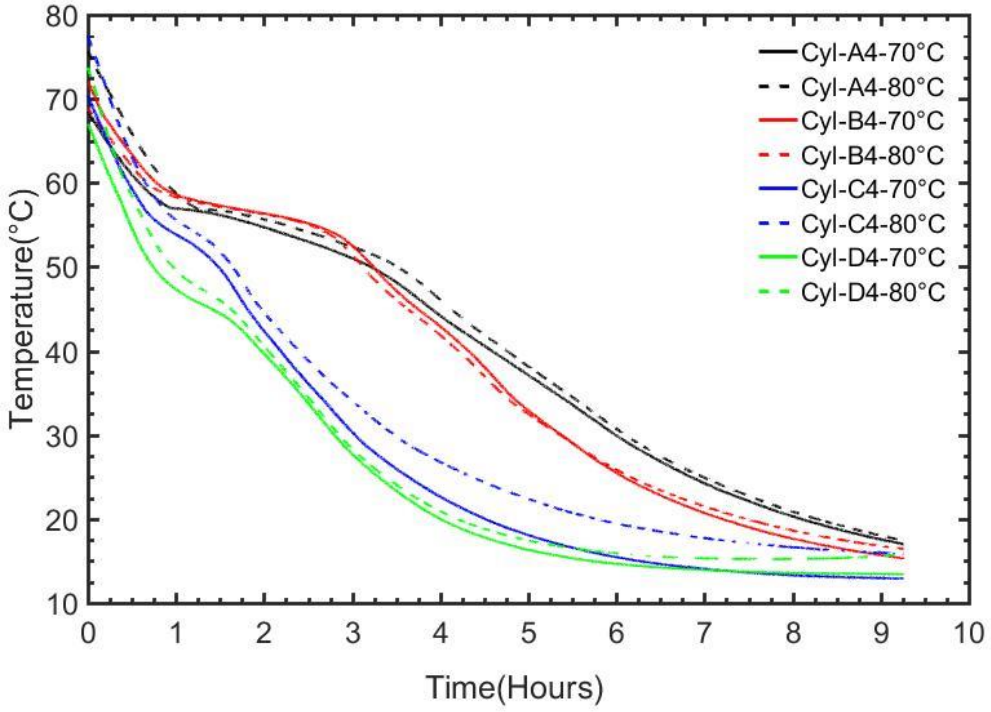

(h) Level 4

Fig. 7.10: Comparison of thermocouple probes located 20mm away from HTF pipe during discharging with HTF at 10 °C after charging at 70 °C and 80 °C and 10 L/min flow rate.

7.4.3.3 Complete charging-discharging cycle

Fig.7.11 (a-d) shows the variation of PCM temperature in a complete charging and discharging cycle for thermocouple probes located 5mm from the inner surface of the acrylic cylinder for each container. The HTF charging temperatures were at 70 °C and 80 °C, with the discharging temperature of 10 °C while the HTF flow rate was kept constant at 10 L/min. It is observed that the overall charging-discharging time is highly dependent on the charging time which is influence by the HTF temperature. Increasing the HTF charging temperature from 70 to 80 °C reduces the complete cycle time to 54, 55, 57, and 63% for cylinders A to D respectively. Reducing the outer to inner diameter ratios from 8.1 to 2.7 between cylinders A and D decreases the overall cycle time to 34% and 40% for the HTF temperature of 70 to 80 °C respectively.

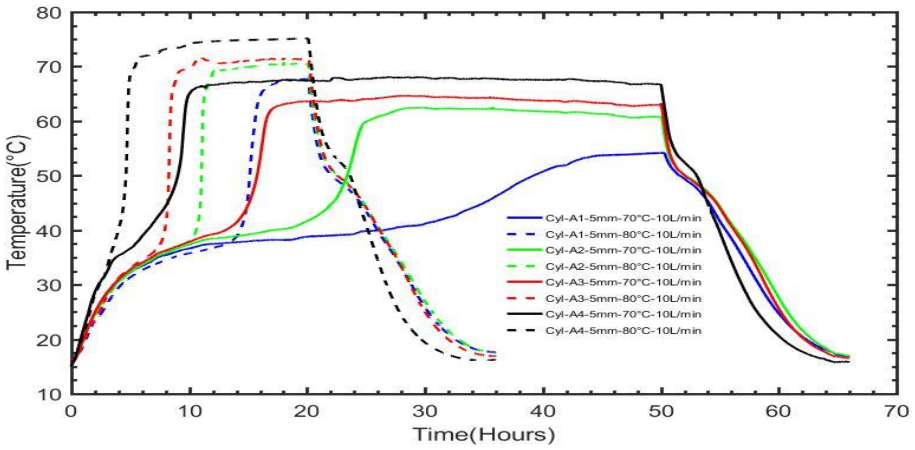

(a) Cylinder A

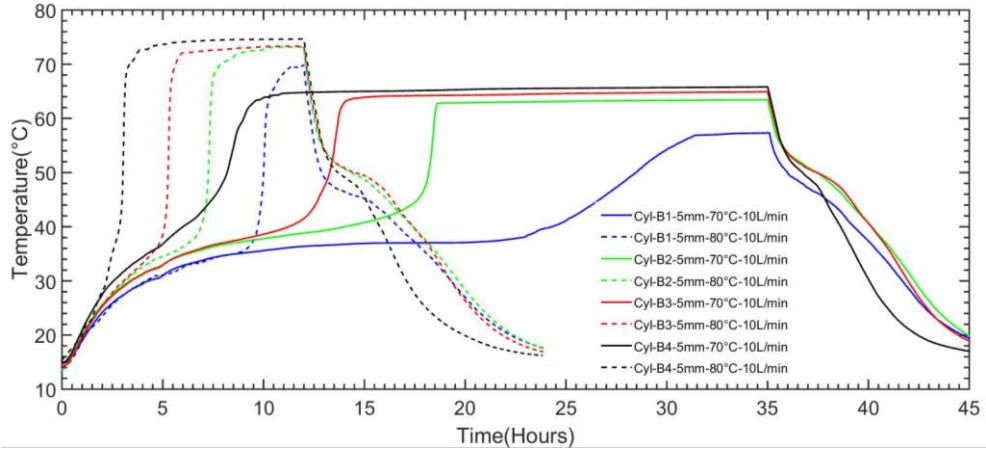

(b) Cylinder B

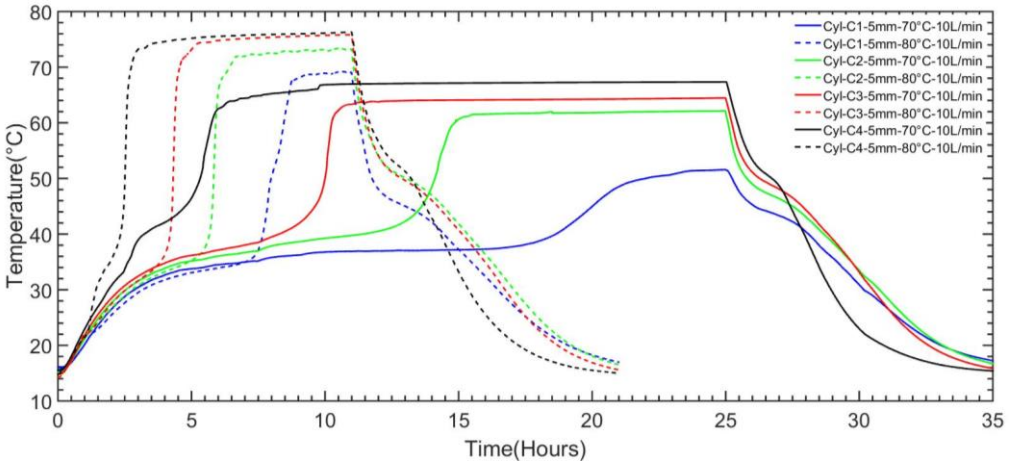

(c) Cylinder C

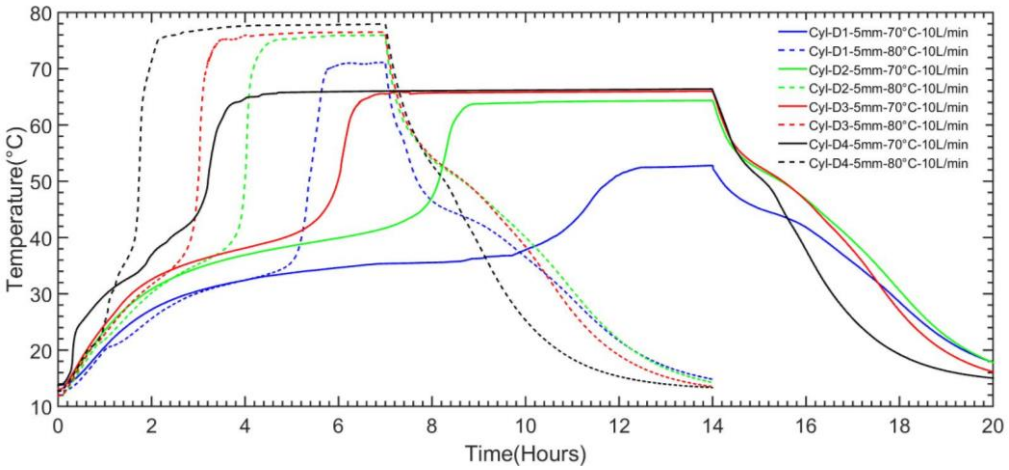

(d) Cylinder D

Fig. 7.11 Complete charging and discharging cycles for thermocouple probes located 5mm away from the inner diameter of the acrylic cylinder.

To conclude what was discussed in this section, Table 3 compare the total charging, discharging, and a complete cycle time of LHTES unit with reference to the cylinder A

Comparing is shown in Table 3.

Table 3: Comparison of time ratios based on cylinder A.

LHTES Unit	Cylinder A	Cylinder B	Cylinder C	Cylinder D
Ratio (Do/Di)	8.10	5.40	4.0	2.70
Charging time ratio (70 °C)	1	0.70	0.50	0.28
Charging time ratio (80 °C)	1	0.66	0.50	0.33
Discharging time ratio	1	0.75	0.63	0.44
Complete cycle time ratio (70 °C)	1	0.70	0.54	0.30
Complete cycle time ratio (80 °C)	1	0.69	0.60	0.40

7.4.4. Comparing LHTES units based on the HTF flow rate

The PCM temperature variation in different LHTES units ere compared with the same HTF flow rate and the same HTF Reynolds number.

7.4.4.1 Comparing with the same HTF flow rate

Fig. 7.12 (a-d) compares the PCM temperature variation during the complete charging-discharging cycle with charging HTF temperature of 70°C, and discharging HTF temperature of 10°C while the HTF flow rate kept at 10 L/min. By reducing the ratio of outer to the inner diameter from 8.1 to 2.7 for cylinders A to D, the charging, discharging, and complete cycle times decrease to 28%, 44%, and 34% respectively.

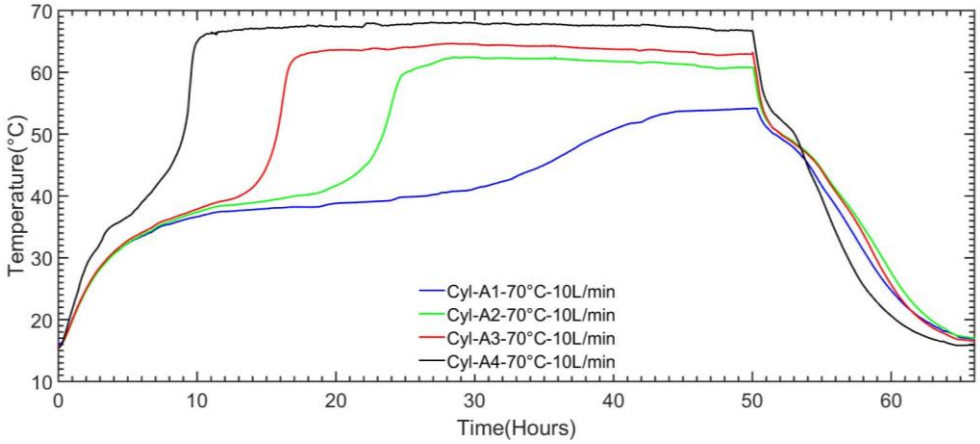

(a) Cylinder A (10 L/min)

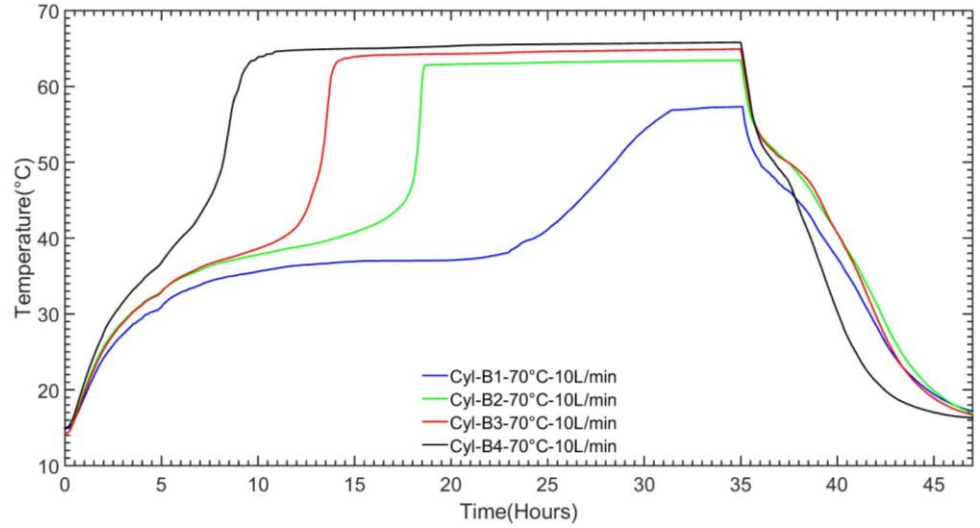

(b) Cylinder B (10 L/min)

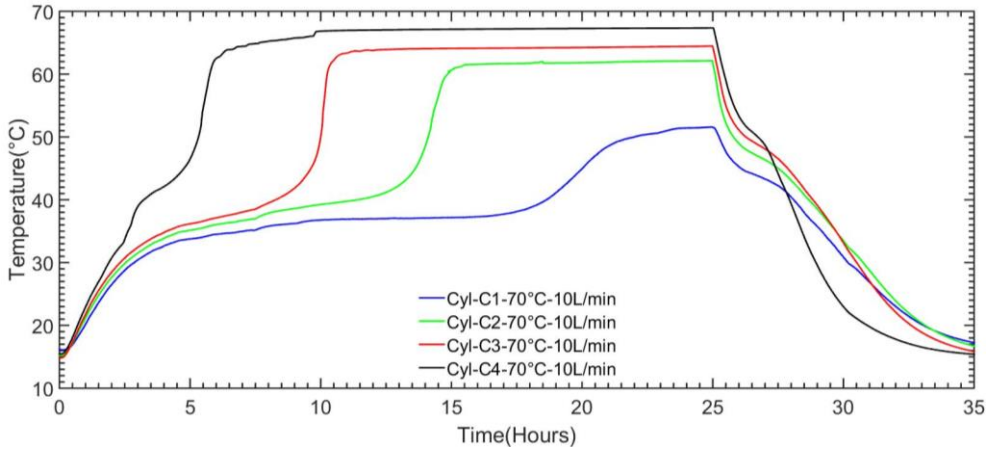

(c) Cylinder C (10 L/min)

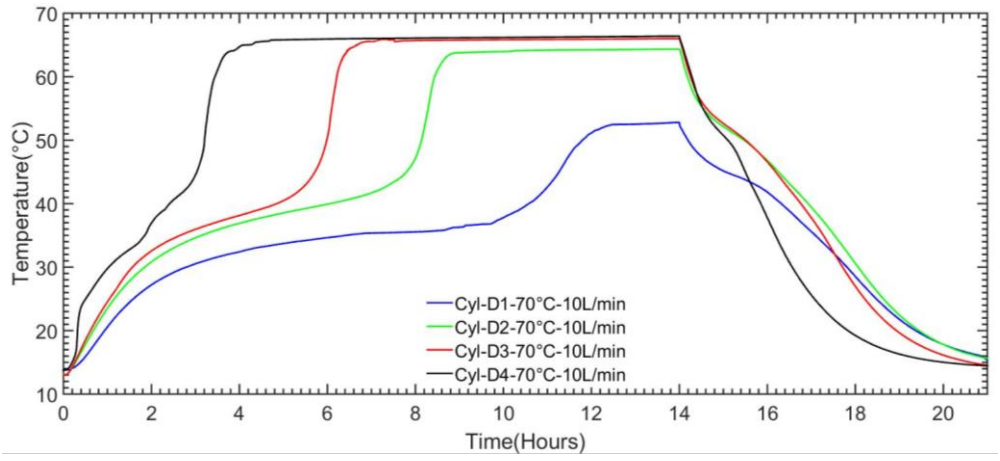

(d) Cylinder D (10 L/min)

Fig. 7.12 PCM temperature variations in a complete charging and discharging cycle.

7.4.4.2 Comparing with the same HTF Reynolds number

Fig. 7.13 (a-d) compares the PCM temperature variation during the complete charging-discharging cycle with charging HTF temperature of 70°C, and discharging HTF temperature of 10°C while the HTF Reynolds number was kept constant. The HTF flow of 5, 7.5, 10, and 15 L/min in cylinders A, B, C, and D respectively provides the same Reynold number and accordingly the same heat transfer coefficient in all LHTES units. It can be seen that reducing the ratio of outer to inner diameters from 8.1 to 2.7 between cylinders A and D decreases the charging, discharging, and complete cycle times to 28%, 44%, and 34% respectively which is similar to the results obtained with the same HTF flow rate. In these experiments, there is little difference between the HTF inlet and outlet temperature (less than 0.5 °C) for any of the LHTES systems. Therefore, a large amount of heat is carried downstream with the HTF, while only a small amount of heat is transferred directly to the PCM. Consequently, for as long as the HTF flow is turbulent, increasing or decreasing the HTF flow rate does not significantly improve the heat transfer rate. It can be concluded that the change in forced convective heat transfer produced by varying the HTF flow rate does not alter the PCM heat transfer rate in the systems which is according to the previous finding in Chapter 5 and 6.

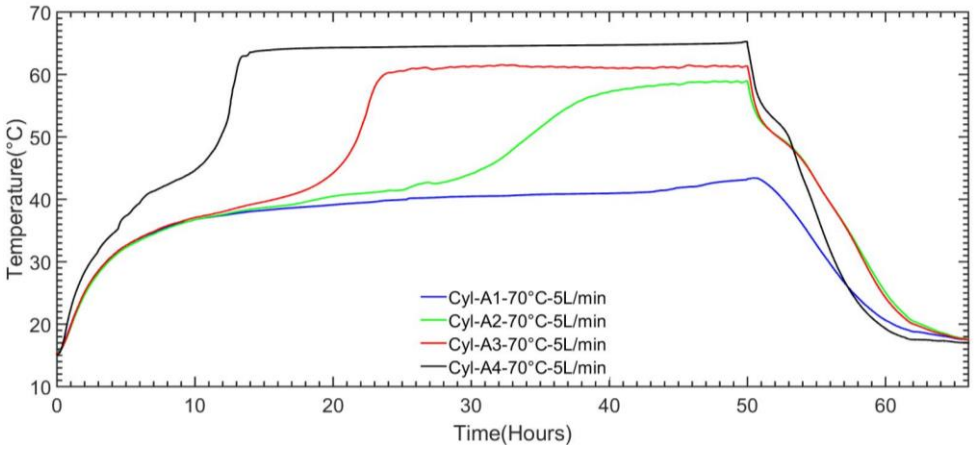

(a) Cylinder A (5L/min)

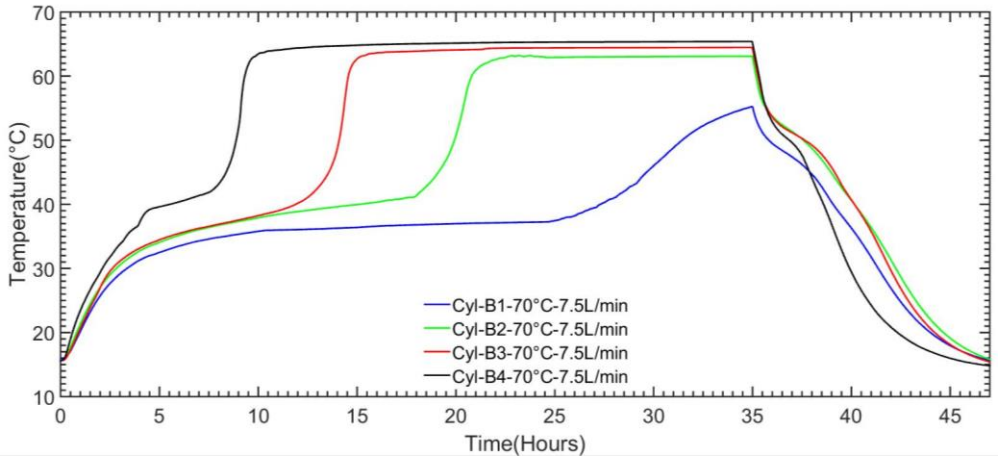

(b) Cylinder B (7.5 L/min)

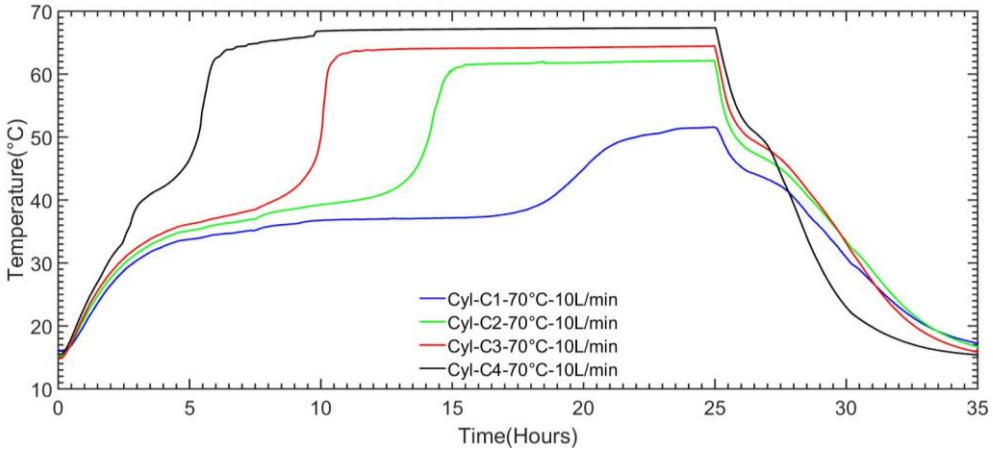

(c) Cylinder C (10 L/min)

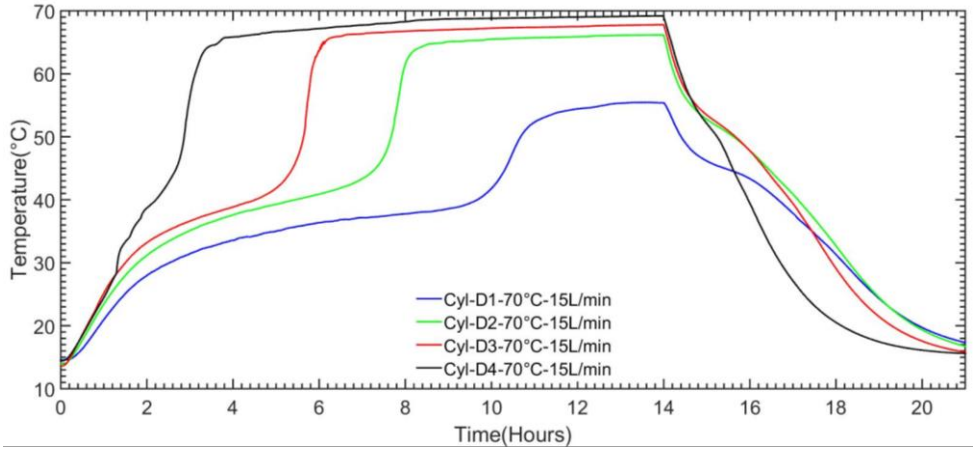

(d) Cylinder D (15 L/min)

Fig. 7.13: Variation of the PCM temperature in a complete charging and discharging cycle in each container with the same Reynolds number.

7.4.5. Comparing the LHTES units based on the stored energy

In this section, the total stored energy and the stored energy per hour are compared to evaluate the performance of LHTEs units. Fig.7.14 (a-b) shows the total stored energy variation in LHTES units with different outer to inner radii ratios during the charging (HTF temperatures of 70 and 80 °C) and discharging (HTF temperatures of 10 °C) processes. In Fig.7.14, the dash lines show the total stored energy in an ideal system without any heat loss, and the solid line are for the real systems under the experiment. Also, the time is taken for each unit to complete the charging and discharging process is mentioned near the bold points.

It can be seen that increasing the diameter ratio raises the total stored energy. This is because a greater volume of PCM exists in the cylinder at higher ratios. However, the greater the total energy stored in higher diameter ratio systems, the longer the time needed for charging or discharging, as the data labels indicate. An interesting observation is that there is a sharp increase in the stored/released energy between diameter ratios of 2.7 and 4 (Cyl D to Cyl C), but this trend slows down between diameter ratios of 4 and 5.4 (Cyl C to Cyl B). Finally, between diameter ratios of 5.4 and 8.1(Cyl B to Cyl A), there is no significant difference in stored/released energy.

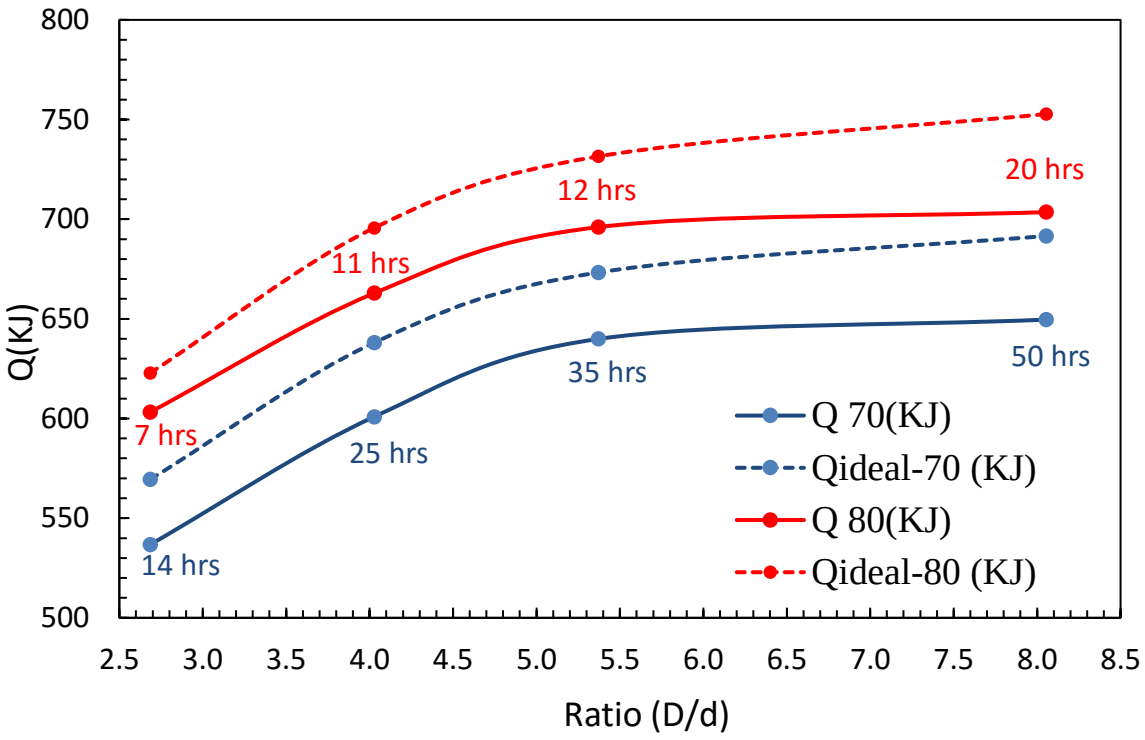

(a) Charging process

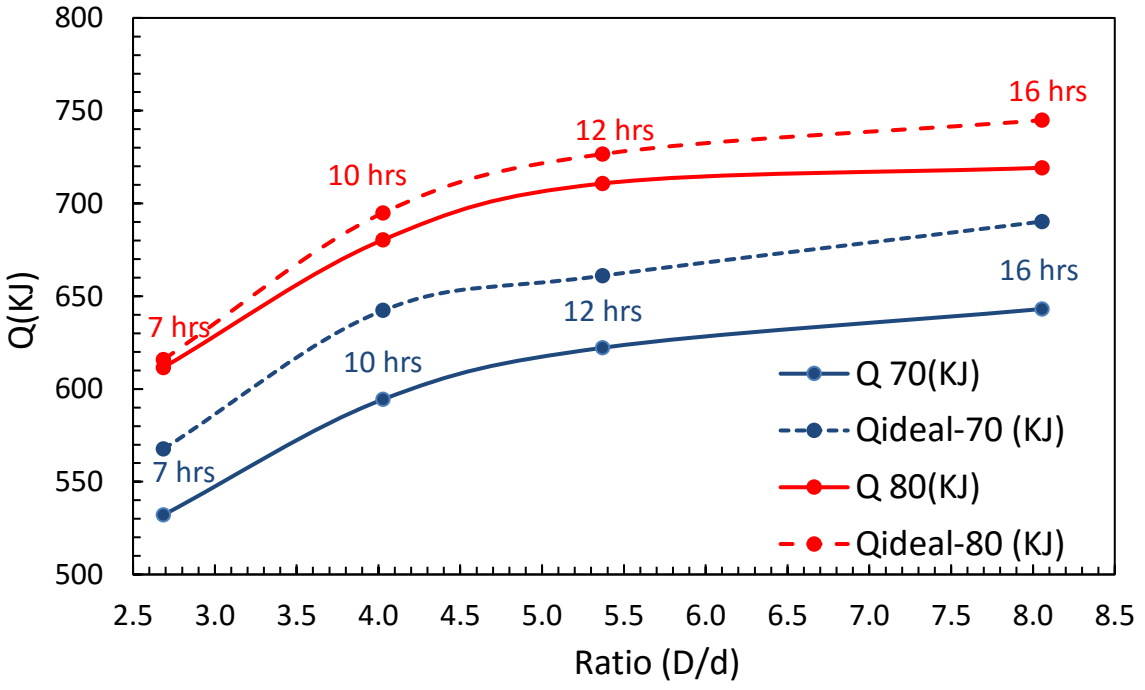

(b) Discharging process

Fig. 7.14: The effect of tube diameter ratios on the total stored energy during a) charging and b) discharging processes.

Furthermore, Fig.7.15 depicts the variation in the energy storage rate per hour obtained during the charging and discharging processes. It can be seen that the LHTES units with higher diameter ratios will store/release less energy per hour. There is a dramatic drop in the stored energy per hour for the charging process as the diameter ratio increases from 2.7 to 4 (Cyl D to Cyl C). However, there is no significant difference in the stored energy as the diameter ratio increases from 4 to 5.4 (Cyl C to Cyl B). It again drops significantly between diameter ratios 5.4 and 8.1 (Cyl B to Cyl A). Diameter ratios between 4 and 5.4 could be more reasonable for design purposes.

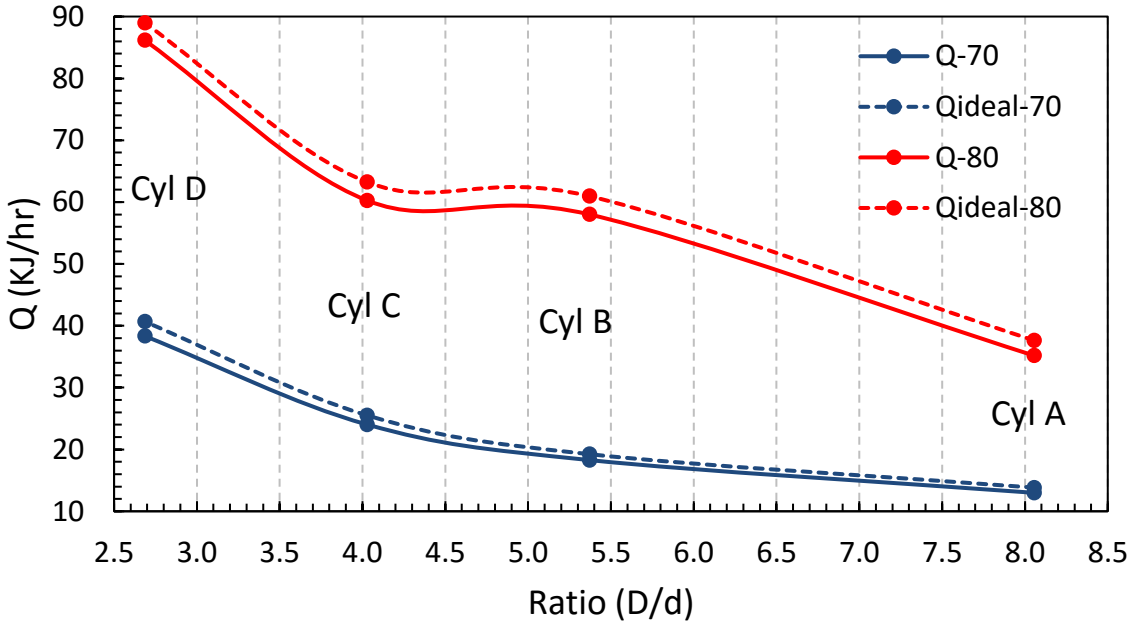

(a) Charging process

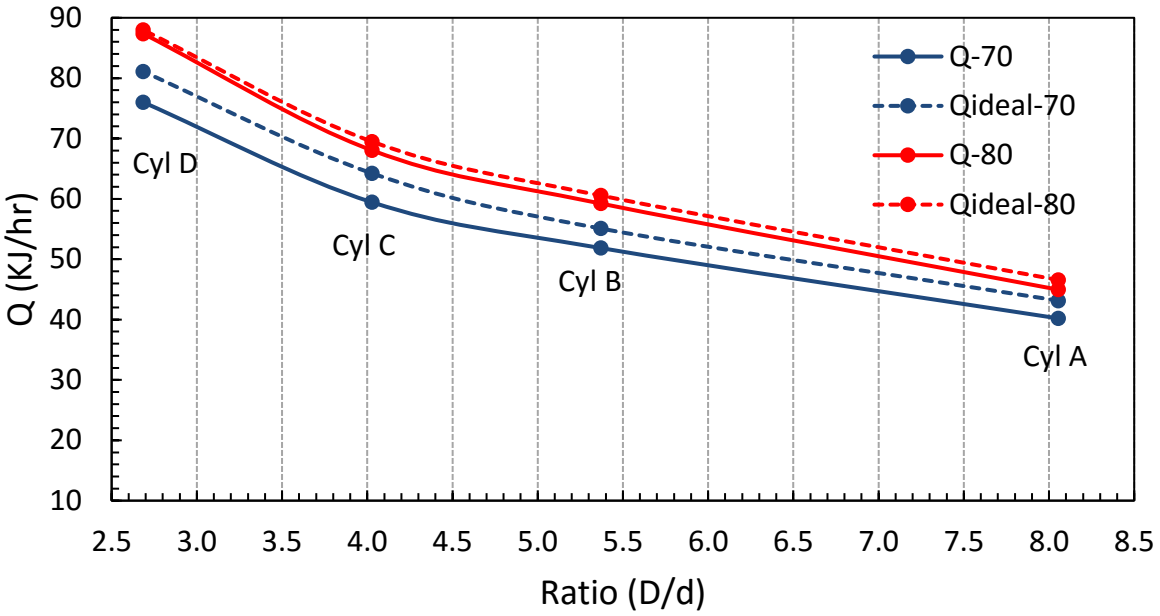

(b) Discharging process

Fig. 7.15 Effect of tube diameter ratio on rate of energy storage during (a) charging and (b) discharging processes.

It can be concluded that the optimum LHTES system is Cyl B with the outer to inner radii ratio of 5.4 and the HTF charging temperature of 80°C. During the charging process, Cyl B stores almost the same amount of energy as the Cyl A which has the highest among these systems in a 60% of time required. During the discharging process, Cyl B released the same energy in only 75% of the time needed by Cyl A. On the other hand, Cyl B stored almost the same amount of energy per hour as Cyl C does. This means that increasing the HTF surface area by reducing the outer to inner radii ratio from 5.4 to 4 does not significantly increase the stored energy. Also, the time needed to complete the charging process in Cyl B and C with the HTF temperature of 80°C is almost the same.

7.5. Conclusion

This chapter studies the effect of geometrical parameters of the vertical cylindrical LHTES unit. For this purpose, four different shell to tube diameter ratios were considered with the PCM

on the shell side and the HTF is passing through on the tube side. The PCM temperature distributions were measured and compared experimentally. The results showed that complete charging and discharging was highly dependent on the ratio of outside to the inside diameter as well as the HTF temperature. The effects of HTF flow rate were also examined experimentally. It is concluded that there was no significant difference in the charging and discharging time by increasing the HTF flow rate as far as the HTF flow was turbulent. For the design purpose, this parameter was highly dependent on the hours of sunlight as well as the output temperature of the solar collector. Having HTF temperature of 80ºC for 12 hours, the outer to inner diameter ratio of 5.4 is the optimum to give the highest stored/released energy. The parameters discussed in this chapter need to be considered in the design and optimization of shell-and-tube LHTES systems.

7.6. References

[1] Agyenim F, Hewitt N, Eames P, Smyth M. A review of materials, heat transfer and phase change problem formulation for latent heat thermal energy storage systems (LHTESS). Renewable and sustainable energy reviews. 2010;14:615-28.

[2] Seddegh S, Wang X, Henderson AD, Xing Z. Solar domestic hot water systems using latent heat energy storage medium: A review. Renewable and Sustainable energy reviews. 2015;49:517-33.

[3] Lacroix M. Numerical simulation of a shell and tube latent heat thermal energy storage unit. Solar Energy. 1993;50(40):357-367.

[4] Esen M, Durmus A, Darmus A, Geometri design of solar-aided latent heat store depending on various parameters and phase change materials. Solar Energy. 1998;62(1):19-28.

[5] Ismail K. A. R, Goncalves M. M. Thermal performance of a PCM storage unit. Energy Conversion and Management. 1999;40:115-138.

[6] Ismail K. A. R, Melo C. A. Convection-based model for a PCM vertical storage unit. International Journal of Energy Research. 1998;22:1249-1265.

[7] Trp A, Lenic K, Frankovic B. Analysis of the influence of operating conditions and geometric parameters on heat transfer in water-parrafin shell and tube latent thermal energy storage unit. Applied Thermal Engineering. 2006;26:1830-1839.

[8] Tao Y. B, He Y. L, Numerical study on thermal energy storage performance of phase change material under non-steady state inlet boundary. Applied Energy.2011;88:4172-4179.

[9] Avci M, Yazici MY. Experimental study of thermal energy storage characteristics of a paraffin in a horizontal tube-in-shell storage unit. Energy conversion and management. 2013;73:271-7.

[10] Hosseini M, Rahimi M, Bahrampoury R. Experimental and computational evolution of a shell and tube heat exchanger as a PCM thermal storage system. International Communications in Heat and Mass Transfer. 2014;50:128-36.

[11] Seddegh S, Wang X, Henderson AD. A comparative study of thermal behaviour of a horizontal and vertical shell-and-tube energy storage using phase change materials. Applied Thermal Engineering. 2016; 93:348-358.

[12] Wang W, Zhang K, Wang L, He Y. Numerical study of the heat charging and discharging characteristics of a shell-and-tube phase change heat storage unit. Applied Thermal Engineering. 2013;58 (1-2):542-553.

[13] Wang W, Wang L, He Y. The energy efficiency ratio of heat storage in one shell and one tube phase change thermal energy storage unit. Applied Energy. 2015;138:169-182.

[14] Tehrani S. S. M, Taylor R. A, Saberi P, Diarece G. Design and feasibility of high temperature shell and tube latent heat thermal energy storage system for solar thermal power plant. Renewable Energy. 2016; 96:120-136.

Chapter8: Conclusion and future research

8.1. Final conclusion

This thesis started with a review of thermal energy storage technologies for solar water heating systems with a particular focus on latent heat thermal energy storage. It was found that the integrated phase change storage vessel was the most common approach. It was also revealed that most of the current research efforts focusing on understanding the performance and heat transfer in the latent heat energy storage unit. Then, a theoretical method was investigated on the heat transfer mechanism in PCM during the charging and discharging processes. Two heat transfer models named pure conduction and combined conduction and convection were developed and the predicted results were validated against available experimental data. It was concluded that the combined conduction and convection model can better describe the energy transfer in the phase change materials during the charging process. In contrast, heat transfer by conduction is most significant during the discharging process. In terms of total solidification time, the two models show little difference.

Using the combined conduction and convection model, the thermal behavior and heat transfer characteristics in the horizontal and vertical shell-and-tube thermal energy storage systems were compared. During the charging process, natural convection is the dominant heat transfer mechanism in both systems. The results indicated that the horizontal orientation has superior thermal performance during charging and in particular during part-load energy charging. In fact, for the horizontal orientation, convective heat transfer has a strong effect on melting of the upper part of the solid PCM and is less significant during melting of the lower half of the solid PCM. However, in the vertical orientation, convective heat transfer is the same

active during the entire charging process. During the discharging process, the thermal behavior does not show any difference between horizontal and vertical systems.

As most experimental works in the literature focused on heat transfer in the horizontal shell-and-tube LHTES system which was significantly different from that in the vertical ones, visualized experiments were performed on the physics of the heat transfer mechanism in vertical cylindrical and conical shell-and-tube LHTES systems. It was found that natural convection dominated heat transfer during the charging process and thermal behavior were very similar in both systems. The results showed that there existed a vertical convective circulation channel around the HTF pipe. The width of this vertical channel did not show significant change once it was formed. Thermal energy was transferred from the HTF to the liquid PCM and then carried upward via vertical convective circulation in the channel. This thermal energy was further transferred in the liquid PCM accumulated at the upper part of the storage system through horizontal convective circulation. Hence heat transfer was more effective at the upper part of the system and PCM melting front moves downward from the top to the bottom of the system. Further comparison study showed that the vertical conical system had better energy storage performance than the cylindrical system. This indicated that a vertical storage unit with geometry having large volume in the upper part and small volume in the lower part could have better energy storage performance. During the discharging process, the experimental and theoretical results showed that the PCM solidifies around the HTF pipe and the solidification front moves both outward and upward. Due to its low thermal conductivity, the PCM behaves as an insulating material and the rate of heat transfer from the HTF to the PCM is reduced. The comparative results show that both systems have similar trend and it takes almost the same time to complete the discharging process.

Finally, the effect of the geometrical parameters on vertical cylindrical shell and tube LHTES systems were investigated. Considering four different shell to tube diameter ratios, the

results show that complete charging and discharging is highly dependent on the ratio of outside to the inside diameter as well as the HTF temperature. It is also concluded that there is no significant difference in the charging and discharging time by increasing the HTF flow rate as far as the HTF flow is turbulent. For the design purpose, this parameter is highly dependent on the hours of sunlight as well as the output temperature of the solar collector.

The research provides useful information and guidance to researchers and engineers for design and optimization of shell-and-tube LHTES systems.

8.2. Future research

The following important aspects need to be addressed in future work in this area:

- A mathematical model is required to compare the performance of SDHW systems with different integration techniques;
- A general numerical model should be developed to simulate the SDHW system performance under different scenarios to optimize the system in terms of performance and economics.
- Developing a standard is necessary to give the optimum configuration of LHTES in SDHW systems;
- An international PCM standard is necessary to unify the research findings and for design purposes.
- Further research is required to incorporate the up-to-date technologies of PCM units into SDHW systems and to better understand the SDHW system performance with these PCM units at different working conditions.
- Further experimental and numerical study should be performed to better understand and evaluate the long term performance of SDHW systems with PCMs under different climate conditions.